



National Library  
of Canada

Canadian Theses Service

Ottawa, Canada  
K1A 0N4

Bibliothèque nationale  
du Canada

Services des thèses canadiennes

## CANADIAN THESES

### NOTICE

The quality of this microfiche is heavily dependent upon the quality of the original thesis submitted for microfilming. Every effort has been made to ensure the highest quality of reproduction possible.

If pages are missing, contact the university which granted the degree.

Some pages may have indistinct print especially if the original pages were typed with a poor typewriter ribbon or if the university sent us an inferior photocopy.

Previously copyrighted materials (journal articles, published tests, etc.) are not filmed.

Reproduction in full or in part of this film is governed by the Canadian Copyright Act, R.S.C. 1970, c. C-30. Please read the authorization forms which accompany this thesis.

**THIS DISSERTATION  
HAS BEEN MICROFILMED  
EXACTLY AS RECEIVED**

## THÈSES CANADIENNES

### AVIS

La qualité de cette microfiche dépend grandement de la qualité de la thèse soumise au microfilmage. Nous avons tout fait pour assurer une qualité supérieure de reproduction.

S'il manque des pages, veuillez communiquer avec l'université qui a conféré le grade.

La qualité d'impression de certaines pages peut laisser à désirer, surtout si les pages originales ont été dactylographiées à l'aide d'un ruban usé ou si l'université nous a fait parvenir une photocopie de qualité inférieure.

Les documents qui font déjà l'objet d'un droit d'auteur (articles de revue, examens publiés, etc.) ne sont pas microfilmés.

La reproduction, même partielle, de ce microfilm est soumise à la Loi canadienne sur le droit d'auteur, SRC 1970, c. C-30. Veuillez prendre connaissance des formules d'autorisation qui accompagnent cette thèse.

**LA THÈSE A ÉTÉ  
MICROFILMÉE TELLE QUE  
NOUS L'AVONS REÇUE**



National Library  
of Canada

Bibliothèque nationale  
du Canada

Ottawa, Canada  
K1A 0N4

TC -

ISE

0-315-23370-2

CANADIAN THESES ON MICROFICHE SERVICE - SERVICE DES THÈSES CANADIENNES SUR MICROFICHE

**PERMISSION TO MICROFILM - AUTORISATION DE MICROFILMER**

• Please print or type - Écrire en lettres moulées ou dactylographier

AUTHOR - AUTEUR	
Full Name of Author - Nom complet de l'auteur	MUHAMMAD RAFIQUL ISLAM
Date of Birth - Date de naissance	JAN 01, 1954
Country of Birth - Lieu de naissance	BANGLADESH
Canadian Citizen - Citoyen canadien	<input type="checkbox"/> Yes / Oui <input checked="" type="checkbox"/> No / Non
Permanent Address - Résidence fixe	C/O MR. SULAIMAN T.B. ROAD LAXMIPUR, RAJSHAHI BANGLADESH

THESIS - THÈSE	
Title of Thesis - Titre de la thèse	AN INVESTIGATION OF THE IMPACT OF FLOW REGIME ON EFFECTIVE PERMEABILITY

Degree for which thesis was presented Grade pour lequel cette thèse fut présentée	M. SC.	Year this degree conferred Année d'obtention de ce grade	1985
University - Université	UNIVERSITY OF ALBERTA	Name of Supervisor - Nom du directeur de thèse	DR. RAMON G. BENTSON

AUTHORIZATION - AUTORISATION	
Permission is hereby granted to the NATIONAL LIBRARY OF CANADA to microfilm this thesis and to lend or sell copies of the film.	L'autorisation est, par la présente, accordée à la BIBLIOTHÈQUE NATIONALE DU CANADA de microfilmer cette thèse et de prêter ou de vendre des exemplaires du film.
The author reserves other publication rights, and neither the thesis nor extensive extracts from it may be printed or otherwise reproduced without the author's written permission.	L'auteur se réserve les autres droits de publication; ni la thèse ni de longs extraits de celle-ci ne doivent être imprimés ou autrement reproduits sans l'autorisation écrite de l'auteur.

ATTACH FORM TO THESIS - VEUILLEZ JOINDRE CE FORMULAIRE À LA THÈSE

Signature	Rafiqul Islam	Date	August 26th, 1985
-----------	---------------	------	-------------------

THE UNIVERSITY OF ALBERTA

AN INVESTIGATION OF THE IMPACT OF FLOW REGIME ON EFFECTIVE  
PERMEABILITY

by

M. Rafiqul Islam

C

A THESIS

SUBMITTED TO THE FACULTY OF GRADUATE STUDIES AND RESEARCH  
IN PARTIAL FULFILMENT OF THE REQUIREMENTS FOR THE DEGREE  
OF Master of Science

IN

PETROLEUM ENGINEERING

DEPARTMENT OF MINERAL ENGINEERING

EDMONTON, ALBERTA

Fall, 1985

THE UNIVERSITY OF ALBERTA

RELEASE FORM

NAME OF AUTHOR M.Rafiqul Islam  
TITLE OF THESIS AN INVESTIGATION OF THE IMPACT OF FLOW  
REGIME ON EFFECTIVE PERMEABILITY  
DEGREE FOR WHICH THESIS WAS PRESENTED Master of Science  
YEAR THIS DEGREE GRANTED 1985

Permission is hereby granted to THE UNIVERSITY OF  
ALBERTA LIBRARY to reproduce single copies of this  
thesis and to lend or sell such copies for private,  
scholarly or scientific research purposes only.

The author reserves other publication rights, and  
neither the thesis nor extensive extracts from it may  
be printed or otherwise reproduced without the author's  
written permission.

(SIGNED) ...*Rafiqul Islam*...

PERMANENT ADDRESS:

C/O MR. M. SULAIMAN  
.....  
T.B. ROAD, LAXMIPUR  
.....  
RAJSHAHI, BANGLADESH  
.....

DATED .August.22nd,.....1985



THE UNIVERSITY OF ALBERTA  
FACULTY OF GRADUATE STUDIES AND RESEARCH

The undersigned certify that they have read, and recommend to the Faculty of Graduate Studies and Research, for acceptance, a thesis entitled AN INVESTIGATION OF THE IMPACT OF FLOW REGIME ON EFFECTIVE PERMEABILITY submitted by M. Rafiqul Islam in partial fulfilment of the requirements for the degree of Master of Science in PETROLEUM ENGINEERING.

*Comay Deaton*

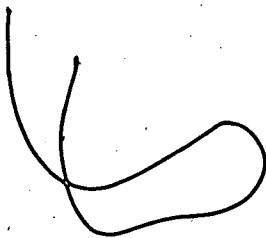
Supervisor

*Amir Qasbi*  
3C 7/10/85

Date..... August 22nd, 1985 .....

**Dedication**

TO  
MY PARENTS,  
AND ALL MY TEACHERS



## ABSTRACT

Currently available techniques for estimating effective permeability are valid only if the displacement is stable and stabilized. That is, only effective permeabilities which are applicable to steady state situations can be measured. As many field displacements are thought to be unstable, there is a need to develop techniques capable of measuring unstable effective permeabilities. The present study proposes one such method. This method enables the estimation of the effective permeabilities in all three flow regimes, namely, unstabilized, stabilized and stable, and unstable displacements.

The proposed method uses the microwave attenuation technique to measure how saturation is distributed along the length of a core. This enables the estimation of the fraction of water flowing at any point along the length of the core. Because a pressure profile is also available, it is possible to relate the fraction flowing to the pressure gradient by means of the differential form of Darcy's law to obtain a dynamic estimate of the effective permeability at any given location (and saturation) along the length of a core. As data acquisition and storage is automated it is possible to obtain a complete set of relative permeability data in less than a day.

Experimental results suggest that effective permeability is a unique function of saturation only if the

displacement is steady-state or if the displacement is stable and stabilized. If the displacement is unstabilized, or if it is unstable, different effective permeability curves are obtained. Moreover, for unstable displacements the effective permeability shows a strong dependence on local heterogeneities.

## Acknowledgement

I would like to express my sincere regards and thanks to Dr. R.G. Bentsen for his kind supervision, guidance and encouragement throughout the period of this study. I am also grateful to Dr. B. Flintoff for kindly helping me understand the micro-computer hardware and programming. Thanks are also due to Prof. P. Dranchuk for his thoughtful suggestions during this work and the production of the thesis.

It is also important to thank Mr. Robert Smith for his help in designing the experimental equipment. Thanks are also due to Mr. Tom Forman who helped me in setting up the computer and other electronic equipment.

I would like to thank the Department of Mineral Engineering and the Faculty of Graduate Studies for providing Research and Teaching Assistantships. Thanks are also due to NSERC and the Coordinating Committee of the Petroleum Aid to Education Trust Fund for the financial aid which made this study possible.

## Table of Contents

Chapter	Page
1. INTRODUCTION .....	1
2. LITERATURE REVIEW .....	3
2.1 BASIC THEORY .....	3
2.1.1 Basic Motion Equation .....	3
2.1.1.1 Channel Flow theory .....	3
2.1.1.2 Cylindrical Flow theory .....	6
2.1.1.3 Structural Models .....	6
2.1.2 Effect of Capillary and Viscous Forces ..	10
2.2 LABORATORY DETERMINATION OF RELATIVE PERMEABILITY .....	19
2.2.1 Steady-State Flow Method .....	19
2.2.2 Unsteady-State Flow Method .....	21
2.2.3 Improved Unsteady-State Flow Method .....	23
2.2.4 Dynamic Method .....	25
2.3 SATURATION MEASUREMENT TECHNIQUES .....	26
2.3.1 Resistivity Technique .....	26
2.3.2 Optical Methods .....	27
2.3.3 X-ray Absorption Method .....	28
2.3.4 Microwave Attenuation Technique .....	29
3. STATEMENT OF THE PROBLEM .....	32
4. THEORY .....	34
4.1 IMMISCIBLE DISPLACEMENT THEORY .....	34
4.1.1 Basic Motion Equation .....	34
4.1.2 Fractional Flow Equation .....	38
4.2 MICROWAVE THEORY .....	44
4.2.1 Dielectric Properties .....	45

4.2.2	Optical Properties .....	49
4.2.3	Physical Properties of Materials .....	52
4.3	STABILIZATION .....	56
4.4	STABILITY .....	56
4.5	CAPILLARY PRESSURE MODEL .....	59
5.	EXPERIMENTAL SET-UP AND PROCEDURE .....	62
5.1	MICROWAVE INSTRUMENTATION .....	62
5.2	FLUID INJECTION SYSTEM, CORE HOLDER, PRESSURE GAUGE, ETC. ....	64
5.3	AUTOMATION OF DATA ACQUISITION AND STORAGE .....	68
5.3.1	HP-9825A Micro Computer .....	68
5.3.2	Multiprogrammer Interface .....	70
5.3.3	Multiprogrammer ....	70
5.3.4	INPUT/OUTPUT cards .....	71
5.3.5	RELAY OUTPUT/REDABACK cards .....	73
5.3.6	Automatic Powermeter HP 432C .....	73
5.3.7	HP 9872A Plotter .....	74
5.4	MICROWAVE SIGNAL VERSUS WATER SATURATION .....	76
5.5	CORE PREPARATION PROCEDURE .....	78
5.6	ESTABLISHMENT OF IRREDUCIBLE WATER SATURATION .....	80
5.7	WATERFLOOD .....	81
5.8	FLUID PROPERTIES .....	82
5.9	CONVERSION OF MICROWAVE RESPONSE TO A SATURATION PROFILE .....	83
5.10	DATA ANALYSIS .....	85
6.	RESULTS AND DISCUSSION .....	90
6.1	MCT5+LAGO OIL DISPLACEMENT .....	90
6.2	DOW CORNING OIL DISPLACEMENT .....	106

6.3	MINERAL OIL DISPLACEMENT .....	113
6.4	BREAKTHROUGH RECOVERY VS. RECIPROCAL CAPILLARY NUMBER .....	126
6.5	EFFECT OF FLOW REGIME ON EFFECTIVE PERMEABILITY .....	128
7.	CONCLUSIONS AND RECOMMENDATIONS .....	132
7.1	CONCLUSIONS .....	132
7.2	RECOMMENDATIONS .....	135
8.	REFERENCES .....	140
9.	APPENDIX - A .....	150
10.	APPENDIX - B .....	153
11.	APPENDIX - C .....	154
12.	APPENDIX - D .....	163
13.	APPENDIX - E .....	172
14.	APPENDIX - F .....	181
15.	APPENDIX - G .....	187
16.	APPENDIX - H .....	196
17.	APPENDIX - I .....	199
18.	APPENDIX - J .....	200
19.	APPENDIX - K .....	222



## LIST OF TABLES

TABLE		PAGE
6.1	Characterstics and results of the MCT5+LAGO oil displacements	91
6.2	Values of dimensionless groups and recoveries for the runs conducted	92
6.3	Characterstics and results of the Dow-Coring oil displacement	107
6.4	Characterstics and results of the mineral oil displacements	115
H-1	Parameters of the capillary pressure curve fit	198
K-1	Parameters of the cumulative recovery curve fit	223
K-2	Parameters of the $\Delta P$ vs. time curve fit	224
K-3	Parameters of the cumulative recovery (at $\xi = 0.45$ and 0.66) curve fit	225

# LIST OF FIGURES

## FIGURE

## PAGE

4.1	Dielectric constants for dipolar liquid .....	48
4.2	Loss factors for some pure liquids .....	53
4.3	Loss factors for aqueous salt solutions.....	54
5.1	Experimental set-up.....	67
5.2	Automation system and interconnections.....	75
6.1	Capillary pressure curve fit for MCT5+LAGO...	93
6.2	Comparison between the JBN and the Dynamic method (Run 1).....	100
6.3	Comparison between the JBN and the Dynamic method (Run 2).....	101
6.4	Comparison between the JBN and the Dynamic method (Run 4).....	103
6.5	Comparison between the JBN and the Dynamic method (Run 5).....	104

6.6	Effective permeabilities at two different points (Run 5).....	105
6.7	Capillary pressure curve fit for Dow-Corning oil.....	109
6.8	Comparison between the JBN and the Dynamic method (Run 7).....	111
6.9	Effective permeabilities at two different points (Run 7).....	113
6.10	Comparison between the JBN and the Dynamic method (Run 8).....	118
6.11	Comparison between the JBN and the Dynamic method (Run 9).....	119
6.12	Comparison between the JBN and the Dynamic method (Run 10).....	120
6.13	Effective permeabilities at two different points (Run 8).....	122
6.14	Effective permeabilities at two different points (Run 9).....	123

6.15	Effective permeabilities at two different points (Run 10).....	124
6.16	Breakthrough recovery versus reciprocal capillary number.....	127
6.17	Effective permeabilities for different runs (Dynamic method).....	129
6.18	Effective permeabilities for stabilized and stable runs (Dynamic method) .....	131
A.1	Example of determination of effective permeabilities (Run 1).....	151
B.1	Some of the experimental saturation profiles (Run 1).....	154
B.2	Some of the experimental saturation profiles (Run 2).....	155
B.3	Some of the experimental saturation profiles (Run 4).....	156
B.4	Some of the experimental saturation profiles (Run 5).....	157

B.5	Some of the experimental saturation profiles (Run 7).....	158
-----	---	-----

B.6	Some of the experimental saturation profiles (Run 8).....	159
-----	---	-----

B.7	Some of the experimental saturation profiles (Run 9).....	160
-----	---	-----

B.8	Some of the experimental saturation profiles (Run 10).....	161
-----	--	-----

C.1	$\Delta P$ curve fit (Run 1).....	163
-----	-----------------------------------	-----

C.2	$\Delta P$ curve fit (Run 2).....	164
-----	-----------------------------------	-----

C.3	$\Delta P$ curve fit (Run 4).....	165
-----	-----------------------------------	-----

C.4	$\Delta P$ curve fit (Run 5).....	166
-----	-----------------------------------	-----

C.5	$\Delta P$ curve fit (Run 7).....	167
-----	-----------------------------------	-----

C.6	$\Delta P$ curve fit (Run 8).....	168
-----	-----------------------------------	-----

C.7	$\Delta P$ curve fit (Run 9).....	169
-----	-----------------------------------	-----

C.8	$\Delta P$ curve fit (Run 10).....	170
-----	------------------------------------	-----

D.1	Cumulative oil production curve fit (Run 1).....	172
D.2	Cumulative oil production curve fit (Run 2).....	173
D.3	Cumulative oil production curve (fit (Run 4).....	174
D.4	Cumulative oil production curve fit (Run 5).....	175
D.5	Cumulative oil production curve fit (Run 7).....	176
D.6	Cumulative oil production curve fit (Run 8).....	177
D.7	Cumulative oil production curve fit (Run 9).....	178
D.8	Cumulative oil production curve fit (Run 10).....	179
E.1	Cumulative oil production curve fit (at $\xi=.45$ ) (Run 5).....	181

E.2	Cumulative oil production curve fit (at $\xi=.45$ ) (Run 7).....	182
E.3	Cumulative oil production curve fit (at $\xi=.45$ ) (Run 8).....	183
E.4	Cumulative oil production curve fit (at $\xi=.45$ ) (Run 9).....	184
E.5	Cumulative oil production curve fit (at $\xi=.45$ ) (Run 10).....	185
F.1	Cumulative oil production curve fit (at $\xi=.66$ ) (Run 1).....	187
F.2	Cumulative oil production curve fit (at $\xi=.66$ ) (Run 2).....	188
F.3	Cumulative oil production curve fit (at $\xi=.66$ ) (Run 4).....	189
F.4	Cumulative oil production curve fit (at $\xi=.66$ ) (Run 5).....	190
F.5	Cumulative oil production curve fit (at $\xi=.66$ ) (Run 7).....	191

F.6	Cumulative oil production curve fit (at $\xi=.66$ ) (Run 8).....	192
F.7	Cumulative oil production curve fit (at $\xi=.66$ ) (Run 9).....	193
F.8	Cumulative oil production curve fit (at $\xi=.66$ ) (Run 10).....	194
G.1	Example of pressure profile curve fit.....	196



## NOMENCLATURE

$a_c$	Constant used in Eq. 4.52
$a_p$	Constant used in Eq. 5.9
$a_2$	Constant used in Eq. 5.6
$a_3$	Constant used in Eq. 5.7
$a_4$	Constant used in Eq. 5.8
$A$	Cross-sectional area of the core holder.
$A_c$	Area under the capillary pressure vs. saturation curve.
$A_{ls}$	Absorbance due to porous slab and core holder.
$A_{st}$	Total Absorbance of the Porous media and oil/water system.
$A_w$	Absorbance due to water, Eq. 5.1
$b_c$	Constant used in Eq. 4.52
$b_p$	Constant used in Eq. 5.9
$b_2$	Constant used in Eq. 5.6
$b_3$	Constant used in Eq. 5.7
$b_4$	Constant used in Eq. 5.8
$B_1$	Constant used in Eq. 5.2
$c$	Velocity of light.
$c_c$	Constant used in Eq. 4.52
$c_p$	Constant used in Eq. 5.9
$c_2$	Constant used in Eq. 5.6
$c_3$	Constant used in Eq. 5.7
$C$	Concentration
$d_c$	Constant used in Eq. 4.52

$d_2$	Constant used in Eq. 5.6
$d_3$	Constant used in Eq. 5.7
$D$	Instantaneous electric displacement, Eq. 4.39
$D_{max}$	Maximum instantaneous electric displacement
$e_c$	Constant used in Eq. 4.52
$e_2$	Constant used in Eq. 5.6
$E$	Instantaneous field strength, Eq. 4.39
$E_{max}$	Maximum instantaneous field strength
$f$	Frequency
$f_c$	Constant used in Eq. 4.52
$f_o$	Fractional flow of oil
$f_w$	Fractional flow of water
$g$	Gravitational acceleration
$h$	Thickness of the core
$i$	$\sqrt{-1}$
$I_r$	Relative Injectivity = $(q/\Delta P)/(q/\Delta P)_i$
$I_{sr}$	Instability number, Eq. 4.50
$I_x$	Attenuated microwave power
$I_o$	Incident microwave power
IOIP	Initial oil in place
$k$	Extinction coefficient per unit of concentration
$k_a$	Molar absorption coefficient
$k_{wa}$	Extinction coefficient of water
$K$	Absolute permeability
$K_e$	Effective Permeability
$K_o$	Effective Permeability to oil
$K_{or}$	Effective Permeability to oil at initial water saturation

$K_{ro}$	Relative Permeability to oil
$K_{rw}$	Relative Permeability to water
$K_w$	Effective Permeability to water
$K_{wr}$	Effective Permeability to water at irreducible oil saturation
$L$	Length of the core
$L_x$	Thickness of the core
$L_y$	Width of the core
$m$	Mass of the sand in core holder
$M_r$	End-point mobility ratio
$n$	Index of refraction
$n^*$	Complex index of refraction, Eq. 4.44
$N_{cl}$	Local Capillary number
$N_{cm}$	Macroscopic Capillary number
$N_g$	Gravity number
$N_p$	Cumulative oil production
$P$	Pressure
$P_b$	Base Pressure
$P_c$	Capillary Pressure
$P_d$	Displacement Pressure
$P_o$	Pressure in oil phase
$P_w$	Pressure in water phase
$q$	Volumetric total flow rate
$q_o$	Volumetric flow rate for oil
$q_w$	Volumetric flow rate for water
$Q_o$	Cumulative oil production
$Q_w$	Cumulative water production
$r_m$	Average macroscopic mean radius of curvature

$S$	Normalized saturation
$S_{nw}$	Non-wetting phase saturation
$S_o$	Oil saturation
$S_{or}$	Residual oil saturation
$S_w$	Water saturation
$S_{we}$	Wetting phase saturation
$S_{wi}$	Initial water saturation
$S_{wr}$	Residual water saturation
$S_{w2}$	Water saturation at the outlet end of the core
$t, T$	Time
$v$	Superficial velocity of the total flow
$v_{oz}$	Superficial velocity of oil phase along z-axis
$v_{wz}$	Superficial velocity of water phase along z-axis
$V$	Volume of the core holder
$V_{pr}$	velocity of propagation, Eq. 4.45
$W_i$	Cumulative water injection
$x, y, z$	Coordinate axes
$\alpha$	Angle between the positive z direction and the vertical taken in the downward direction
$\gamma$	Interfacial tension for oil/water system
$\delta$	Phase angle
$\Delta P$	Total Pressure drop across the core
$\epsilon$	Dielectric constant
$\epsilon'$	Real part of dielectric constant, Eq. 4.41
$\epsilon''$	Imaginary part (loss factor) of dielectric constant, Eq. 4.42
$\mu$	Viscosity
$\mu_o$	Oil viscosity

$\mu_w$	Water viscosity
$\xi$	Normalized distance, $x/L$
$\pi$	3.14159.....
$\rho$	Density
$\rho_g$	Grain density of Ottawa sand
$\rho_o$	Density of oil
$\rho_w$	Density of water
$\sigma$	Interfacial tension for oil/water system
$\sigma_e$	Effective interfacial tension for an oil/water/sand system
$\tau$	Dimensionless time
$\phi$	Porosity
$\Phi$	Potential
$\Phi_o$	Potential in the oil phase
$\Phi_w$	Potential in the water phase
$(\Phi_o)_w$	Potential of the oil phase in water phase
$(\Phi_w)_w$	Potential of the water phase in water phase

## 1. INTRODUCTION

Waterflooding is one of the most widely used techniques adopted to improve the recovery efficiency of oil fields. As each one percent increase in recovery efficiency adds about four billion barrels to the recoverable reserves, it is important to properly determine the fluid flow properties which pertain during the immiscible displacement of one fluid by another, such as occurs in waterflooding.

One of the most important properties needed to make a waterflood prediction is the water-oil relative permeability characteristics of the reservoir rock. Many techniques have been proposed to estimate effective permeabilities for water/oil systems. Unfortunately, none of the currently available techniques is applicable to a displacement which is not stable and stabilized. As most field displacements are believed to be unstable, any application of effective permeabilities measured in the laboratory with the aid of the conventional techniques is questionable.

In the past, the effects of the viscous and capillary forces have been studied using the viscosity ratio and interfacial tensions as individual parameters. However, no researchers have successfully studied the displacement process with the aid of different scaling groups, such as the instability number or the macroscopic capillary number, which really dictate the nature of the flow regime. Therefore, in determining the effect of viscous and

capillary forces, there has been a consistent lack of understanding the combined effect of the viscosity ratio and interfacial tension. As a matter of fact, an investigation in terms of the above scaling groups is of more value to field applications than is an individual investigation of the different parameters that affect the flow.

Moreover, no work has been done to understand how the effective permeability should behave under flow regimes which are unstabilized or unstable. Such work has not been undertaken primarily because a technique capable of measuring effective permeabilities under all flow conditions has not been successfully devised. As it is important to ensure that the flow regime in the laboratory is the same as that in the field, one has to develop a method capable of measuring effective permeabilities under all flow conditions. Only at this stage is it possible to investigate the impact of flow regime on effective permeability. Thus, it is the purpose of this study to develop a method capable of measuring effective permeability under all three flow regimes, namely, unstabilized, stable and stabilized, and unstable.

## 2. LITERATURE REVIEW

### 2.1 BASIC THEORY

#### 2.1.1 Basic Motion Equation

Since the early work of Darcy (1865), Darcy's law has been widely accepted for single phase flow through a porous medium. Even though Darcy's law seems to properly describe single phase flow through porous media, its extension to multiphase flow has been a controversial problem. There have been numerous attempts to describe and visualize the flow paths while two fluids are flowing simultaneously through a porous medium. Consequently, several theories as to how fluids distribute themselves during an immiscible displacement have been put forward. These theories are outlined in the following discussion.

##### 2.1.1.1 Channel Flow theory

It has been intuitively understood for a long time that the concept of permeability established for the flow of a single phase fluid through a porous medium may be applied to two-phase flow by modifying its value according to the relative amount of the fluid present at a given cross section of the porous medium. Consequently, one can visualize an experiment involving the simultaneous steady flow of two fluids (1 and 2) through a horizontal porous medium of constant cross section  $A$  and finite length  $L$ . Let constant rate pumps



discharge at rates  $Q_1$  for fluid 1 and  $Q_2$  for fluid 2 through the column. Also let two pairs of manometers give the pressure drops  $\Delta P_1$  for fluid 1 and  $\Delta P_2$  for fluid 2 at a distance  $L$  along the column. Once a steady flow has been established for both fluids, one may assume that the channel open to each fluid is invariant too. Thus, Darcy's law originally describing the flow of a single phase fluid completely saturating the porous medium can be extended to describe the flow of each of the two immiscible fluids flowing simultaneously through the column. Wyckoff and Botset (1936) used this concept first, and experimentally showed that the following equations hold.

$$q_1 = - \frac{K_1}{\mu_1} \frac{\Delta P_1}{L} \quad (2.1)$$

and,

$$q_2 = - \frac{K_2}{\mu_2} \frac{\Delta P_2}{L} \quad (2.2)$$

where  $q_1$  and  $q_2$  are the specific discharges ( $q_1=Q_1/A$ ); ( $q_2=Q_2/A$ ) and  $\mu_1$  and  $\mu_2$  are the dynamic viscosities of fluid 1 and 2, respectively. The parameters  $K_1$  and  $K_2$  are called the effective permeabilities for fluid 1 and 2, respectively. The effective permeabilities depend on the structure of the porous medium involved, especially on the absolute permeability,  $K$ , of the porous medium and the

respective saturations. For this reason, the ratios  $K_{r1} = K_1/K$  and  $K_{r2} = K_2/K$  are often used. They are called the relative permeabilities of fluid 1 and 2, respectively.

Ever since this simplified description by Wyckoff and Botset (1936), there has been substantial experimental evidence for the contention that (Chatenev r and Calhoun, 1952; Yadav et al., 1984) for two immiscible fluids flowing simultaneously through a porous medium, each fluid establishes its own tortuous path which usually forms a very stable channel. If the degree of saturation of one of the fluids is not extreme (near its residual value), there should be a direct relation between the channel area open to the flow of the fluid and the saturation of that fluid (de la Cruz and Spanos, 1983). That is to say, if one considers a wetting fluid ( $S_{we}$ ) and a nonwetting fluid ( $S_{nw}$ ), as  $S_{nw}$  is reduced, the cross-sectional area of channels of the nonwetting fluid tends to decrease until only isolated regions of it remain (i.e, residual non wetting fluid saturation). Similarly, as  $S_{we}$  is decreased, the channels of the wetting fluid tend to break down and become discontinuous (irreducible wetting fluid saturation). As a fluid becomes discontinuous, its flow can not take place under ordinary conditions (unless flow conditions or fluid properties are changed to mobilize the isolated ganglia) (de la Cruz and Spanos, 1983; Chatzis et al., 1984; Morrow et al., 1984).

### 2.1.1.2 Cylindrical Flow theory

Even though the concept, as depicted above, of each fluid establishing its own channel of flow through the porous medium is easy to manipulate and makes the flow description easy, it is questionable due to the fact that one of the fluids preferentially wets the solid and adheres to its surfaces with nonwetting fluid everywhere surrounded by wetting fluid. This second observation brings to mind, rather, a Poiseuille type of concentric flow in a tube (Yuster, 1951). Moreover, as wettability, in itself, is subject to hysteresis, it is clear that relative permeability is also affected by this phenomenon, i.e., it depends on how the two fluids are distributed within the pore space. Therefore, depending upon the equilibrium distribution of the two fluids within the pore space, there may be many possible pairs of values of relative permeability due to the many possible flow paths of the two fluids. This suggests that the relative permeability curves may depend on the manner in which the experiment is performed.

### 2.1.1.3 Structural Models

Apart from the simplified concept of channel or concentric flow of two phases through porous medium, porous media have also been represented by network models recognizing their complex structure. Such a model was first introduced by Fatt (1956a,b,c). Since the early work of Fatt structural models of the porous media have become a useful tool to understand flow

behaviour. As this approach avoids over-simplification of the porous media, there has been a lot of interest in this area for almost two decades. The model originally proposed by Fatt (1956a) was modified by Dodd and Kiel (1959) to allow entrapment of the wetting phase in calculating capillary pressure as a function of saturation during drainage of the wetting phase. Chatzis and Dullien (1977) extended the above model to three dimensions in computing the drainage capillary pressure. In 1982, Koplik and Lasseter used a structural model to describe unsteady-state flow. Lin and Slattery (1982) developed a structural model in the context of local volume-averaged equations of motion. However, this was meant to describe steady-state displacement only. The first attempt to describe unsteady-state flow in the context of local volume-averaged equations was taken by Alemán-Gómez et al. (1984). They recognized the unsteady-state displacement as being composed of a series of incremental increases in capillary pressure, the increases being greater than a threshold value required to displace the fluid residing in a pore. They distinguished between free (or forced) and restricted imbibition in a displacement process. The free or forced imbibition is attributed to the mechanism where the pressure drop over a capillary partially filled with the wetting phase reinforces the action of the interfacial tension forces. As a consequence, for free

or forced imbibition, all capillaries are invaded as soon as they are brought into contact with the wetting phase. On the other hand, they referred to restricted imbibition as that where the pressure drop over a capillary partially filled with the wetting phase acts counter to the interfacial tension forces. This classification permitted the determination of when a multiple flooded zone would develop in a displacement process; that is, multiple flooded zones would develop only during the restricted imbibition case. This observation recognizes, therefore, that during unstable displacements, a reversal of the sign of capillary pressure may occur which gives rise to the growth of viscous fingers of the displacing fluid. That is, in such a case the pressure would be higher in the wetting phase than in the non-wetting phase.

All the models described so far took into consideration the fact that both the fluids in a displacement process are continuous. However, in a displacement process, one may expect one fluid to be discontinuous (in the form of droplets) but still mobile whereas the other is continuous and mobile. In this case the conventional approach of volume averaging to describe two-phase flow cannot be taken. In this regard, de la Cruz and Spanos (1983) undertook a new approach to the use of local volume averaging to describe flow phenomena when one fluid is discontinuous but mobile. They pointed out that in order to find a

criterion for when trapped oil ganglia in a water wet porous media might be mobilized, an approach different from the conventional one is required. They questioned the application of Darcy's equation and the relative permeability concept when the system contains one continuous phase with mobilized droplets of the other phase, especially in the frontal region during immiscible displacement. In their derivation of the two-phase flow equations by using the volume averaging method (Whitaker, 1967; Slattery, 1967) they expressed the shear force term of the Navier-Stokes equation in powers of velocity and kept only the lowest order term. Thus, four different parameters were introduced in the flow equation describing each phase. However, this derivation has the advantage of describing the criterion for mobilization of oil droplets. It was shown that the magnitude of the difference between the two terms containing the capillary number and the pressure gradient of a given phase has to be greater than the magnitude of an integral of a term containing the interfacial curvature over the area common to the two phases. Even though a practical application of this criterion would require further theoretical and experimental investigation, this study may be termed a pioneer work in understanding the flow mechanism when only one of the two phases is continuous, but yet both phases are mobile.

### 2.1.2 Effect of Capillary and Viscous Forces

Since the early work of Leverett (1939), there have been numerous attempts to investigate the effect of both capillary and viscous forces on relative permeability. Analyzing the different displacement tests performed, there seems to be two types of displacements: macroscopic displacements, wherein the saturations change slowly, and incremental displacements wherein the saturations change quickly. Warren and Calhoun (1955), Paez et al. (1955) used unsteady-state, macroscopic displacements to show the dependence of relative permeability on interfacial tension. The same experiment, but with much more detail, was performed by Lefebvre du Prey (1973). He investigated the influence of capillary and viscous forces on liquid-liquid relative permeabilities in various consolidated porous media. He expressed the ratio of capillary to viscous forces in terms of a dimensionless group,  $N_{c1}$ , defined as

$$N_{c1} = \sigma / \mu v \quad (2.3)$$

This equation was derived using dimensional analysis. He showed that for a contact angle range of  $0^\circ$  to  $30^\circ$  and a viscosity ratio of 1, the relative permeabilities obtained were strongly affected by variations in  $N_{c1}$ . He found that the relative permeability, for certain saturations, decreases as the value of  $N_{c1}$  is increased. Physically, the effect of  $N_{c1}$  on relative permeability curves can be

understood by realizing that viscous forces in the absence of capillary forces would cause a uniform distribution of each phase in every capillary, in proportion to its saturation (Dullien, 1979). Therefore, in the complete absence of capillary forces the relative permeabilities would be represented by two symmetrical diagonal lines, intersecting at 50% saturation, as found by Bardon and Longeron (1980). At low values of the capillary forces (as compared to the viscous forces), viscous forces have a homogenizing effect which causes a uniform fluid distribution. This effect is more pronounced in the larger capillaries where the velocity is greater, while in the smaller capillaries the distribution of the different phases is still dictated by the capillary forces.

Since the capillary number as defined by Lefebvre du Prey was derived by dimensional analysis, it is capable of describing the fluid distribution only at the microscopic level. Hereafter such numbers will be referred to as local capillary numbers ( $N_{cl}$ ). However, it is more useful to obtain a capillary number capable of describing fluid distribution at the macroscopic level. Such a capillary number was derived by Bentsen (1976) using inspectional analysis and is given by

$$N_{cm} = \frac{A_c K_{wr}}{v L \mu_w} \quad (2.4)$$

Using this capillary number he showed (Bentsen, 1978)



theoretically that, if the capillary number,  $N_{cm}$  is less than 0.01, then the capillary term in the fractional flow equation may be neglected and the Buckley-Leverett solution may be accepted. This capillary number, being applicable at the macroscopic level, enabled him to postulate the range of values of  $N_{cm}$  over which the steady-state solution may be applied. Hereafter such numbers will be referred to as macroscopic capillary numbers ( $N_{cm}$ ).

Talash (1976) and Batycky and McCaffery (1978) used incremental displacements to show the dependence of relative permeability on interfacial tension. A detailed investigation of the effect of interfacial tension on relative permeability curves was also undertaken by Amaefule and Handy (1982). They found experimentally that relative permeability has a strong dependence on interfacial tension for values lower than  $10^{-1}$  N/m. However, they did not find any dependence at higher interfacial tension values. They found that the dependence at lower interfacial tension values was such that:

- (1) relative permeabilities increase with decreasing interfacial tensions at a given water saturation.
- (2) the curvature of the relative permeability curves decreases with decreasing interfacial tension, and at very low interfacial tension values, a linear relationship between relative permeabilities and saturation is obtained.
- (3) end point saturation values decrease with decreasing interfacial tension.

Another important observation was that a higher local capillary number (defined as  $v\mu/\gamma$ ) was required to mobilize the wetting phase than the nonwetting phase residual saturations.

In 1985, Fulcher et al. studied the effect of capillary number on two-phase relative permeability curves. They used the steady-state method to measure the relative permeabilities. They found that as the interfacial tension decreased below 5.5 N/m, the oil permeability increased and the water permeability decreased. However, the effect of interfacial tension was more pronounced on the oil permeability curves than on the water permeability curves.

Another factor affecting the relative permeabilities that has been studied and reported by many authors is the effect of the interference that one fluid exerts on the other within the pore space as a result of the difference in their viscosities. The fact that the sum of  $(K_w + K_o)$  is less than  $K$  suggests that the viscosity should have an effect on relative permeability curves.<sup>^</sup>

Osoba et al. (1951) investigated the influence of factors such as boundary effects, hysteresis, viscosity ratio and flow rate upon relative permeability by using five different methods of steady-state relative permeability measurement. They concluded that the viscosity ratio had no effect on the relative permeability. They also concluded that if the boundary effects were minimized, no effect of rate was observed on the measured relative permeabilities. They suggested that higher flow rates would minimize the

boundary effect.

Scott and Rose (1953) undertook a theoretical investigation of the effect of viscosity on relative permeability. They showed, by replacing portions of the fluid-fluid interface by a thin impervious wall, that there would be a corresponding decrease in relative permeability upon an increase of the viscosity ratio.

Paez et al. (1955) investigated the effect of interfacial tension and pressure gradient on oil recovery (in terms of residual oil saturation) and used  $\gamma/\Delta P$  as a correlating variable. They concluded that both the interfacial tension and the pressure differential had an influence on the total recovery and hence, on the relative permeability. A similar conclusion was reached by Warren and Calhoun (1955).

Sandberg et al. (1958) used radioactive tracers to measure the saturation during steady-state displacements conducted for the purpose of measuring relative permeability. They found that the relative permeability to water and oil was a unique function of saturation and independent of flow rate. They concluded, as did Osoba et al. (1951), that the viscosity ratio did not have any effect on the relative permeability curves, if the flow rate is high enough to minimize the boundary effects.

For the oil and water case Russel and Charles (1959) argued that the presence of a thin layer of water on the solid surfaces, analogous to a thin layer of water on the surface of a pipe, acts as a "lubricant", thus reducing the

resistance to flow. This phenomenon indicates that a transfer of viscous forces takes place across the fluid-fluid interfaces within the pore space.

Odeh (1959) measured relative permeabilities, using the steady-state method, to investigate the effect of viscosity ratio on the relative permeability curves. He concluded that the viscosity ratio did not have any effect on the wetting phase relative permeability. He observed that the viscosity ratio had no effect on the nonwetting phase relative permeabilities for samples with high absolute permeability. However, for low absolute permeabilities, the nonwetting phase relative permeability was found to increase with an increase of the viscosity ratio with a maximum increase at the lowest nonwetting phase saturation. This observation may be explained by the fact that a maximum capillary effect would arise at lower wetting phase saturations.

Rose (1960) took an interesting approach by considering the fact that one fluid passing over another contiguous immiscible fluid will always impart a motion to the second fluid. He considered a model where two phases, 1 and 2, are flowing while separated, in part, by a fluid-fluid interface, and, in part, by a thin impervious wall. With the aid of this model, he was able to show the magnitude of the "lubrication effect" and concluded that the volumetric throughput of a fluid partially filling a pore space is sometimes greater than its throughput when it completely fills the pore space. This condition of increased relative

permeability occurs when the saturation of the considered fluid approaches unity, as long as the contiguous fluid has a lower viscosity. He also showed the effect of the viscosity ratio on the relative permeability resulting from a nonzero velocity at the fluid-fluid interfaces.

Huppler (1970) stated that, with significant heterogeneities, waterflood results would be sensitive to flooding rates. He recommended that for cores with large lens structures, a better approximation may be obtained by performing waterfloods in both longitudinal and transverse directions and taking the average. To be noted here is that the heterogeneity may cause perturbations during high flow rates that would cause viscous fingering and thus could cause unstable displacement.

In 1973, Lefebvre du Prey used macroscopic displacement tests to investigate the effect of viscosity and flow rate on relative permeability. He concluded that both viscosity ratio and flow rate affect relative permeability data.

In 1975, Brandner and Slotboom investigated the difficulties in oilflooding heterogeneous cores. They used an upward waterflood followed by a downward oilflood over a range of different velocities. They found that if the sample length is less than the height of capillary rise, while vertically flooding a heterogeneous core with nonwetting phase, the fluids would be unable to maintain a proper distribution and, as a consequence, the displacement results may be chaotic.

In 1985, Fulcher et al., while investigating the effect of capillary number, also investigated the effect of flow rate on two-phase relative permeabilities. By using the steady-state method for measuring relative permeabilities, they found no flow rate dependence of the relative permeability.

In brief, it is clear that there are a large number of experimental observations which contradict one another. Rose (1979) contended that none of the researchers have conclusively demonstrated the dependence or non-dependence of relative permeability on the capillary and viscous forces. In order to make a definitive remark on the above-mentioned theoretical and experimental observations, one may refer to the conclusions of Handy and Datta (1966). They demonstrated that for consolidated porous media the relative permeabilities depend on whether the method uses incremental displacements leading to small changes in saturations or macroscopic displacements resulting in larger saturation changes. Slattery (1974) discussed this same observation and demonstrated that an incremental displacement would normally be a restricted imbibition displacement, which would result in the nonwetting phase being trapped in the larger pores, whereas macroscopic displacements of the nonwetting phase would be free or forced imbibition displacements, which result in it being trapped in the smaller pores. A discussion was carried out along similar lines by Lin and Slattery (1982) who argued that the fraction of the displaced phase trapped and

stranded depends on the ratio of the viscosity of the displacing phase to that of the displaced phase and upon the magnitude of the pressure gradient. Therefore, the relative permeabilities measured using macroscopic displacements exhibit dependence on both the viscosity ratio and the magnitude of the pressure gradient. However, such a dependence is not expected from relative permeabilities measured by the steady-state method, as they are carried out under so slow saturation changes that the effects of the viscous forces and of the magnitude of the pressure gradient upon the saturation history can be neglected with respect to those of the interfacial forces. Alemán-Gómez et al.

(1984) used this argument to justify, in retrospect, why researchers (Warren and Calhoun, 1955; Paez et al., 1955; Lefebvre du Prey, 1973), using macroscopic displacements, found that relative permeability depended on the pressure gradient and the viscosity ratio, whereas others (Osoba et al., 1951; Sandberg et al., 1958), using incremental displacements, concluded that the viscosity ratio or the pressure gradient did not have any effect on the relative permeabilities. This comment is also valid for the recent study of Fulcher et al. (1985), who found no dependence of relative permeability on flow rates by using steady-state method.

## 2.2 LABORATORY DETERMINATION OF RELATIVE PERMEABILITY

The methods available for the measurement of relative permeabilities can be divided into two broad categories: steady-state and unsteady-state techniques.

### 2.2.1 Steady-State Flow Method

Typically, in the steady-state method, two different fluids are injected simultaneously at fixed and known flow rates. When inflow equals outflow and/or the pressure drop across the core reaches a constant value, steady-state is assumed to be attained. It should be noted that the attainment of steady-state flow may take a long time, depending on the method used. Once steady-state is reached, if the flow rate for each phase is known along with the pressure drop across the core, one may use Darcy's law for each phase and thus obtain relative permeability values for each phase at that particular saturation. The saturation, in turn, may be determined by different methods, e.g., direct weighing, X-ray absorption, electric resistivity measurement, or the use of a volumetric balance on the fluids passing through the cores. Within this overall description of the method, a large number of different techniques have been reported. These techniques differ from one another in the manner in which the boundary or end effect is minimized and in the manner in which the two fluids are introduced into the core. Scheidegger (1974) has discussed in detail the relative merits of each method.



The steady-state method uses the fewest assumptions in determining the relative permeability curves. Consequently, it has become general practice to use this method as the standard against which all other techniques are compared.

However, this method is time consuming and may take over a week, depending on the technique used, to establish steady state. Apart from being time consuming, steady-state methods may not be applicable to systems where saturations change with time and show spatial gradients (Rose, 1968). Unfortunately, in most field situations the displacement is dynamic and thus the application of steady-state relative permeabilities to describe unsteady-state flow behaviour is questionable from the conceptual point of view. In this regard, it should be noted that many researchers have found disagreement between unsteady-state and steady-state relative permeabilities (Kimbler and Caudle, 1957; Schneider and Owens, 1970; Archer and Wong, 1973). This confusion as to what extent steady-state relative permeabilities are applicable to a system where, truly speaking, only unsteady-state displacement is taking place was not resolved until the recent study by Alemán-Gomez et al. (1984). With the aid of their structural model derived by volume averaging of the flow equations, they demonstrated that there should be a considerable difference between steady-state and unsteady-state relative permeabilities if the local capillary number is large. As a consequence, as the local capillary number would be the largest in the immediate vicinity of the displacement front, even if the

interfacial tension is very small or the pressure gradient is very large, one should employ only the unsteady-state relative permeabilities in the immediate vicinity of the displacement front. They also commented that, if a discrepancy between steady-state and unsteady-state relative permeabilities were not observed by a certain experiment, it was most probably because of the fact that the unsteady-state method was not capable of measuring truly unsteady-state relative permeabilities.

### 2.2.2 Unsteady-State Flow Method

This method is often called the external drive method. It involves displacing one phase by another and calculating the relative permeability from the produced fluid ratios.

Welge (1952) used the Buckley-Leverett (1942) frontal advance equation to develop a method to compute the average saturation and hence the oil recovery. His aim was actually to find out fluid recovery once the relative permeability curves were available. In other words, if the fractional recovery of one fluid phase is known, the ratio of relative permeabilities might be obtained from the above mentioned method. Johnson et al. (1959) extended the pioneer work of Welge to permit calculation of the individual relative permeabilities. This method has the advantage of being very fast as it takes only a few hours to obtain the same information as that of the steady-state method.

A great deal of work has been done to check if the unsteady-state method can reproduce the results of the

steady-state methods. Most of the results seem to confirm that the unsteady-state method gives the same results as the steady-state techniques. However, as already discussed, some of the experiments are found to be exceptions to the above observation (Owens et al., 1965; Schneider and Owens, 1970; Archer and Wong, 1973).

The external drive method is based on the assumption that Buckley-Leverett (1942) theory is valid. This requires that the displacements used for measuring relative permeability curves be stabilized and one dimensional (pressure and saturation uniform in any cross section). Moreover, a Lagrangian formulation of the fluid displacement problem must be permissible. These limitations eliminate the possibility of applying the external drive method to displacement processes where the flow is either unstabilized or unstable, or where the experimental saturation profiles are not monotonic (Bentsen and Saeedi, 1981).

The only experimental method proposed so far to determine unsteady-state relative permeabilities is that of Johnson-Bossler-Naumann (JBN). Unfortunately, this technique estimates the relative permeabilities at saturations corresponding to those pertaining at the outlet face of a one dimensional flow system and, as Alemán-Gomez et al. (1984) have pointed out, the displacement front coincides with the outlet face only at one point in time. Alemán-Gomez et al. (1984) have also shown that the relative permeabilities measured by the JBN method correspond to small values of the local capillary number and

thus are indistinguishable from those measured by the steady-state flow method, unless the core is subjected to an unusually large pressure gradient. Unfortunately, such a large pressure gradient might cause instability in the system and a Lagrangian formulation would not be possible; hence, the JBN method can no longer be applied. Rose (1979) compared the application of the Buckley-Leverett equation to a situation where viscous fingering prevails to applying Navier-Stokes equations to turbulent flow. This makes the application of the JBN method to measure unsteady-state relative permeability questionable.

Archer and Wong (1973) reported that, as the JBN method uses the water breakthrough as an important factor, the calculated relative permeabilities will not represent the properties of the bulk of the core sample and anomalous relative permeabilities would result, if the breakthrough time observed is somewhat earlier than that of the actual main front. Anomalous relative permeability curves were also observed for cores with intermediate wettability. This same observation was reconfirmed by Sigmund and McCaffery (1979).

### 2.2.3 Improved Unsteady-State Flow Method

In order to avoid having strangely shaped relative permeability curves, Archer and Wong (1973) proposed the use of a reservoir simulator to obtain relative permeability curves from a laboratory experiment. This approach has also been used, in a modified form, by Sigmund and McCaffery

(1979). This method eliminates the possibility of having strangely shaped relative permeability curves as obtained from the JBN method. The numerical reservoir simulator is used to match the production data, using a history matching technique. It involves assuming a set of relative permeability curves (that might be the ones originally calculated by the JBN method) and matching the observed production and pressure data with that generated by solution of the finite difference approximations to the Buckley-Leverett equations. The new set of relative permeabilities are such that the difference between the observed and calculated production and pressure data is minimized.

Unfortunately, history matching is not necessarily unique. Therefore, the fact that the shape of the relative permeability curves is reasonable would not necessarily confirm that the new set of relative permeabilities obtained with the aid of a reservoir simulator truly represents the flow phenomena. Furthermore, this method will give results different from those of the JBN method only in cases of intermediate wettability or heterogeneous formations. Hence, all the shortcomings of the JBN method would also be applicable to this method, except in a few cases where having strangely shaped relative permeability curves may be avoided by this method.

#### 2.2.4 Dynamic Method

As has already been pointed out, the theory, upon which the external drive methods for measuring unsteady-state relative permeability is based, requires that the flow velocity be constant at all the cross sections of the linear porous body. Therefore, there is a need to develop a new technique to measure the relative permeabilities in a truly dynamic system under all flow conditions. In this context, Rose (1968) argued that the only valid way of dealing with the displacement process would be to observe saturations simultaneously and continuously as a function of time and space. Then, he suggested that the so-called dynamic relative permeability functions (of saturation) be deduced by solving the Buckley-Leverett equation along with the capillary function (of saturation) simultaneously. But, once again, as the Buckley-Leverett equation is not applicable for situations where viscous fingers occur (unstable displacement), or where the capillary forces are dominant over viscous forces, the only option left is to use directly the differential form of Darcy's equation in two-phase flow by using an averaged form of the fractional flow curve as determined from the saturation profiles. This exploitation of the saturation profiles would, therefore, allow one to obtain relative permeability data with the most reliable theoretical basis. In brief, this method will require the saturation profiles together with the pressure profile along the length of the core.

## 2.3 SATURATION MEASUREMENT TECHNIQUES

The ability to measure the saturation contained in an elemental volume is not a recent innovation. Since the early work of Wyckoff and Botset (1936) many methods for measuring in-situ or global saturation in a sample core have been proposed. Among these, the following methods have gained popularity in different periods of time.

### 2.3.1 Resistivity Technique

This technique was first used for measuring the oil/water saturation of a porous sample by Wyckoff and Botset (1936). They utilized the difference in brine and hydrocarbon resistivity to determine the saturation at various flow conditions. This technique involves developing a conductivity saturation curve for each system. The use of brine instead of pure water is necessary to render the water conductive. Leverett (1939) used the same technique to study the effect of flow rate and viscosity on the relative permeability curves. Levine (1954) used the resistivity technique to measure the saturation distribution and velocity of each of the two flowing phases. The resistivity technique was also used by Perkins (1957) who used a constant viscosity ratio in order to measure saturation profiles at high and low flow rates. Bail and Marsden (1957) used the same technique to measure the saturation profiles during the displacement of oil by brine in a system where a residual brine saturation was initially present.

This is one of the oldest methods used for determining in-situ saturations in a porous sample. This method requires that the distilled water be replaced by brine, but no foreign material has to be added to the water-oil system. However, the major problem with this technique is that the saturations estimated by this method are a kind of integrated average between two fixed points (containing electrodes). Increasing the number of electrodes would cause interference between adjacent electrodes and the estimated saturation values will not represent truly local saturations, and still a continuous saturation profile would remain beyond question. Moreover, this technique is cumbersome to use.

### 2.3.2 Optical Methods

Problems associated with the resistivity technique called for a more advanced technique. The optical method is one such method. One of the first applications of optical methods to measure the saturation profile was undertaken by Steber and Marsden (1956). They suggested a method based on matched refractive indices.

Hagoort (1974), with a view to studying the displacement stability of the water-drive process, measured saturation profiles in a water-wet connate water bearing reservoir model. He used a transparent flow model with matched refractive indices of fluids and porous material, thus enabling a photometric measurement of local fluid saturations. This photometric method involved making use of



the transparency of the model and the light absorption properties of the fluids. This required an addition of 1% (by weight) cobalt-chloride to the water phase to colour it blue. As the oil phase showed no absorption, it was possible to find the water saturation along the length of the core. He used different flow rates to study the stability of the displacement process but did not report any saturation profiles for the situations when the displacement was believed to be unstable.

This method overcomes the problem of having estimated saturations only at discrete points, as in the resistivity technique, and successfully generates continuous saturation profiles along the length of the core. However, this method involves doping one of the fluids with a foreign substance and, therefore, the fluid characteristics might be changed. Moreover, the reported saturation profiles as calculated by this technique are not of high quality.

### 2.3.3 X-ray Absorption Method

This method calls for using the X-ray absorption property of aqueous solutions. Morgan et al. (1950) were among the first to use the X-ray absorption method to measure the saturation profile along the length of a core. The method involves measuring continuously the intensities of the signals from an X-ray tube at the input and of the beam after it has passed through the core under test. As the intensity of the X-ray beam that is transmitted by the core is related to the saturation of the aqueous solution,

by knowing the output intensity one can calculate the saturation of the aqueous phase. This technique was used later on by Lipson (1951) who showed that the saturations, as measured by X-ray absorption method, are not single-valued and show some hysteresis effects. Geffen and Gladfelter (1952) used this same technique and showed that for all cases the X-ray method gives single valued saturations and no hysteresis was observed.

This method gives results clearly superior to those of resistivity or optical methods but still the saturation data are not accurate enough to give quantitative estimations of the saturation (Morgan et al., 1950), as the reproduction of the relative permeability was not possible with the saturations estimated by this method. This method involves using X-rays that, in themselves, are not safe to use. Moreover, for X-rays to be effective, the water has to be doped with Sodium Iodide or Iodo-Benzene has to be added to the liquid hydrocarbons.

#### 2.3.4 Microwave Attenuation Technique

Because of the unreliability of the data, and because of the need to add foreign material to the fluids, there was a need to develop a method for measuring saturations which did not suffer these defects. The microwave attenuation technique overcomes these difficulties and generates a continuous saturation profile along the length of the core. Parsons (1975) was the first researcher to report having used the selective absorption of electromagnetic radiation.

He chose microwaves at a fixed frequency of 21.2 GHz at which frequency the microwaves are strongly absorbed by water, and negligibly by the hydrocarbons used for the displacement tests. He presented saturation profiles that were superior in quality to any previously published. These saturation profiles were very similar to those one would expect from a Buckley-Leverett type displacement. Once the superiority of this method was recognized, other studies reporting the use of the microwave attenuation technique appeared in the literature. Parsons and Jones (1977) used this technique to measure saturation profiles in micellar flooding in order to develop the concept of linear scaling.

So far, none of these studies reported a comparison of measured saturation profiles with those obtained theoretically (by solving the continuity and flow equations including the capillary term). Bentsen and Saeedi (1981) reported the use of the microwave attenuation technique to measure a series of saturation profiles with different viscosity ratios ( $\mu_o/\mu_w$ ) ranging from 1.22 to 73.33. They considered flow rate as a parameter too, and for the first time, they compared the experimental saturation profiles with the theoretical ones. The agreement between the two was quite good. Most importantly, they also reported that at very high flow rates, when the viscous forces are completely dominant, and at very slow flow rates, when the capillary forces are completely dominant, the saturation profiles deviate considerably from standard Buckley-Leverett profiles. They also showed some saturation profiles at flow

rates believed to be unstable according to a criterion obtained later on by Bentsen (1985a). While they successfully demonstrated the difference between saturation profiles obtained during unstabilized, stabilized and stable, and unstable displacements, the data acquisition technique not being automated, they could not use the saturation profiles for any further analysis, e.g., calculating fractional flow at any point. As a consequence, they could not explain in terms of relative permeability why differences in saturation profiles should arise in different flow regimes. Moreover, one of the major difficulties of this study was that the saturation profile was unmeasurable for a water saturation above 60%, primarily because the input power of the microwave was limited to only 6mw and the thickness of the core was relatively high.

### 3. STATEMENT OF THE PROBLEM

As the literature review in the previous chapter revealed, there is not a single technique that is capable of estimating the effective water and oil permeabilities during unstable or unstabilized displacement. In past years, there has been much effort spent on investigating the impact of viscosity, flow rate and interfacial tension separately.

Unfortunately, none of these factors form any scaling group alone that would govern the flow regime in a displacement test. Therefore, there has been a consistent lack of understanding of how effective permeabilities would vary with the variation of capillary or viscous forces. It is, therefore, of interest to investigate the effect of flow regime as dictated by the instability number or capillary number.

As all the currently available techniques for measuring effective permeabilities are applicable only in steady-state or stable and stabilized displacements, a new technique capable of measuring effective permeabilities during unstable or unstabilized displacement needs to be devised.

The present study attempts to devise such a method and thereby investigate the impact of different flow regimes on the effective permeabilities. Special attention is focused on the effective permeabilities during unstable displacement, as most of the field displacements are believed to be unstable and, in order to apply the effective

permeabilities to the field calculations, one should have a better understanding of the nature of the effective permeability curves when the displacement is unstable.

## 4. THEORY

### 4.1 IMMISCIBLE DISPLACEMENT THEORY

#### 4.1.1 Basic Motion Equation

If  $\alpha$  is the angle measured between the positive  $z$  direction (the direction of flow) and the vertical taken in the downward direction, then the force potential may be written as (Hubbert, 1956; Bentsen, 1985a):

$$\Phi = -gz\cos\alpha + \int_{P_b}^{P+P_c} \frac{dP}{\rho} \quad (4.1)$$

If one is measuring pressures in the water, then it is necessary to assume that the fluids are being injected on the water side of the interface. For this case,

$$(\Phi_w)_w = -gz\cos\alpha + \int_{P_b}^{P_w} \frac{dP}{\rho_w} \quad (4.2)$$

If it can be assumed that  $\rho_w$  is independent of pressure, then

$$(\Phi_w)_w = -gz\cos\alpha + \frac{P_w - P_b}{\rho_w} \quad (4.3)$$

If the porous media is water wet, then

$$P_c = P_o - P_w \quad (4.4)$$

Hence,

$$(\Phi_o)_w = -gz \cos \alpha + \int_{P_o=P_b}^{P_o=P_w+P_c} \frac{dP}{\rho_o} \quad (4.5)$$

$$= -gz \cos \alpha + \int_{P_o=P_b}^{P_o=P_w} \frac{dP}{\rho_o} + \int_{P_o=P_w}^{P_o=P_w+P_c} \frac{dP}{\rho_o} \quad (4.6)$$

If  $\rho_o = \text{constant}$ ,

$$(\Phi_o)_w = -gz \cos \alpha + \frac{P_w - P_b}{\rho_o} + \frac{P_c}{\rho_o} \quad (4.7)$$

Writing Darcy's law for the water phase,

$$v_{wz} = - \frac{K_w \rho_w}{\mu_w} \frac{\partial (\Phi_w)_w}{\partial z} \quad (4.8)$$



$$= - \frac{K_w \rho_w}{\mu_w} \left[ -g \cos \alpha + \frac{1}{\rho_w} \frac{\partial P_w}{\partial z} \right] \quad (4.9)$$

$$= - \frac{K_w}{\mu_w} \left[ -g \rho_w \cos \alpha + \frac{\partial P_w}{\partial z} \right] \quad (4.10)$$

As,

$$q_w = v_{wz} \cdot A = f_w \cdot q \quad (4.11)$$

one obtains,

$$f_w = - \frac{K_w A}{\mu_w q} \left[ \frac{\partial P_w}{\partial z} - g \rho_w \cos \alpha \right] \quad (4.12)$$

or,

$$K_w = - \frac{\mu_w f_w}{\frac{\partial P_w}{\partial z} - g \rho_w \cos \alpha} \cdot q/A \quad (4.13)$$

Similarly,

$$v_{oz} = - \frac{K_o \rho_o}{\mu_o} \frac{\partial (\Phi_o)}{\partial z} \quad (4.14)$$

$$= - \frac{K_o \rho_o}{\mu_o} \left[ -g \cos \alpha + \frac{1}{\rho_o} \frac{\partial P_w}{\partial z} + \frac{1}{\rho_o} \frac{\partial P_c}{\partial z} \right] \quad (4.15)$$

$$= - \frac{K_o}{\mu_o} \left[ -g \rho_o \cos \alpha + \frac{\partial P_w}{\partial z} + \frac{\partial P_c}{\partial z} \right] \quad (4.16)$$

As,

$$q_o = v_{oz} \cdot A = q \cdot f_o \quad (4.17)$$

one obtains,

$$f_o = - \frac{K_o A}{\mu_o q} \left[ \frac{\partial P_w}{\partial z} - g \rho_o \cos \alpha + \frac{\partial P_c}{\partial z} \right] \quad (4.18)$$

Taking  $P_c$  as function of saturation alone,

$$\frac{\partial P_c}{\partial z} = \frac{dP_c}{dS_w} \frac{\partial S_w}{\partial z} \quad (4.19)$$

Therefore, one obtains,

$$f_o = - \frac{K_o A}{\mu_o q} \left[ \frac{\partial P_w}{\partial z} - g \rho_o \cos \alpha + \frac{dP_c}{dS_w} \frac{\partial S_w}{\partial z} \right] \quad (4.20)$$

$$K_o = - \frac{\mu_o f_o}{\frac{\partial P_w}{\partial z} - \rho_o g \cos \alpha + \frac{dP_c}{dS_w} \frac{\partial S_w}{\partial z}} \cdot q/A \quad (4.21)$$

For saturations greater than the floodfront saturation,  $\partial S_w / \partial z$  is small. Moreover,  $dP_c / dS_w$  will also be small. As a consequence, the product  $(dP_c / dS_w)(\partial S_w / \partial z)$  may be neglected, provided this condition is met.

#### 4.1.2 Fractional Flow Equation

One of the major difficulties associated with experimentally determining the relative permeability curves is that it is extremely difficult to measure directly the fraction of a particular phase which is flowing at a given cross section of the core. However, this difficulty can be eased if a saturation profile along the length of the core is available. In this respect, two approaches can be taken: the Lagrangian approach and the Eulerian approach.

If the Lagrangian approach is taken, one starts with the Lagrangian form of the continuity equation (Bentsen, 1976), i.e.,

$$\frac{\partial \xi(S, \tau)}{\partial \tau} = \frac{\partial f_w(S, \tau)}{\partial S} \quad (4.22)$$

By integrating Equation 4.22 for a specific saturation,

$$\xi(S, \tau) dS = \int_0^{\tau} \frac{\partial f_w}{\partial S} d\tau dS \quad (4.23)$$

or,

$$\int_0^{S^*} \xi(S, \tau) dS = \int_0^{S^*} \int_0^{\tau} \frac{\partial f_w}{\partial S} d\tau dS \quad (4.24)$$

At this point if  $(\partial f_w / \partial S)$  is well behaved, the order of integration may be changed and one obtains,

$$\int_0^{S^*} \xi(S, \tau) dS = \int_0^{\tau} \int_0^{S^*} \frac{\partial f_w}{\partial S} dS d\tau \quad (4.25)$$

$$= \int_0^{\tau} [ f_w(S^*, \tau) - f_w(0, \tau) ] d\tau \quad (4.26)$$

As  $f_w(0, \tau) = 0$ , it follows that

$$\int_0^{S^*} \xi(S, \tau) dS = \int_0^{\tau} f_w(S^*, \tau) d\tau \equiv Q_w(S^*, \tau) \quad (4.27)$$

Thus  $Q_w(S^*, \tau)$  may be obtained by integrating the area under

the saturation profile at a specific time, the integral being evaluated between 0 and  $S^*$ . If  $Q_w(S^*, \tau)$  is evaluated at a number of different times, it becomes possible to plot  $Q_w(S^*, \tau)$  versus  $\tau$ . If such data is curve fitted, then  $f_w(S^*, \tau)$  may be estimated by differentiating with respect to  $\tau$ , the model equation used to fit  $Q_w(S^*, \tau)$ .

When applying this approach, the pressure has to be known at many points along the length of the core. Unfortunately, the pressures were known only at seven points along the length of the core and a curve fit of these points to obtain a continuous profile did not give satisfactory results when slopes were calculated from the curve fit. As a consequence a different approach, namely the Eulerian approach, was taken. This approach requires the slope of the pressure profile at local points only and such a slope could be estimated by using linear interpolation between two adjacent known pressures. For this approach, one has to start from the Eulerian form of the continuity equation (Bentsen, 1976), i.e.,

$$\frac{\partial f_w}{\partial \xi}(\xi, \tau) = - \frac{\partial S}{\partial \tau}(\xi, \tau) \quad (4.28)$$

By integrating this equation at some specific point in time, say  $\tau^*$ , one may obtain a relationship between the fraction flowing at a particular location in the core, say  $\xi^*$ , and the area under the saturation profile between  $\xi=0$  and  $\xi=\xi^*$  as follows.

For some specific time, say,  $\tau^*$ ,

$$df_w = \frac{\partial f_w}{\partial \xi} d\xi + \frac{\partial f_w}{\partial \tau} d\tau \quad (4.29)$$

$$= \frac{\partial f_w}{\partial \xi} d\xi \quad (4.30)$$

As  $\tau$  has been assumed constant at  $\tau = \tau^*$ , one has

$$\frac{\partial f_w}{\partial \xi} = \frac{df_w}{d\xi} \quad (4.31)$$

Using 4.28 and 4.29 one obtains,

$$df_w(\xi, \tau^*) = - \frac{\partial S}{\partial \tau}(\xi, \tau^*) d\xi \quad (4.32)$$

or,

$$\int_0^{\xi^*} df_w = - \int_0^{\xi^*} \frac{\partial S}{\partial \tau} d\xi \quad (4.33)$$

If  $S(\xi, \tau^*)$  is continuous then the order of integration and differentiation may be interchanged, i.e.,

$$f_w(\xi^*, \tau^*) - f_w(0, \tau^*) = - \frac{\partial}{\partial \tau} \int_0^{\xi^*} S(\xi, \tau^*) d\xi \quad (4.34)$$

In as much as  $f_w(0, \tau^*) = 1$ , it follows that

$$f_w(\xi^*, \tau^*) - 1 = - \frac{\partial}{\partial \tau} \int_0^{\xi^*} S(\xi, \tau^*) d\xi \quad (4.35)$$

or,

$$f_o(\xi^*, \tau^*) = \frac{\partial}{\partial \tau} \int_0^{\xi^*} S(\xi, \tau^*) d\xi \quad (4.36)$$

Integrating both sides,

$$\int_0^{\tau^*} f_o(\xi^*, \tau) d\tau = \int_0^{\xi^*} S(\xi, \tau^*) d\xi \quad (4.37)$$

or,

$$\int_0^{\tau^*} f_o(\xi^*, \tau) d\tau = Q_o(\xi^*, \tau^*) = \int_0^{\xi^*} S(\xi, \tau^*) d\xi \quad (4.38)$$

Thus  $Q_o(\xi^*, \tau^*)$  may be obtained by integrating the area under the saturation profile at a specific time, the integral being taken up to the same point in space every time. Once  $Q_o(\xi^*, \tau^*)$  is obtained as a function of time for a given point, a curve of cumulative oil production is obtained as a function of time. By taking the slope of this curve, one may obtain the  $f_o(\xi^*, \tau^*)$  value at any particular time.

This approach has some practical problems such as taking slopes of experimental data. However, this problem may be resolved by curve fitting the recovery data. As this approach does not need a continuous pressure profile, it was used for the present study.

An example of the calculation of the effective permeabilities is discussed in the Appendix A.



## 4.2 MICROWAVE THEORY

Electromagnetic radiation is called microwave radiation when the frequency ranges from  $4 \cdot 10^8$  Hz to  $4 \cdot 10^{11}$  Hz.

Understanding the laws governing microwave behaviour of any material is important in using this technique for measuring saturation profiles. If materials are classified in terms of interactions with microwaves, one would have the following basic types of materials:

- (1) Conductors
- (2) Insulators
- (3) Dielectrics

Conductors are those materials that reflect microwaves; thus, they may be used to contain and guide the microwaves. Insulators are those materials that transmit microwaves without any appreciable loss of power; i.e., microwaves can travel across them without losing their strength.

Dielectrics are those materials that absorb microwaves; i.e., once they are exposed to the path of microwaves only a small part of them can cross the material. However not all dielectrics absorb microwaves in the same proportion, and in order to predict the absorption, one may describe them in terms of either dielectric or optical phenomena. However, as the materials being dealt with are non-magnetic, this discussion will be limited to the electric field-medium interactions.

#### 4.2.1 Dielectric Properties

When a material is placed in a static electric field, a redistribution of electric charges in the field occurs. This polarization, partial or total, may be caused by several simultaneous effects:

- (1) The relative displacement of the negative electron cloud and the positive nucleus.
- (2) Displacement of atoms or ions.
- (3) Alignment with the field by molecules with permanent dipoles.
- (4) An interfacial phenomenon in emulsions.

Once polarization occurs, if the external field is removed, the polarization effect would return to its normal state. However, the time required to return to the normal state, often called the relaxation time, may be very short or very long depending on the nature of the electric field involved. For instance, relaxation time would be very short for small displacements and high electron mobility. However, molecular dipole relaxation times would be relatively longer because of the separation of charges and the local retardation of molecular reorientation.

Now, if the electric field is alternating, i.e., the external field is applied and removed alternately with a certain frequency, the electric charges would be set into alternating polarization and relaxation. As is known, an electromagnetic radiation is an alternating field, and thus, would set the electron field into oscillation. However, the frequency of the electron field that is put in oscillation

and that of the electromagnetic wave may not match and may differ by some phase angle,  $\delta$ . Therefore, at any time, instantaneous field strength and electric displacement may be defined by:

$$E = E_{\max} \cdot \cos 2\pi f t \quad (4.39)$$

and,

$$D = D_{\max} \cdot \cos(2\pi f t - \delta) \quad (4.40)$$

The displacement and the electric field strength would be in phase if  $\delta=0$ . In order to compare the displacement with the electric field strength the concept of dielectric constant is introduced. Dielectric constant is defined by  $\epsilon = D/E$  when  $\delta=0$ . However, when  $\delta \neq 0$ , i.e., when the  $D$  and  $E$  vectors are not colinear, the dielectric constant is considered in two parts. The first part

$$\epsilon' = \frac{D_{\max} \cos \delta}{E_{\max}} \quad (4.41)$$

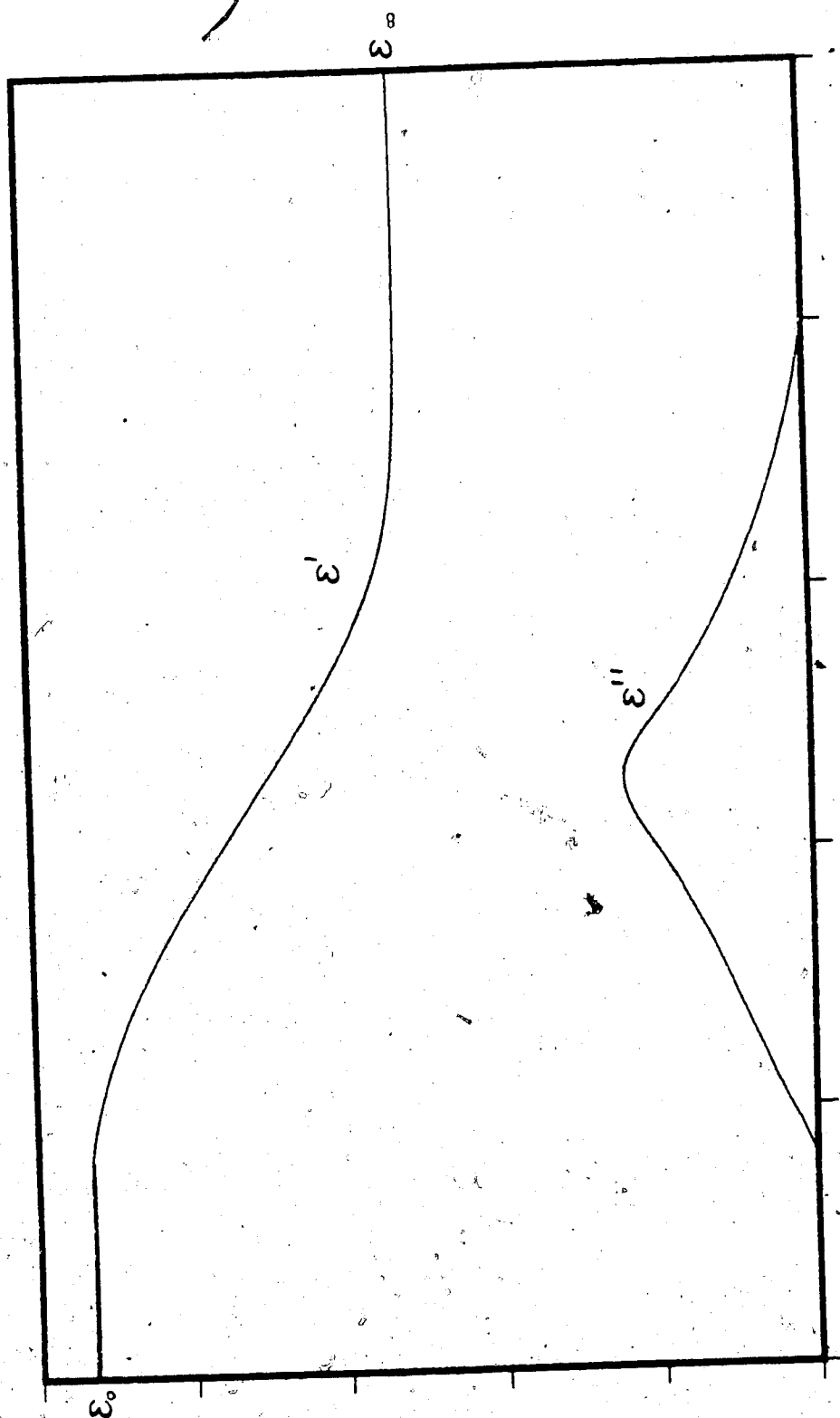
represents the normal dielectric constant, or the proportionality constant, between  $E_{\max}$  and the component of  $D_{\max}$  that is in phase with the field. The other part,

$$\epsilon'' = \frac{D_{\max} \sin \delta}{E_{\max}} \quad (4.42)$$

represents the loss factor, which is essentially the ratio of the  $90^\circ$  out of phase part of  $D_{\max}$  to  $E_{\max}$ . As one can see, these two terms,  $\epsilon'$  and  $\epsilon''$ , may be considered as real and imaginary parts of the dielectric constant. These constants may be measured experimentally and are functions of the material, the environment, and the field frequency.

As a moving or oscillating charge is an electric current, if the dielectric molecules behave like a perfect capacitor, the displacement current would always follow the field and  $\epsilon''$  would be zero and hence the material would be transparent to the radiation. Therefore, only the out-of-phase part of the displacement current contributes to energy that is absorbed and ultimately dissipated as heat.

In the microwave frequency range dipole relaxation, as explained earlier, is mainly responsible for the energy absorbing process. For dipolar materials, the dielectric constant would be dependent on the frequency as can be predicted from the expression for the two parts of the dielectric constant. Figure 4.1 shows this dependence of both parts of dielectric constants on the frequency of a dipolar liquid. As one can see in this figure, at very low frequencies, the dipole alignment occurs at the same frequency as the field oscillations and therefore  $\epsilon''=0$  and  $\epsilon'=\epsilon_0$ , the static value. In the intermediate range of



## LOG FREQUENCY

FIG. 4.1 DIELECTRIC CONSTANTS FOR DIPOLAR LIQUID (After Parsons, 1975)

frequency, there is a frequency band where the dipoles cannot keep in step with the field, and thus the loss factor,  $\epsilon''$ , is a bell-shaped curve that can be characterized by a single relaxation time,  $t$ , associated with the  $\epsilon''$  peak. At very high frequencies, the field changes so rapidly with respect to the dipole's ability to keep in step that the dipole orientations practically become random and thus do not contribute to a displacement current. Once again  $\epsilon''$  becomes 0 but  $\epsilon'$ , on the other hand, remains at the optical dielectric constant  $\epsilon_\infty$ , which is different from  $\epsilon_0$ .

#### 4.2.2 Optical Properties

If a medium is such that it absorbs electromagnetic radiation, while the electromagnetic radiation travels through this medium, the maximum electric strength diminishes with distance. The instantaneous field strength can be represented as a function of time and position in terms of optical properties by the following relationship:

$$E(x,t) = E_i \exp\left[-\frac{2\pi f k x}{c}\right] \exp\left[i2\pi f\left(t - \frac{nx}{c}\right)\right] \quad (4.43)$$

where,

$E(x,t)$  = electric field strength after travelling a distance,  $x$ .

$E_i$  = maximum electric field strength of the incident radiation, i.e., at  $x=0$ .

In the above expression, the first exponential term accounts for the absorption of energy as radiation passes through the medium. Therefore, it contains the extinction coefficient,  $k$ . The second exponential term accounts for the sinusoidal variation of the field with time. The above equation can be simplified by using a complex index of refraction which is defined as:

$$n^* = n - ik \quad (4.44)$$

For a non-negative insulator, the velocity of propagation is given by

$$v_{pr} = c/\sqrt{\epsilon'} = c/n \quad (4.45)$$

The above equation leads to

$$\epsilon' = n^2$$

Similarly one has,

$$\epsilon^* = N^{*2} \quad (4.46)$$

where  $\epsilon^* = \epsilon' - i\epsilon''$  is the complex dielectric constant. This equation leads to the following relations among physically measurable quantities,

$$\epsilon' = n^2 - k^2 \quad (4.47)$$

and,

$$\epsilon'' = 2nk \quad (4.48)$$

Both of these parameters are thus measurable as dielectric or optical properties. [ A more detailed derivation of the above may be found in Parsons' (1975) ]

The Lambert absorption law is obtained by applying Equation (4.43) to the change in intensity of the radiation upon passing through some material. It states that, for homogeneous, multicomponent mixtures, each molecule contributes to the wave attenuation as if the other molecules were not present. Therefore, when the absorption ability of one species is much larger than the others (much larger extinction coefficient), then the total absorption in a sample is a direct function of the number of those molecules in the path of the electromagnetic radiation. Thus, the Beer-Lambert law states that:

$$\frac{I_x}{I_0} = \exp(-K_a Ch) \quad (4.49)$$

where,

$I_x$  = radiation intensity leaving the sample.

$I_0$  = radiation intensity entering the sample.

and

$K_a$  = molar absorption coefficient



However, if more than one component in the mixture absorbs radiation, this law states that the absorbance would be additive.

Besides absorption phenomena, the microwaves are subject to the usual optical laws of reflection, refraction, diffraction, etc. However, as the microwaves have wave lengths relatively longer than ordinary light, it happens that the particle size of the components of the currently used experiments ( sand grains, oil droplets, water droplets, micro-emulsions, etc. ) are smaller than the wave length (approximately 1 cm for 27 GHz), and thus the composite medium appears homogeneous in the "sight" of the microwaves.

#### 4.2.3 Physical Properties of Materials

At microwave frequencies, most of the solids and gases have a negligible loss factor. It turns out that, even though some gas molecules have permanent dipoles, their low density may cause an insignificant absorption. On the other hand, the loss factor varies greatly for pure liquids.

The magnitude of the loss factor depends not only on the molecular structure of the medium but also on the temperature. For water, dissolved salt content may cause a significant change also in the loss factor. These effects are depicted in Figures 4.2 and 4.3. However, the effect of dissolved salt content in water is second order. As can be seen in Figures 4.2 and 4.3, a majority of crude oil molecules are nonpolar and show extremely small microwave

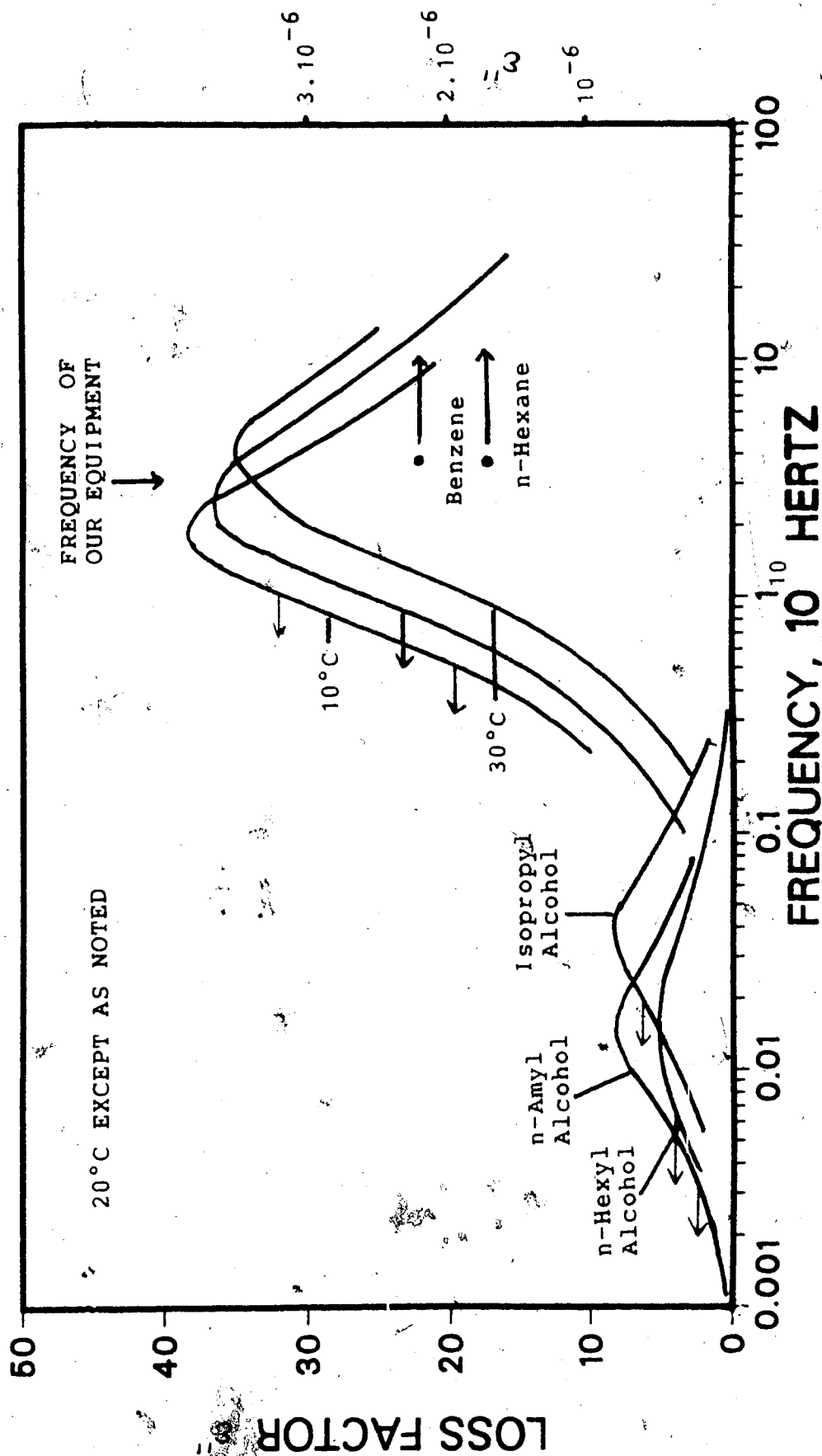


FIG. 4.2 LOSS FACTORS FOR SOME PURE LIQUIDS (After Parsons, 1975)

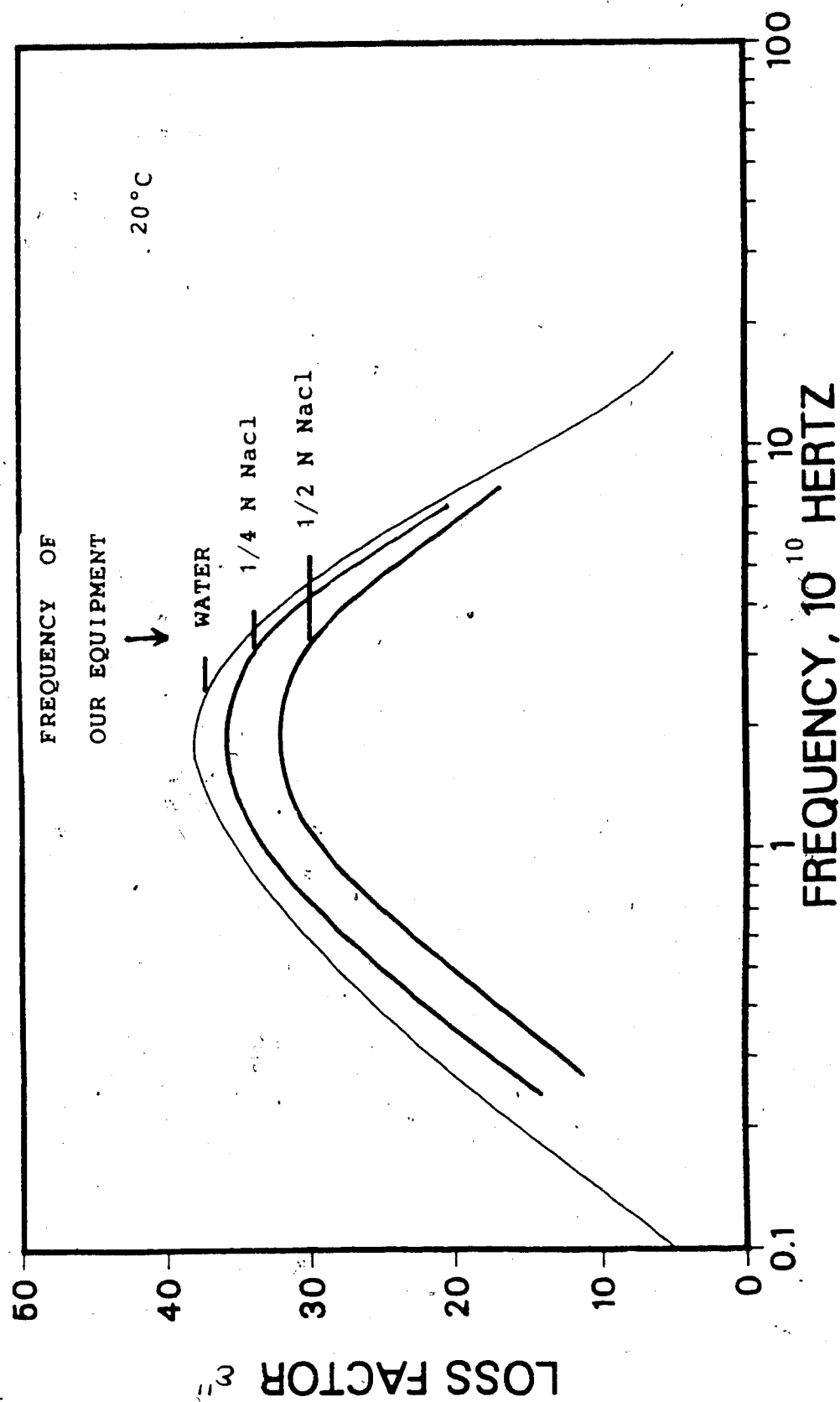


FIG. 4.3 LOSS FACTORS FOR AQUEOUS SALT SOLUTIONS (After Parsons, 1975)

losses.

For the present study, a frequency of 27 GHz was chosen for the microwaves. At this frequency range, water has about the maximum loss factor. Thus, as the microwave travels across a mixture of water and oil, the water's loss factor overshadows that of oil and the oil may be considered "transparent" to the microwaves. Therefore, the loss of energy may be attributed primarily to the water and partly to the core-holder material, etc. which are again much more "transparent" than water.

### 4.3 STABILIZATION

Stabilization is achieved for an immiscible displacement process when fractional flow becomes invariant with time, i.e., the shape of the fractional flow curve and the saturation profiles do not change shape with time. The displacement equation proposed by Buckley and Leverett is equivalent to the long-time solution of a Lagrangian formulation of the one-dimensional, immiscible fluid displacement process (Bentsen, 1978). As already discussed, the external drive method for determining relative permeabilities is based on the assumption that the Buckley-Leverett equation is applicable. As a consequence, before the external drive technique may be applied, stabilized flow must be achieved. It has been demonstrated (Bentsen, 1978) that if the macroscopic capillary number as defined by the Equation 2.4 is less than 0.01, then the displacement is essentially stabilized.

### 4.4 STABILITY

If we consider two fluids which are initially separated by a plane interface in a porous medium, the displacement of one of these fluids by the other can take place under two completely different displacement regimes. The first one is stable displacement during which a transition region between these two fluids will develop as they travel through a porous medium. Depending on the balance between the viscous, capillary, and gravity forces and the pore size distribution, the size and the shape of the transition zone

changes. Conventional one-dimensional, immiscible displacement theory may be used only to predict the shape of the saturation profiles when the displacement is stable. If the displacement is truly ideal the two fluids will continue to be separated by a sharp front or saturation discontinuity as long as the flow paths are identical.

The second type of displacement is unstable displacement. In this kind of displacement the interface separating the two fluids becomes unstable causing viscous fingers to appear. In this case, the heterogeneities in the porous medium and the balance between viscous, capillary and gravity forces will determine the extent of viscous fingering. It is expected that the flow behaviour in an immiscible displacement would vary considerably depending on whether the displacement is stable or unstable (Bentsen, 1985a). That is why it is important to be able to predict the boundary separating stable displacements from unstable displacements. This boundary was predicted in the present study with the aid of a new theory developed by Bentsen (1985a). This theory suggests that, for rectangular shaped systems, the displacement will be stable provided the instability number defined by Equation 4.50

$$I_{sr} = \frac{v (M_r - 1 - N_g)}{K_{wr} \sigma_e} \frac{(M_r^{1/3} + 1)}{(M_r + 1) (M_r^{1/3} + 1)^2} \frac{4L_x^2 L_y^2}{L_x^2 + L_y^2} \quad (4.50)$$

does not exceed  $\pi^2$ . Here,  $\sigma_e$  represents the pseudo or

effective interfacial tension between the displaced and displacing fluids. In order to estimate  $\sigma_e$ , one may make use of a recently developed mechanistic model (Bentsen, 1985b) that requires the capillary pressure versus saturation curve. Given that such a curve is available  $\sigma_e$  may be obtained from

$$\sigma_e = \frac{A_c \phi (1 - S_{wi} - S_{or})}{2/r_m} \quad (4.51)$$

where  $2/r_m = 1$  and where  $A_c$  is the area under the capillary pressure versus saturation curve. In order to avoid integrating experimental data, an imbibition capillary pressure model of the experimental data may be used.

#### 4.5 CAPILLARY PRESSURE MODEL

It is usually assumed that capillary pressure may be expressed as a function of saturation only, as the capillary pressure at any point is directly related to the mean curvature of the interface, which, in turn is a function of saturation (Leverett, 1941). Melrose (1970) pointed out that the trapping mechanism for the non-wetting phase during imbibition is different from that for the wetting phase during drainage. This is because, during drainage, the wetting phase is trapped in the small pores, whereas during imbibition the probability for the large pores to be bypassed is the largest. Even though a distinct difference in shape is observed between drainage and imbibition capillary pressure curves, Szabo (1972) argued that the concavity of the drainage capillary pressure curve at the maximum saturation is due to the effect of gravity on cores of finite dimensions and is not a characteristic of the drainage capillary pressure versus saturation relationship itself. Therefore, if the gravity effect is neglected the shape of the imbibition and drainage capillary pressure curves would be much closer.

To date, only empirical models have been proposed for describing capillary pressure as a function of saturation. In order to have a consistent capillary pressure model, several conditions have to be fulfilled (Golaz and Bentsen, 1980). However, the task here is to obtain an empirical model that is applicable to an imbibition capillary pressure curve. So far, no effort has been undertaken to derive an



imbibition capillary pressure model. In order to propose such a model, it was expected that the model would have a similar form to that suggested by Golaz and Bentsen (1980). However, in order to obtain a better fit to the experimental data, the following form (Bentsen, 1984) was used.

$$P_c = - \frac{a_c(S+c_c)^{(1-d_c)}}{1-d_c} - \frac{b_c(1+e_c-S)^{(1-f_c)}}{1-f_c} + \frac{a_c}{1-d_c}(1+c_c)^{(1-d_c)} - \frac{b_c}{1-f_c}e_c^{(1-f_c)} \quad (4.52)$$

In this model the  $P_d$  term is neglected as this is an imbibition model. For this model, the area under the capillary pressure curve is given by,

$$A_c = \frac{a_c(c_c^{(2-d_c)} - (1+c_c)^{(2-d_c)})}{(1-d_c)(2-d_c)} + \frac{b_c((1-e_c)^{(2-f_c)} - e_c^{(2-f_c)})}{(1-f_c)(2-f_c)} + \frac{a_c}{1-d_c}(1+c_c)^{(1-d_c)} - \frac{b_c}{1-f_c}e_c^{(1-f_c)} \quad (4.53)$$

As one can see from the above equation, the only requirement on this capillary pressure model is that (so that the area  $A_c$  is finite)

$$d_c \neq 1$$

$$d_c \neq 2$$

$$f_c \neq 1$$

$$f_c \neq 2$$

It should be noted that  $S = \frac{S_w - S_{wi}}{1 - S_{wi} - S_{or}}$ , because for imbibition capillary pressure data, one starts from a water saturation of  $S_{wi}$ ; thus the total range of water saturation variation is from  $S_{wi}$  to  $(1 - S_{or})$ . For the present study, only the imbibition model was used as the displacement tests performed to measure relative permeability data were of the imbibition type.

## 5. EXPERIMENTAL SET-UP AND PROCEDURE

For the present study, the instruments may be classified under the following categories:

- (1) Microwave instrumentation
- (2) Fluid injection system and pressure measuring devices
- (3) Data aquisition, automation and storage equipment.

### 5.1 MICROWAVE INSTRUMENTATION

The microwave attenuation technique is conceptually simple. It requires a stable source of microwaves, a sample and a detection system. The different components of this system are :

(a) **Klystron and Power supply:** The Klystron supplies a very stable, single frequency microwave signal with all waves in phase. The microwave generator has a frequency range of 26-30 GHz. The generator was operated at a frequency of 27 GHz. The generator can supply a maximum output power of 1100 mW.

(b) **Tuners:** Micrometer plungers in both the electrical and magnetic planes fine tune the frequency of the generator.

(c) **Attenuator:** The microwave signal can be reduced to any desired amount with the attenuator.

(d) **Horns:** For measuring water saturations a pyramidal horn with a lens antenna to alter the pattern was selected. This horn transmits a spherical wave with primary and secondary lobes; however, when a lens is placed on the mouth of the horn, the spherical wave is converted to a plane wave if the refractive index and shape of the lens surfaces are properly chosen.

(e) **Sample:** A sample of constant thickness was used. It was large enough to prevent diffraction effects when exposed to the microwave beam.

(f) **Detector:** An HP-8484 sensor was used for detecting the microwave energy. A sensitive, thin-film thermocouple detects the temperature rise caused by the conversion of microwave energy to heat in the detector point.

(g) **Powermeter:** The sensor or detector electromotive force is amplified to a usable level and is directly connected to the powermeter. The powermeter that is used to measure the attenuated microwaves is an HP-432C which is equipped with a binary coded digital output facility. Hence, data can be transmitted directly to a digital computer, provided an adequate interface is available.

## 5.2 FLUID INJECTION SYSTEM, CORE HOLDER, PRESSURE GAUGE, ETC.

A constant-rate Ruska pump was used to inject mercury into a cylinder. As the mercury cylinder was connected to two cylinders containing water and oil, the injected mercury could be used to displace either water or oil by simply opening the proper valves. The fluid-containing cylinders were, in turn, connected to the core holder by flexible tygon tubing. Once again, by choosing the proper valve, one could inject either water or oil into the core holder. At the entrance of the core holder a Heise Pressure gauge (range 0 - 50 psia) was connected so as to have a qualitative idea of the inlet pressure.

The core holder was fabricated from PVC to avoid any appreciable attenuation of microwave power when microwaves traveled across it. The core holder had a constant, rectangular cross section so that the thickness exposed to microwaves was constant. At the outlet end of the core holder was attached a small rectangular chamber that enabled the detection of oil or water drops as soon as they came out of the sand-packed core. This chamber was made of transparent lucite. A similar lucite chamber was used at the inlet end as well to permit one to view the fluid distribution at the beginning of each displacement test.

The PVC core holder had a thickness of .75 cm. This small thickness was required to decrease the microwave attenuation as the amount of attenuation is directly proportional to the thickness of the core holder. This enabled the measurement of saturation profiles up to a water saturation of 100 %. A

greater thickness may be used in the future as a more sensitive power meter (HP-436A) has been acquired. Only one core holder was used during this study. The characteristics of the core holder are reported in Table 6.1.

In order to measure the pressure profile along the length of the core, seven equally spaced transducers were placed on the core holder. These transducers were especially made for low-range pressure measurement. Two sets of transducers were used (one set with a range of 0 - 12 psia, the other set with a range of 0 - 25 psia) to obtain maximal accuracy during the pressure measurement. Higher pressure measurements were not required as the major constraint on pressure was due to the design of the core holder, as it could support a maximum pressure of only 30 psia.

To collect the liquids at the outlet end a fractional collector was used. It was equipped with 10 cc tubes to be able to measure the fractional volume of produced fluids with higher accuracy. The fractional collector was connected to a controller that could be monitored manually or automatically. The core holder was mounted on brackets with wheels. A fractional collector with wheels was mechanically connected to the core holder to synchronize their movement. Both of these units were driven on rails by a chain drive, which was run by a variable speed d.c. motor. To be able to start a complete scan from the same point of the core holder, a stopper was fixed on the bench. The bracket containing the core holder was automatically

retracted after each saturation scan and was stopped by the stopper so as to enable the start of the next scan from the same point.

The experimental set-up is sketched in the Figure 5.1.

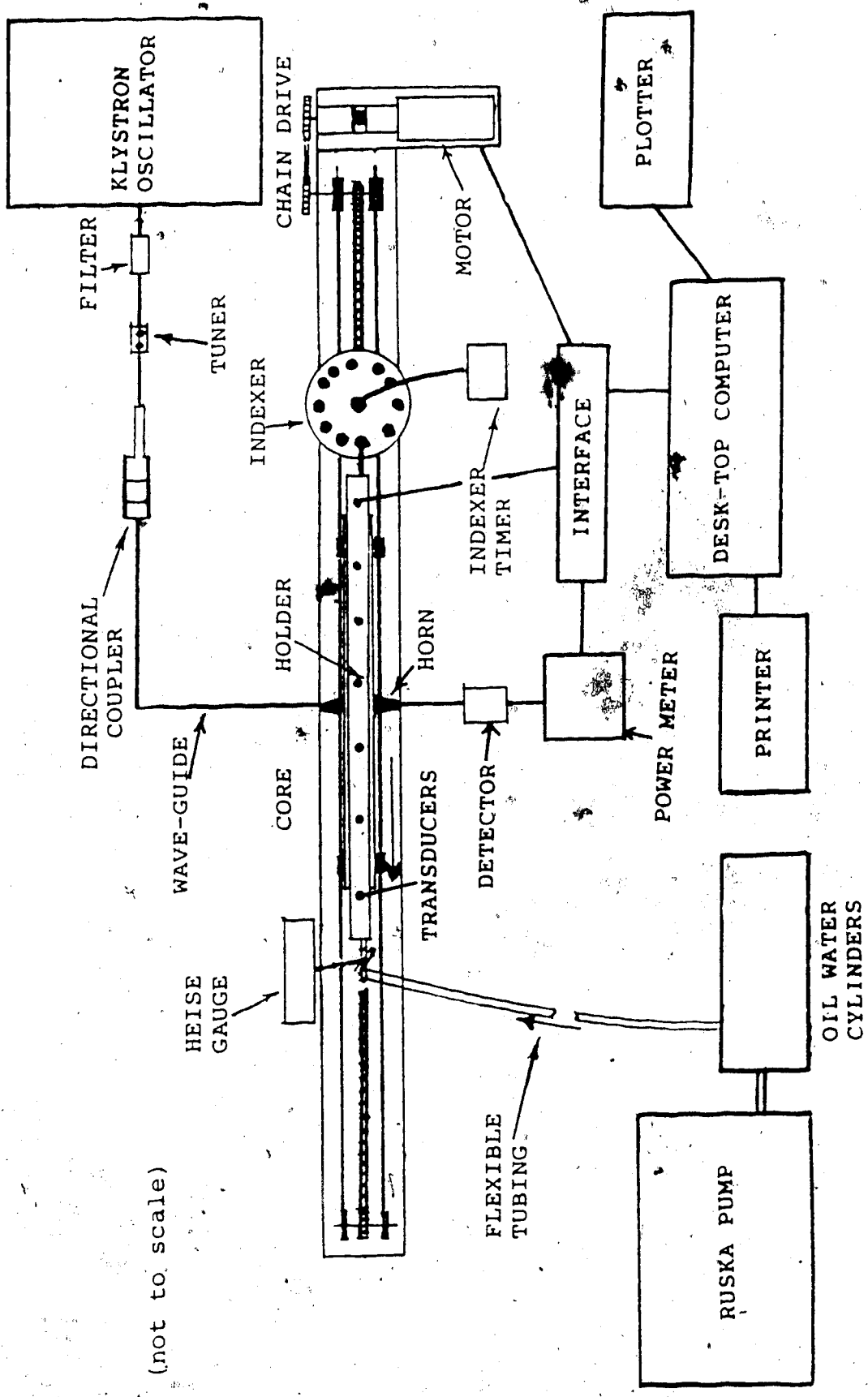


FIG. 5.1 EXPERIMENTAL SET-UP



### 5.3 AUTOMATION OF DATA AQUISITION AND STORAGE

Automation involves making the microwave output power measurement and the transducers' pressure measurements automatic. Also, the scanning of the core holder had to be automated. A HP-9825 microcomputer was used for this purpose.

The powermeter used to measure the output power of the microwave was an HP-432C that had a binary coded digital output. Hence, it could be directly connected to the interface of the digital computer.

In order to automate data collection for the powermeter output and the pressure data and to automatically scan the core holder, the following equipment was used:

#### 5.3.1 HP-9825A Micro Computer

This micro computer is the main data acquisition and control device. It works along with its peripherals in order to maintain Input/output (I/O) communication with external devices and to store data. It has the following characteristics:

##### (a) Memories

It uses two types of memory : Read/write memory and read only memory. The read/write memory is used to store programs and data. That is, when one stores a program or data, he "writes" into the memory. When one accesses a line of a program or a data element, one "reads" from memory; thus the the term read/write. Read only memory differs in

that it is permanent. When the computer is turned off, the contents of read/write memory are lost, whereas the read only memory (ROM) is unaffected. ROM cards can be plugged into the ROM slots on the front of the computer. This makes it possible to expand the language.

Program and data in read/write memory can be saved for future use by recording the information on the tape cartridge.

(b) Language:

The language used by the HP 9825A is called HPL. The basic programming unit is the statement. Statements are typed using lower case abbreviated mnemonics, such as "prt" for print. Multi-statement lines can be stored by separating with semicolons.

Two other characteristics of this language are implied multiplication and the assignment operator. Implied multiplication is a standard algebraic notation such as  $5X$ . The assignment operator  $\rightarrow$  points to the variable being assigned a value, such as  $5 \rightarrow D$ . Further details of the language are available in the HP 9825A manual.

(c) Error messages:

When an error occurs, the computer beeps and displays an error number. The number references a description that will help pinpoint the cause of the error.

### 5.3.2 Multiprogrammer Interface

A model HP 59500A is used as an interface between the multiprogrammer and the computer. This interface buffers and transmits data and control signals between the HP-IB (Interface bus) and the multiprogrammer, 6940B. It converts the serial ASCII alphanumerics of the HP-IB to the 16-bit parallel format required by the 6940B multiprogrammer. The 59500A also adapts the 3-wire handshake process used on the HP-IB to the 2-wire method (Gate/Flag) employed by 6940B.

The 59500A's interface circuits are contained on a multilayer printed circuit board which contains over 60 integrated circuits. Operating voltage for the interface circuits is provided by a +5 volts regulated power supply.

The 59500A/6940B can function on the HP-IB as a talker or as a listener and has source handshake, acceptor handshake, and service request capabilities. Further details of these different modes and the electric characteristics are available in the HP 59500A manual.

### 5.3.3 Multiprogrammer

A model 6940B is used as an interface between the system and the computer. The 6940B can be used in a single-unit system employing from one to fifteen plug-in input/output cards, or in a multi-unit system consisting of one 6940B master unit and up to fifteen 6941B extender units. Each extender unit can also accommodate up to fifteen input/output cards, allowing a multiprogrammer system that may be expanded up to a maximum of 240

input/output channels. Hence, the multiprogrammer system can be used to convert a single computer I/O channel to a total of 240 I/O channels.

The multiprogrammer system is controlled by a digital computer which supplies 16-bit binary words to

(1) Control the mode of operations of the system (for example, to allow the multiprogrammer to time share input and output functions, to establish timing synchronization between the computer and I/O devices through the multiprogrammer, etc.)

(2) Address output cards and supply the output quantity, in binary coded form, to be developed by the output cards for application to the output device.

(3) Address input cards for the reception of binary-coded input data.

One can refer to the HP 6940B manuals for a detailed descriptions of the multiprogrammer.

#### 5.3.4 INPUT/OUTPUT cards

The function of the output cards is to develop a signal which corresponds to programmed data, and to deliver this signal to the user's system. The output cards are similar to one another in that each contains address gates, data storage, and output data conversion circuits. The nature of the output conversion circuits determines the card type.

Further details on how to address and program an output card are available in the output card manuals. The peculiarity of the output cards is that when they are programmed to a particular output value, they hold that value until they are readdressed and the programmed data are changed. The digital output card was used to send a signal of 2.5 Volts that was amplified to 110 Volts in order to start the d.c. motor at selected times. The motor used a chain-drive to move the core-holder for a complete scan.

The function of the input cards is to receive data from the user's system and convert it to a form which could be used in the program. Each of the input cards contains an address gate and input data interface circuits. Two input cards were used to transfer microwave output power data to the computer. A third input card was used along with the output/read back card to measure the data from the transducers.

When an input/output card is plugged into a particular slot of a particular unit, it assumes the address of that slot and unit, and will either receive and store data (output cards) or transmit data (input cards) only when that unit and slot are addressed. Unit selection is accomplished by decoding control words (that may be found in the manual), but slot address decoding is accomplished by directly wiring a unique combination of four slot address bits to each of the 15 input/output slots. If a card is moved to a new slot it assumes the address of that slot.

### 5.3.5 RELAY OUTPUT/READBACK cards

A model HP69433A is used for this purpose. It provides 12 separate contact outputs that reflect the status of 12 previously programmed data bits to the computer. This was used to read data from the seven pressure transducers by using only one digital input card. The steps involved in programming a relay card are:

- a. Enabling the relay output of the card by programming the system enable (SYE) bit.
- b. Addressing first the multiprogrammer unit, and then the slot in that unit.
- c. Programming data that will provide the desired output relay contact configuration.
- d. Programming an input select (ISL) bit so that the data programmed in step (c) can be read back to the computer.

### 5.3.6 Automatic Powermeter HP 432C

This powermeter, which is used to measure the attenuated power, was under automatic control. The powermeter uses the HP Interface Bus (IB). The automatic powermeter enables the following functions.

#### (i) Zero-setting:

Accurate zerosetting is critical when measuring power on the lower ranges of the powermeter. Zero-set drift is caused by the power sensing element experiencing a temperature change or temperature gradient since the last zero-setting. Likely sources of temperature change are atmospheric changes,

thermal conduction down the power transmission line, and sources of heat near the power sensing element. The sequences to follow in order to zero set are available in the HP 432C manual.

(ii) Triggering:

This is a feature available via remote programming, i.e., standby, triggered, or free-running operation. It has specific capabilities like Hold, Trigger immediate, Trigger with delay, Free run at maximum rate, Free run with delay, etc.

(iii) Data storage:

An array is used for storing measured attenuated power. As automatic scale changing is performed, another array that contains flags for the scales used is also stored simultaneously. Both the stored arrays may be retrieved later on and the actual power values may be calculated by a program capable of decoding binary coded numbers.

### 5.3.7 HP 9872A Plotter

In order to plot the saturation profile, a model HP 9872A plotter was chosen. The plotter ROM enabled the desktop computer to control the plotter and to provide hard copy graphic solutions to problems solved by the computer.

The automation system and interconnection between different devices are depicted by the Figure 5.2.

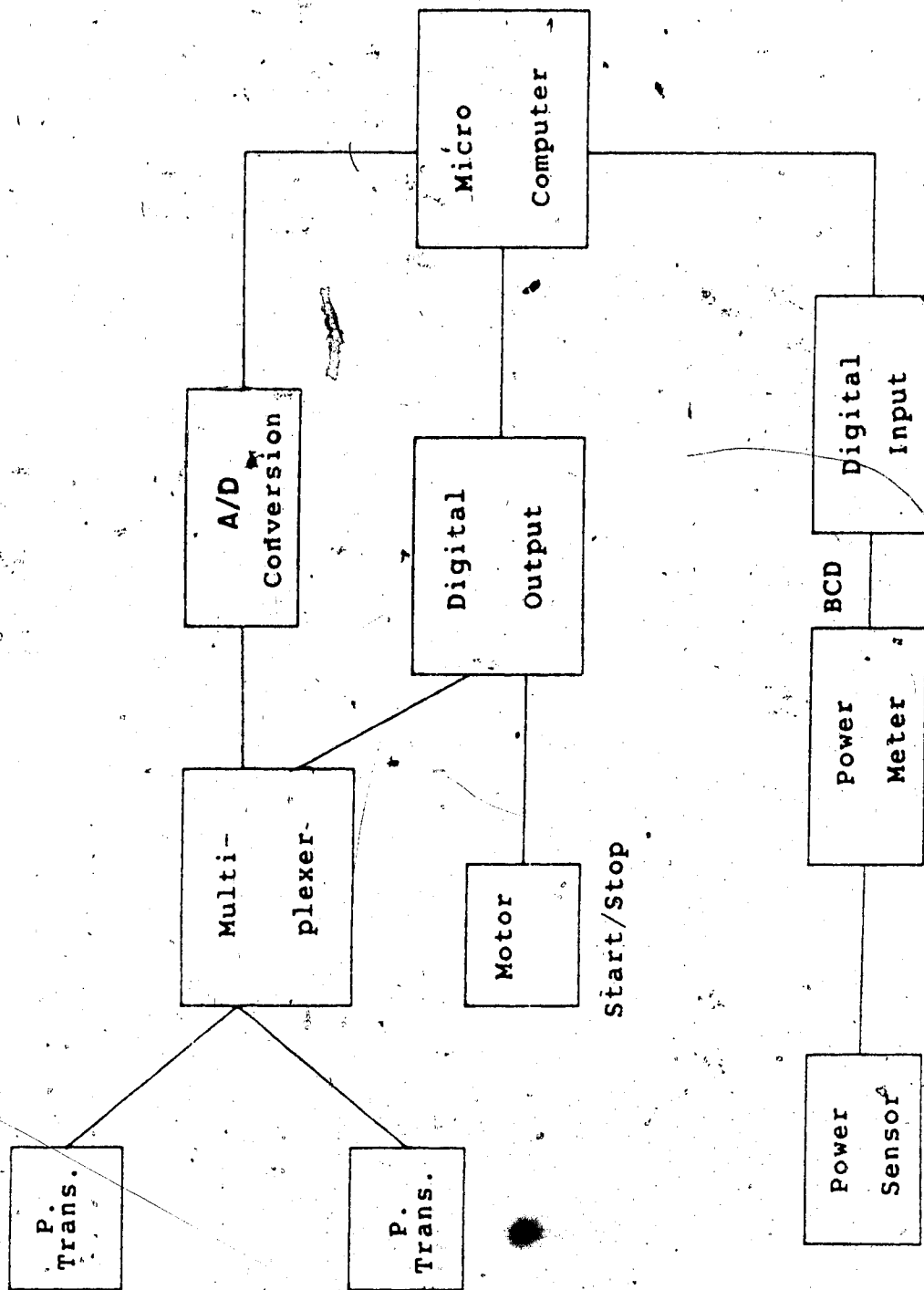


FIG. 5.2 AUTOMATION AND DATA ACQUISITION SYSTEM



#### 5.4 MICROWAVE SIGNAL VERSUS WATER SATURATION

If water were the only absorptive material in the system then it would be possible to derive a theoretical relationship between the microwave signal and the water saturation. However, as the Ottawa sand and the PVC core holder also absorb a part of the microwave signal, the overall system may be considered to have two absorptive components, i.e., water and everything else. In this regard, the absorbance due to materials other than water has to be determined experimentally. Note that the absorbance constant,  $A_{1s}$ , not only accounts for the losses due to the core holder and sand, but also for other losses such as those due to reflection. The absorbance caused by the water may be expressed as

$$A_w = - \frac{4 \pi f k_{wa} h \phi S_w}{2.303 c} = B_1 S_w \quad (5.1)$$

As absorbances are additive, the total absorbance may be written as:

$$A_{st} = A_{1s} + B_1 S_w = \ln \left( \frac{I_o}{I_x} \right) \quad (5.2)$$

where  $I_o$  and  $I_x$  are the power at the inlet and outlet respectively. As the data collection was automated, it was possible, by means of a dry scan ( $S_w=0$ ), to estimate  $A_{1s}$  at 500 points along the length of the core. Similarly by scanning the core when the water saturation was 100 percent, it was possible to estimate  $B_1$  at the same 500 points.

Thus, it was possible to determine independent correlations between absorbance and water saturation at each of 500 discrete points along the length of the core. As a consequence, it was not necessary to assume that each point along the length of the core had the same response characteristics. To be noted that this response could vary along the length of the core due to local heterogeneities.

### 5.5 CORE PREPARATION PROCEDURE

Unconsolidated Ottawa sand (80-120 mesh) was used during all the runs. Ottawa Silica sand (70-130 mesh) as received from the suppliers was sieved to obtain 80-120 mesh sand. The wet packing technique was used to obtain packs with consistent properties. In order to pack the core, the core holder was suspended in a vertical position and filled with distilled water up to a few centimeters height. In this process, sand was dropped into the core holder through a constant height of distilled water so as to have a water head on top of the sand. After the core holder was filled with sand, a 12 cm long transparent (lucite) extension with the same shape as the core holder was used to maintain about a 6 cm high water head on top of about 6 cm of extra sand in the extension. The core holder was vibrated overnight in a vertical position. Once packed, the extension was removed and the end plate was put on the end of the core holder. Then the core holder was tested for leaks at a water pressure of 25 psia.

Once the core was wet packed the sample was dried to obtain the microwave scan at zero percent water saturation. The drying was performed by flowing dry air through the sample until a microwave response equivalent to that of dry sand was obtained. The average time for drying was five days. This long time was required because the air flow rate was kept low in order to maintain a maximum inlet pressure of 20 psia. The core holder was weighed both empty and with dry sand in order to have an estimate of the mass of the

sand pack. This enabled subsequent calculation of the pore volume. As dry scans were very similar to scans taken at the irreducible water saturation it was felt that consistent packings of the cores were obtained. Also, the dry scans looked alike for different runs showing good reproducibility. The microwave response data at 0% water saturation were stored for subsequent saturation calculations.

After the dry scan was taken, the core was resaturated by imbibition of distilled water into the sand which was under vacuum. To saturate the core, it was connected to a beaker containing a volume of distilled water greater than the previously estimated pore volume of the sand pack. The pore volume was estimated by making the following calculation:

$$\text{Pore volume} = \left( V - \frac{m}{\rho_g} \right), \text{ cc}$$

where,

$m$  = mass of the sand in core holder

$V$  = volume of the core holder

and

$\rho_g$  = grain density of Ottawa sand

Once the sand in the core holder has imbibed distilled water of about the same volume as that estimated above, the inlet was connected to the Ruska pump and water was pumped through the core at a flow rate of about 200 cc/hr. An accurate

material balance, thus, gave the exact pore volume of the sand. The flow was allowed to stabilize (when the pressure drop along the length of the core is constant). This pressure drop was noted for that particular flow rate in order to be able to calculate the absolute permeability of the core.

Once the core was saturated, a microwave scan was taken at 100% water saturation. Following the same procedure as for the dry scan, the microwave response data were recorded and stored by the computer.

The sand pack with 100% water saturation was allowed to sit for about twelve hours to render it water wet.

The speed of the d.c. motor was adjusted so that the core travel time was 30 seconds (time required for the computer to collect 500 data points). This adjustment was made for every run. Also, the position of the inlet and outlet horns were aligned and immobilized with a stand.

## 5.6 ESTABLISHMENT OF IRREDUCIBLE WATER SATURATION

In order to establish an irreducible water saturation,  $S_{wi}$ , an oilflood was conducted. So as to avoid any effect of flow rate on the irreducible water saturation, all the oil floods were carried out at a constant flow rate for a given series of runs. Also the oilfloods were carried out at a favourable mobility ratio.

Microwave scans were done randomly during the oilflood. Once several pore volumes were injected, very little change was observed in the microwave signal. A water cut of less

than one percent of the total outlet flow was obtained after injecting four pore volumes of oil. This was assumed to be the criterion for establishing the irreducible water saturation. The irreducible water saturation profiles were similar for all the runs and for a given run, the saturations along the core were more or less constant. This observation reconfirmed the earlier one that the sand packing was consistent.

When the irreducible water saturation was reached, another microwave scan was performed and the microwave response data were stored as usual. Neglecting local heterogeneities, one could attribute an average value of the microwave response to the average  $S_{wi}$  value as calculated from the material balance. Otherwise, this response data could be used as a check on the microwave response curve for different known values of the saturation, such as 0%, 100%, and  $S_{wi}$ .

## 5.7 WATERFLOOD

For each run, a waterflood was performed at a constant rate. The flood front was allowed to advance at least up to one-fifth of the total length of the core before starting regular interval microwave scanning. The microwave scan interval was 5-6 minutes for slower flow-rates (below 100cc/hr) and 3-4 minutes for higher flow-rates (above 100cc/hr). As the powermeter used was able to change scale automatically, unlike the procedure used in a previous study (Saeedi, 1979), a single scan was performed at each time.

During each scan 500 data points were recorded and stored by the computer for future use.

As waterflooding continued the pressures along the length of the core were recorded at seven different points by the pressure transducers. The computer recorded pressure data at one minute intervals. A delay of 2 seconds from the first to the last transducer was recorded. This delay was considered to be negligible and the pressures were assumed to be instantaneous.

The waterflooding was continued until the oil-cut became less than one percent of the total outlet flow. At this point the irreducible oil saturation was assumed to be reached, and the waterflooding was stopped.

## 5.8 FLUID PROPERTIES

For the present study, three different fluids were used as displaced fluid along with distilled water in the displacement tests. These fluids were

- (1) MCT5+LAGO
- (2) Dow-Corning
- (3) Mineral oil (Heptane+Paraffin oil)

Imbibition capillary pressure curves were obtained for the oils MCT5+LAGO and Dow-Corning by using the "Restored State" method. The interfacial tension between each of the oils and water was estimated using the Pendant drop technique. The viscosity of each of these fluids was measured using a Brookfield digital viscometer. The densities were determined by using a specific gravity bottle

and a precision balance.

### 5.9 CONVERSION OF MICROWAVE RESPONSE TO A SATURATION PROFILE

For all the scans, the input power of the microwave generator was fixed at 10mW. The reason why such a low power input was used is that the power measuring sensor (HP-8484) was not capable of measuring any power beyond 10mW and a further increase in power would cause damage to the sensor at the inlet of the core. As the core was sufficiently thin this input power was enough to obtain a measurable response at the other side of the core. However, recently a new power meter capable of measuring high as well as low power has been obtained. This would enable the use of higher power at the inlet. For every run the frequency was fixed at 27 GHz. The extinction coefficient is constant as is the porosity and thickness at each point. Therefore, one should obtain a linear relationship between  $\ln(I_x)$  and  $S_w$ .

In order to obtain the straight line relationship between  $\ln(I_x)$  and  $S_w$  for each of the 500 points along the core, one can use any two of the known saturation values and thus interpolate or extrapolate the intermediate values of the saturations. If more than one point is known, then one could use an average value for the characteristic straight line. As it was intended to allow for the possibility of having different irreducible water or oil saturations along the length of the core, it seemed appropriate to use the 0% and 100% water saturations as reference points. However,



once the irreducible water and oil saturations along the length of the core were calculated using 0% and 100% water saturation values as references, it was evident that both water and oil irreducible saturation values were more or less the same along the length of the core. As the microwave responses were stored for each of the above cases for 500 points along the length of the core, the computer could calculate the intermediate points during each scan. As a characteristic straight line was determined for each point, it was possible to handle local heterogeneities.

The conversion from the output power to saturation by using Equations 5.1 and 5.2 was undertaken at each of the 500 points along the length of the core. The water saturations were plotted against the normalized distance,  $x$ . First, the irreducible water saturation profile was plotted. As a large amount of water was injected to establish the irreducible water saturation ( four pore volumes ), a fairly uniform irreducible water saturation was observed for all the mobility ratios. For all the cases the irreducible water saturation ranged from 0.1 to 0.12 as determined from material balance. Also, this value did not change significantly along the length of the core.

The next step was to convert the waterflood data. Equations 5.1 and 5.2 were used to calculate the saturation profiles. The saturation profiles were not strictly a monotonic function of distance and local perturbations were evident for all the runs at all times. This behaviour is probably due to the minor irregularities found in any real

porous medium. The plot of  $S_w$  versus  $t$  was used to obtain the fractional flow at different positions of the core for each scan conducted during waterflooding. It was done following the procedure described in the theory.

For each run conducted, the irreducible oil saturation was established. As a large amount of water was injected to obtain the irreducible oil saturation, the saturation profiles were quite uniform along the length of the core. Also, no significant effect of mobility ratio on the irreducible oil saturation was observed.

#### 5.40 DATA ANALYSIS

In order to check the proposed technique for measuring the relative permeabilities with a conventional technique, the external drive technique proposed by Johnson, Bossler and Naumann (1959) was chosen for comparison. It should be kept in mind that such comparisons are valid only when the displacement is stabilized and stable. If the displacement is unstabilized, or if it is unstable, the JBN method is not expected to give reliable results because the assumptions underlying Buckley-Leverett theory are violated. In brief, the JBN method is based on the following equations:

$$f_o = \frac{1}{1 + \frac{K_{rw}\mu_o}{K_{ro}\mu_w}} = \frac{d(N_p)}{d(W_i)} \quad (5.3)$$

$$S_{w2} - S_{wi} = N_p - W_i f_o \quad (5.4)$$

$$\frac{f_o}{K_{ro}} = \frac{d\left[\frac{1}{W_i I_r}\right]}{d\left[\frac{1}{W_i}\right]} \quad (5.5)$$

As the dynamic method proposed in the present study makes all the above information available, the same data may be used to obtain the relative permeability curves by the JBN method. The JBN method as well as the dynamic method calls for taking slopes of experimental data. For the JBN method, the slopes of the  $N_p$  versus  $W_i$  and  $1/(W_i I_r)$  versus  $1/W_i$  curves have to be known, whereas for the dynamic method the slopes of  $N_p$  versus time and pressure versus distance have to be obtained. As taking slopes directly on experimental data may lead to strangely shaped relative permeability curves, mathematical models for the above mentioned curves were curve fitted to the experimental data by a simplex algorithm (Nelder and Mead, 1965). For the JBN method, it was decided to curve fit the  $N_p$  versus time curve (which would lead to the determination of  $1/(W_i I_r)$  versus  $1/W_i$  curve). The following functional forms were used, as they gave the best results.

$$N_p = a_2 \ln(T+c_2) + b_2 (\ln(T+d_2))^2 + e_2 \quad (5.6)$$

$$\Delta P = \exp [ a_3 \ln(T+c_3) + b_3 (\ln(T+c_3))^2 + d_3 ] \quad (5.7)$$

For the proposed dynamic method, the following functional form was used to fit the recovery data.

$$N_p = a_4 \tanh (T/b_4) \quad (5.8)$$

The reason why a different function was used for the dynamic method is that a good fit was obtained by using only two free parameters. Such a good fit was not obtained for the production data at the outlet end of the core. This may be because of the fact that the production data at the outlet end was collected for a longer time and the function used for the dynamic method does not fit well for a very long time. As a consequence a five parameter function was used for the production data of the JBN method. The quality of curve-fit for these data may be seen in the Appendices C-F. Some of the cumulative oil recovery (as determined by the Dynamic method) curves show erratic changes in slope. This usually occurs just before the irreducible oil saturation is reached. Slug flow of oil is expected at this stage of the displacement. This would explain changes in slope of the oil recovery curve. When processing the data, some erratic points were removed to obtain a more realistic recovery curve. The values of the parameters for the different curve fits are reported in Appendix K.

At first, the pressures at seven different points along the length of the core were curve fitted using the polynomial function given by Eq. 5.9,

$$P = a_p - b_p \xi - c_p \xi^2 \quad (5.9)$$

where  $\xi$  is the dimensionless distance. However, it was observed that the inlet and outlet pressures were not consistent with those measured internally. Appendix-G shows some of the curve fits for pressure profiles where the pressures measured outside the core holder can be seen as being different from the curve fit. A possible explanation may be given by the fact that a saturation discontinuity occurs as the fluid leaves or enters the core. For this reason the pressures measured outside the core holder were not used for any further analysis. While using slopes obtained from Equation 5.9, it was found that they varied significantly from those obtained using linear interpolation between two adjacent pressure transducers. Moreover, anomalous effective permeabilities were obtained by using the slopes of the model equation. For this reason, and also as the absolute permeability may not be constant along the length of the core, it was decided to estimate local pressure gradients rather than fit a curve to the entire pressure profile. This was done by assuming that the pressure profile was linear between adjacent pressure transducers. As the distance between the adjacent transducers was about 12.5 cm, the actual pressure gradient at a particular location and that estimated by linear interpolation may have differed somewhat because of local variations in permeability, perturbations on the saturation profiles, and so forth.

It is to be noted that for several reasons (Miller and Ramey, 1983) the absolute permeability was taken as the base for calculating the relative permeabilities when the JBN method was being used. Also, when the JBN method was used, it was noted that, by using the difference of the pressure at the inlet end (outside the core holder) and the outlet end (1 atm), an anomalous shape of the relative permeability curve was obtained. This problem was eliminated by using an estimated inlet pressure as derived by extrapolating the pressures inside the porous media. The pressures in the porous media were extrapolated linearly to obtain an estimation of the inlet pressure.

## 6. RESULTS AND DISCUSSION

Immiscible displacement studies were carried out using water-wet sand packs. Several displacement fluids were used and for each run the dimensionless scaling groups were calculated. In total, ten displacement runs were carried out, but relative permeabilities were calculated for only 8 different runs using the proposed dynamic method and the JBN method. For the other two runs, even though dimensionless scaling groups were calculated, the saturation profile data being lost due to a technical difficulty the relative permeabilities were not calculated. The results are discussed in the different sections according to the displaced fluid used.

### 6.1 MCT5+LAGO OIL DISPLACEMENT

The properties of the fluids and the core used in these displacements are reported in Table 6.1. The fluid was especially blended so as to be transparent to the microwave beam. The values of the scaling groups for this series of runs are reported in Table 6.2. In order to obtain an estimate of the effective interfacial tension, a complete set of imbibition capillary pressure data was obtained by using the "Restored State" method. These data were curve fitted using Equation 4.52. The parameters calculated by curve fitting the capillary pressure data are reported in Appendix-H. Figure 6.1 shows the curve fit along with the

TABLE 6.1

Characterstics and Results of the MCT5+LAGO oil Displacement

$\mu_o = 11 \text{ mPa}\cdot\text{sec}$				$q(\text{oil flood}) = 0.0333 \text{ cc/sec}$			
$\mu_w = 1.0 \text{ mPa}\cdot\text{sec}$				(while establishing $S_{wi}$ )			
$\rho_o = 840 \text{ kg/m}^3$				$\rho_w = 1000 \text{ kg/m}^3$			
$L = 116 \text{ cm}$				$A = 3.7 \text{ cm}^2$			
$\sigma = 11 \text{ dynes/cm}$				$A_c = 0.014 \text{ atm}$			
Run No.	$q$ cc/sec*	$K$ ( $\mu\text{m}^2$ )	P.V. (cc)	$S_{wi}$ (%)	$K_{or}$ ( $\mu\text{m}^2$ )	$K_{wr}$ ( $\mu\text{m}^2$ )	$S_{or}$ (%)
1.	0.0167	13.5	172	11.0	7.50	4.9	80.2
2.	0.0222	13.0	170	11.0	7.50	5.1	79.6
3.	0.0278	13.7	174	11.5	7.50	5.4	80.0
4.	0.0333	13.0	172	11.0	7.40	5.5	80.3
5.	0.0417	13.8	173	11.5	7.50	5.8	79.8
6.	0.0444	13.5	172	11.0	7.45	5.8	80.0

\* Waterflood



TABLE 6.2

Values of Dimensionless Groups and Recoveries  
for the Runs Conducted

Run No.	$M_r$	$N_c$	$I_{sr}$	Recovery " IOIP	$\mu_o/\mu_w$	Fluid
1.	7.19	0.14	1.27	.33	11	MCT5+LAGO.
2.	7.48	0.11	1.72	.38	11	"
3.	7.92	.093	2.2	.422	11	"
4.	8.17	0.08	2.71	.454	11	"
5.	8.51	0.067	3.18	.46	11	"
6.	8.56	0.062	3.67	.469	11	"
7.	6.82	0.049	3.46	.47	9.35	Dow-Corning
8.	13.8	0.052	9.90	.30	35	Mineral
9.	13.9	0.048	10.3	.28	35	"
10.	16.	0.046	13.7	.23	35	"

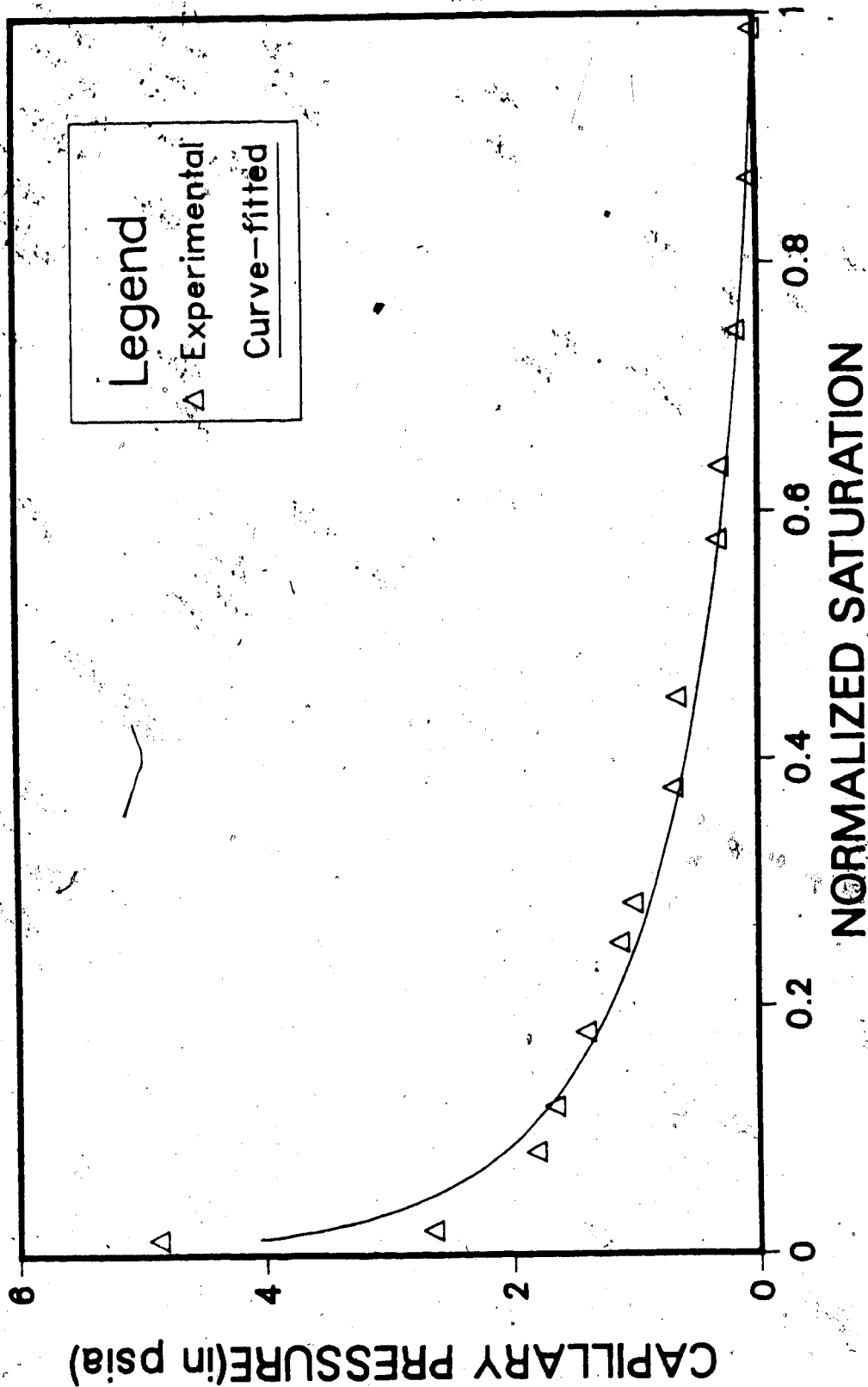


FIG. 6.1 CAPILLARY PRESSURE CURVE FIT FOR MCT5+LAGO.

experimental data. As the experimental data and the curve fit suggest, the imbibition capillary pressure curve does not have a steep slope near the irreducible oil saturation, i.e., near the end of the imbibition test. To be noted also is that, in order to obtain an imbibition capillary pressure curve, one has to start from an initial water saturation of  $S_{wi}$ . By curve fitting the capillary pressure data one can estimate the area under the capillary pressure versus normalized saturation curve. This area enabled the effective interfacial tension to be calculated using Equation 4.53. Finally the capillary number and the instability number were calculated by using Equations 2.4 and 4.50 respectively.

A flow rate of 120 cc/hr was used for all the runs during the establishment of the irreducible water saturation. The water-cut was reduced below 1% of the total outlet flow after a cumulative oil injection of four pore volumes. At this point the microwave response became constant with time showing that a constant value of irreducible water saturation had been reached. The oilflood was stopped after four pore volumes of oil injection. At this point the irreducible (initial) water saturation was estimated from the volumetric balance on the oil injected and oil produced. The irreducible water saturations for the different runs of this series are reported in Table 6.1. The irreducible water saturations are very close to each other for all the runs. This shows that good reproducibility has been obtained in packing the cores.

In terms of  $K_{or}$ , all the runs show very close agreement. To be noted, however, is that the flow rate for establishing the irreducible oil saturation was kept constant for all the runs. Therefore, there was no question of observing any difference in  $K_{or}$  due to variations in the oil flooding rate.

Waterfloods were carried out at different flow rates as reported in Table 6.1. Waterflooding was continued until the oil-cut fell below 1% of the total outlet flow. At this point, the microwave response became fairly constant with time showing that a constant value of the irreducible oil saturation had been reached. The effective permeabilities to water at the irreducible oil saturation are reported in Table 6.1. These  $K_{wr}$  values are very close to each other for all the runs conducted in this series. These values range from 4.9 darcies for the lowest waterflood rate to 5.8 for the highest flow rate. For intermediate values of the waterflooding rate the  $K_{wr}$  values vary from 4.9 to 5.8, showing a continuous increase with increasing flow rate. The dependence of  $K_{wr}$  on the waterflood rate is expected for very high flow rates (Melrose and Brandner, 1974; de la Cruz and Spanos, 1983). There is not much experimental evidence for such a dependence when the flow rate is very small and when the flow is not stabilized. However, if the displacement is not stabilized (high values of the capillary number) variables such as breakthrough recovery are expected to vary until a sufficiently low capillary number is reached (Bentsen, 1978; Demetre et al., 1981). Similarly, one may

expect a dependence of  $K_{wr}$  on flow rate for unstabilized flow. This same dependence was previously observed by Saeedi (1979) who contended that such a dependence may either be due to a different flow regime for lower flow rates or simply due to the fact that a different saturation is assumed to be the irreducible oil saturation for each flow rate. However, he did not establish any irreducible oil saturations for any of his runs but rather he estimated the  $K_{wr}$  values by extrapolation of the pressure data. In the present study, the irreducible oil saturation has been reached by injecting a sufficient amount of water (at least three pore volumes), and the same criterion, i.e., an oil-cut lower than 1% of the total outlet flow, was used for determining that the irreducible oil saturation was reached. Moreover, a volumetric balance on the water injected and produced showed that similar values of irreducible oil saturation were obtained for all the runs (ranging from 79.6% to 81%). Therefore, the differences observed in the present study are most likely due to the fact that, if the displacement is not stabilized, the value of  $K_{wr}$  will continue to vary until a fairly stabilized displacement is established.

As the instability numbers suggest (all numbers less than  $\pi^2$ ), all the displacements of this series were stable. However, the capillary numbers were quite high for the slower flow rates as compared to the value of .01 required for stabilized flow (Bentsen, 1978). Therefore, all the displacements performed in this series of displacements are

expected to be dominated by capillary effects. However, the form of the saturation profiles suggests that capillary forces dominate flow for flow rates less than about 120 cc/hr (See Figures B-1 and B-2). At higher flow rates (starting from 120 cc/hr) the saturation profiles look very similar to Buckley-Leverett profiles even though the capillary numbers are still higher than .01. In this respect, the value of .01 for the capillary number appears to be quite restrictive. Such a comment was made in an earlier study as well (Bentsen and Saeedi, 1981).

The theory suggests that if the flow is not stabilized the JBN method should not be applied (Johnson et al., 1959). Despite this, a comparison is made between the effective permeabilities calculated by the JBN method and those calculated by the dynamic method suggested in the present study, in order to investigate the range of velocities over which the two methods give essentially similar results. The results obtained using the different flow rates are depicted in Figures 6.2 through 6.5. In these figures, the effective permeabilities calculated by the JBN method are shown by smooth curves while those calculated by the proposed method are shown as data points. The reason for this is, for the JBN method, both the recovery and pressure curves are fitted as a function of time and thus, for a given time, the effective permeability is calculated by using smooth functional forms only. On the other hand, for the dynamic method, the recovery curve is fitted as a function of time. The effective permeabilities obtained by the dynamic method

could have been smoothed if the slopes at given points of the pressure profile had been fitted as a function of time. However, this was not done for the present study because of time limitations. It should be noted that the pressure gradients at a particular location in the core decreased monotonically with time and, as a consequence, smoothing of the pressure gradient data probably would not have been difficult.

The proposed dynamic method is applied at two points along the length of the core. These points are chosen such that they are not too close to the inlet or the outlet so as to be able to avoid any end effect on the measurement data. One more advantage of this method is that, as the saturation is estimated by microwave power measurement and not by physical sampling as in the JBN method, lower water saturations may be detected by microwave response and thus a larger portion of the relative permeability curve is obtained by the dynamic method. On the other hand, due to data storage problems, the dynamic method was not continued beyond 2 hours after the front reached the point within the core where the pressures and saturations were being measured, whereas data for the JBN method were collected for a longer period, as it needed no extra data storage. Therefore, for very slow flow rates, the dynamic method covered (because of data storage problems) only the lower portion (below 65% water saturation) of the effective permeability curve. However, for high but stable flow rates, the dynamic method covers almost the whole saturation

range of the effective permeability curves.

At very low flow rates (see Fig. 6.2 and 6.3) where the capillary forces dominate the flow, one can observe that the effective permeability to water as calculated by the dynamic method and by the JBN method are quite close. On the other hand, effective permeabilities to oil do not match very well, even though the difference is smaller at higher water saturations. It is to be noted, however, that the JBN method should not be applied to unstabilized flow such as these two cases where the capillary numbers are quite high. In this respect, a closer agreement between the results by the two methods is not expected. Regardless, an explanation as to why the oil permeability curves are more different may be given. That is, the product  $\frac{dP_c}{dS_w} \frac{\partial S_w}{\partial x}$  has been

neglected in the calculation of the effective permeability to oil (see Equation 4.21) and neglect of this term may not be justified, especially at low values of saturations where  $(dP_c/dS_w)$  and  $(\partial S_w/\partial x)$  are both quite high. As a consequence, the actual effective permeability would be somewhat smaller than that predicted by the dynamic method used here. This suggests that if the  $(dP_c/dS_w)(\partial S_w/\partial x)$  term were not neglected there would be a better agreement in the oil permeabilities calculated by the two methods. However, calculation of this term requires knowledge of how capillary pressure varies with saturation in a dynamic situation, as there are doubts that capillary pressure data acquired in an equilibrium experiment would be applicable to a dynamic



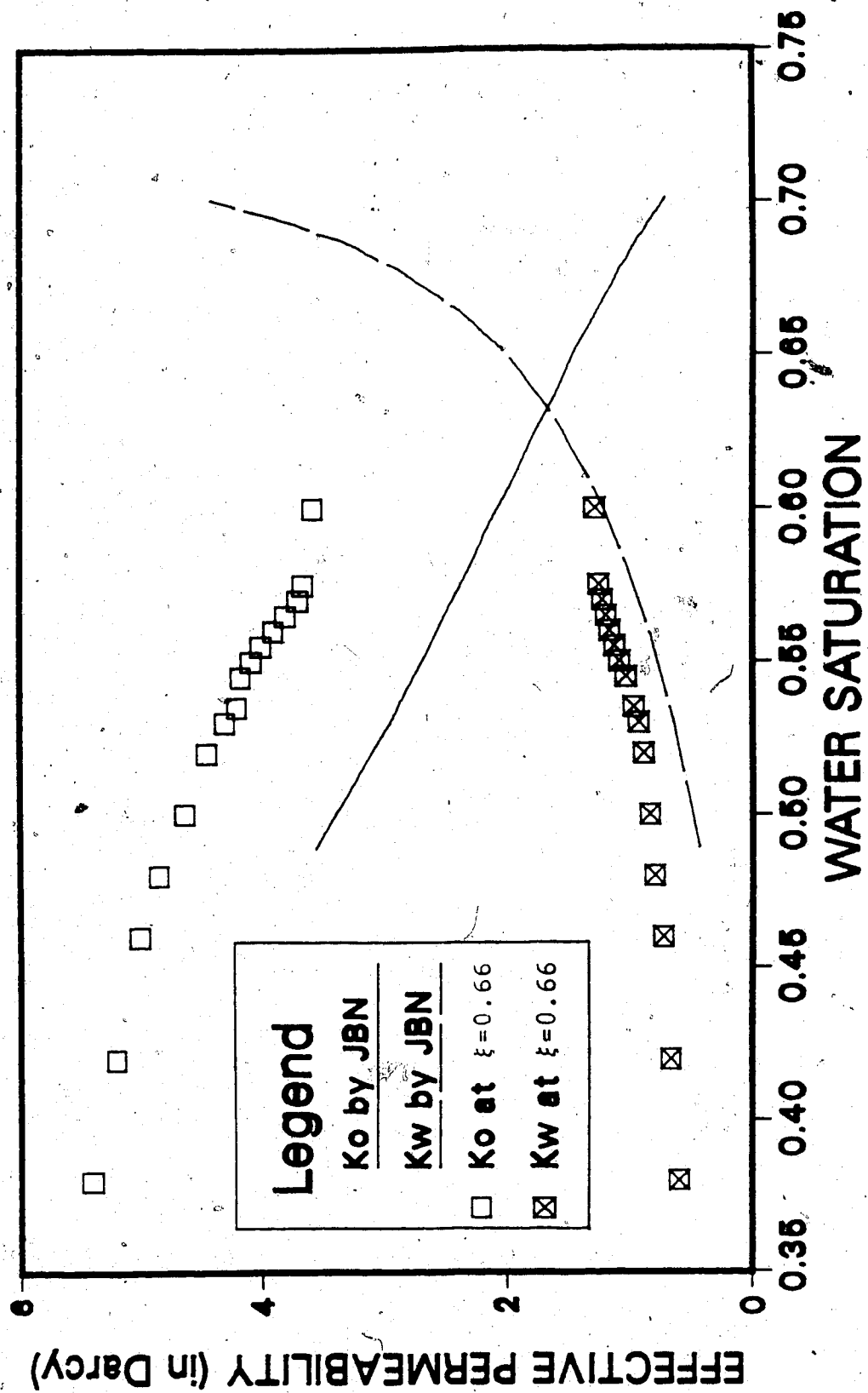


FIG. 6.2 COMPARISON BETWEEN THE JBN AND THE DYNAMIC METHOD (RUN 1)

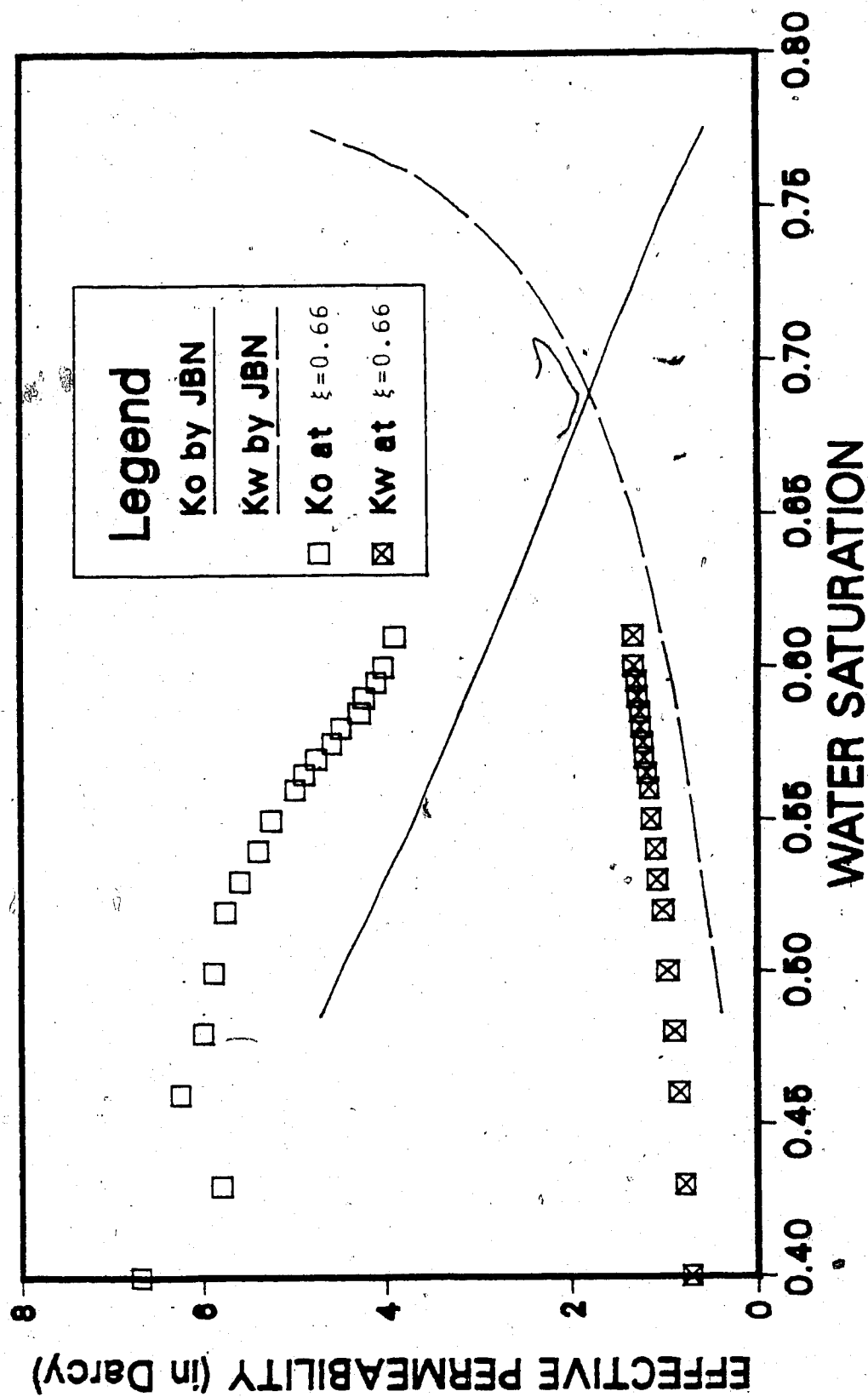


FIG. 6.3 COMPARISON BETWEEN THE JBN AND THE DYNAMIC METHOD (RUN 2)

situation. As the present equipment does not allow the measurement of capillary pressure in dynamic situation no effort was undertaken to estimate the correction term.

It is usually accepted that the JBN method is applicable when the flow regime is stable and stabilized. Runs 4, 5 and 6 fall into this category. A comparison of Runs 4 and 5 is depicted in Figures 6.4 and 6.5. In these cases the results of the two methods agree quite well. There is no particular trend that would suggest that the inclusion of the  $(dP_c/dS_w) \cdot (\partial S_w/\partial x)$  term would have given better agreement. This neglect of the product  $(dP_c/dS_w) \cdot (\partial S_w/\partial x)$  would appear to be justified, provided the displacement is stable and stabilized. It is to be noted, however, that the capillary numbers of these runs are still higher than 0.01, the theoretical value required for stabilized flow. Runs with still lower values of capillary number are performed with other displacement fluids. They will be discussed in the following section.

Theory suggests that if the pressure and saturation do not vary appropriately along the length of the core, there may be substantial differences between effective permeabilities determined at different points along the length of the core. For this reason, the effective permeabilities were obtained at two different points for the flow rate of 150 cc/hr (Run 5). At this flow rate, the capillary number for the total system indicates that the displacement is close to stabilization. Figure 6.6 compares the effective permeabilities calculated at two different

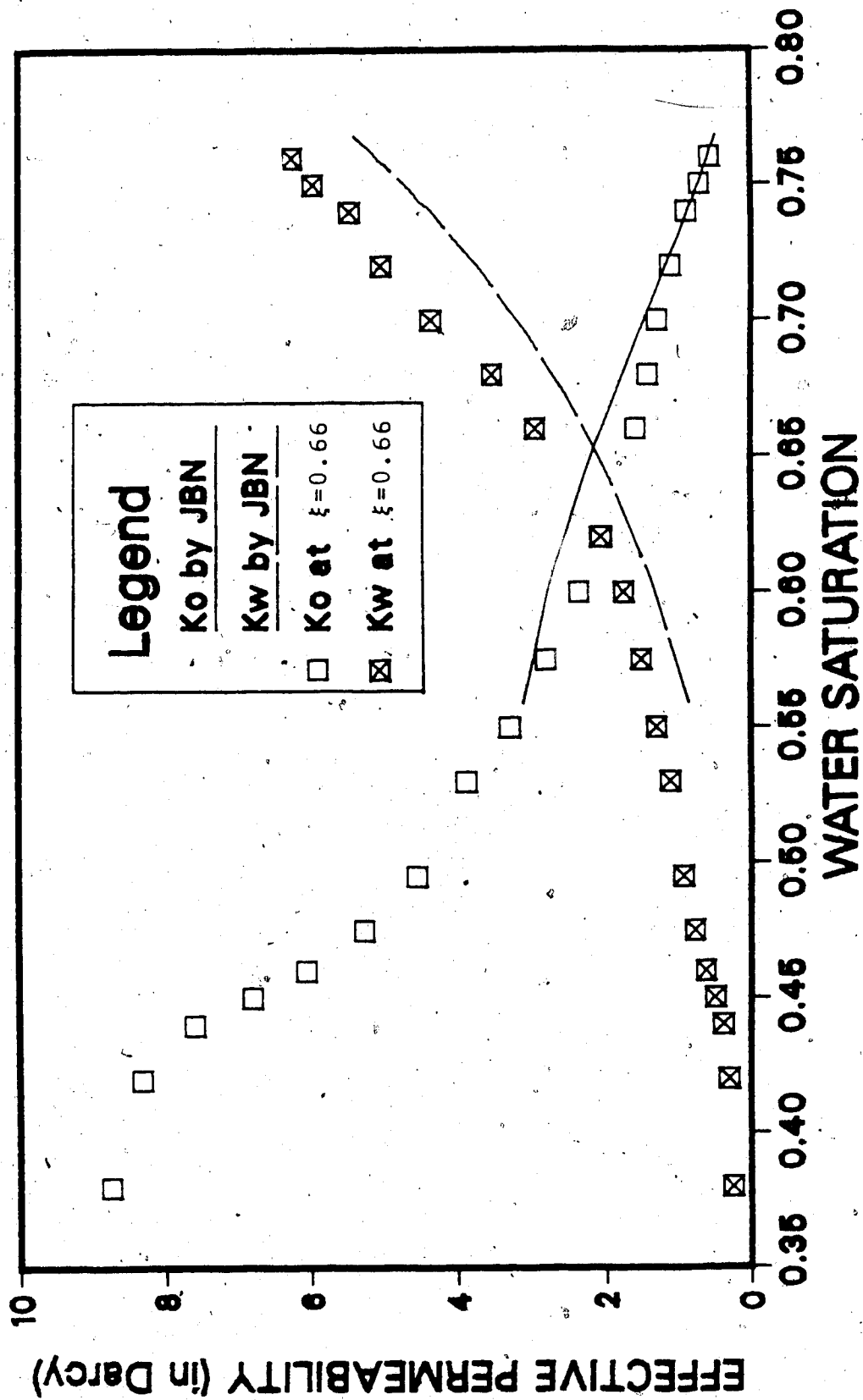


FIG. 6.4 COMPARISON BETWEEN THE JBN AND THE DYNAMIC METHOD (RUN 4)

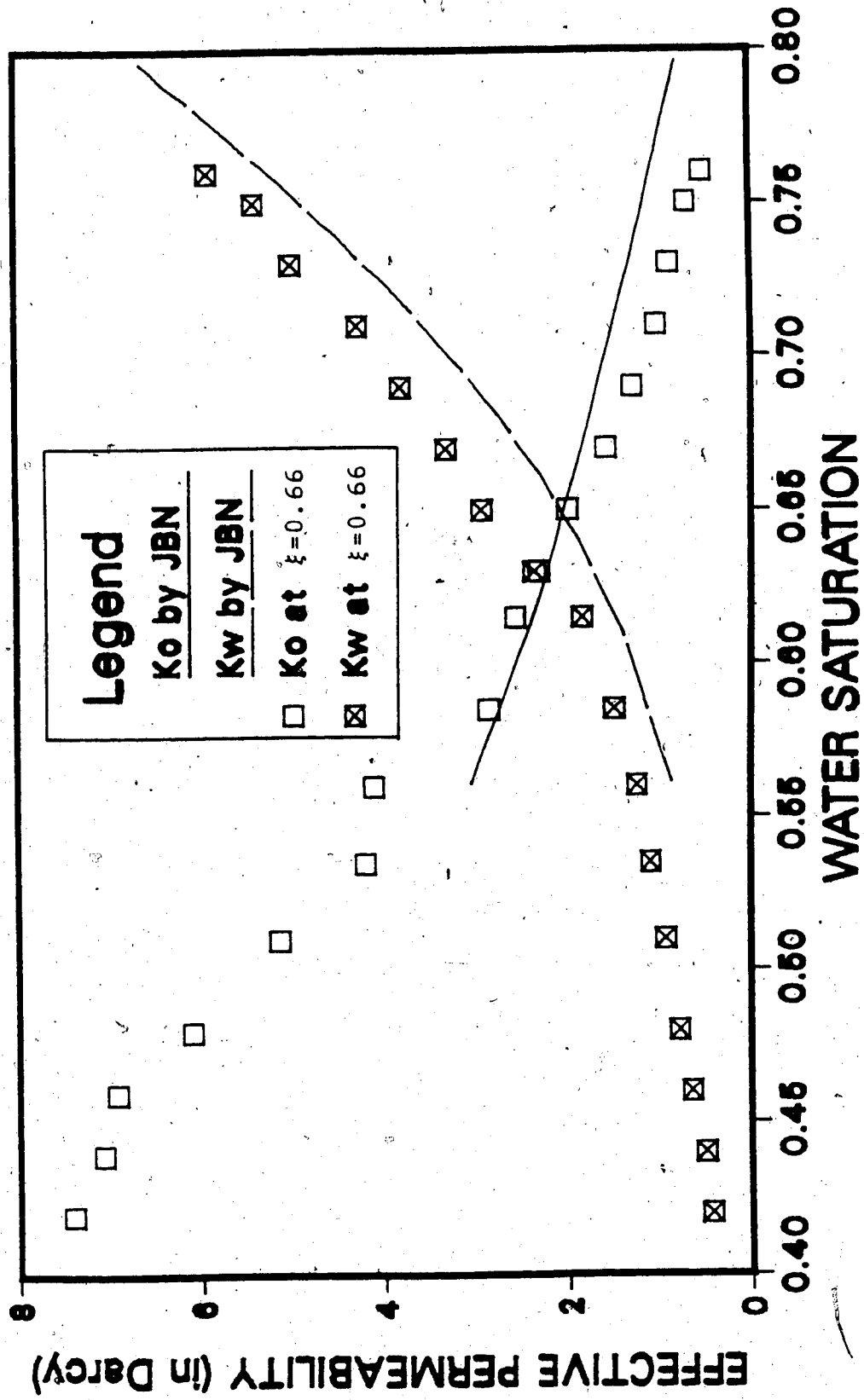


FIG. 6.5 COMPARISON BETWEEN THE JBN AND THE DYNAMIC METHOD (RUN 5)

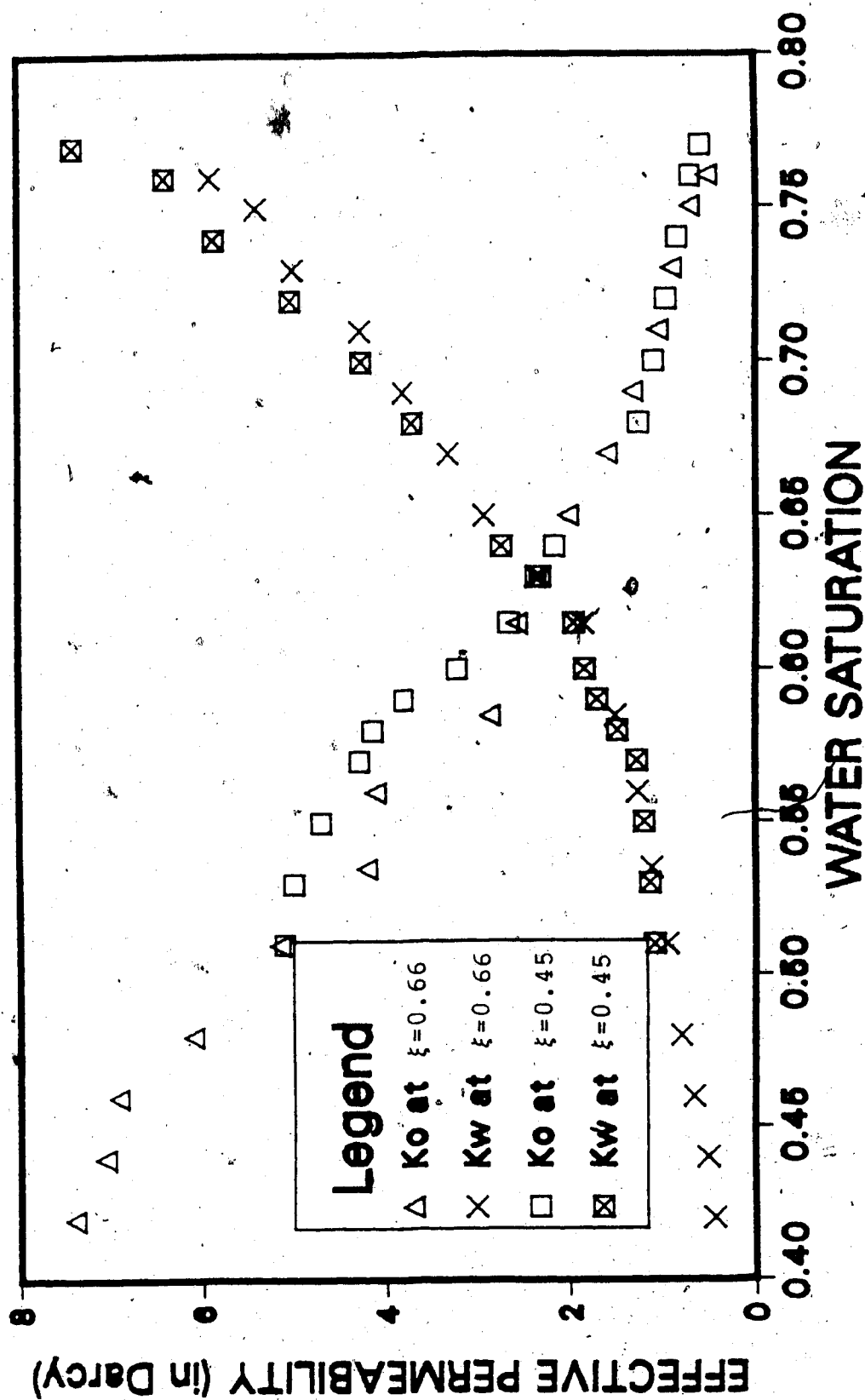


FIG. 6.6 EFFECTIVE PERMEABILITIES AT TWO DIFFERENT POINTS (RUN 5)

points along the length of the core. Because these two different points have different effective lengths, they also have different capillary numbers. Nevertheless, the fairly close agreement in effective permeabilities suggests that, at least for this flow regime, the effective permeability is invariant in space and hence, a unique function of saturation. This observation confirms the theoretical expectation in the stable and stabilized flow regime.

## 6.2 DOW CORNING OIL DISPLACEMENT

The properties of the fluids and cores used in this displacement are reported in Table 6.3. For this particular oil, only one displacement run was performed. The main reason for performing this particular run was to use a different viscosity ratio ( $\mu_o/\mu_w$ ) and a more stabilized flow. An unstable flow regime was not possible to achieve even with this fluid as the effective interfacial tension is relatively high for this fluid. In order to obtain an estimate of the effective interfacial tension, a set of imbibition capillary pressure data was made available by using the "Restored State" method. As was the case for the previously used fluid, the capillary pressure data were curve fitted by using Equation 4.52. Once the capillary pressure data were curve fitted, it was possible to estimate the area under the capillary pressure curve by using Equation 4.53. The parameters of Equation 4.53 after fitting the capillary pressure data of this fluid/water system are reported in Appendix-H. The model equation along

TABLE 6.3

## Characteristics and Results of the Dow-Coring

## Oil Displacement

---

$\mu_o = 9.35 \text{ mPa}\cdot\text{sec}$	$q(\text{oil flood}) = 0.0333 \text{ cc/sec}$
$\mu_w = 1.0 \text{ mPa}\cdot\text{sec}$	(while establishing $S_{wi}$ )
$\rho_o = 934 \text{ kg/m}^3$	$\rho_w = 1000 \text{ kg/m}^3$
$L = 116 \text{ cm}$	$A = 3.7 \text{ cm}^2$
$\sigma = 19.4 \text{ dynes/cm}$	$A_c = 0.016 \text{ atm}$

---

Run No.	$q$ cc/sec*	$K$ ( $\mu\text{m}^2$ )	P.V. (cc)	$S_{wi}$ (%)	$K_{or}$ ( $\mu\text{m}^2$ )	$K_{wr}$ ( $\mu\text{m}^2$ )	$S_{or}$ (%)
7.	0.0555	13.5	171	11	6.8	5.1	81.0

---

\* Waterflood



with the capillary pressure data are depicted in Figure 6.7. Now, as the area under the capillary pressure curve is known for at least two fluids (Dow-Corning and MCT5+LAGO), it was possible to check the relationship between  $A_c$  and the interfacial tension of the oil/water system as determined by the Pendant Drop technique. It was found that the area under the capillary pressure curve, and hence the effective interfacial tension, is approximately proportional to the interfacial tension of the water/oil system. This observation was also reported previously by Peters (1979). Therefore, the proportionality constant between  $A_c$  and the interfacial tension was determined for the Mineral oil by averaging those of MCT5+LAGO and Dow-Corning oil. As the interfacial tension for the Mineral oil/water was known it was possible to estimate  $\sigma_e$ , using Equation 4.51, for the Mineral oil/water/sand system by knowing the interfacial tension between Mineral oil and water.

Once the effective interfacial tension for this oil/water/porous medium was known, it was possible to determine the capillary number and instability number by using Equations 2.4 and 4.50, respectively. These values are reported in Table 6.2.

A flow rate of 120 cc/hr was used to establish the irreducible water saturation. As was the case in the previous series of runs, oil was injected until the water-cut was reduced below 1% of the total outlet flow. An oil injection of 4 pore volumes was required to reach this criterion. At this point the microwave response became

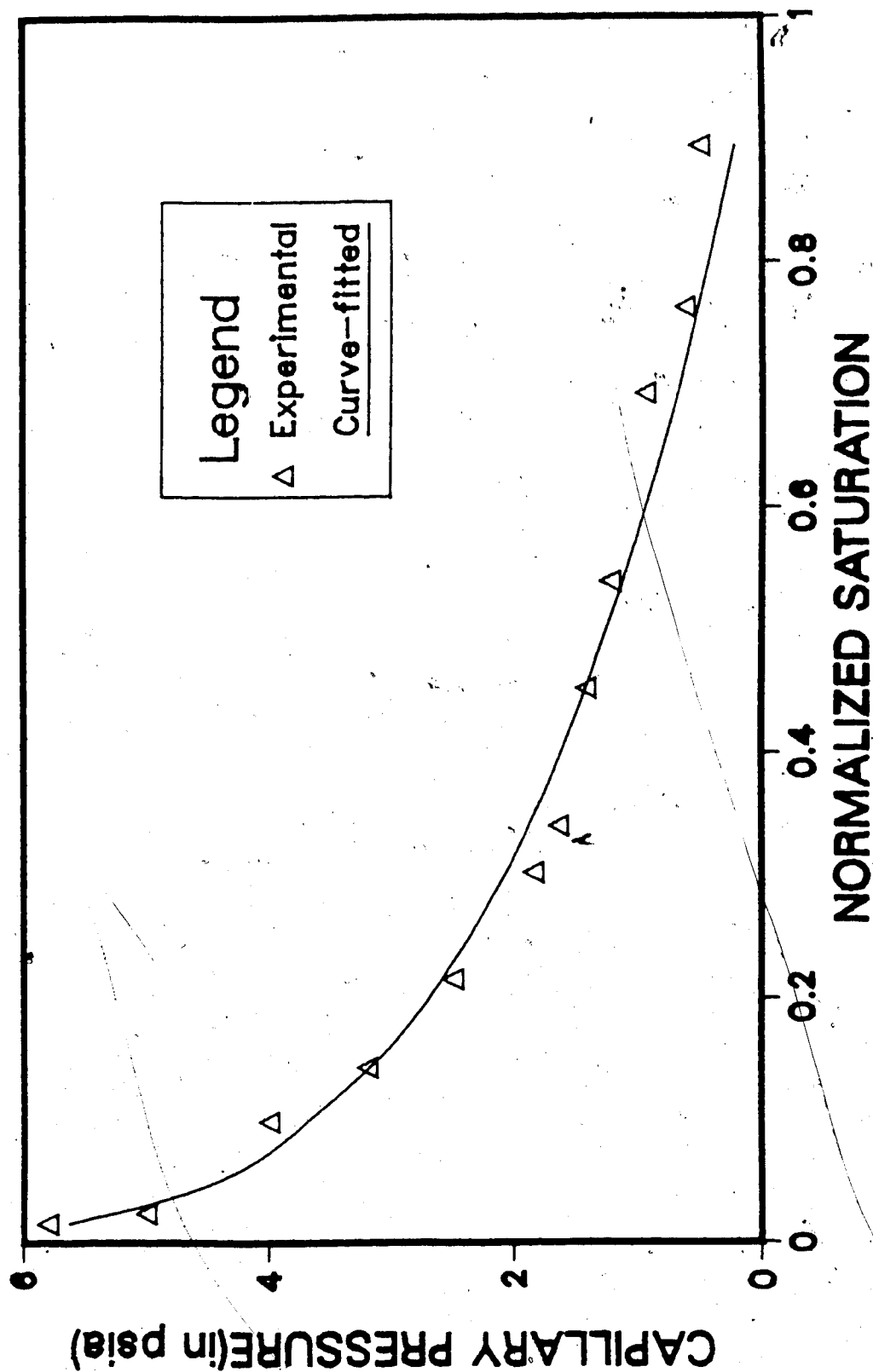


FIG. 6.7 CAPILLARY PRESSURE CURVE FIT FOR DOW-CORNING OIL

invariable with time and therefore a constant irreducible water saturation was assumed to have been reached. The irreducible water saturation value was then calculated by volumetric balance on the oil injected. This value is reported in Table 6.3. This value (11%) is the same as previously observed for the MCT5+LAGO oil. However, the two oils did not have very different viscosities and the effective interfacial tensions were fairly close.

The waterflood was continued at 200cc/hr until the oil cut dropped below 1% of the total outlet flow. At this point the microwave response became constant with time and the irreducible oil saturation was assumed to have been reached. The effective permeability to water at irreducible oil saturation is reported in Table 6.3. This value is very close to that obtained with MCT5+LAGO oil. However, it is slightly lower than that of the stable and stabilized flow of MCT5+LAGO oil. This difference is not sufficient to justify making any comment on the dependence of  $K_{wr}$  on the viscosity ratio.

The instability number suggests that the displacement was stable. Also the capillary number is relatively small showing that the displacement was close to stabilization. The saturation profiles of this run suggest that the displacement was of the Buckley-Leverett type (See Figure B-5). These saturation profiles, therefore, confirm the theoretical expectation of stable and stabilized flow.

Effective permeabilities were calculated by the JBN method as well as the dynamic method. Figure 6.8 depicts

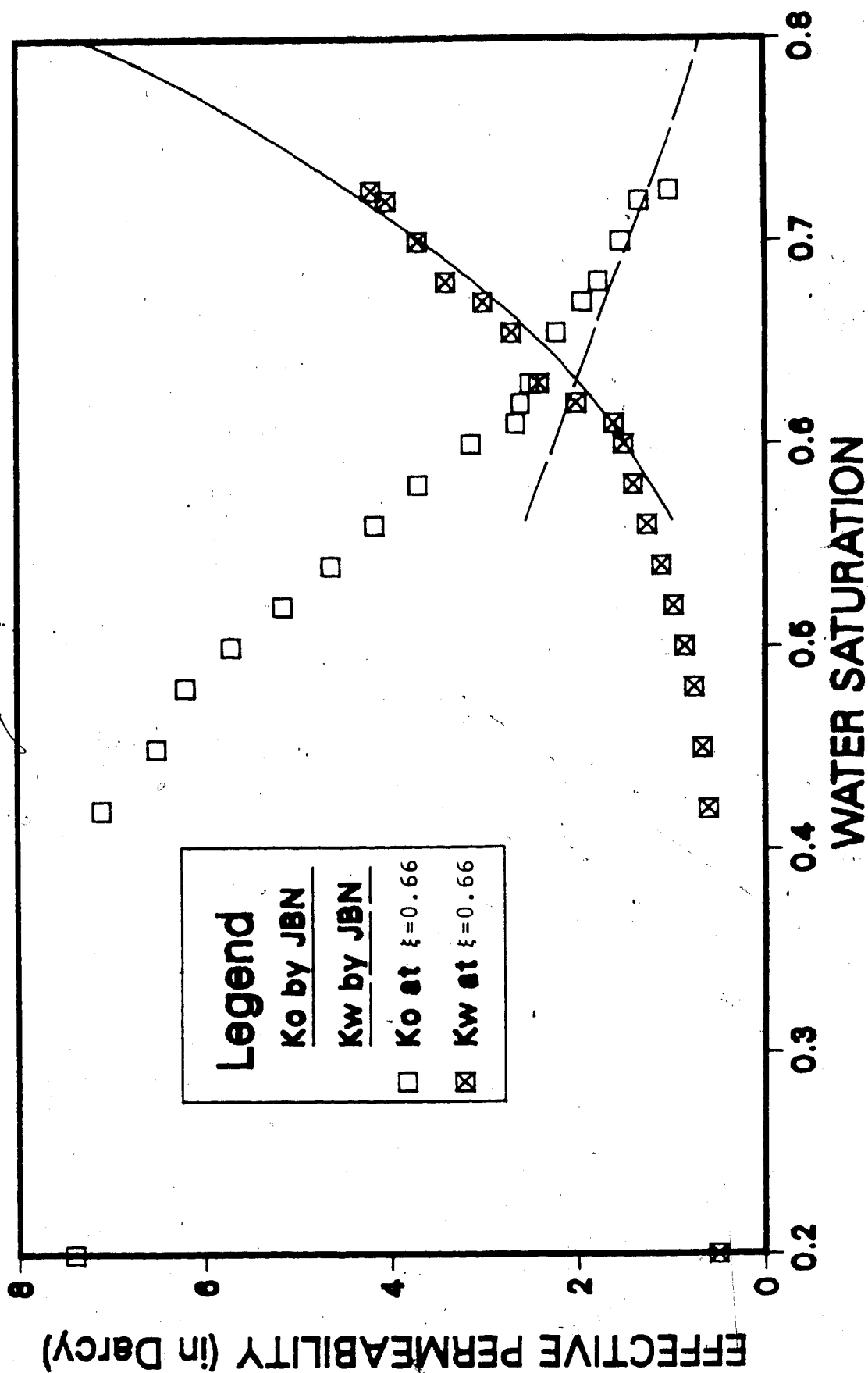


FIG. 6.8 COMPARISON BETWEEN THE JBN AND THE DYNAMIC METHOD (RUN 7)

the comparison of the effective permeabilities as calculated by the two methods. The permeabilities as calculated by the two methods are fairly close. However, the agreement in oil permeability values is better for higher values of saturation. It seems that a better agreement in oil permeability would occur if the  $(dP_c/dS_w) \cdot (\partial S_w/\partial x)$  term were included in the calculation. In order to check how the effective permeabilities vary along the length of the core, the effective permeabilities were obtained at two different points for this particular run. Figure 6.9 compares the effective permeabilities calculated at two different points along the length of the core. Because these two different points have different effective lengths, they also have different capillary numbers. Even though these points have different capillary numbers, the agreement in effective permeabilities is fairly close. As in the case of MCT5+LAGO oil, the effective permeability is invariant with space for stable and stabilized flow. This observation reconfirms that the dynamic method is consistent in calculating effective permeabilities in the stable and stabilized flow regime.

### 6.3 MINERAL OIL DISPLACEMENT

One of the major objectives of the present study was to estimate relative permeabilities during unstable displacements. As the previously mentioned fluids had properties such that an unstable displacement was impossible to reach with the existing equipment (as the required flow

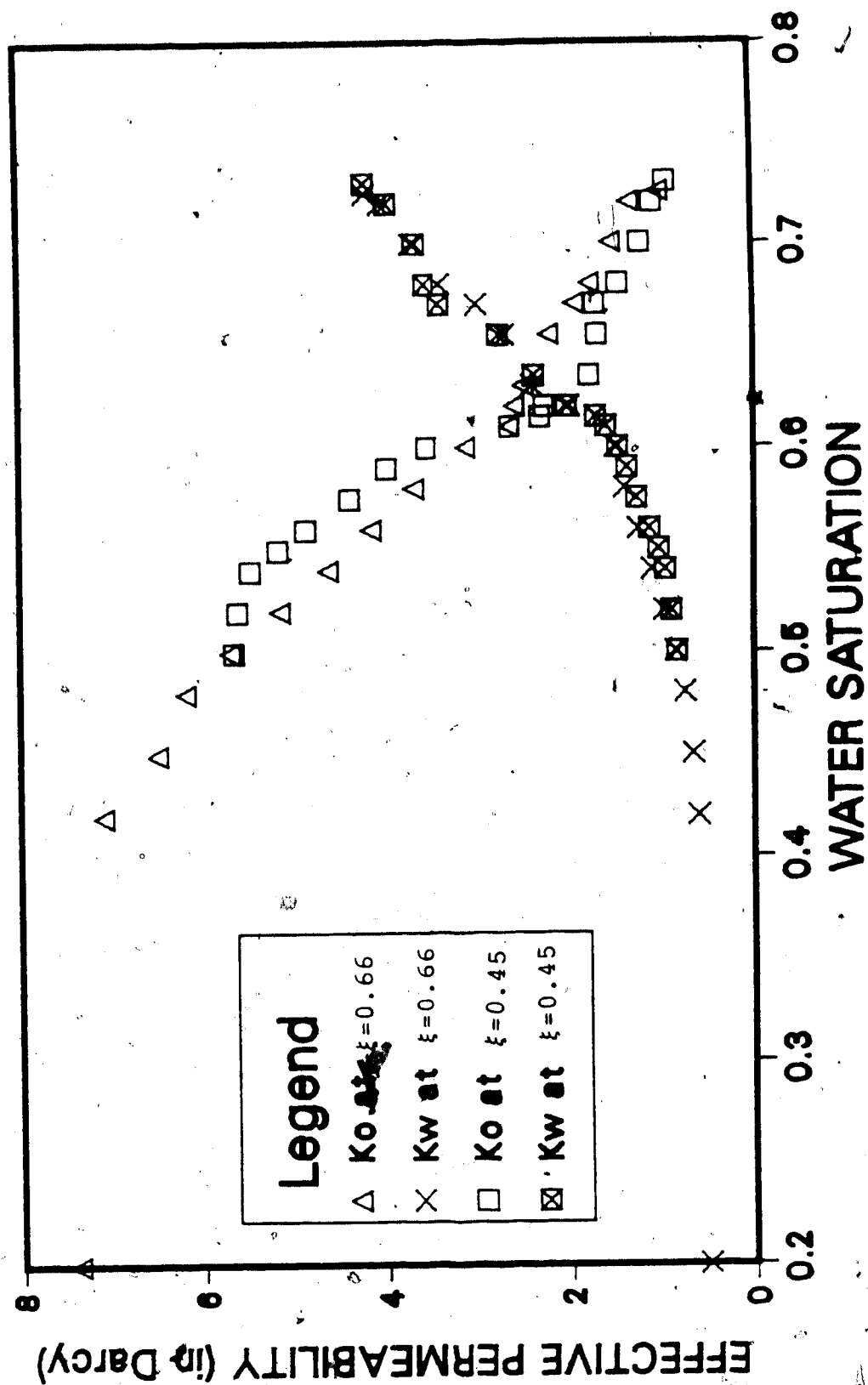


FIG. 6.9 EFFECTIVE PERMEABILITIES AT TWO DIFFERENT POINTS (RUN 7)

rate would cause excessive pressure at the inlet end of the core), a new fluid with a high viscosity and a relatively lower interfacial tension had to be chosen. For this purpose, a mixture of paraffin oil and heptane was prepared. The fluid properties are reported in Table 6.4. For this particular fluid, a set of capillary pressure data was not available. However, this was not felt necessary as the other two sets of capillary pressure data showed that the area under the capillary pressure curve could be considered as being linearly proportional to the interfacial tension of the oil/water system. Therefore, a theoretical estimate of the area under the capillary pressure curves could be obtained by knowing the interfacial tension of this oil/water system. This enabled the estimate of the effective interfacial tension of the oil/water/porous media system. Once the effective interfacial tension was estimated, the instability number and the capillary number could be calculated as well. These values for these displacement runs (Runs 8-10) are reported in Table 6.2.

In order to establish the irreducible water saturation an oil flow rate of 120 cc/hr was used. The oilflooding was continued until four pore volumes of oil was injected when the water-cut fell below 1 % of the total outlet flow and the microwave response became constant with time. At this point, the irreducible water saturation was assumed to have been reached. These values are reported in Table 6.4. These values are the same as those obtained with the previous oils. However, the mineral oil has a viscosity

TABLE 6.4

Characteristics and Results of the Mineral Oil  
Displacement

$\mu_o = 35 \text{ mPa}\cdot\text{sec}$	$q(\text{oil flood}) = 0.0333 \text{ cc/sec}$
$\mu_w = 1.0 \text{ mPa}\cdot\text{sec}$	(while establishing $S_{wi}$ )
$\rho_o = 850 \text{ kg/m}^3$	$\rho_w = 1000 \text{ kg/m}^3$
$L = 116 \text{ cm}$	$A = 3.7 \text{ cm}^2$
$\sigma = 11 \text{ dynes/cm}$	$A_c = 0.01 \text{ atm(estimated)}$

Run No.	$q$ cc/sec*	$K$ ( $\mu\text{m}^2$ )	P.V. (cc)	$S_{wi}$ (%)	$K_{or}$ ( $\mu\text{m}^2$ )	$K_{wr}$ ( $\mu\text{m}^2$ )	$S_{or}$ (%)
8.	0.0333	13.8	172	11	11.9	4.7	79.8
9.	0.0389	13.5	171	11	12.0	5.0	80.4
10	0.0444	13.7	173	11	12.0	5.5	80.1

\* Waterflood



much higher than that of the Dow-Corning or MCT5+LAGO. Therefore, one may conclude that the irreducible water saturation was independent of the viscosity ratio. However, the  $K_{or}$  values for this series of runs were significantly higher than those obtained in previous runs. Such an observation was also made by Saeedi (1979) who also used a very viscous oil. While establishing the irreducible water saturation, the displacement is more stable for a more viscous oil. Therefore, the  $K_{or}$  values as reported for mineral oil may be the correct ones. As already mentioned in the previous chapter, if the effective permeability is estimated using the inlet pressure measured just outside the inlet face of the core (rather than just inside), the estimated effective permeability may not be correct. As a consequence the pressures inside the core should have been used. This was not possible in the present study as the pressure was measured only outside the core and the pressure profile was made available only during waterflooding.

As the instability numbers for the different runs suggest, all the displacements in this series were unstable. However, Run 8 was almost on the stability boundary. Runs 8 and 9 were supposed to be unstable. The saturation profiles for these runs are quite perturbed and do not appear as Buckley-Leverett type profiles (See Figures B-6 to B-8). This shows the validity of the predic of the recently developed stability theory (Bentsen, 1985a).

It is thought that the JBN method is not applicable in the unstable displacement regime. However, the dynamic

method is capable of obtaining relative permeabilities in unstable displacements. Even though the saturation profiles are not monotonic in these cases, an average may be taken in order to estimate the fractional flow at a given point of the core. The average is taken, as for other runs, by integrating the experimental data numerically and then by curve fitting the resulting fractional flow values as a function of time. The resulting effective permeabilities are plotted along with those calculated by the JBN method in Figures 6.10 to 6.12. As the figures show, the comparison is good only for the water permeabilities. For the oil permeabilities, the dynamic method predicts lower values than those calculated by the JBN method. This observation is in contrast to that observed in unstabilized or stabilized and stable flow, where the dynamic method calculated somewhat higher oil permeabilities than those calculated by the JBN method. As the predicted oil permeabilities are smaller, a correction for the  $(dP_c/dS_w)(\partial S_w/\partial x)$  term would only increase the difference unless the correction term is negative, which is possible only at local points in unstable displacements. Moreover, any correction would involve the calculation of  $dP_c/dS_w$ , and there are doubts if the capillary pressure curves as obtained under static and equilibrium conditions would be applicable to dynamic, unstable cases. Consequently no further attempt to make the above correction was taken in the present study.

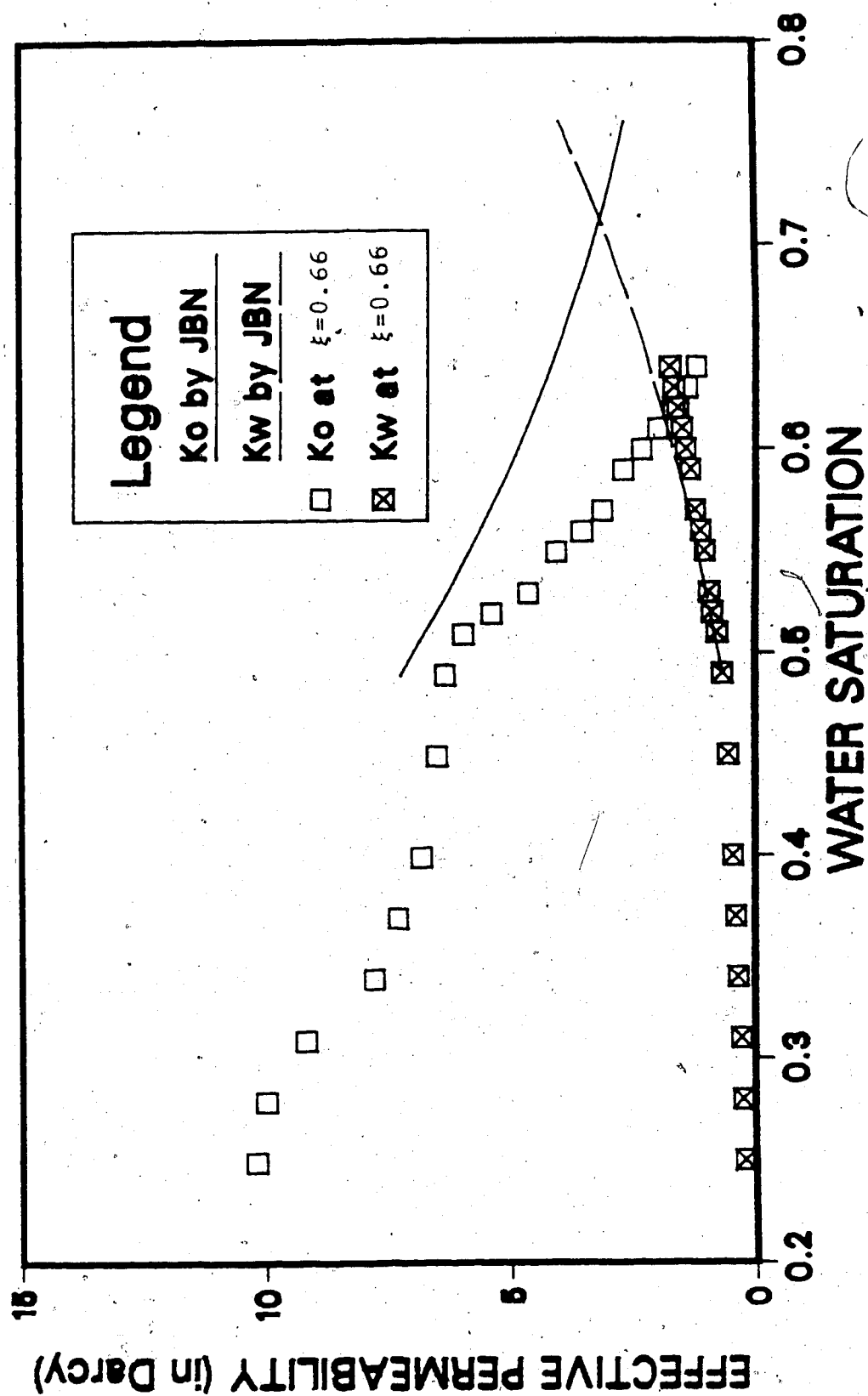


FIG. 6.10 COMPARISON BETWEEN THE JBN AND THE DYNAMIC METHOD (RUN 8)

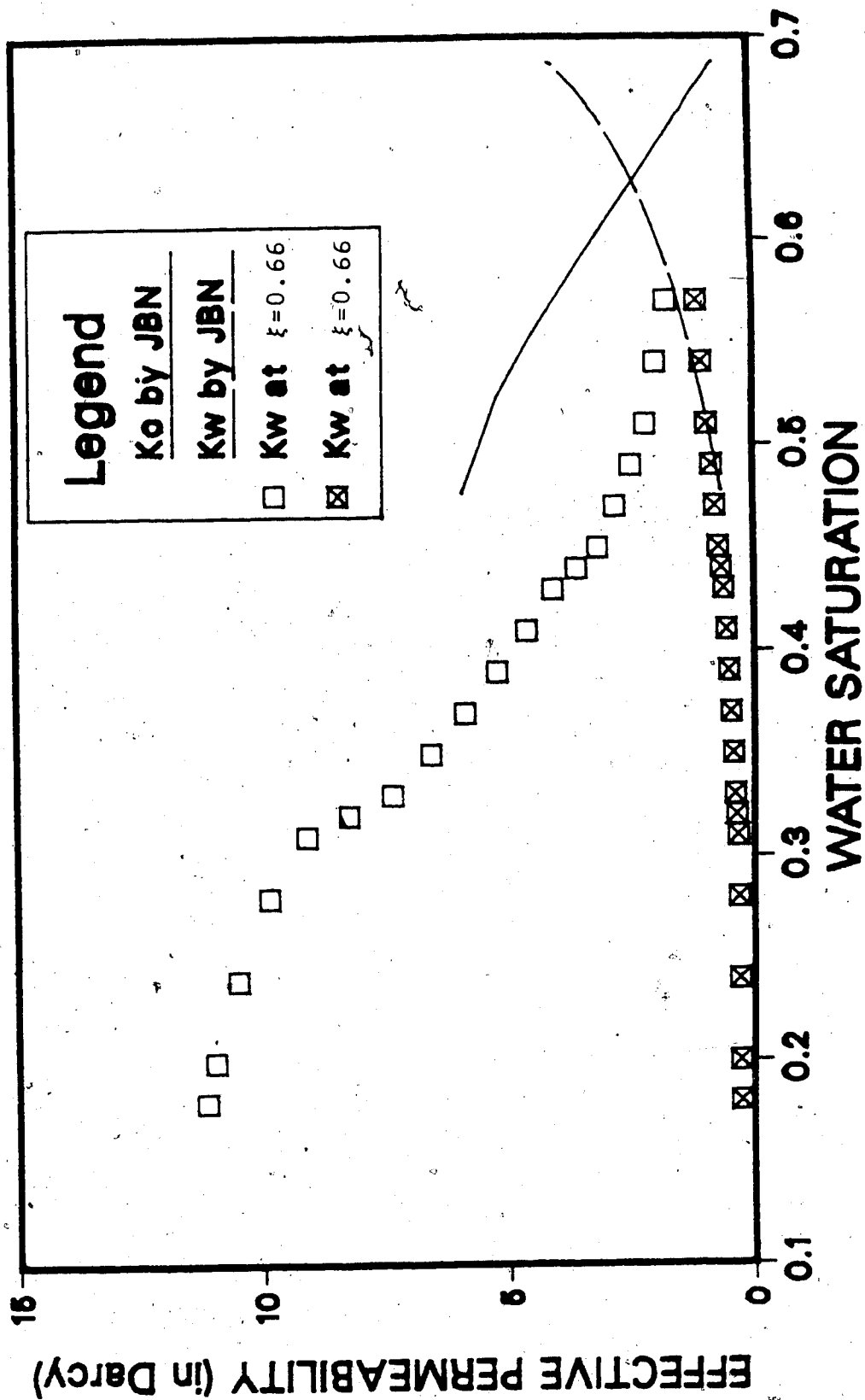


FIG. 6.11 COMPARISON BETWEEN THE JBN AND THE DYNAMIC METHOD (RUN 9)

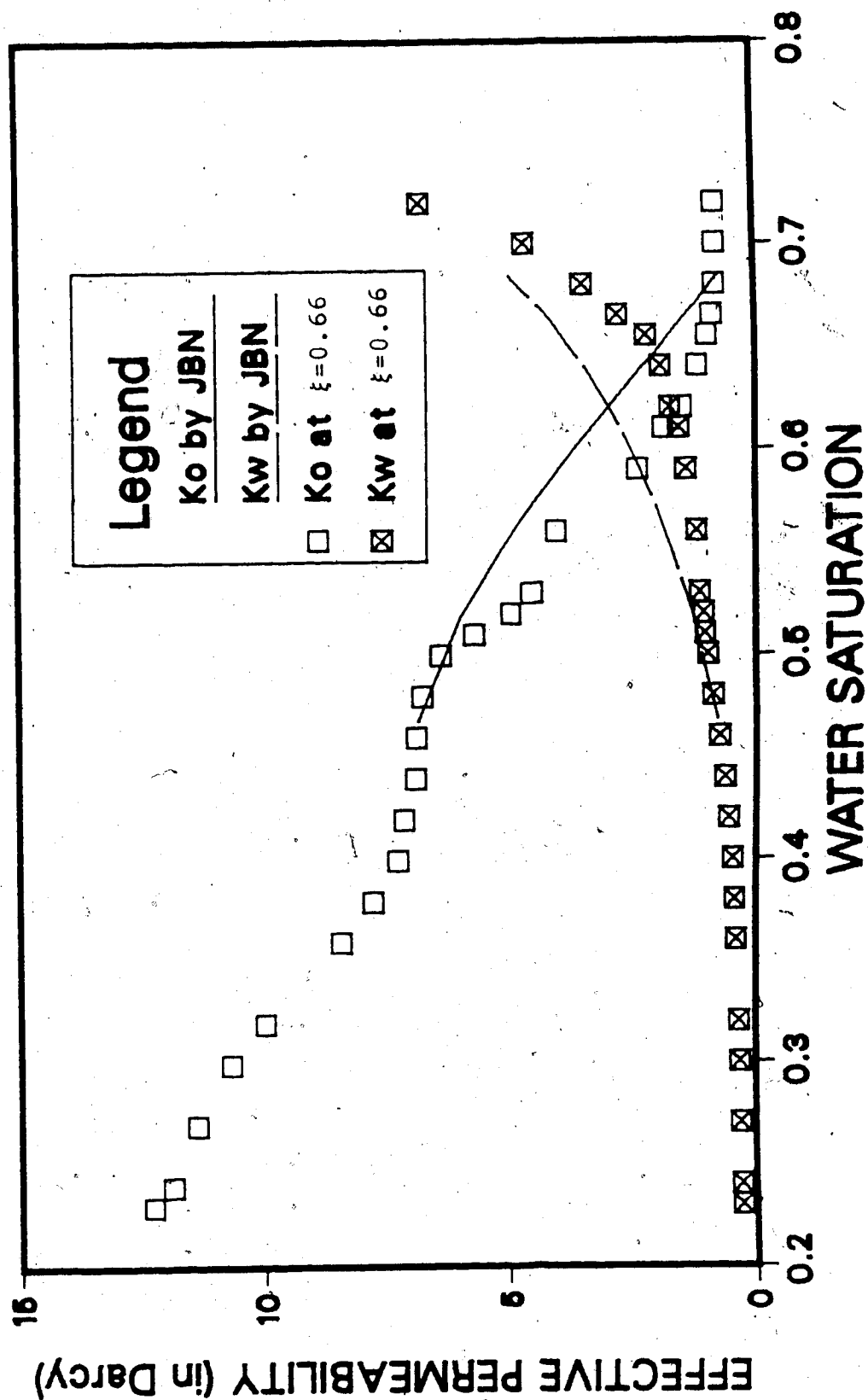


FIG. 6.12 COMPARISON BETWEEN THE JBN AND THE DYNAMIC METHOD (RUN 10)

It has not been confirmed that any unique set of relative permeability curves would properly define the displacement process in the unstable displacement case. One of the objectives of the present study was to observe if the effective permeabilities were unique functions of saturation even when the displacement was unstable. Figure 6.13 shows the effective permeabilities at two different points for a flow rate of 120 cc/hr. For this particular run, the instability number is very close to the stability boundary. Figure 6.13 shows that both the oil and water permeability curves are fairly close for both positions, confirming that the effective permeabilities do not vary much along the length of the core. However, for Run 9 (140 cc/hr), even though the water permeabilities are very close for both positions (Figure 6.14), the oil permeability curve is different at both locations. This difference in oil permeability at different points along the length of the core suggests that the effective permeability to oil may not be a unique function of saturation when the displacement is unstable. Figure 6.15 shows the effective permeabilities at two different points for Run 10 (170 cc/hr). Once again the effective permeabilities to water, at intermediate values of  $S_w$ , seem to be invariant with location. Also, the difference in effective permeabilities to oil for the two locations is less pronounced than is the case for Run 9. As the difference in effective permeabilities to oil is maximum in the case of an intermediate instability number, one can not say that the difference increases as the instability

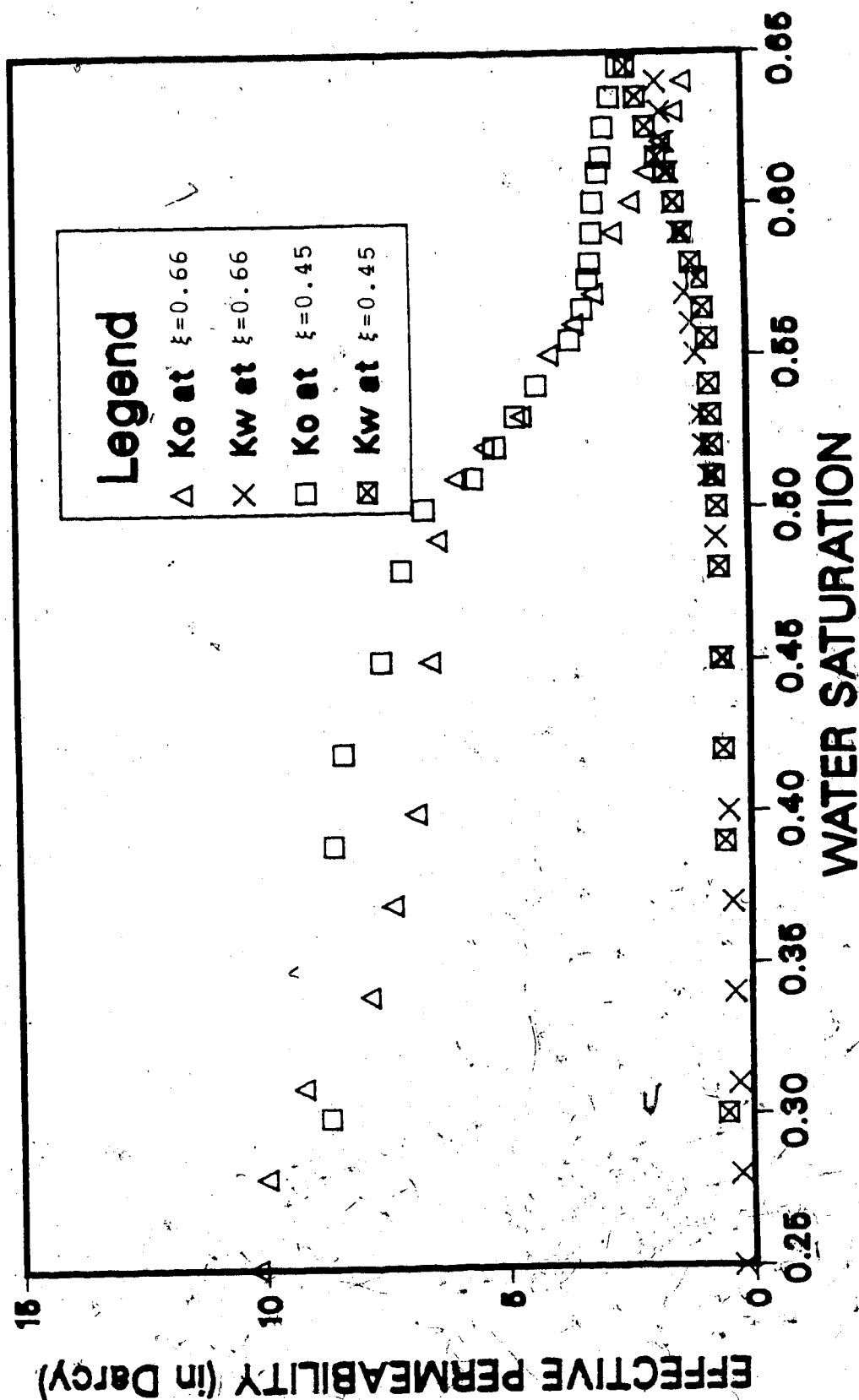


FIG. 6.13 EFFECTIVE PERMEABILITIES AT TWO DIFFERENT POINTS (RUN 8)

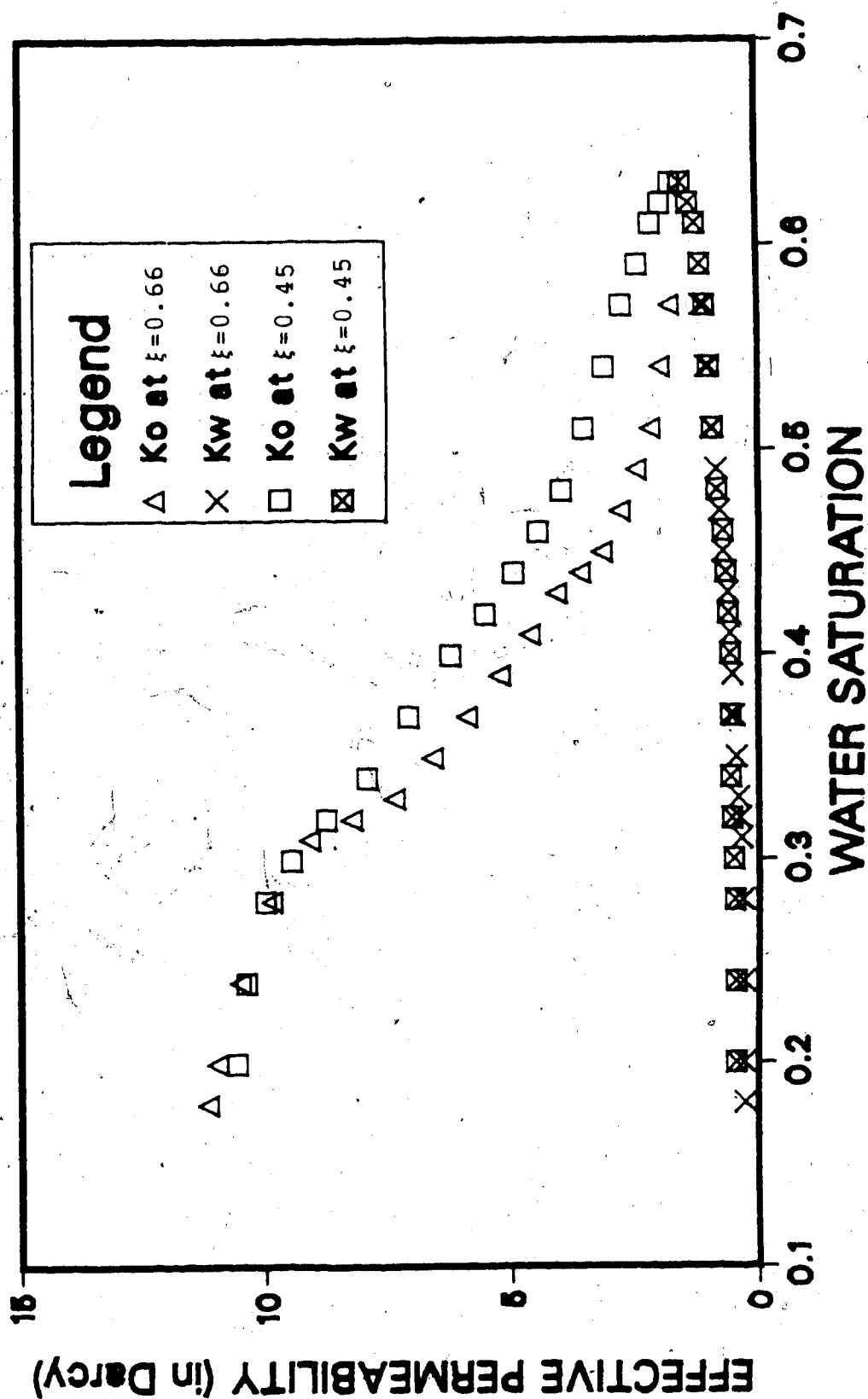


FIG. 6.14 EFFECTIVE PERMEABILITIES AT TWO DIFFERENT POINTS (RUN 9)



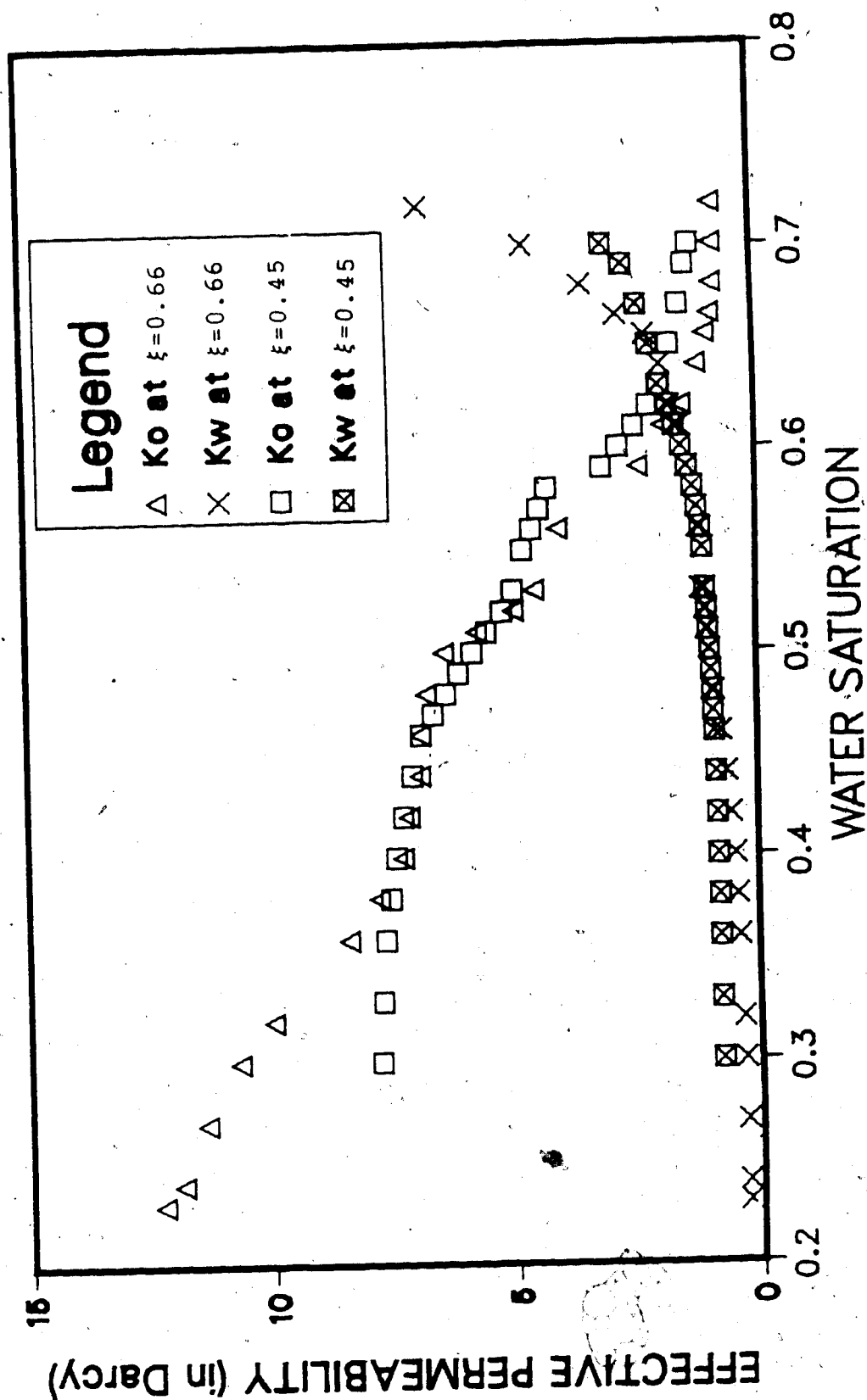


FIG. 6.15 EFFECTIVE PERMEABILITIES AT TWO DIFFERENT POINTS (RUN 10)

number increases. This difference appears to be probabilistic once the flow regime becomes unstable.

Different permeabilities at different locations along the length of the core are most likely due to heterogeneity effects. It has been shown for the Hele-Shaw model (Coskuner and Bentsen, 1985) that as the flow regime becomes more and more unstable the flow behaviour becomes more chaotic and the effect of heterogeneity is more pronounced. Similar behaviour is expected for porous media and thus as the viscous forces take over, the effect of heterogeneity is more and more pronounced. However, no particular trend is observed in terms of the distance of the considered point from the inlet end. For Run 9, the oil permeability is higher at  $\xi = 0.45$  than that at  $\xi = 0.66$ , whereas for Run 10, the oil permeability is higher at  $\xi = 0.66$  than at  $\xi = 0.46$ . As the capillary pressure curve is obtained under equilibrium conditions and as the displacement is taking place under dynamic conditions, there seems to be little justification in applying the  $(dP_c/dS_w)(\partial S_w/\partial x)$  correction to the unstable case. However, because of the extremely chaotic behaviour observed when the flow is unstable, there may be a reversal of slope of the  $dP_c/dS_w$  curve. The correction would then improve the agreement between the results as obtained by the dynamic and the JBN methods.

#### 6.4 BREAKTHROUGH RECOVERY VS. RECIPROCAL CAPILLARY NUMBER

The experimental breakthrough recovery may be correlated with the reciprocal capillary number as has been done by Bentsen (1978) and Demetre et al. (1981). They stated that the experimental breakthrough versus reciprocal capillary number curve should asymptotically reach a steady state value. This steady state value is reached once stabilized flow is attained. However, if the flow regime falls into the unstable region the breakthrough recovery drops drastically and a further decrease continues until a very high instability number is reached (Demetre et al., 1981). In order to verify the predicted stability boundary, breakthrough recoveries are plotted against the reciprocal capillary number. This plot is shown in Figure 6.16. As can be seen in the figure, the experimental breakthrough recovery is quite low at lower flow rates. As the capillary number decreases the experimental breakthrough recoveries increase steadily and a fairly constant value is obtained at the lowest capillary numbers, provided the displacement is still stable. However, when the displacement is unstable (Runs 8, 9 and 10), a sudden decrease occurs in the experimental breakthrough values. It is to be noted that these unstable displacement runs have instability numbers higher than  $\pi^2$  and thus they are predicted to be unstable by the recently developed stability theory (Bentsen, 1985a). This observation, therefore agrees with that observed in a previous study (Demetre et al., 1981).

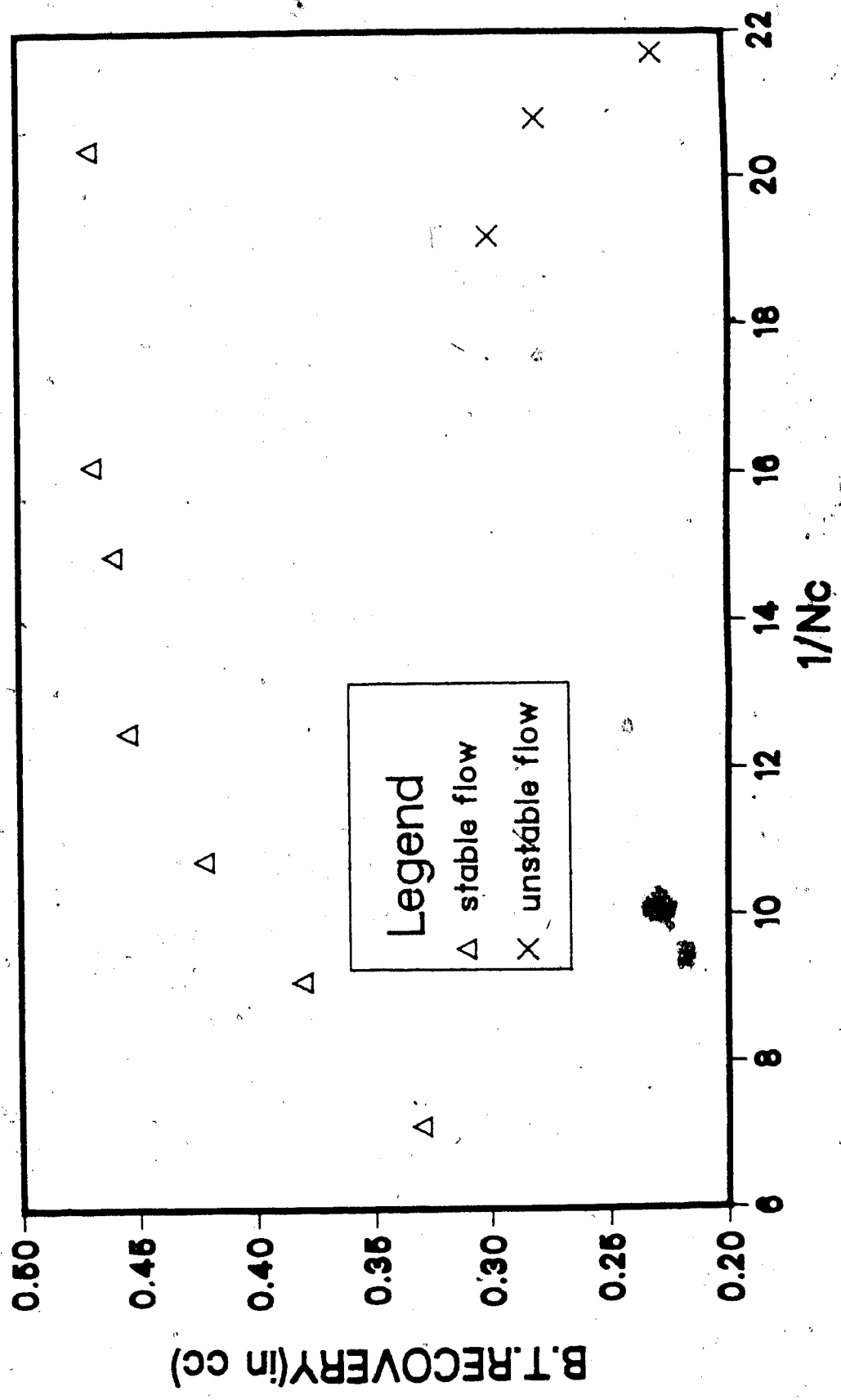


FIG. 6.16 BREAKTHROUGH RECOVERY VERSUS RECIPROCAL CAPILLARY NUMBER

## 6.5 EFFECT OF FLOW REGIME ON EFFECTIVE PERMEABILITY

As the literature survey revealed, many of the researchers did a great deal of work in order to investigate the effect of viscosity, flow rate and interfacial tension on the relative permeability curves. However, none of these factors forms a scaling group alone to govern the flow regime in a displacement test. Therefore, in the present study, the effect of stable, unstable and unstabilized flow regime rather than the effect of independent factors was investigated. Whether a displacement is stable or unstable depends on the instability number that incorporates the effect of viscosity, interfacial tension and the flow rate. However, whether a flow regime is unstabilized or stabilized depends on the macroscopic capillary number (defined by Bentsen, 1978) that incorporates the end point effective permeabilities and the area under the capillary pressure versus saturation curve. The present study enabled checking how the effective permeabilities vary as different scaling groups vary; in other words, how effective permeabilities vary as the flow regime changes. Figure 6.17 shows the effective water and oil permeabilities for all the displacement tests performed. These are the effective permeability values estimated by the dynamic method. As one can see, all the effective water permeabilities fall on the same line, showing no dependence on any of the factors such as flow rate, viscosity, etc., at least over the range of variables studied here. This shows the insensitivity of the effective water permeabilities to viscous or capillary

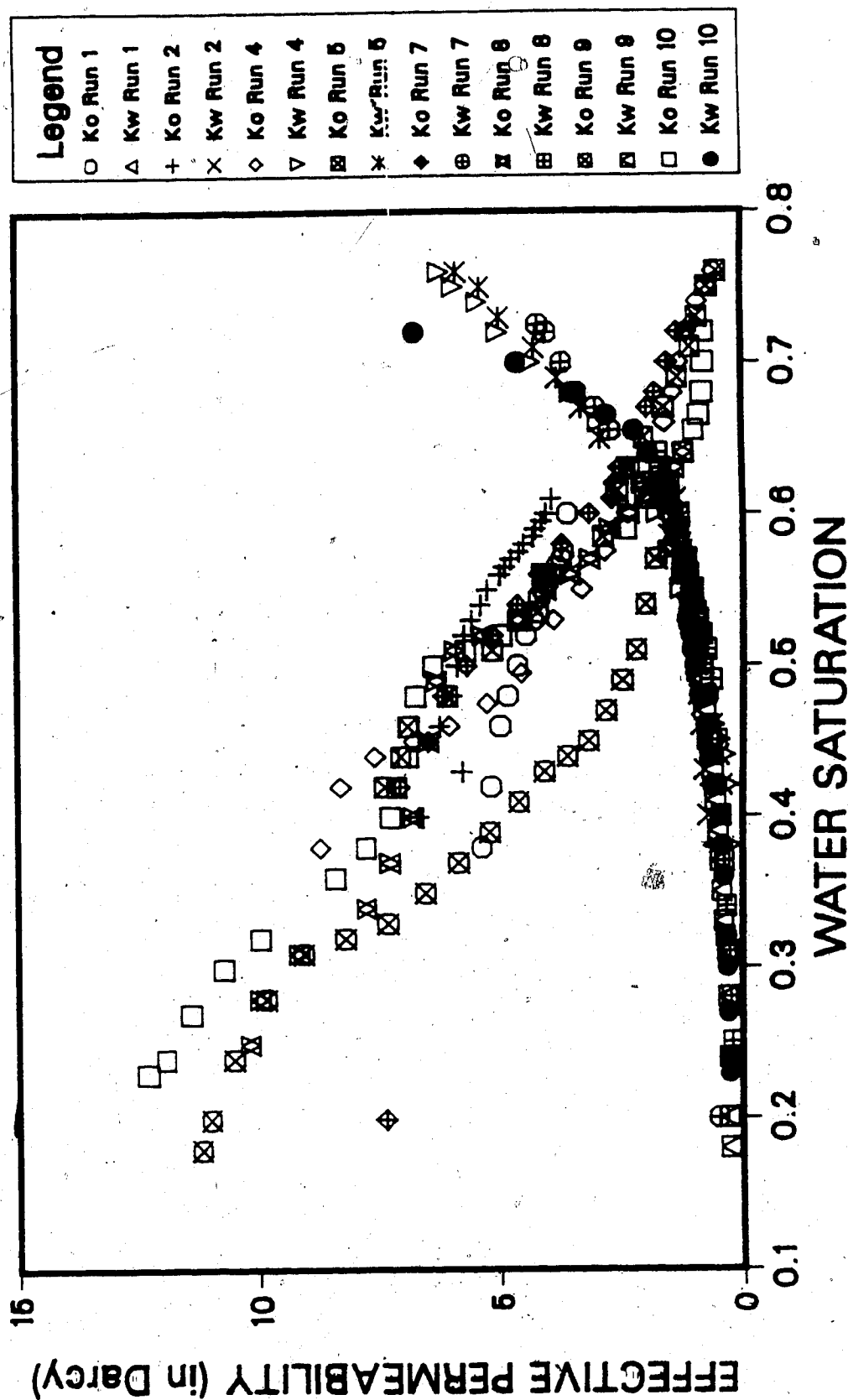


FIG. 6.17 EFFECTIVE PERMEABILITIES FOR DIFFERENT RUNS (DYNAMIC METHOD)

forces. On the other hand, the effective permeabilities to oil are not all the same. The effective oil permeabilities are very similar for Runs 4, 5 and 7 (See Figure 6.18). Runs 4 and 5 were performed with MCT5+LAGO, whereas Run 7 was performed with Dow-Corning. All three of these runs may be categorized as being stable and stabilized displacements. On the other hand, Runs 1 and 2 were unstabilized displacements. Moreover, these two runs have effective oil permeabilities very similar to each other but different from those of stabilized and stable displacements. Effective oil permeabilities for Run 8 fall very close to those of the stable and stabilized displacements. To be noted here is that this particular run has an instability number very close to the stability boundary. Runs 9 and 10 are both unstable. The effective oil permeabilities for Run 9 are consistently lower than those of the stable and stabilized runs. The effective oil permeabilities for Run 10 fall in between those for Runs 8 and 9, showing no particular trend as the saturation increases. One can see that the effective oil permeabilities for the unstable displacements do not correlate well with those of stable displacements, but as the number of unstable runs is limited it is difficult to draw any conclusions on the way effective oil permeabilities for unstable displacements vary as the instability number is increased.

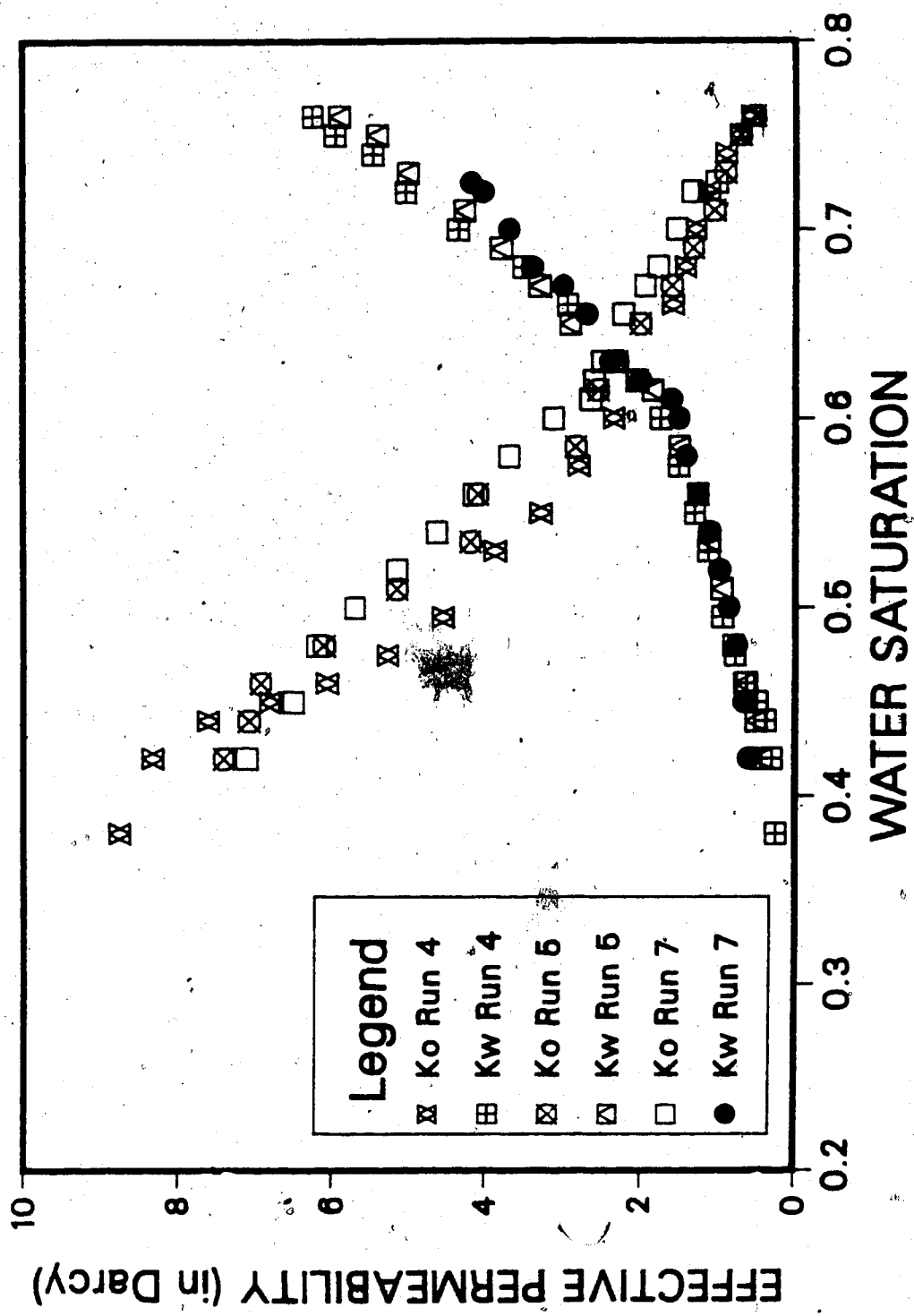


FIG. 6.18 EFFECTIVE PERMEABILITIES FOR STABILIZED AND STABLE RUNS (DYNAMIC METHOD)



## 7. CONCLUSIONS AND RECOMMENDATIONS

### 7.1 CONCLUSIONS

A technique capable of measuring effective permeabilities under all flow regimes has been developed. The effective permeabilities have been estimated using both the conventional JBN method and the proposed dynamic method. The flow regimes have been determined using scaling groups such as the instability number and the capillary number. In order to check the variation in effective permeabilities for all the flow regimes, three different fluids have been used as the displaced fluid along with distilled water as the displacing fluid.

Based on the experimental results presented herein, and keeping in mind the limited range of velocities over which the experiments have been conducted, the following conclusions may be drawn:

1. Equation 4.50, which arises out of recently developed instability theory (Bentsen, 1985a), correctly predicts the boundary between stable and unstable displacements. As a consequence, it may also be inferred that Equation 4.51 correctly predicts the pseudo-interfacial tension for the displacement.
2. The dynamic method, as proposed in this study, predicts the same oil and water permeabilities as predicted by the JBN method, provided the displacement is stable and stabilized. This is consistent with the assumptions

underlying the two methods. However, the dynamic method covers a broader range of saturations than does the JBN method.

3. When the displacement is unstabilized, the dynamic method should not predict the same effective permeabilities as the JBN, as the assumptions underlying the JBN method are violated. Despite this, the dynamic method predicts effective permeabilities to water which are similar to those predicted by the JBN method. However, the oil permeabilities predicted by the dynamic method presented herein are higher than those predicted using the JBN method. Had a correction for the capillary pressure term been included in the dynamic method, closer agreement between the two methods for estimating the oil permeabilities would have been achieved. As no other existing method can predict the effective permeability in the unstabilized flow regime, it was not possible to comment on the quality of predictions of the dynamic method in this flow regime.
4. When the displacement is unstable, the dynamic method predicts water permeabilities similar to those predicted by the JBN method. Thus, contrary to theoretical expectations, the JBN method appears to give reasonable results, provided the instability number is only slightly greater than  $\pi^2$ . However, the oil permeabilities, contrary to the unstabilized case, are lower than those predicted by the JBN method. No attempt was made to assess the impact of the capillary

term on the estimated values for the oil permeabilities, as the effect of capillarity in unstable flow is unknown.

5. The effective permeability to water is invariant with location along the length of the core for all the flow regimes considered. However, the effective permeability to oil depends on location whenever the flow is unstable. Moreover, for unstable flows, the effect of location on oil permeability increases as the flow rate increases. In addition, the way in which the oil permeability is affected does not seem to be related to where along the length of the core the measurement is taken. This suggests that, as the flow becomes unstable, local heterogeneities have a larger and larger impact on the measured oil permeabilities. As a consequence, oil permeabilities may not be unique functions of saturation when the displacement is unstable. As to why the flow regime should affect only the oil permeability, one may give the following explanation. For a water-wet system, water adheres to the rock and resistance to flow is due primarily to the interaction between the water and the adjacent solid. As a consequence, changes in the flow regime appear to have only a marginal effect on the effective permeability to water. On the other hand, the oil phase is surrounded by water-oil interfaces only, provided the porous medium is water wet. Hence, rock-oil interactions should have little if any effect on the

resistance to flow for oil. This, in turn, suggests that changes in flow pattern, brought about by a change in flow regime, have a large impact on the effective permeability to oil.

## 7.2 RECOMMENDATIONS

In order to improve the quality of the present work any future project in a similar direction should consider the following recommendations.

1. The thickness of the core holder used in the present study was 0.75 cm. The thickness was limited by the fact that any increase in thickness would decrease the microwave output signal to a certain point that the power sensor HP-8484 (that was used in the present study) cannot measure it. However, as recently a more sensitive power sensor (HP-8486) has been made available along with the power meter HP-436A, for any future study the thickness of the core holder may be increased up to a thickness of 1.25 cm. As a matter of fact, the thickness should be increased as much as possible to obtain a more representative sample of porous media. Moreover, as the instability number increases with the increase in thickness of the sample, an unstable displacement would be attained more easily with a thicker sample. Therefore, any future study should plan for a core holder of about 1.25 cm thickness.
2. As the form of the saturation profiles suggest, the



present study could not eliminate the end effect problems at the inlet end of the core. In the present study, water or oil was directly injected into the porous system through the inlet; therefore, there was insufficient time for the injected fluid to spread across the total height of the core. This problem might be minimized by introducing a porous glass plate at the inlet end that would disperse the injected fluid rather than creating a jet at the inlet.

3. The present system of automation is not very sophisticated. A computer signal is amplified to activate an electric magnet that makes the contact between the driving chain (run by the d.c. motor continuously) and the bracket containing the core holder. This enables the start of the scanning at the scheduled time, but every time the electric magnet is activated it gives a blow to the core holder-bracket system, and a perturbation is observed in the saturation profiles. Even though this perturbation is not very significant in terms of the fractional flow across a certain point of the core, it is of interest to minimize any perturbations, especially when one has to comment on the stability of the displacement mechanism from the shape of the saturation profile. In order to avoid perturbations of this type, one should use a two-directional motor with an automatic controller. This would enable activation of the motor itself with the computer signal, and the motor would start only when

the signal is given to start scanning.

1. A problem that was encountered in the present study is that the data storage system was not large enough to store the data for a lengthy run (e.g., for the case of a very slow displacement rate). Therefore, data storing capacity should be increased.
5. Determination of the effective permeabilities should be done by the proposed dynamic method at many points along the length of the core to see the trend of any variation, especially in the unstable displacement case. Moreover, if a more pressure-resistant core holder can be built, there should be more investigation on the nature of the effective permeabilities in displacements with very high instability numbers. As the field displacements are believed to have a very high instability number, this investigation would give a feeling for the effective permeabilities in field displacements.
6. The present study did not estimate quantitatively the effect of the  $(dP_c/dS_w)(\partial S_w/\partial x)$  term on the effective oil permeability. Such corrections should be made using capillary pressure data acquired during dynamic displacement rather than using equilibrium capillary pressure data as obtained by the "Restored state" method. Such data could be obtained by estimating the oil and water pressure with the aid of transducers that have diaphragms preferentially wet by oil and water, respectively. This would enable calculation of the

effective oil permeability without any assumption on the capillary pressure data. Moreover, it would be interesting to observe how the oil pressures vary during an unstable displacement.

7. In the present study the JBN method has been used to obtain the effective permeability at the outlet end whereas the dynamic method has been calculated at points inside the core holder. However, an estimation of the effective permeabilities by the JBN method may also be obtained at any point along the length of the core using the fractional flow as obtained by integrating the area under the saturation profiles. If both the dynamic and the JBN method are applied at the same point of the core, there would be more justification in comparing the effective permeabilities as obtained by the two methods. Such a comparison should be made in the future.
8. As has been discussed in the previous chapter, the pressure profile should be obtained not only during the waterflood but also during estimation of the absolute permeability and the irreducible water saturation. This would enable determining whether the permeability varied along the length of the core by applying Darcy's law at different points inside the core. As it was found that the inlet pressure (outside the core holder) was not truly representative of the pressure inside the porous media, the pressures inside the core holder should be obtained during the oilflood as well.
9. As was mentioned in the theory section, it is more

proper to use a model equation for the pressure profile along the length of the core. However, a continuous pressure profile is required for this approach. Therefore, the number of transducers should be increased. Moreover, the pressures would be more representative if the transducers were placed inside the flow stream rather than at the top of the core holder (as in the present study). Once oil and water pressures are obtained at more frequent points along the length of the core, the slope of the pressure profiles should be used along with the fractional flow as obtained by applying both the Eulerian and the Lagrangian formulation to saturation profiles.

10. In the present study, the equation used to curve-fit the cumulative recovery data (as determined by the dynamic method) does not fit the experimental data very well. The fit is particularly poor when the displacement is unstable. A systematic statistical analysis should be undertaken to obtain a model equation that would fit the recovery data properly. More investigation should be directed towards finding a different model equation for the unstable displacement runs.



## 8. REFERENCES

Alemán-Gomez, M., T.R. Ramamohan, and J.C. Slattery., 1984, "A Statistical Model for Unsteady-State Displacement in Porous Media", SPE 13265, 59th Annual Technical Conference and Exhibition of the Society of Petroleum Engineers of AIME, Houston, Texas.

Amaefule, J.O, and L.L. Handy, 1982, "The Effect of Interfacial Tension on Relative Permeabilities of Consolidated Porous Media", Soc. Pet. Eng. J., vol. 22(2), p.371.

Archer, J.S., and S.W. Wong, 1973, "Use of A Reservoir Simulator to Interpret Laboratory Waterflood Data", Soc. Pet. Eng. J., vol. 13(4), p. 343.

Bail, P.T., and S.S. Marsden, 1957, "Saturation Distribution in a Linear System During Oil Displacement", Producer's Monthly, vol. 21(June), p. 417.

Bardon, C., and D. Longeron, 1980, "Influence of Very Low Interfacial Tensions on Relative Permeability", Soc. Pet. Eng. J., vol. 20(4), p.391.

Batycky, J.P. and F.G. McCaffery, 1978, "Low Interfacial Tension Displacement Studies", paper no. 78-29-26, presented at the 29th Annual Technical Meeting of the Petroleum Society of CIM in Calgary.

Bear, J., 1970, "Two-Liquid Flows in Porous Media", Advances in Hydroscience, vol. 6, p.141.

- Bentsen, R.G., 1976, "Scaled Fluid-Flow Models with Permeabilities Differing from that of The Prototype", J. Can. Pet. Tech., vol. 15(3), p. 46.
- Bentsen, R.G., 1978, "Conditions Under Which the Capillary Term may be Neglected", J. Can. Pet. Tech., vol. 17(4), p. 25.
- Bentsen, R.G., 1984, "Personal Communication", University of Alberta, Edmonton, Canada.
- Bentsen, R.G., 1985a, "A New Approach to Instability Theory in Porous Media", Soc. Pet. Eng. J., October.
- Bentsen, R.G., 1985b, "A Functional Relationship for Macroscopic Capillary Pressure", SPE No. 13831.
- Bentsen, R.G., and J. Saeedi, 1981, "Liquid-Liquid Immiscible Displacement in Unconsolidated Porous Media", J. Can. Pet. Tech., vol. 20(1), p. 93.
- Brandner, C.F., and R.A. Slotboom, 1975, "Vertical Immiscible Displacement Experiments in a Non-Homogeneous Flow Cell", J. Can. Pet. Tech., vol. 14(1), p. 27.
- Buckley, S.E., and M.C. Leverett, 1942, "Mechanism of Fluid Displacement in Sands", Trans. AIME, vol. 146, p. 107.
- Chatenever, A., and J.C. Calhoun, 1952, "Visual Examination of Fluid Behavior in Porous Media", Trans. AIME, vol. 195, p. 149.
- Chatzis, I., and F.A.L. Dullien, 1977, "Modelling Pore Structure by 2-D and 3-D networks with Application to Sandstones", J. Can. Pet. Tech., vol. 16(1), p. 97.

Chatzis, I., M.S. Kuntamukkula, and N.R. Morrow, 1984, "Blob-Size Distribution as a Function of Capillary Number in Sandstones", SPE 13213; paper presented at the 59th Annual Technical Conference and Exhibition of the SPE of AIME, held in Houston, Texas.

Coskuner, G. and R.G. Bentsen, 1985, "Experimental Study of A New Approach to Instability Theory in Porous Media", CIM paper no. 85-36-3, presented at the 36th Annual Technical Meeting, Edmonton.

Darcy, H., 1856, "La Fontaine de la ville de Dijon", Victor Dalmont, Paris.

de la Cruz, V., and T.J.T. Spanos, 1983, "Mobilization of Oil Ganglia", AICHE J., vol. 29(5), p. 854.

Demetre, G.P., R.G. Bentsen, and D.L. Flock, 1981, "A Multi-dimensional Approach to Scaled Immiscible Fluid Displacement", CIM paper no. 81-32-7, presented at the 32nd Annual Technical meeting, Edmonton.

Dodd, C.G., and O.G. Kiel, 1959, "Evaluation of Monte Carlo Methods in Studying Fluid Wettability in Porous Rock", J. Phys. Chem., vol. 63, p. 1646.

Dullien, F.A.L., 1979, Porous Media Fluid Transport and Pore Structure, Academic Press, New York, ch. 6, p. 263.

Fatt, I., 1956a, "The Network Model of Porous Media I. Pressure Characteristics", Trans. AIME, vol. 207, p. 144.

Fatt, I., 1956b, "The Network Model of Porous Media II. Dynamic Properties of a Single Size Tube Network", Trans. AIME, vol. 207, p. 160.

- Fatt, I., 1956c, "The Network Model of Porous Media III. Dynamic Properties of Networks with Tube Radius Distribution", Trans. AIME, vol. 207, p. 164.
- Fulcher, R.A., E.Turgay, and C.D. Stahl, 1985, "Effect of Capillary Number and Its Constituents on Two-phase Relative Permeability Curves", Soc. Pet. Eng. J., 24(1), p. 249.
- Geffen, T.M., and R.E. Gladfelter, 1952, "A Note on the X-Ray Absorption Method of Determining Fluid Saturations in Cores", Trans. AIME, vol. 195, p. 322.
- Golaz, P., and R.G. Bentsen, 1980, "On the Use of the Centrifuge to Obtain Capillary Pressure Data", CIM paper no. 80-31-38, presented at the 31st Annual Technical Meeting, Calgary.
- Handy, L.L., and P. Datta, 1966, "Fluid Distributions During Immiscible Displacements in Porous Media", Soc. Pet. Eng. J., vol. 6(3), p. 261.
- Hagoort, J., 1974, "Displacement Stability of Water Drives in Water-wet Connate Water Bearing Reservoirs" Soc. Pet. Eng. J., vol. 14(1), p. 63.
- Hubbert, M.K., 1956, "Darcy's law and the Field Equations of the Flow of Underground fluids", Trans. AIME, vol. 207, p. 222.
- Huppler, J.D., 1970, "Numerical Investigation of the Effects of Core Heterogeneities on Waterflood Relative Permeabilities", Trans. AIME, vol. 249, p. 381.

- Johnson, E.F., D.P. Bossler, and V.O. Naumann, 1959, "Calculation of Relative Permeability from Displacement Experiments", Trans. AIME, vol. 216, p. 370.
- Kimbler, O.K., and B.H. Caudle, 1957, "New Technique for Study of Fluid Flow and Phase Distribution in Porous Media", Oil & Gas J., vol. 55(50), p. 85.
- Koplik, J., and T.J. Lasseter, 1982, "Two-Phase Flow in Random Network Models of Porous Media", SPE 11014, 57th Annual Fall Technical Conference and Exhibition of the Society of Petroleum Engineers of AIME, New Orleans, LA.
- Lefebvre du Prey, E.J., 1973, "Factors Affecting Liquid-Liquid Relative Permeabilities of a Consolidated Porous Medium", Soc. Pet. Eng. J., vol. 13(1), p. 39.
- Leverett, M.C., 1939, "Flow of Oil-Water Mixtures Through Unconsolidated Sands", Trans. AIME, Vol. 132, p. 149.
- Leverett, M.C., 1941, "Capillary Behaviour in Porous Solids", Trans. AIME, vol. 142, p. 152.
- Levine, J.S., 1954, "Displacement Experiments in a Consolidated Porous System", Trans. AIME, vol. 201, p. 57.
- Lin, C.Y., and J.C. Slattery, 1982, "Three Dimensional, Randomized, Network Model for Two Phase Flow through Porous Media", AIChE J., vol. 28, p. 311.
- Lipson, B.L., 1951, "Theoretical Note on Linear Absorption Methods of Determination of Fluid Saturation in Porous Media", Trans. AIME, vol. 192, p. 375.

Melrose, J.C., and C.E. Brandner, 1974, "Role of Capillary Forces in Determining Microscopic Displacement Efficiency", J. Can. Pet. Tech., vol. 13, p. 54.

Miller, M.A., and H.J. Ramey, 1983, "Effect of Temperature on Oil-Water Relative Permeabilities of Unconsolidated and Consolidated Sands", SPE 12116, presented at the 58th Annual Technical Conference and Exhibition of the Society of Petroleum Engineers, San Francisco, California.

Morgan, F., J.M. McDavell, and E.C. Dotty, 1950, "Improvement in the X-Ray Saturation Technique of Studying Fluid Flow", Trans. AIME, vol. 189, p. 183.

Morrow, N.C., H.T. Lim, J.S. Ward, 1984, "Effect of Crude-Oil-Induced Wettability Changes on Oil Recovery", SPE 13215, presented at the 59th Annual Technical Conference and Exhibition of the Society of Petroleum Engineers, Houston, Texas.

Nelder, J.A., and R. Mead, 1965, "A Simplex Method for Function Minimization", Computer Journal, vol. 7, p. 308.

Odeh, A.S., 1959, "Effect of Viscosity Ratio on Relative Permeability", Trans. AIME, vol. 216, p. 346.

Osoba, J.S., J.G. Richardson, J.K. Kerver, J.A. Hafford and P.M. Blair, 1951, "Laboratory Measurements of Relative Permeability", Trans. AIME, vol. 192, p. 47.

- Owens, W.W., D.R. Parrish, and W.E. Lamoreaux, 1965, "An Evaluation of a Gas Drive Method for Determining Relative Permeability Relationships", Trans. AIME, vol. 207, p. 275.
- Parsons, R.W., 1975, "Microwave Attenuation -- A New Tool for Monitoring Saturations in Laboratory Flooding Experiments", Soc. Pet. Eng. J., vol. 15(3), p. 302.
- Parsons, R.W., and S.C. Jones, 1977, "Linear Scaling in Slug-Type Processes -- Application to Micellar Flooding", Soc. Pet. Eng. J., vol. 17(3), p. 11.
- Paez, J., P. Reed, and J.C. Calhoun, 1955, "Relationship Between Oil Recovery, Interfacial Tension, Pressure Gradient and Water-Wet Porous Media", Producer's Monthly, vol. 19(May), p. 34.
- Perkins, F.M., 1957, "An Investigation of the Role of Capillary Forces in Laboratory Waterfloods", Trans. AIME, vol. 210, p. 409.
- Peters, E.J., 1979, "Stability Theory and Viscous Fingering in Porous Media", Ph.D. dissertation, Department of Mineral Engineering, University of Alberta, Edmonton, Alberta, Canada.
- Rose, W., 1960, "Fluid Flow in Petroleum Reservoirs, III. Effect of Fluid-Fluid Interfacial Boundary Condition", Geol. Surv. Circ., vol. 291, p. 18.

- Rose, W., 1968, "Some Problems Connected with the Use of Classical Description of Fluid/Fluid Displacement Processes", Trans. Symp. on Fundamentals of Transport Phenomena in Porous Media, Haifa, Israel, p. 229.
- Rose, W., 1979, "Discussion", Soc. Pet. Eng. J., vol. 19(1), p. 270.
- Russel, T.W.F., and M.E. Charles, 1959, "Effect of the Less Viscous Liquid in the Laminar Flow of Two Immiscible Liquids", Can. J. Chem. Eng., vol. 37, p. 18.
- Saeedi, J., 1979, "A Comparison of Theoretical and Experimental Saturation Profiles in Porous Media", M.Sc. Thesis, Department of Mineral Engineering, University of Alberta.
- Sandberg, C.R., L.S. Gournay, and R.F. Sippel, 1958, "The Effect of Fluid-Flow Rate and Viscosity on Laboratory Determination of Oil-Water Relative Permeabilities", Trans. AIME, vol. 213, p. 36.
- Scheidegger, A.E., 1974, Physics of Flow Through Porous Media, Univ. of Toronto Press, Toronto, Canada, ch. 10, p. 250.
- Schneider, F.N., and W.W. Owens, 1970, "Sandstone and Carbonate Two- and Three-Phase Relative Permeability Characteristics", Soc. Pet. Eng. J., vol. 10(1), p. 75.
- Scott, P.H., and W. Rose, 1953, "An Explanation of the Yuster Effect", Trans. AIME, vol. 198, p. 323.



- Sigmund, P.M. and F.G. McCaffery, 1979, "An Improved Unsteady-State Procedure for Determining the Relative Permeability Characteristics of Heterogeneous Porous Media", Soc. Pet. Eng. J., vol. 19(1), p. 260.
- Slattery, J.C., 1967, "Flow of Viscoelastic Fluids Through Porous Media", AICHE J., vol. 13, p. 1066.
- Slattery, J.C., 1974, "Interfacial Effects in the Entrapment and Displacement of Residual Oil", AICHE J., vol. 20, p. 1145.
- Steber, and S.S. Marsden, 1956, "The Determination of Liquid Saturations in a Porous Medium by a Method of Matched Refractive Indices", Producer's Monthly, vol. 20(April), p. 48.
- Szabo, M.T., 1972, "The Role of Gravity in Capillary Pressure Measurements", Soc. Pet. Eng. J., vol. 22(1), p. 85.
- Talash, A.W., 1976, "Experimental and Calculated Relative Permeability Data for Systems Containing Tension Additives", SPE 5810, paper presented at SPE-AIME Symposium on Improved Oil Recovery, Tulsa, OK, March 22-24.
- Warren, J.E., and J.C. Calhoun, 1955, "A Study of Waterflood Efficiency in Oil-Wet Systems", Trans. AIME, vol. 204, p. 22.
- Welge, H.J., 1952, "A Simplified Method for Computing Oil Recovery by Gas Water Drive", Trans. AIME, vol. 195, p. 91.

- Whitaker, S., 1967, "Diffusion and Dispersion in Porous Media", AICHE J., vol. 13, p. 420.
- Wyckoff, R.D., and H.G. Botset, 1936, "The Flow of Gas-Liquid Mixtures Through Unconsolidated Sands", Physics, vol. 7, p. 325.
- Yadav, G.D., F.A.L. Dullien, I. Chatzis, I.F. MacDonald, 1984, "Microscopic Distribution of Wetting and Non-Wetting Phases in Sandstones During Immiscible Displacements", SPE 13212, presented at the 59th Annual Technical Conference and Exhibition of the Society of Petroleum Engineers, Houston, Texas.
- Yuster, S.T., 1951, "Theoretical Considerations of of Multiphase Flow in Idealized Capillary Systems", Proc. 3rd World Pet. Congr., The Hague, vol.2, p. 436.

## 9. APPENDIX - A

### EXAMPLE OF THE DETERMINATION OF EFFECTIVE PERMEABILITIES

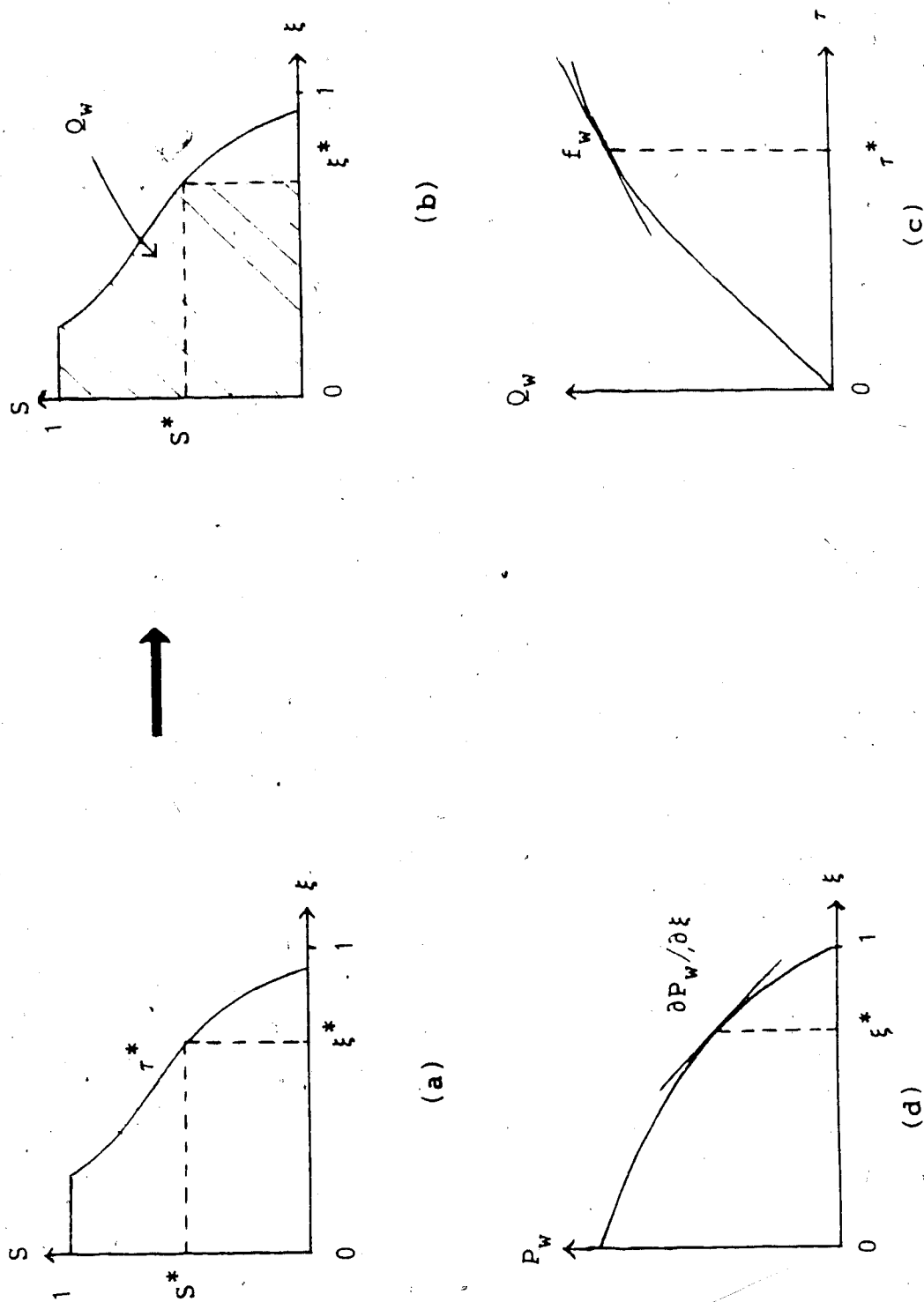


FIG. A-1 EXAMPLE OF THE DETERMINATION OF EFFECTIVE PERMEABILITIES

### DETERMINATION OF THE EFFECTIVE PERMEABILITIES

For a specific time, one may obtain the area under the saturation profile. This would give the cumulative water flowing,  $Q_w$ , up to a specific point,  $\xi^*$ . Therefore, one may obtain a curve  $Q_w$  versus time,  $\tau$ . For a specific time,  $\tau^*$ , one has the pressure ( $P_w$ ) profile available over the distance,  $\xi$ . Therefore, one may obtain  $\partial P_w / \partial \xi$  for a specific point  $\xi^*$ . On the other hand, for the same time,  $\tau^*$ , one has  $f_w$  which is the fractional water flowing (as shown in Figure A-1(c)). Now in Figure A-1(a),  $\xi^*$  corresponds to a saturation of  $S^*$  and a time  $\tau^*$ . For the same time when the saturation becomes  $S^*$  at the point  $\xi^*$ ,  $\partial P_w / \partial \xi$  and  $f_w(S^*, \tau^*)$  are available. Therefore, Equations 4.13 and 4.21 may be used to obtain  $K_w$  and  $K_o$  respectively for the saturation  $S^*$ .

10. APPENDIX - B

SATURATION PROFILES FOR DIFFERENT RUNS

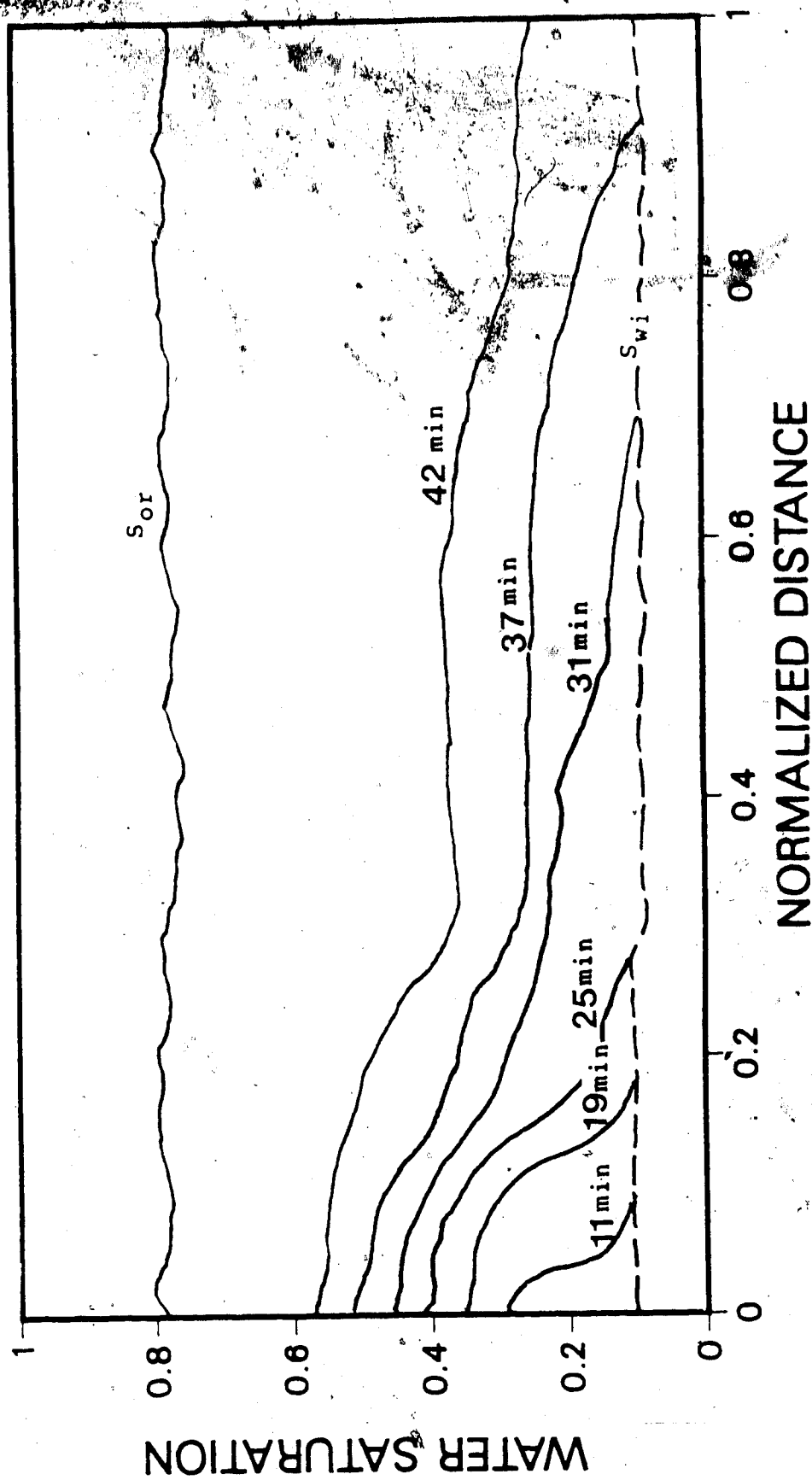


FIG. B-1 SOME OF THE EXPERIMENTAL SATURATION PROFILES (RUN 1)

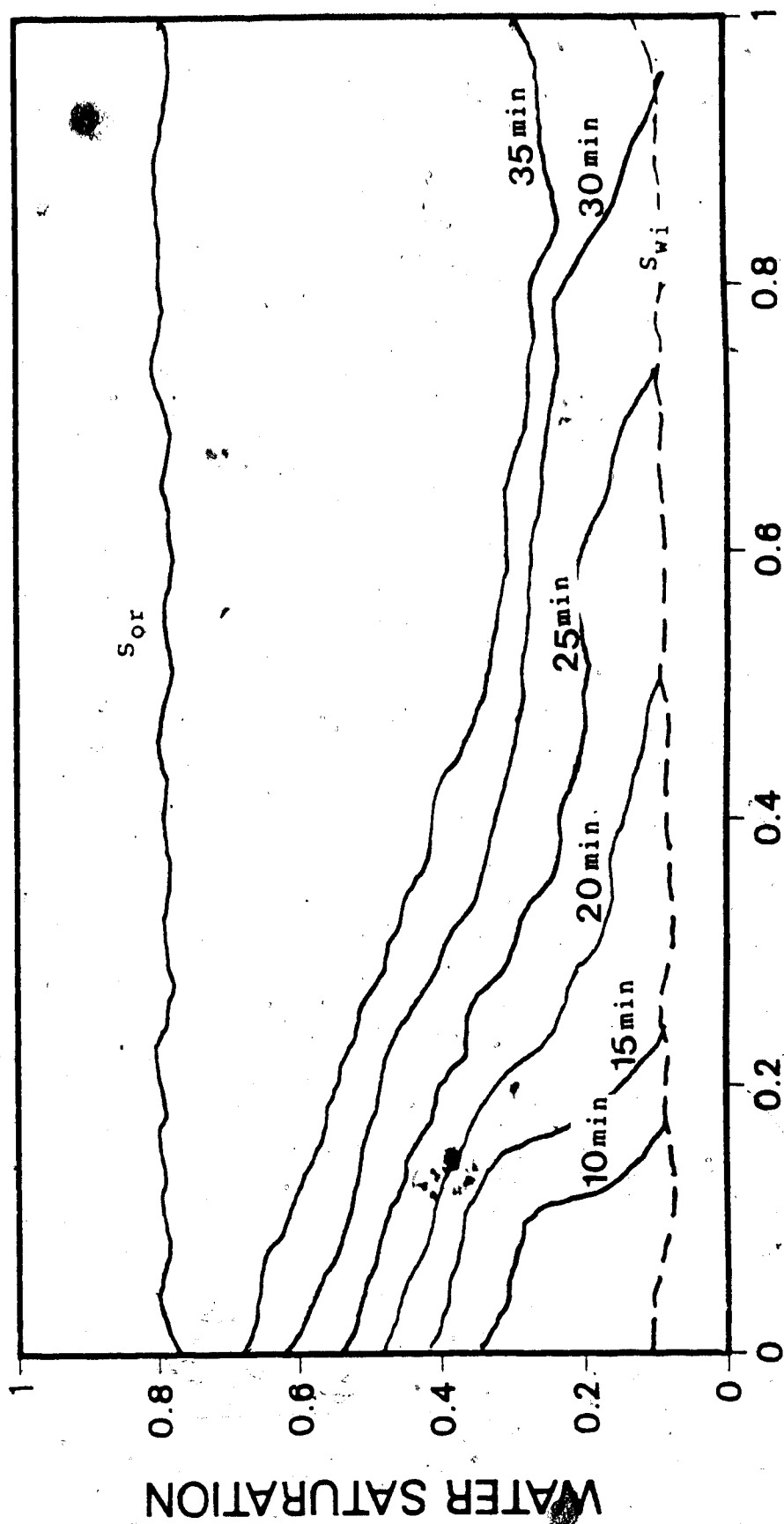


FIG. B-2 SOME OF THE EXPERIMENTAL SATURATION PROFILES (RUN 2)



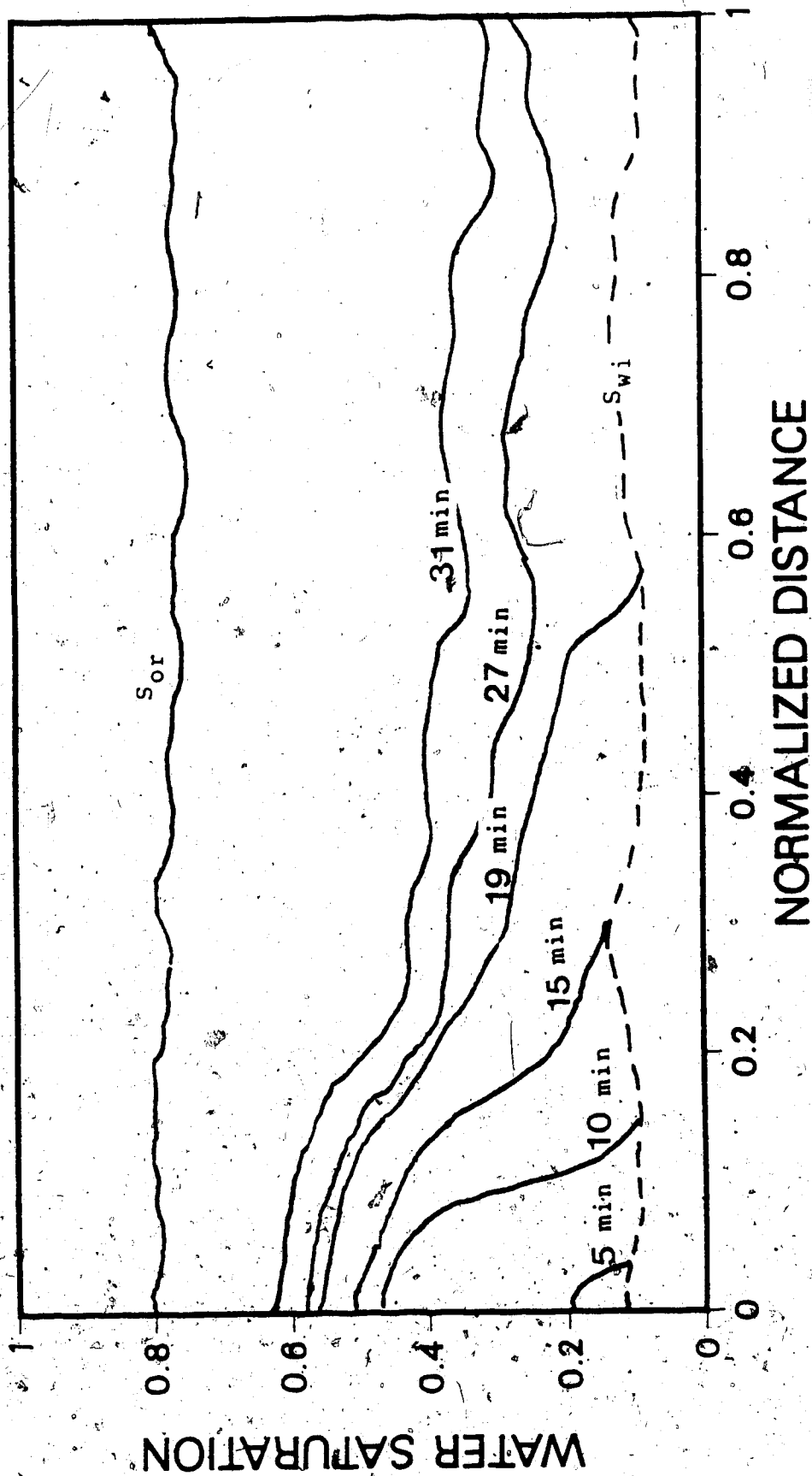


FIG. B-3 SOME OF THE EXPERIMENTAL SATURATION PROFILES (RUN

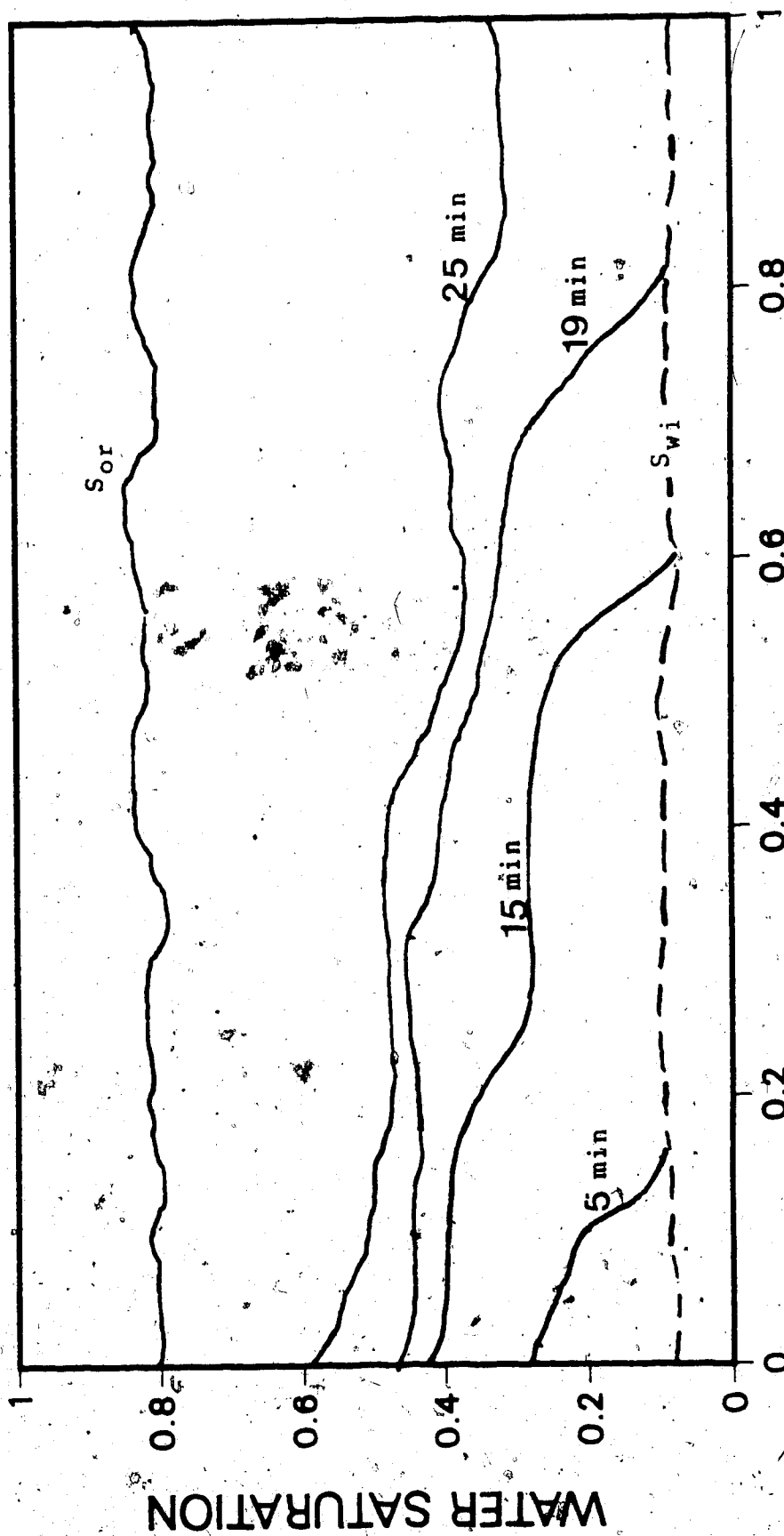


FIG. B-4 SOME OF THE EXPERIMENTAL SATURATION PROFILES (RUN 5)

NORMALIZED DISTANCE

WATER SATURATION

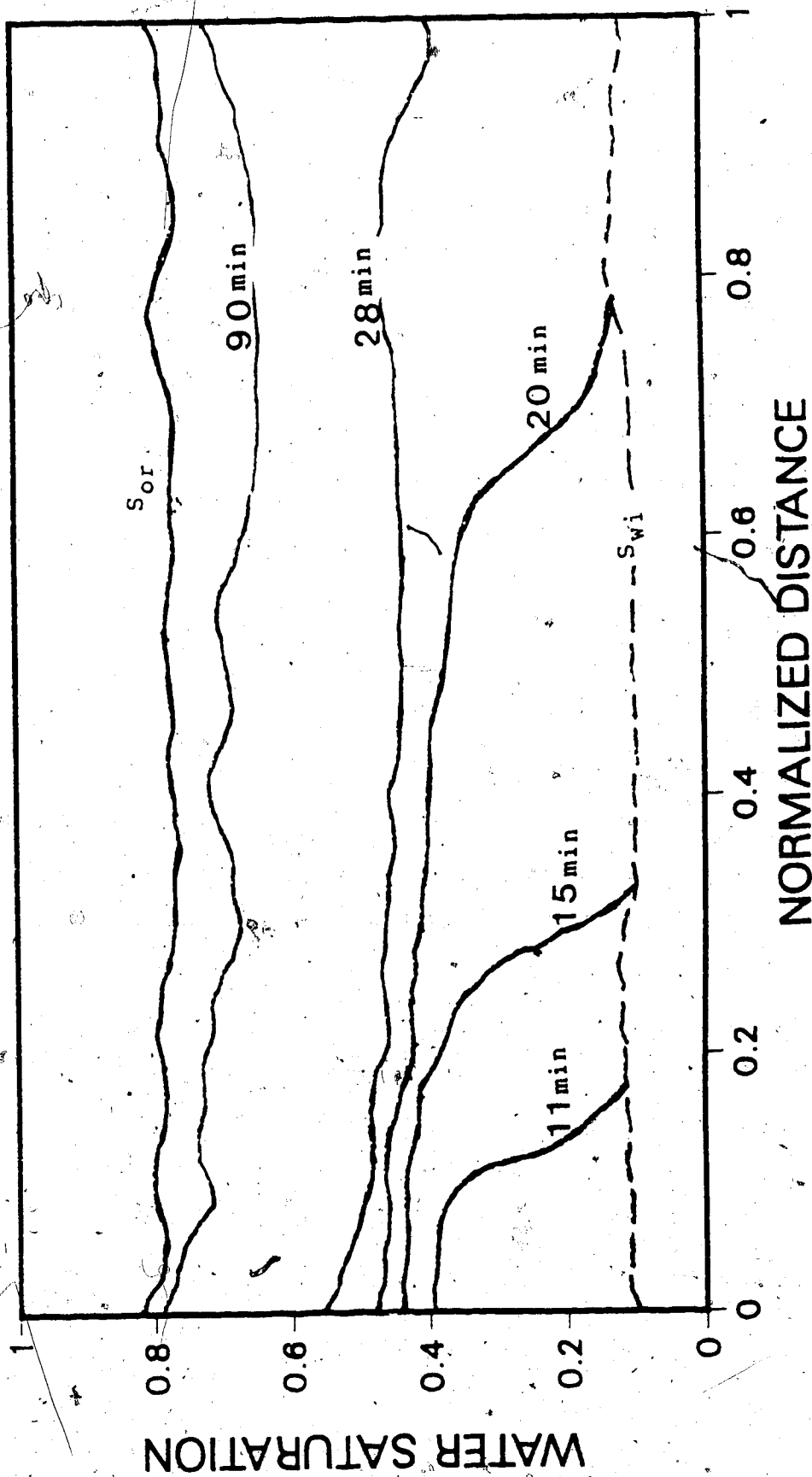


FIG. B-5 SOME OF THE EXPERIMENTAL SATURATION PROFILES (RUN 7)

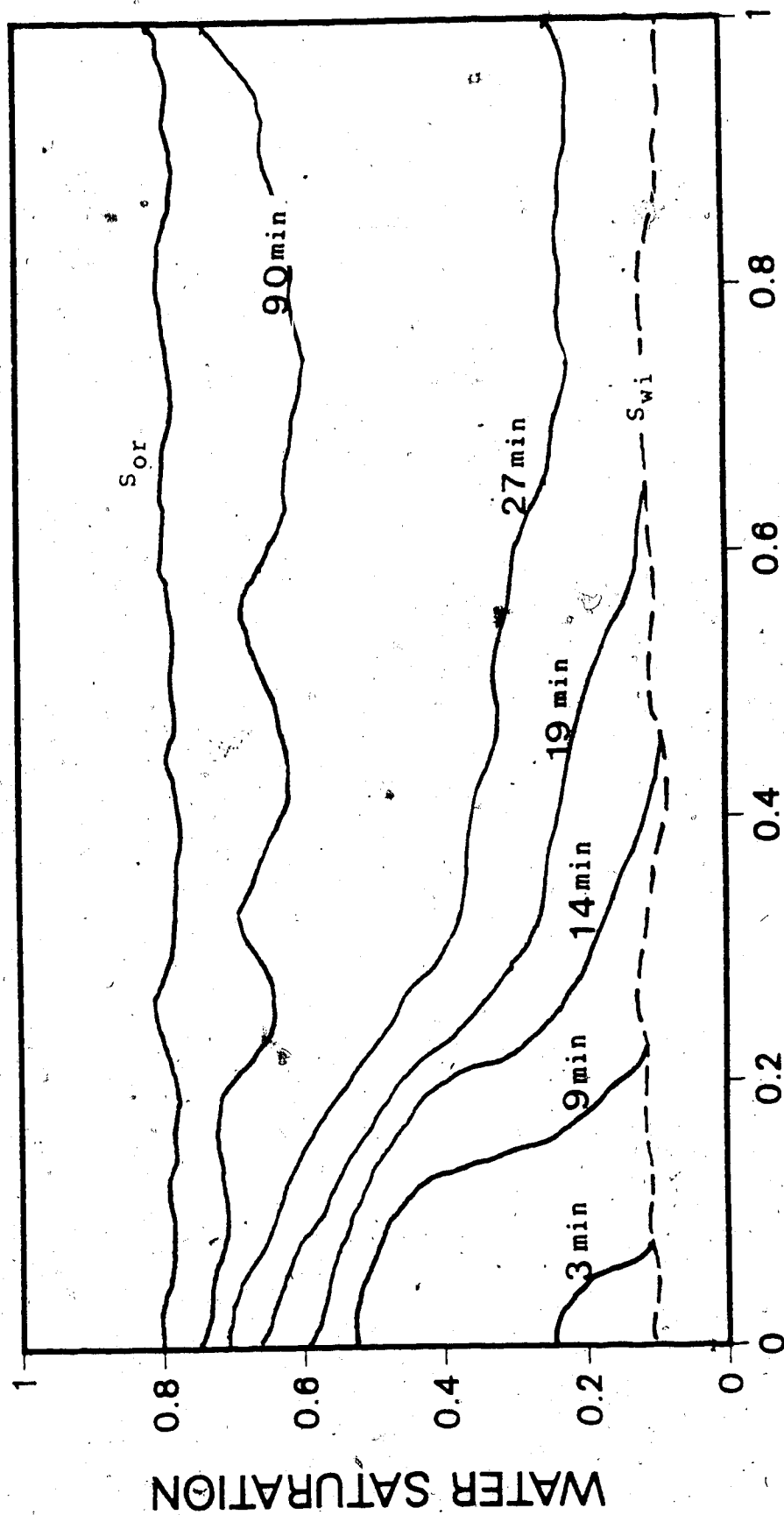
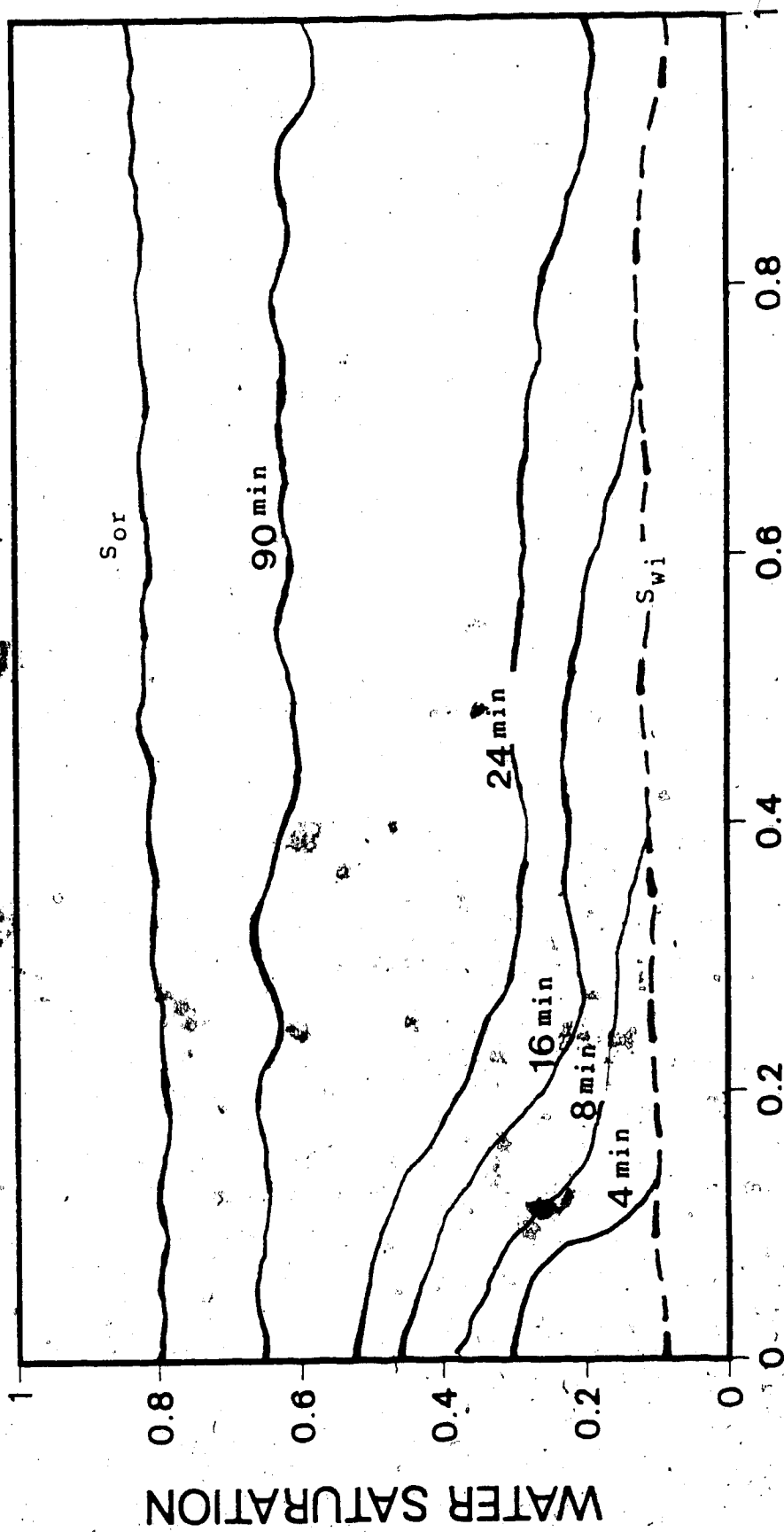


FIG. B-6 SOME OF THE EXPERIMENTAL SATURATION PROFILES (RUN 8)



### NORMALIZED DISTANCE

FIG. B-7 SOME OF THE EXPERIMENTAL SATURATION PROFILES (RUN 9)

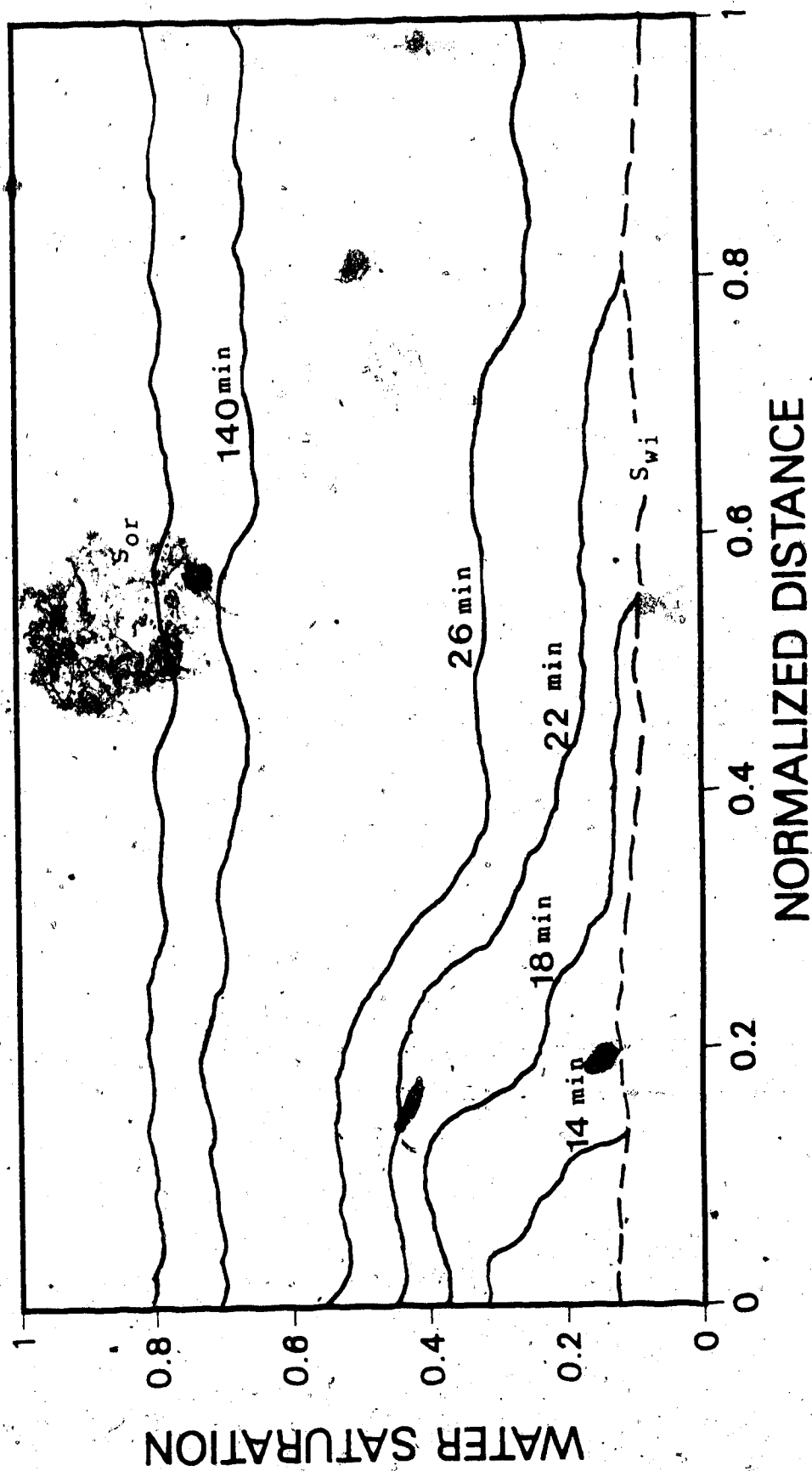
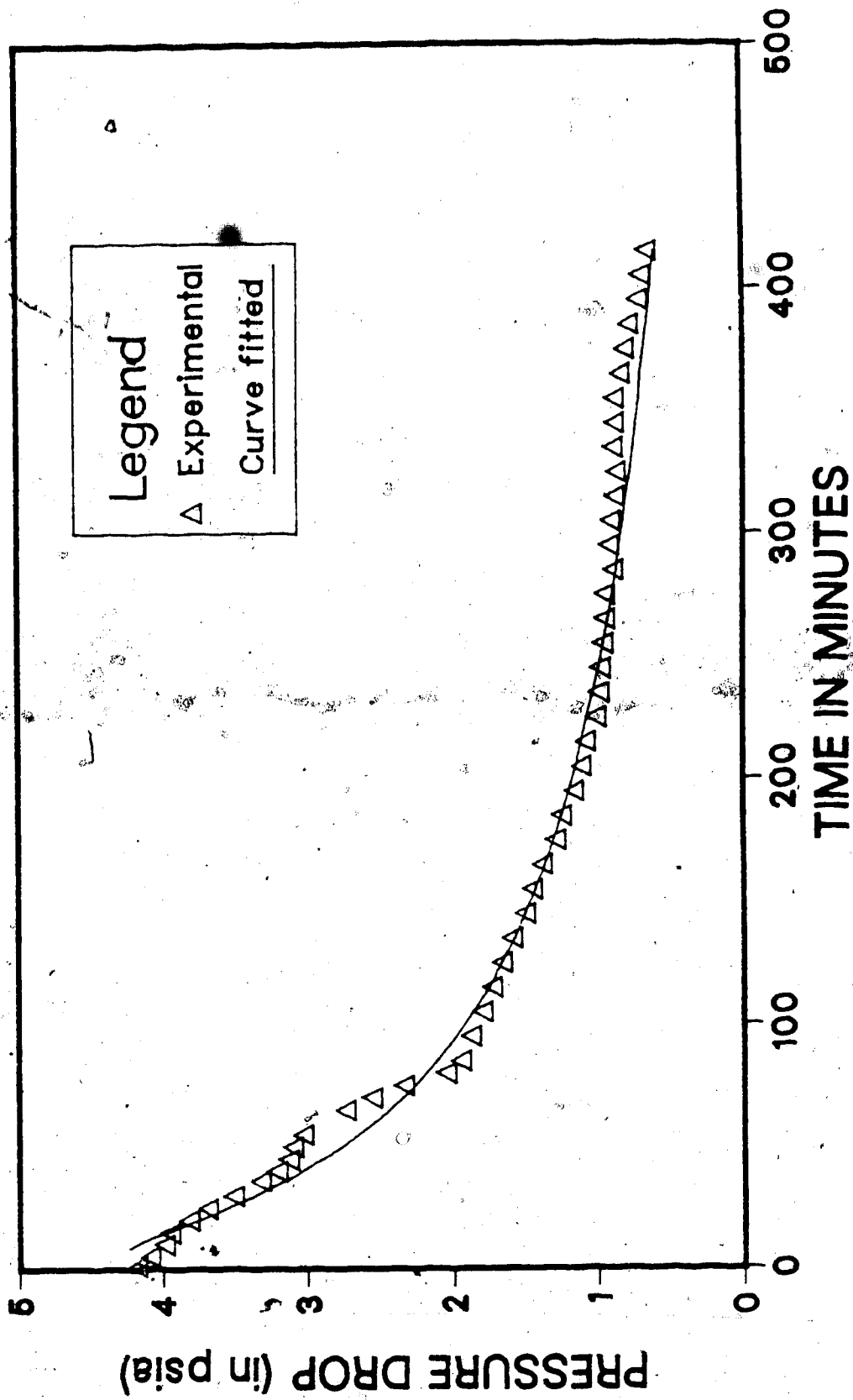


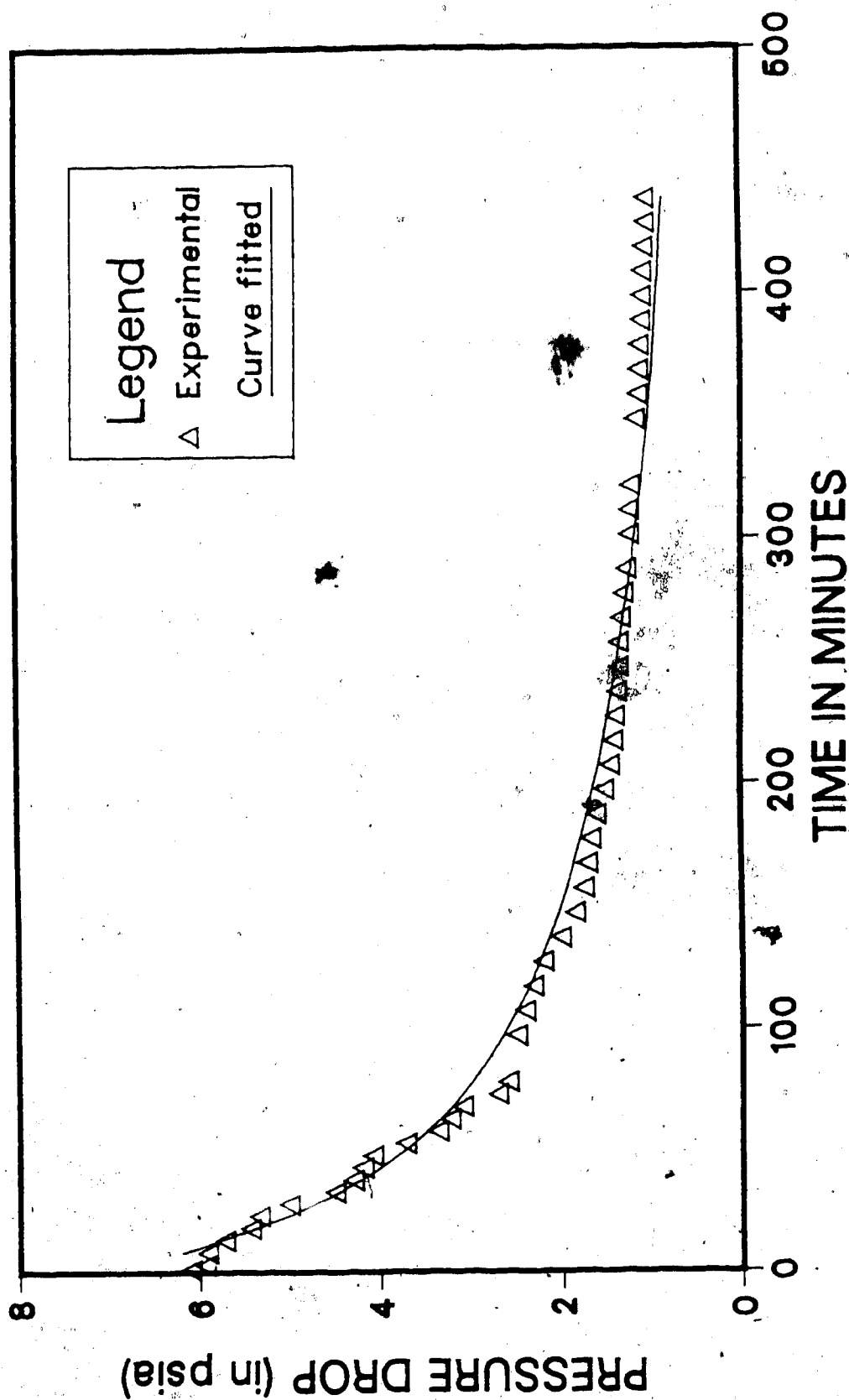
FIG. B-8 SOME OF THE EXPERIMENTAL SATURATION PROFILES (RUN 10)

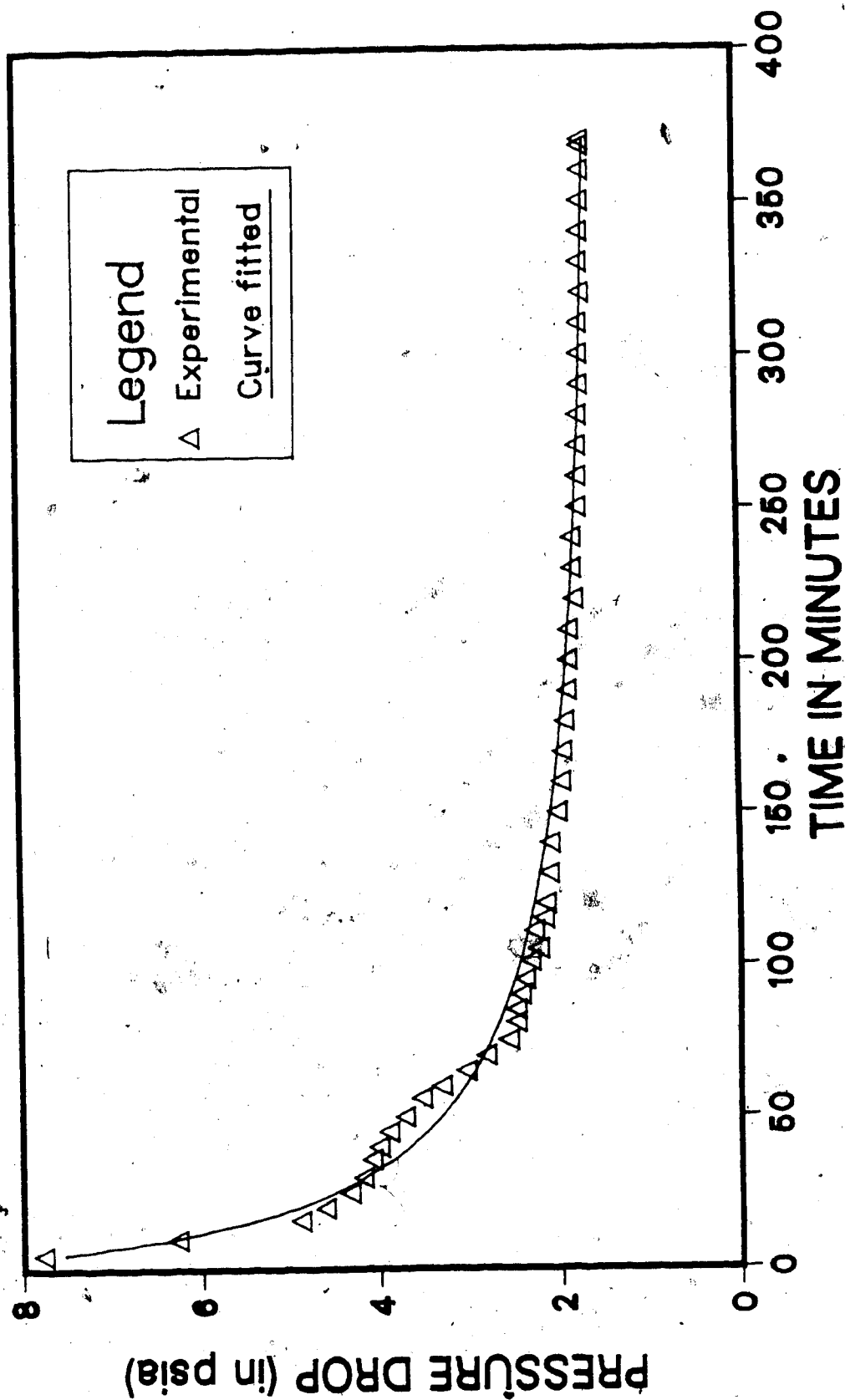
11. APPENDIX - C

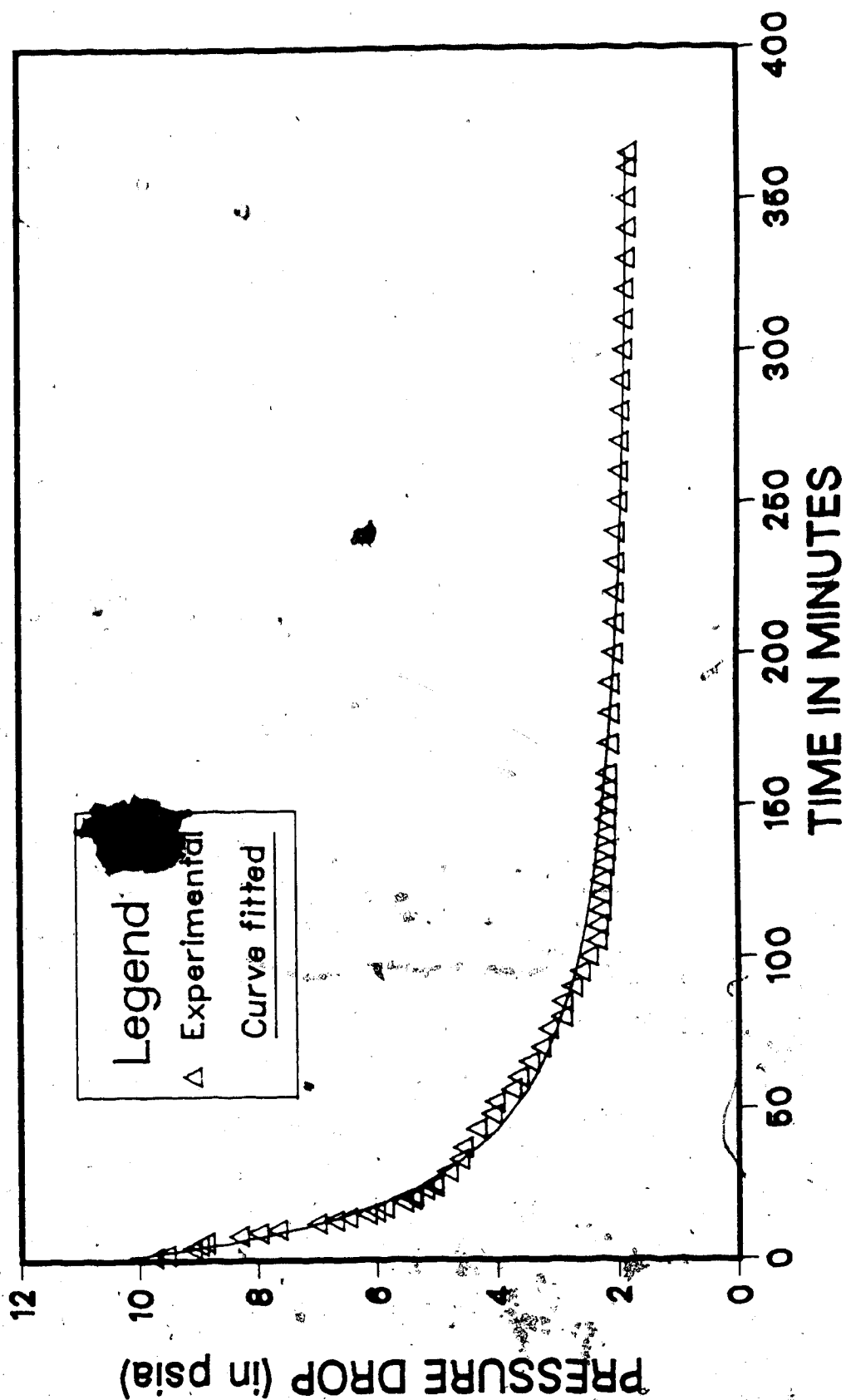
$\Delta P$  VERSUS TIME CURVE FIT

FIG. C-1  $\Delta$ P CURVE FIT (RUN 1)



FIG. C-2  $\Delta P$  CURVE FIT (RUN 2)

FIG. C-3  $\Delta P$  CURVE FIT (RUN 4)

FIG. C-4  $\Delta P$  CURVE FIT (RUN 5)

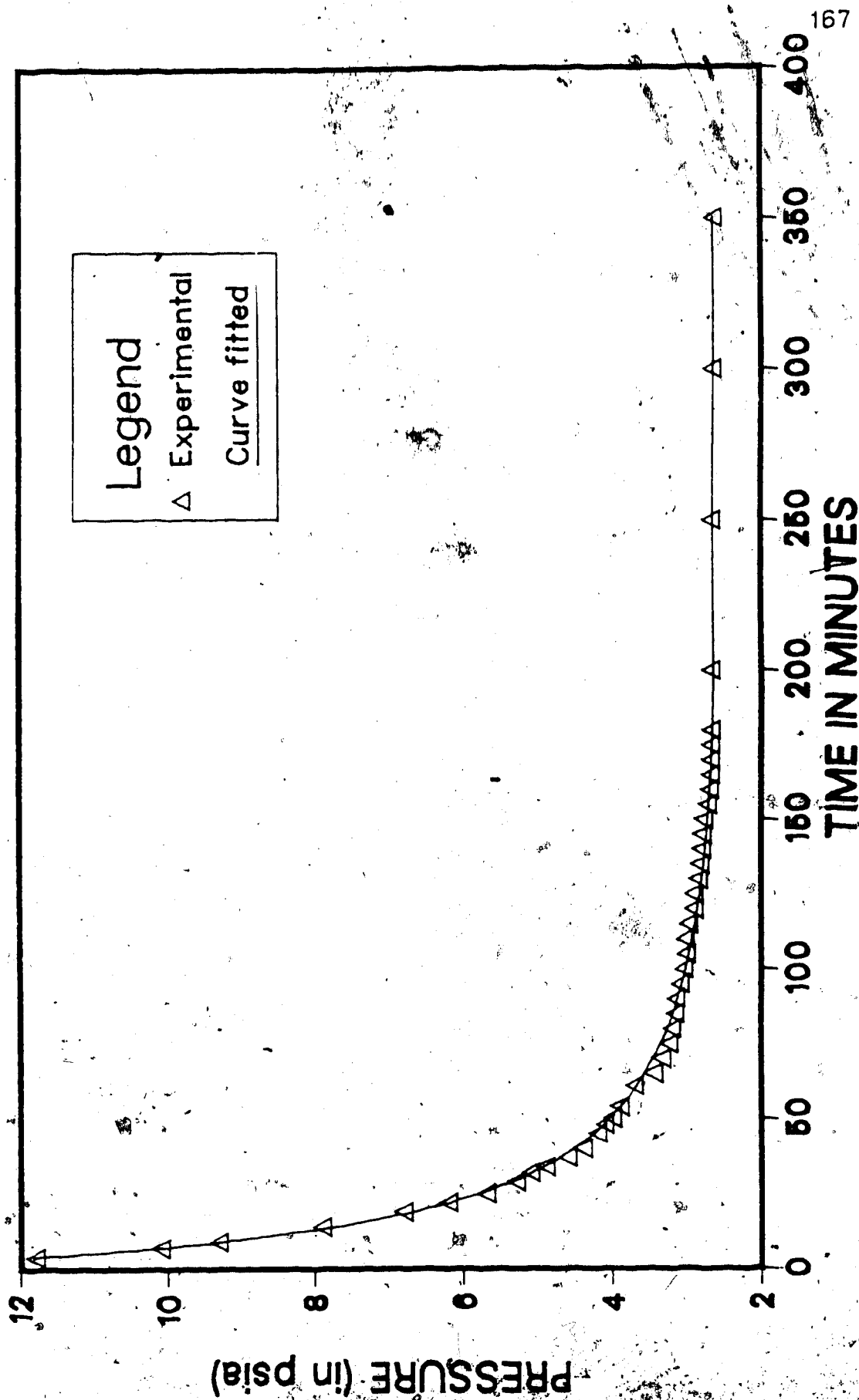


FIG. C-5 ΔP CURVE FIT (RUN 7)

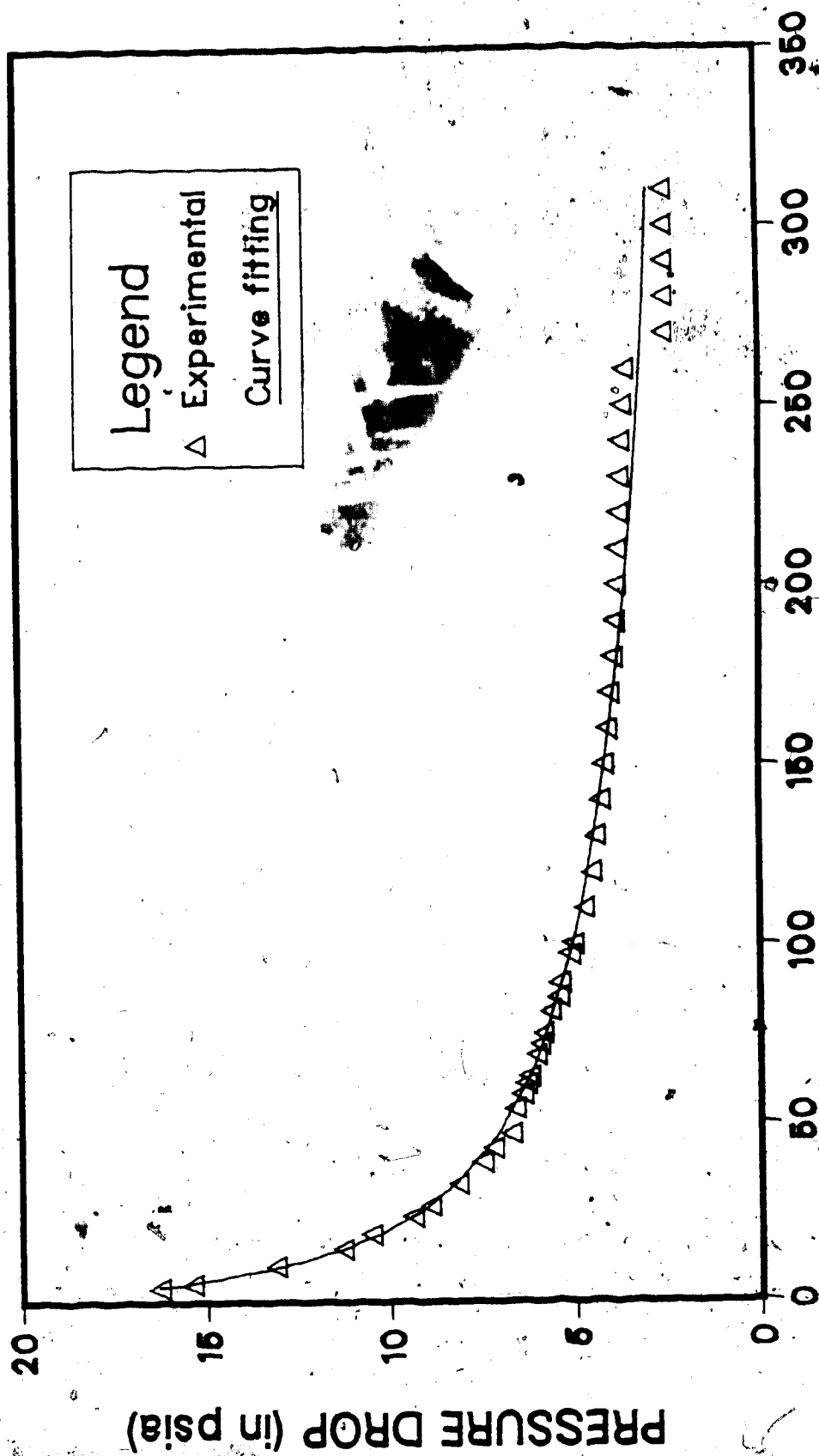


FIG. C-6  $\Delta P$  CURVE FIT (RUN 8)

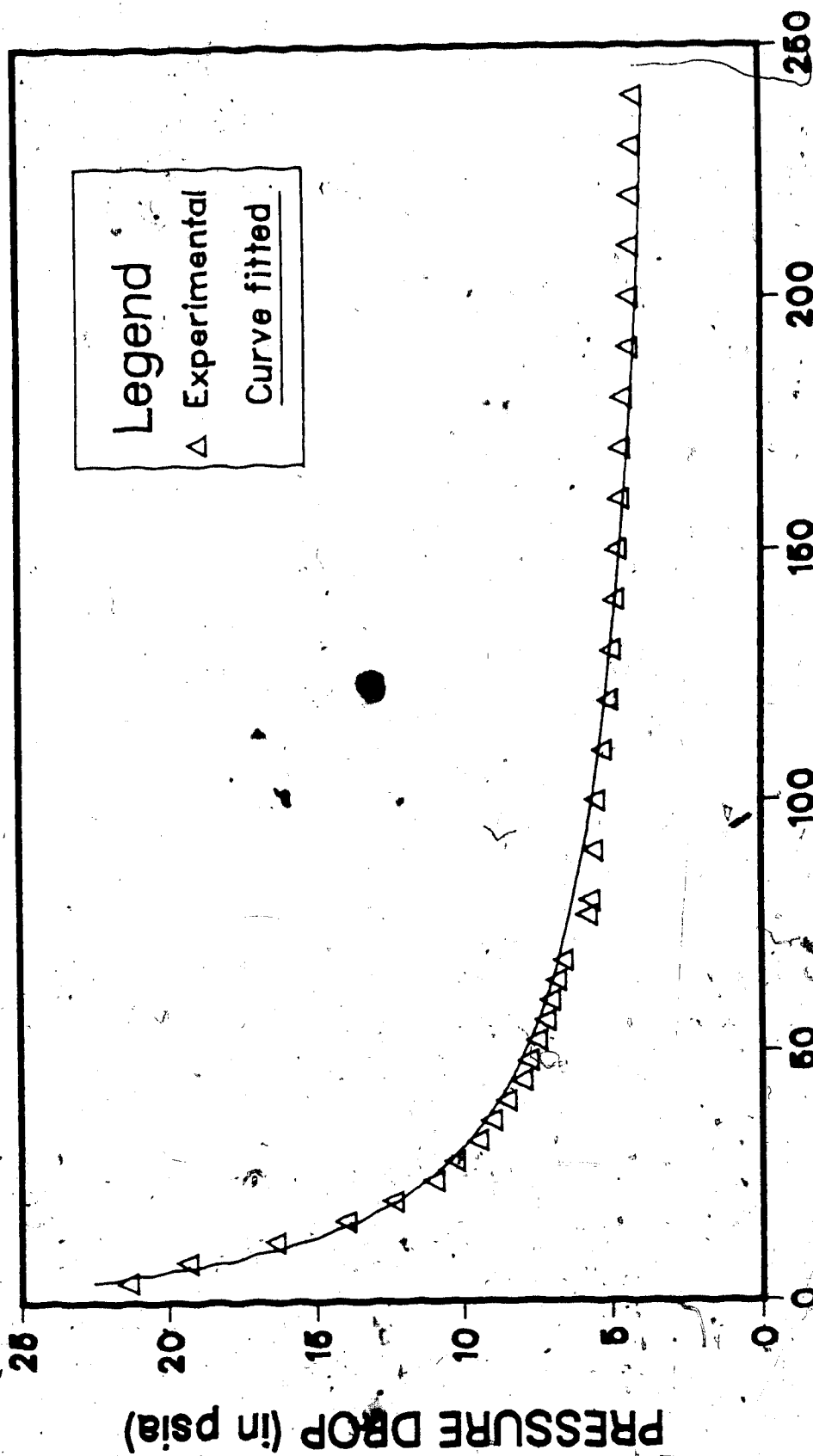
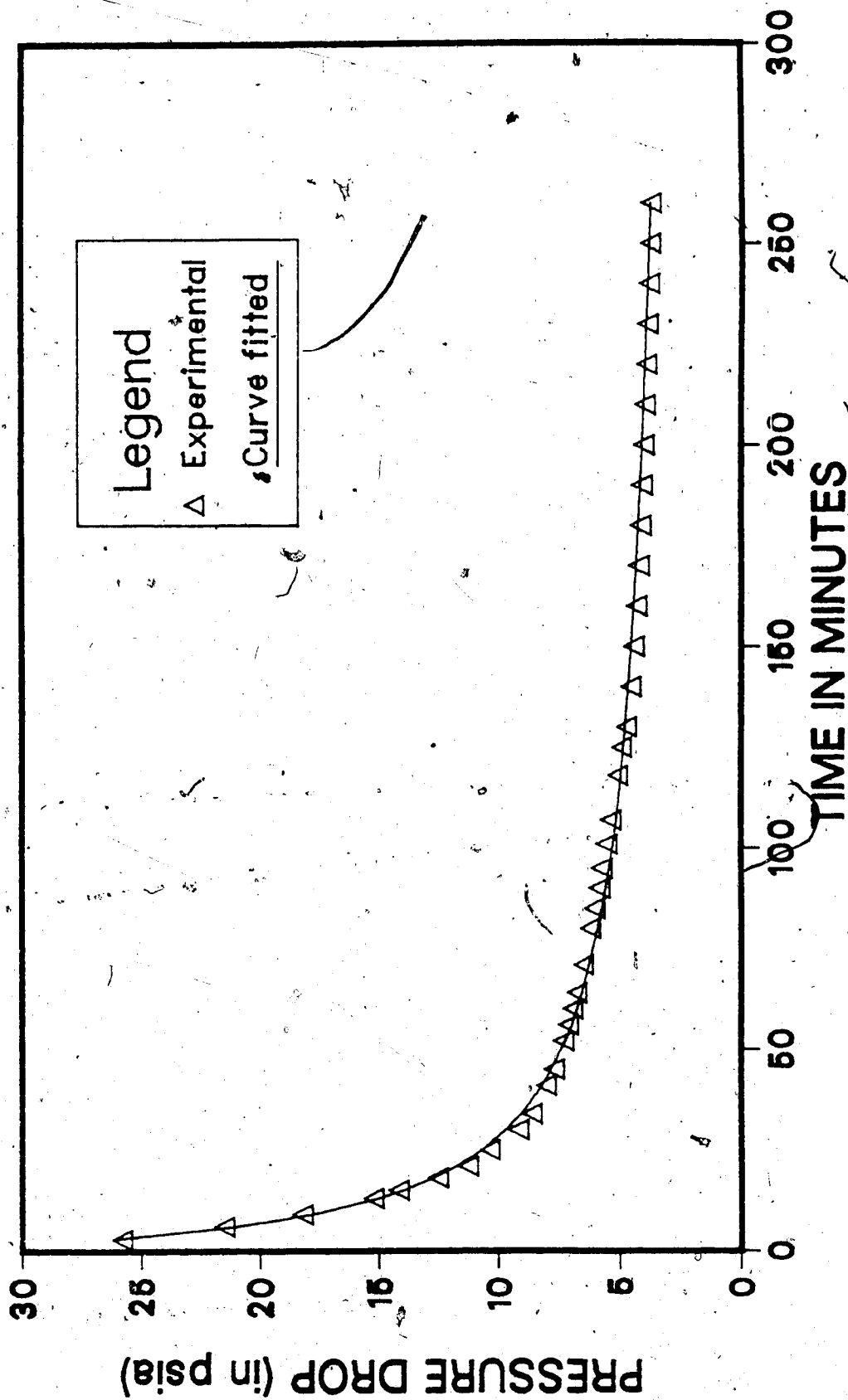


FIG. C-7  $\Delta P$  CURVE FIT (RUN 9)

FIG. C-8  $\Delta P$  CURVE FIT (RUN 10)

12. APPENDIX - D

CUMULATIVE OIL RECOVERY VERSUS TIME CURVE FIT



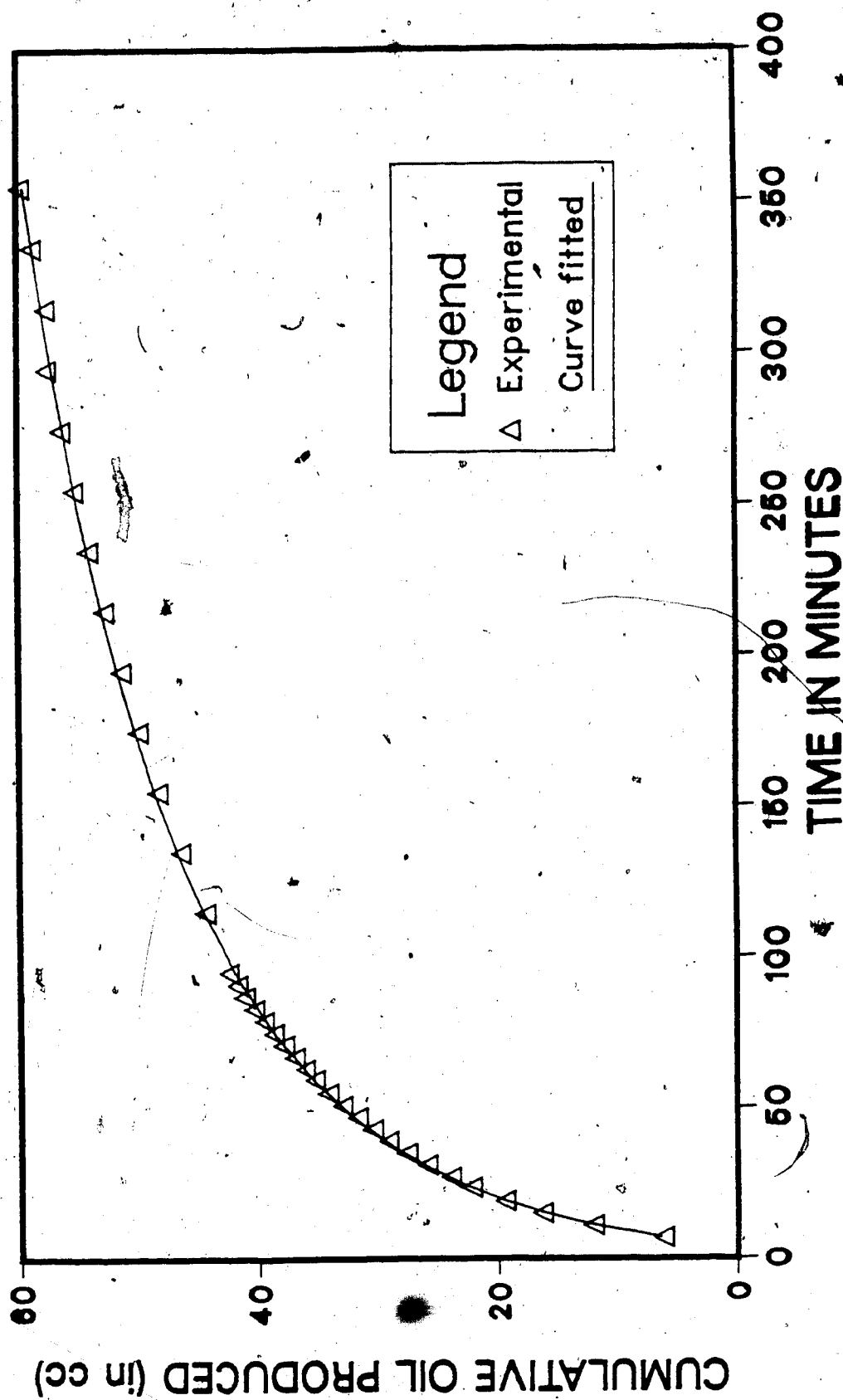


FIG. D-1 CUMULATIVE OIL PRODUCTION CURVE FIT (RUN 1)

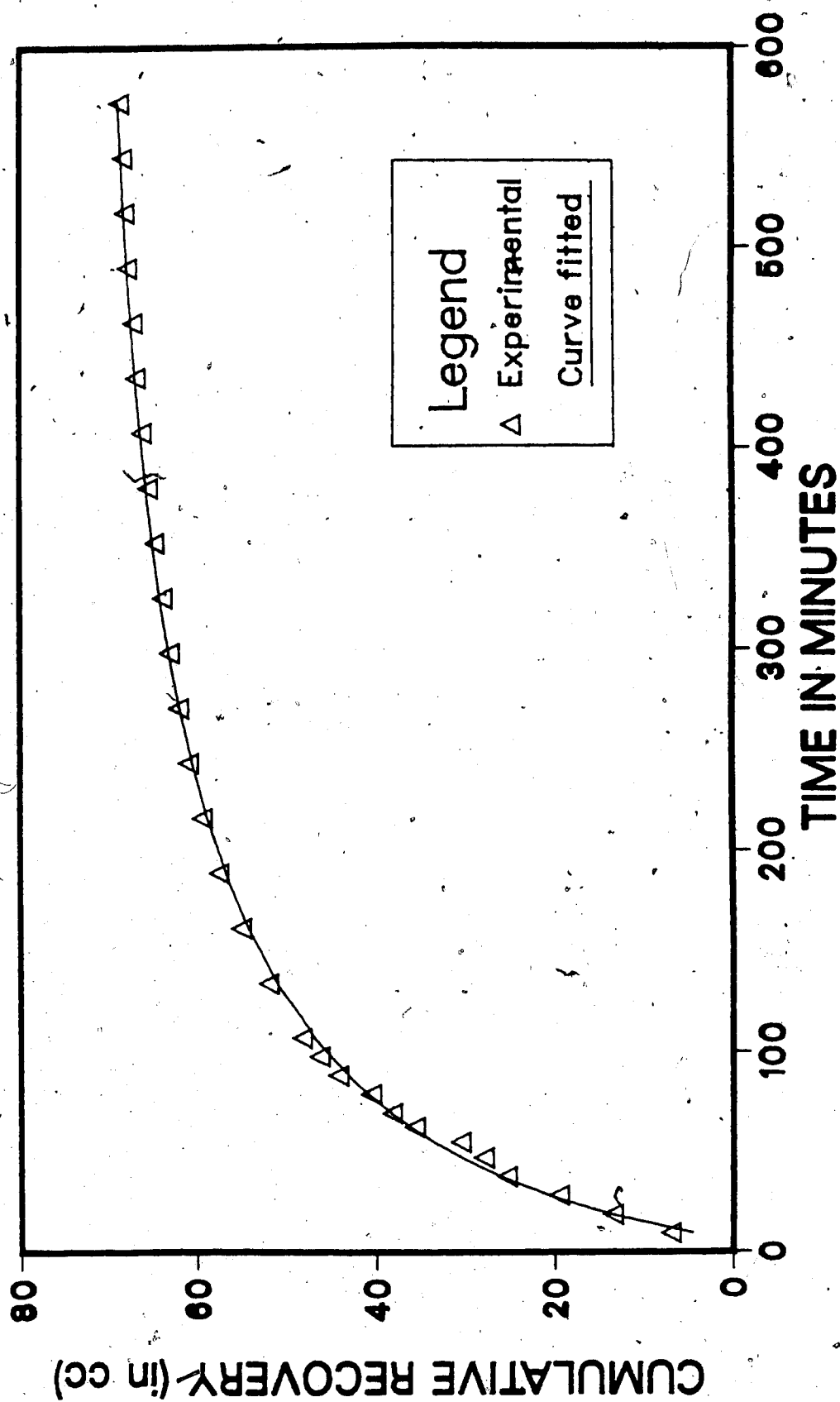


FIG. D-2 CUMULATIVE OIL PRODUCTION CURVE FIT (RUN 2)

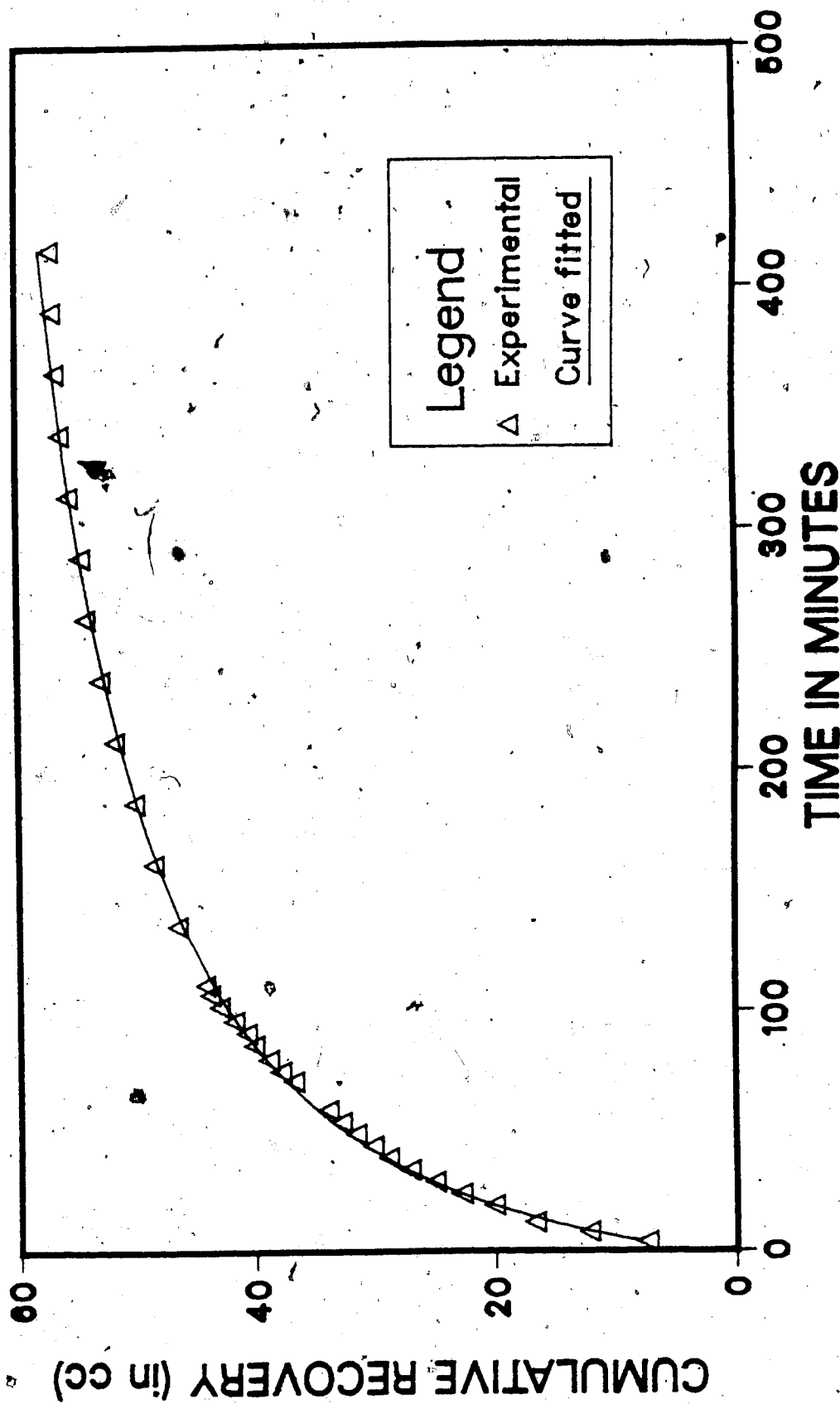


FIG. D-3 CUMULATIVE OIL PRODUCTION CURVE FIT (RUN 4)

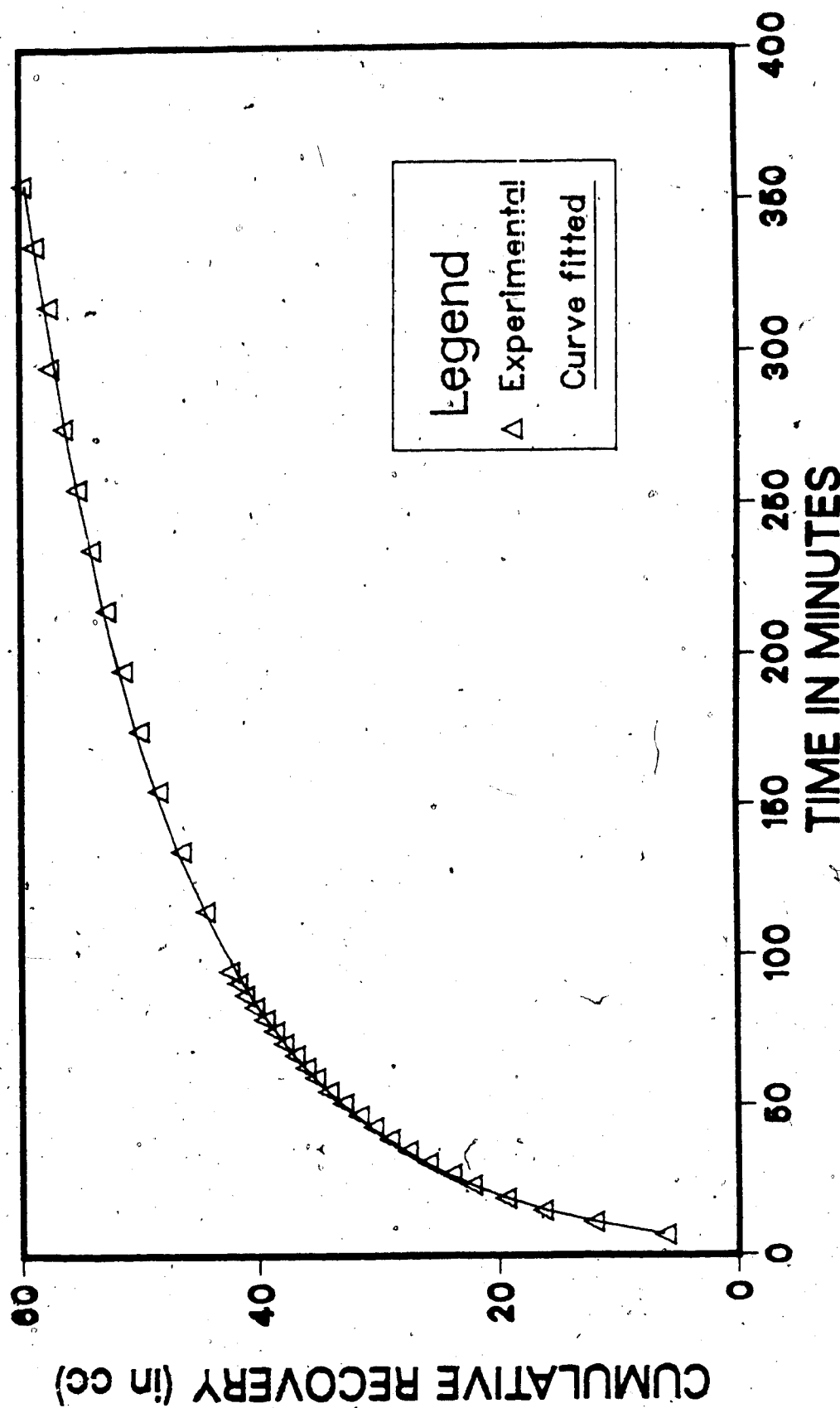


FIG. D-4 CUMULATIVE OIL PRODUCTION CURVE FIT (RUN 5)

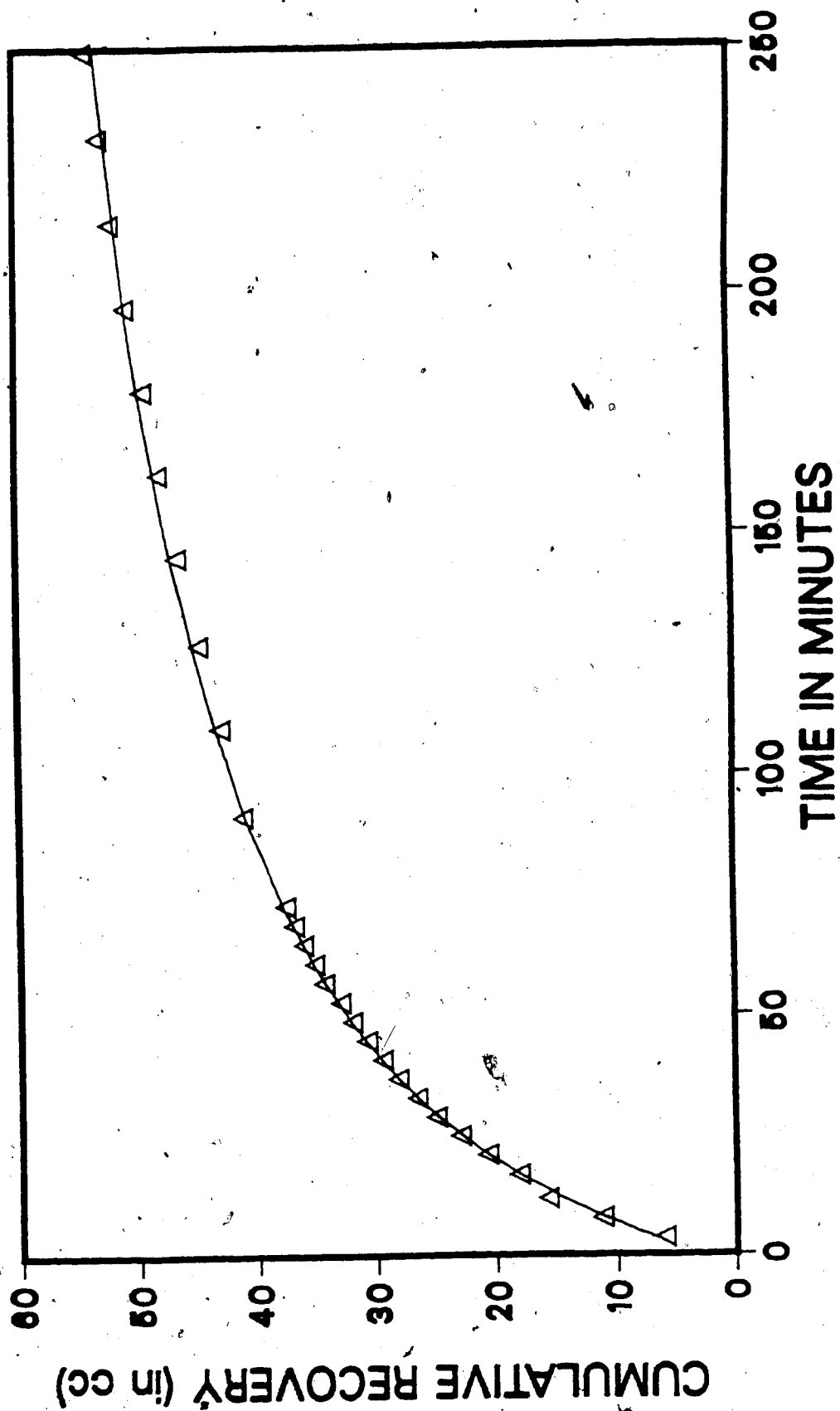


FIG. D-5 CUMULATIVE OIL PRODUCTION CURVE FIT (RUN 7)

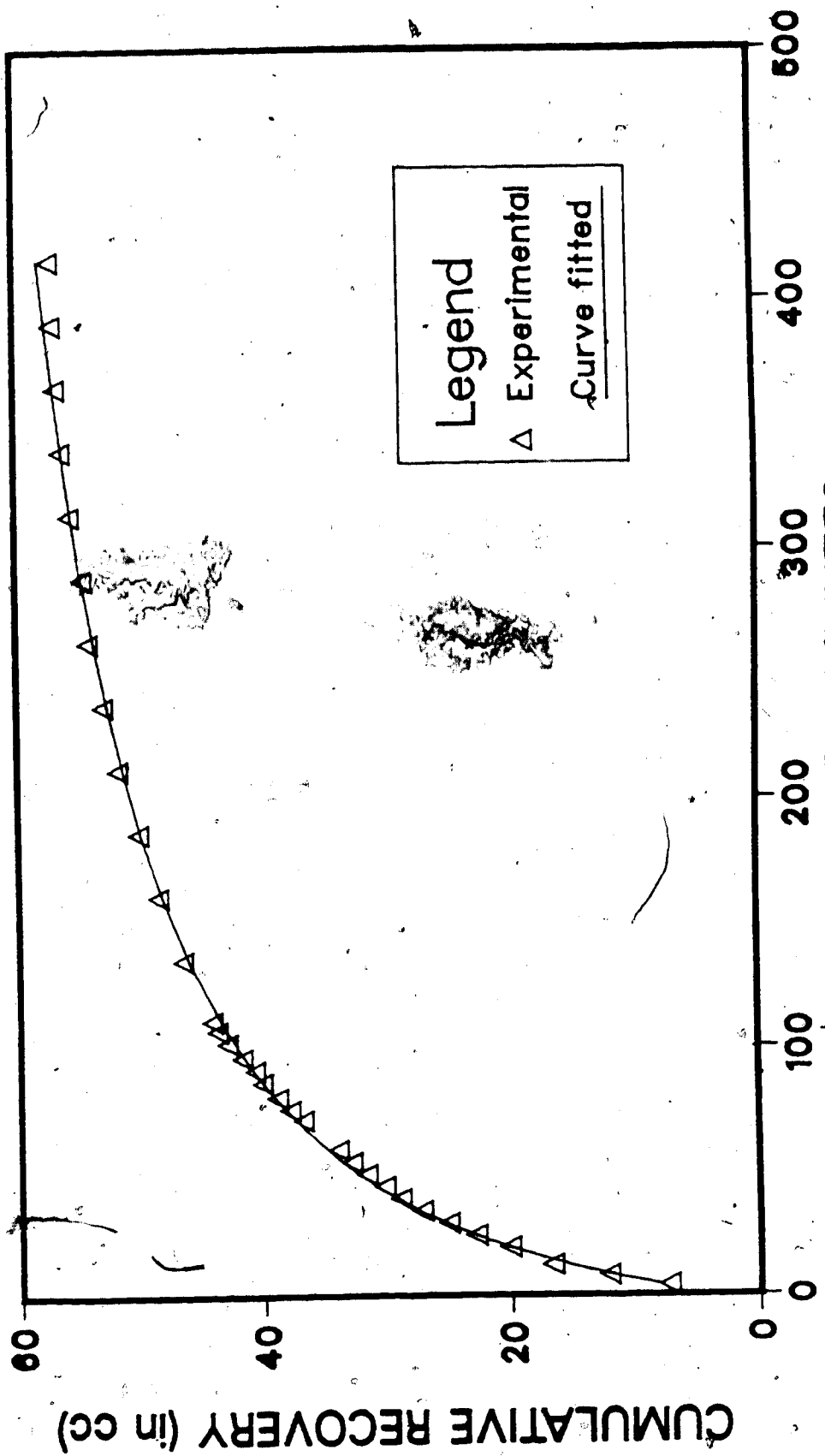


FIG. D-6 CUMULATIVE OIL PRODUCTION CURVE FIT (RUN 8)

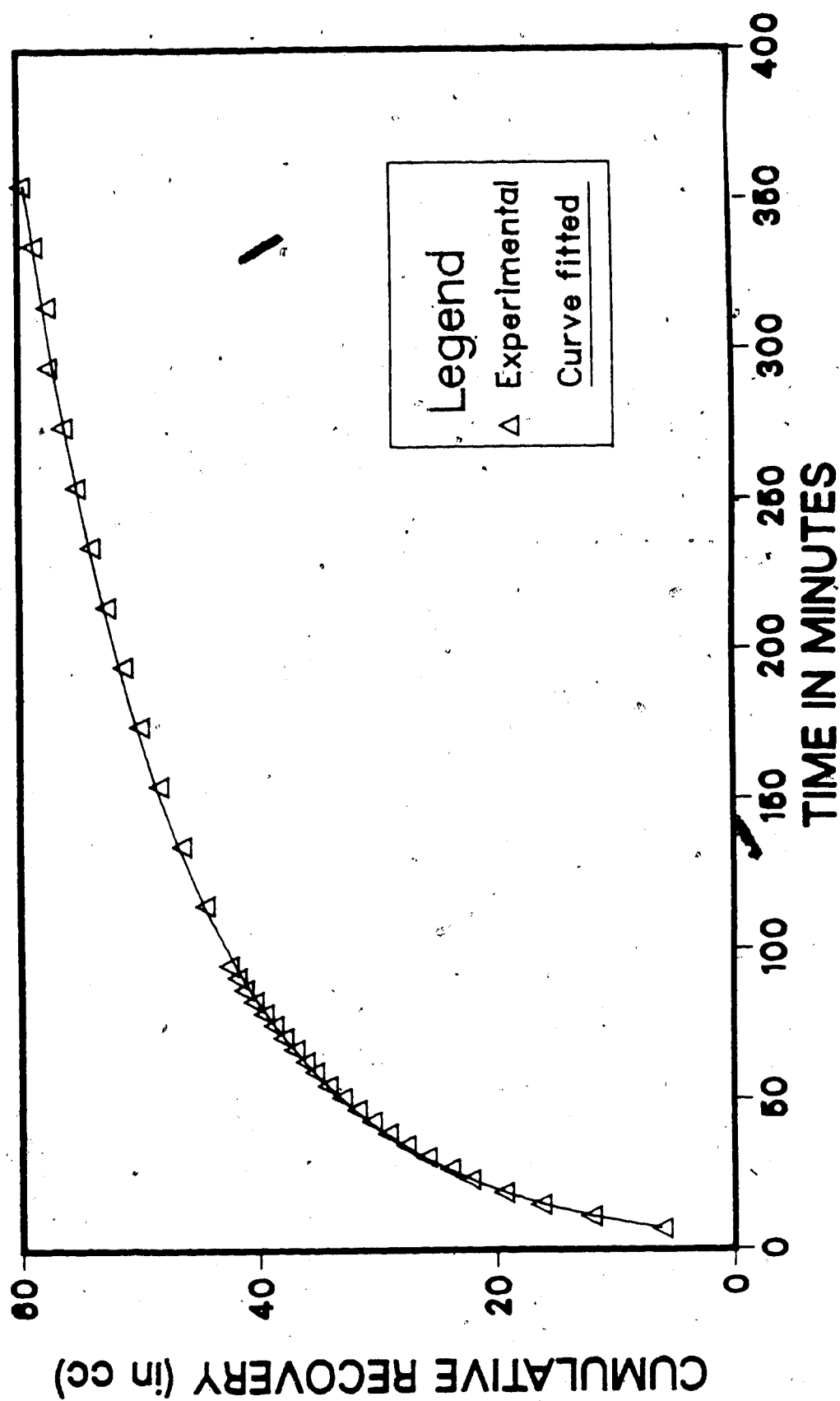


FIG. D-7 CUMULATIVE OIL PRODUCTION CURVE FIT (RUN 9)

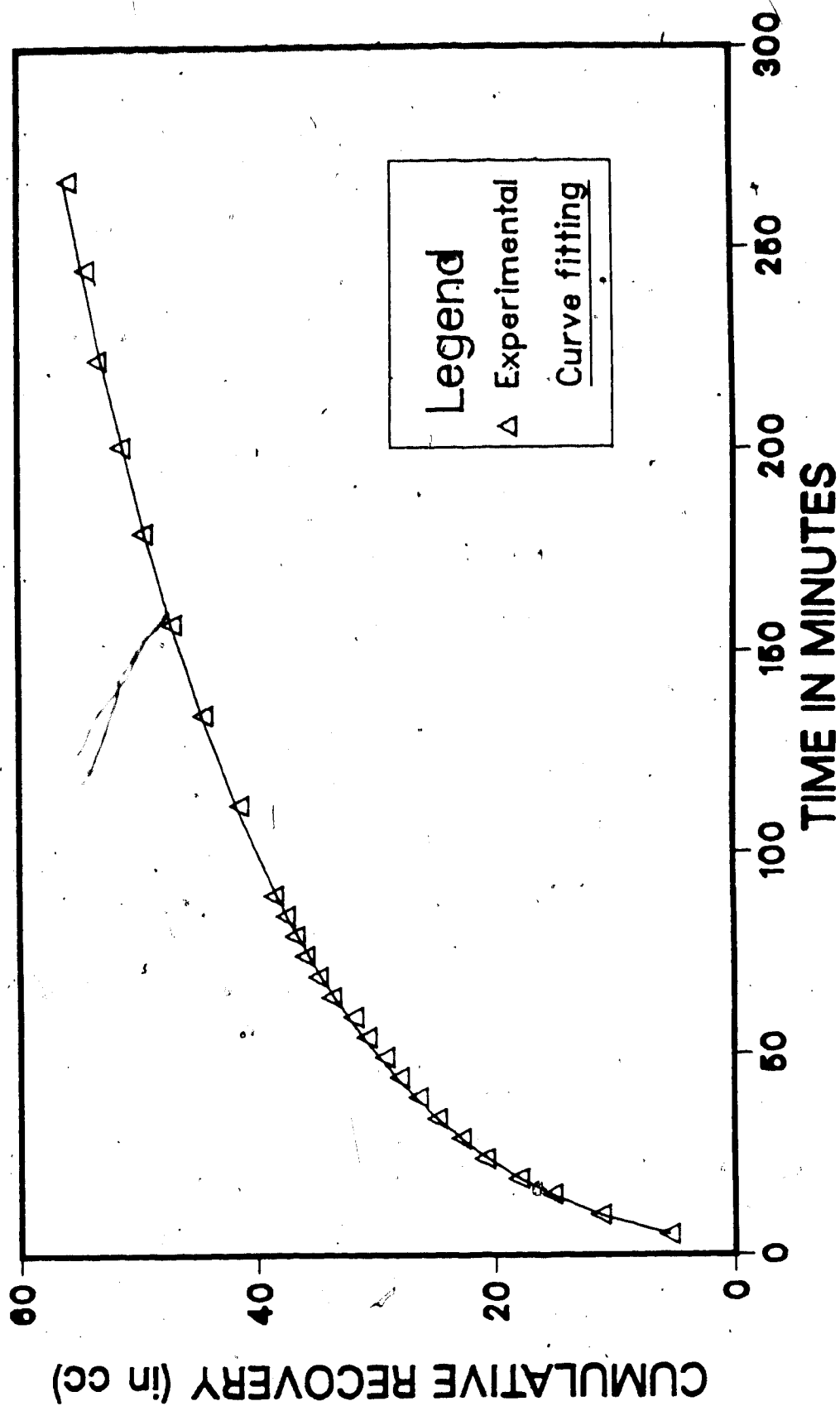


FIG. D-8 CUMULATIVE OIL PRODUCTION CURVE FIT (RUN 10)



13. APPENDIX - E

CUMULATIVE OIL RECOVERY (at  $\xi = 0.45$ ) VERSUS TIME CURVE FIT

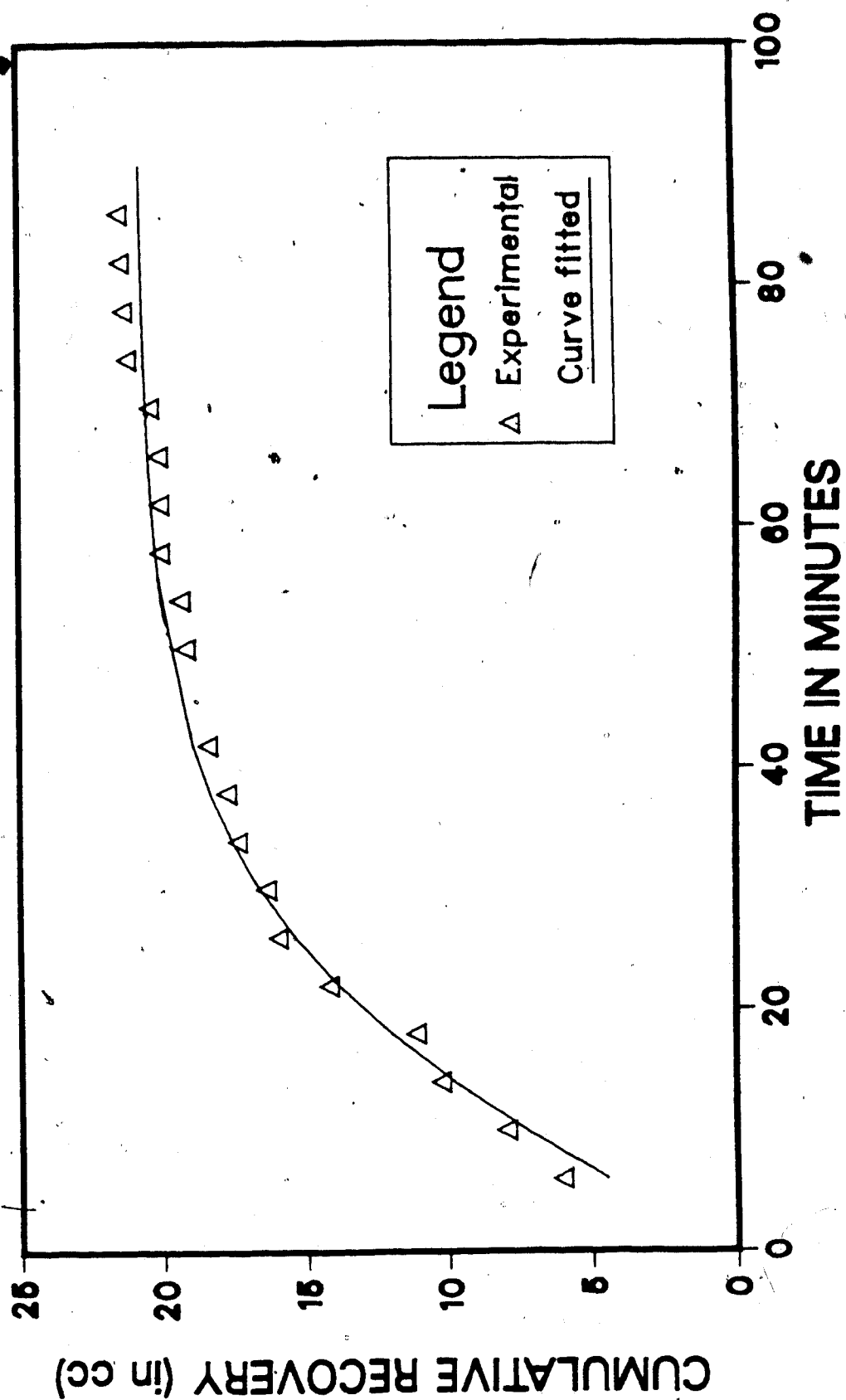


FIG. E-1 CUMULATIVE OIL PRODUCTION CURVE FIT (AT  $\xi = .45$ ) (RUN 5)

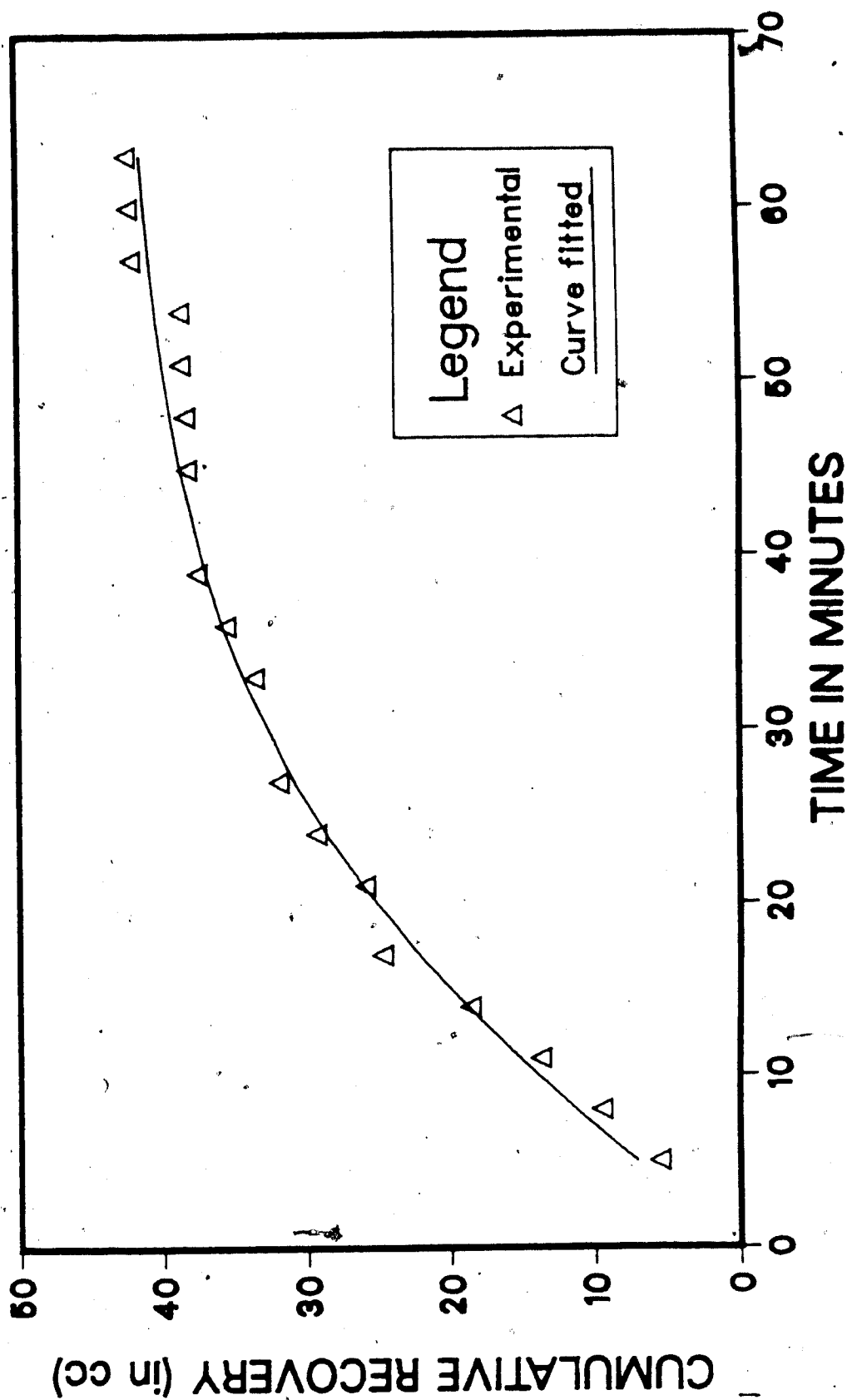


FIG. E-2 CUMULATIVE OIL PRODUCTION CURVE FIT (AT  $\xi = .45$ ) (RUN 7)

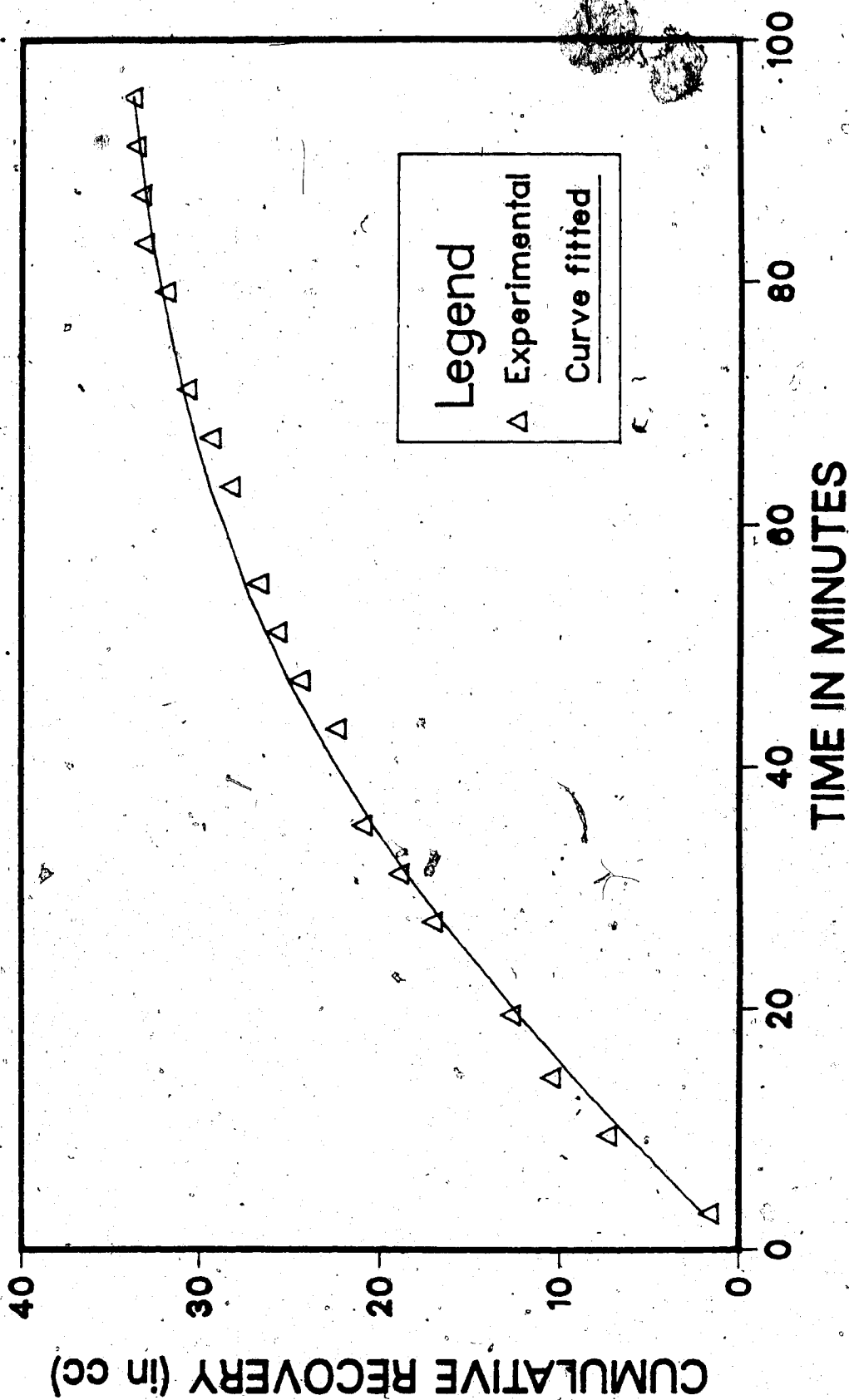


FIG. E-3 CUMULATIVE OIL PRODUCTION CURVE FIT (AT  $\xi = .45$ ) (RUN 8)

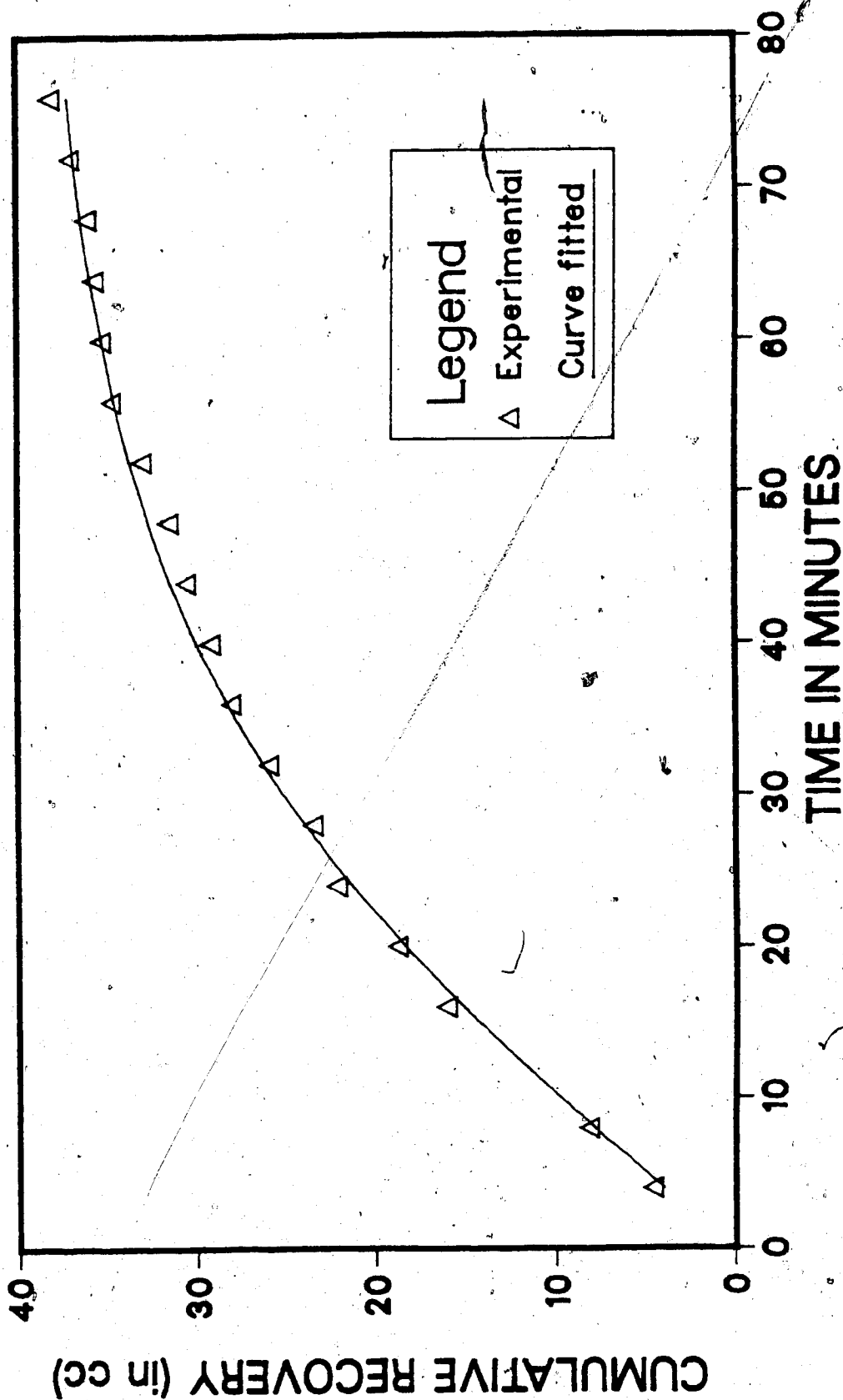


FIG. E-4 CUMULATIVE OIL PRODUCTION CURVE FIT (AT  $\xi = .45$ ) (RUN 9)

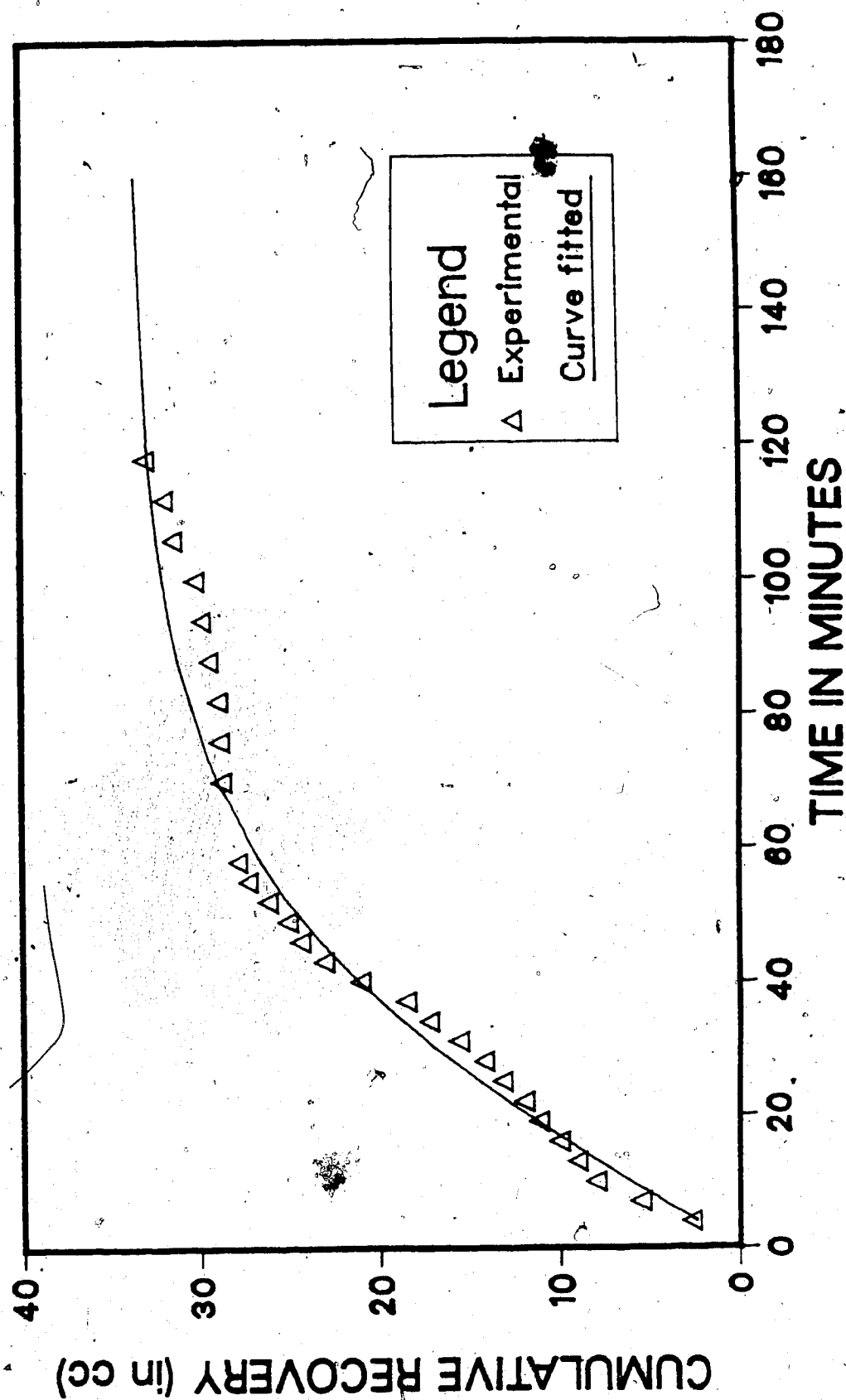


FIG. E-5 CUMULATIVE OIL PRODUCTION CURVE FIT (AT  $\xi = .45$ ) (RUN 10)

#### 14. APPENDIX - F

CUMULATIVE OIL RECOVERY (at  $\xi = 0.66$ ) VERSUS TIME CURVE FIT

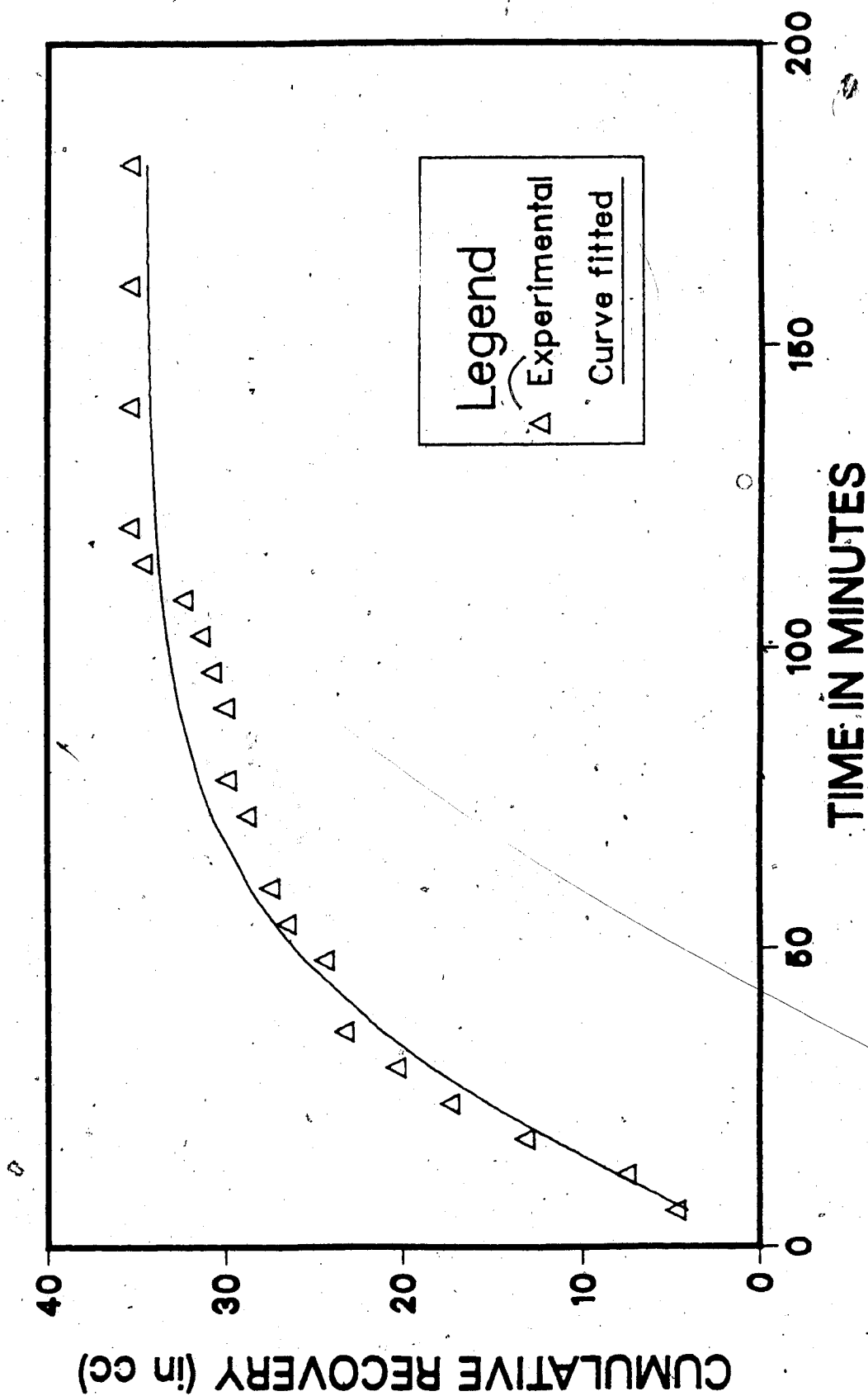


FIG. F-1 CUMULATIVE OIL PRODUCTION CURVE FIT (AT  $\xi = .66$ ) (RUN 1)



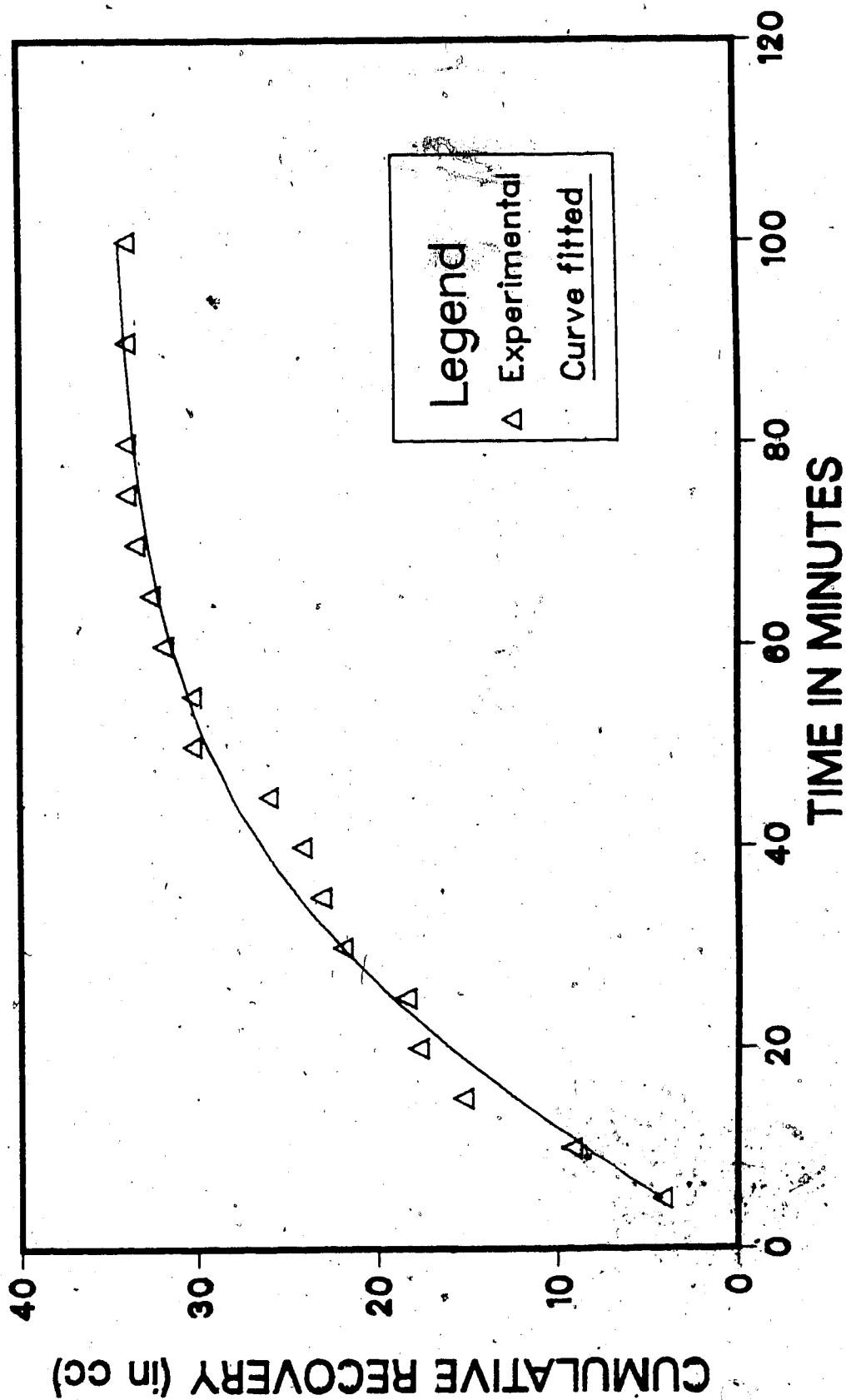


FIG. F-2 CUMULATIVE OIL PRODUCTION CURVE FIT (AT  $\xi = .66$ ) (RUN 2)

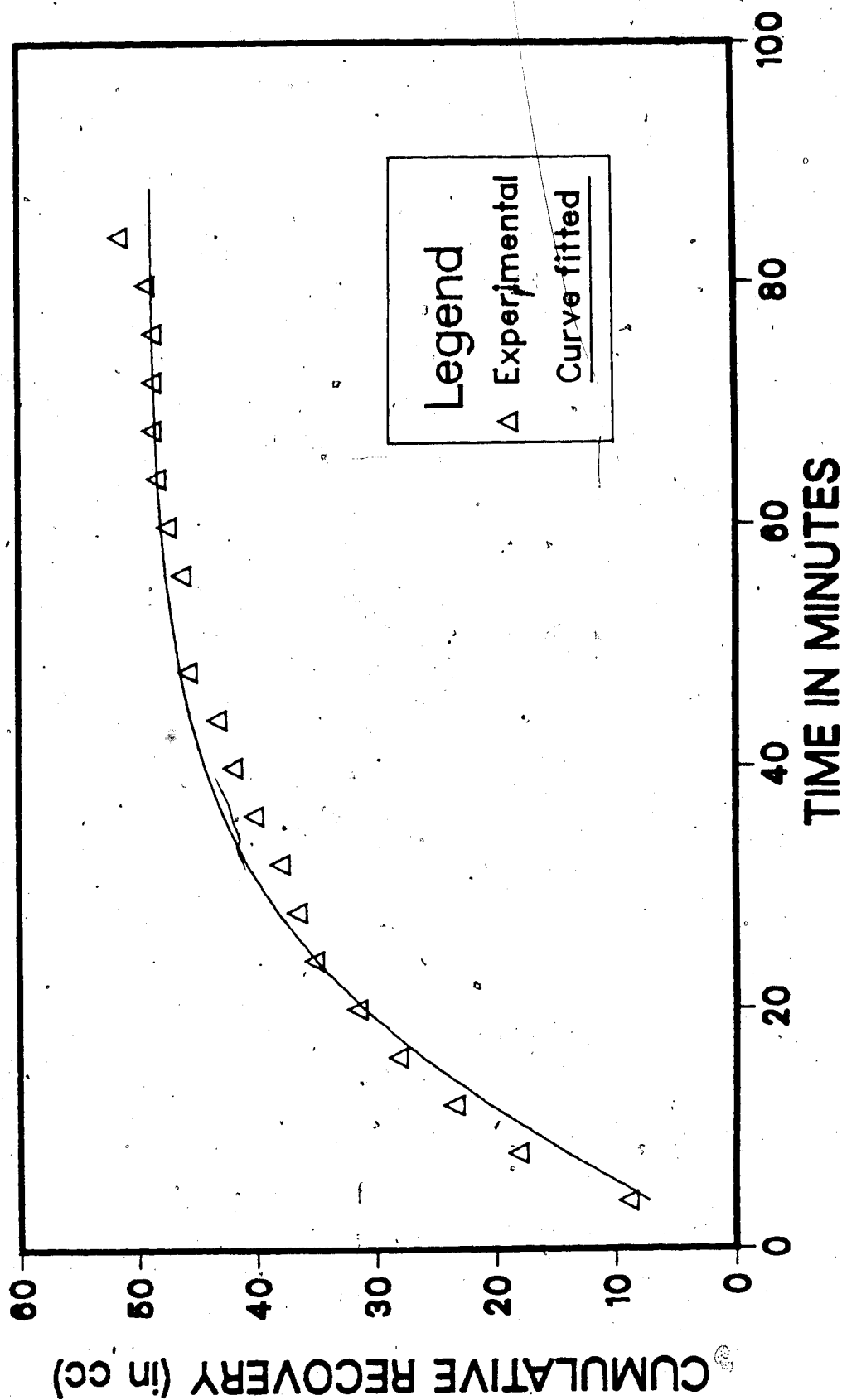


FIG. F-3 CUMULATIVE OIL PRODUCTION CURVE FIT (AT  $\xi = .66$ ) (RUN 4)

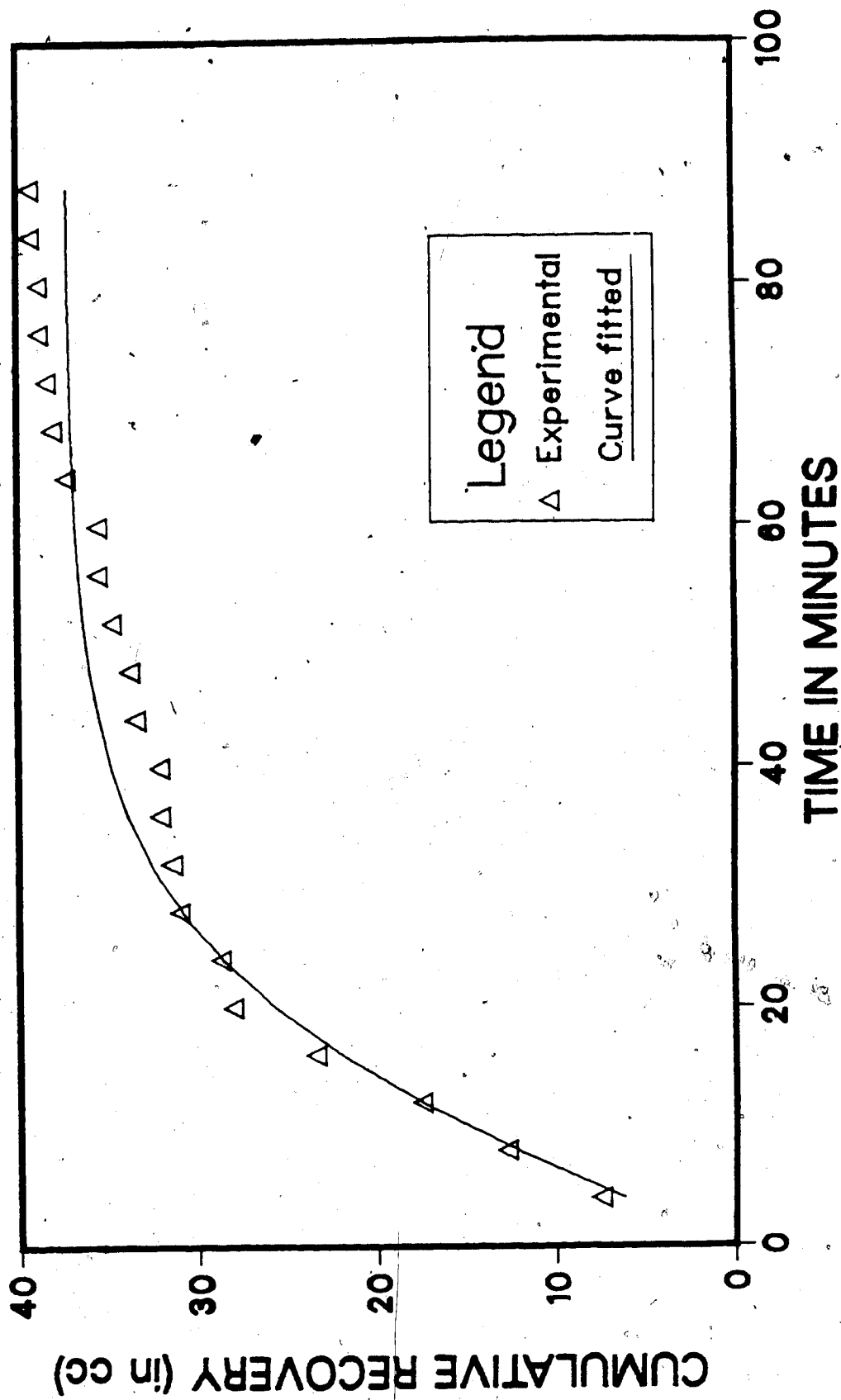


FIG. F-4 CUMULATIVE OIL PRODUCTION CURVE FIT (AT  $\xi = .66$ ) (RUN 5)

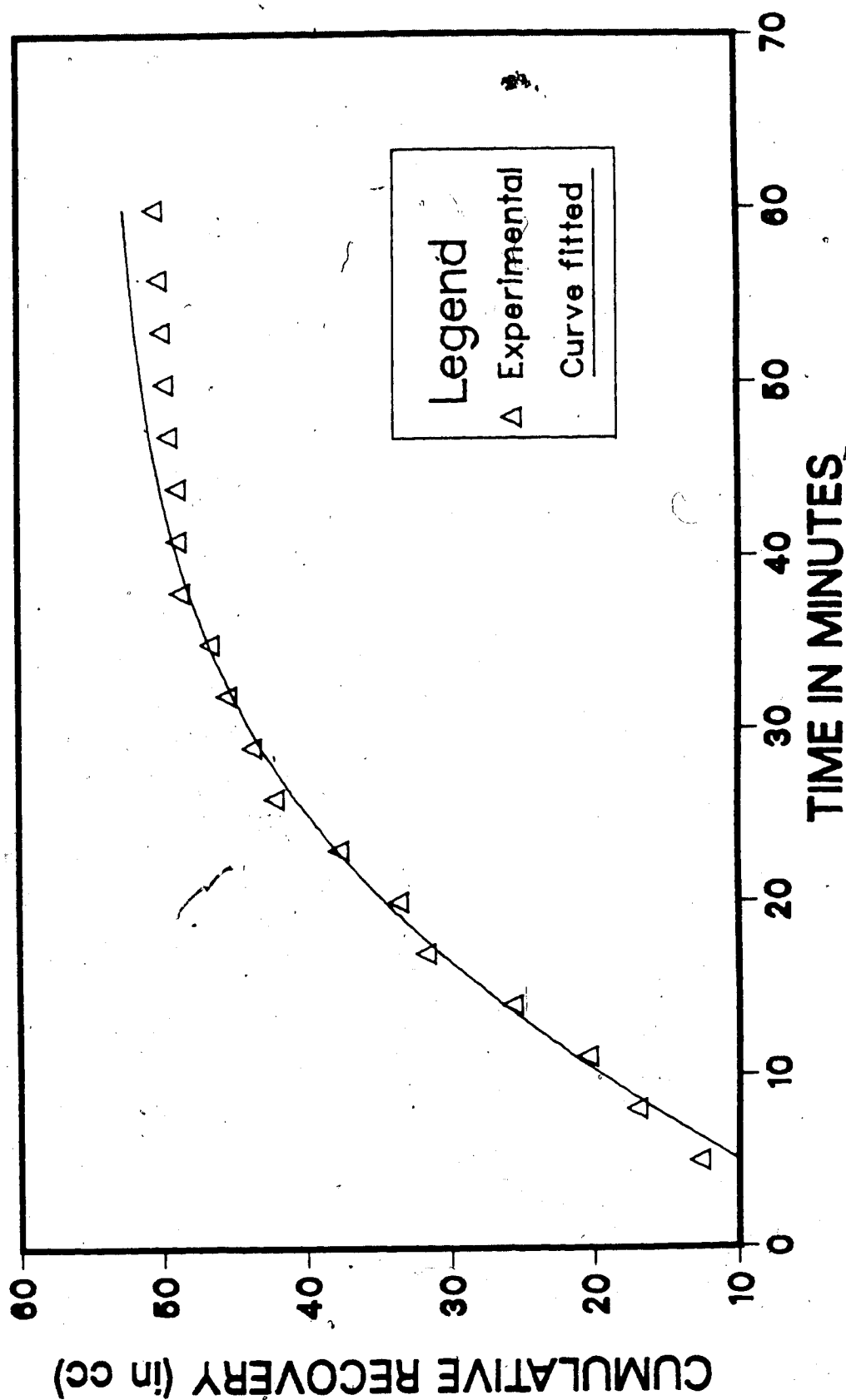


FIG. F-5 CUMULATIVE OIL PRODUCTION CURVE FIT (AT  $\xi = .66$ ) (RUN 7)

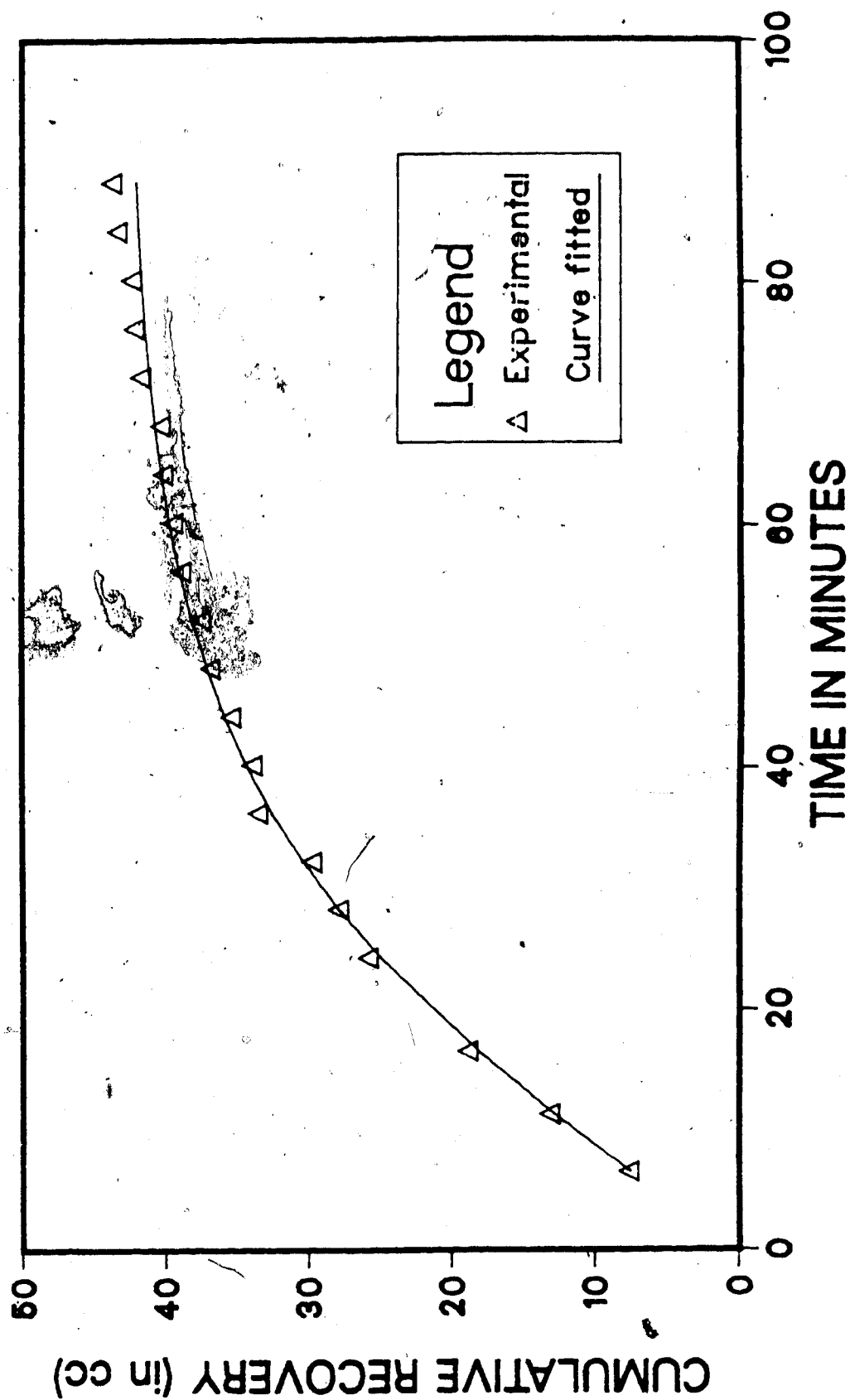


FIG. F-6 CUMULATIVE OIL PRODUCTION CURVE FIT (AT  $\xi = .66$ ) (RUN 8)

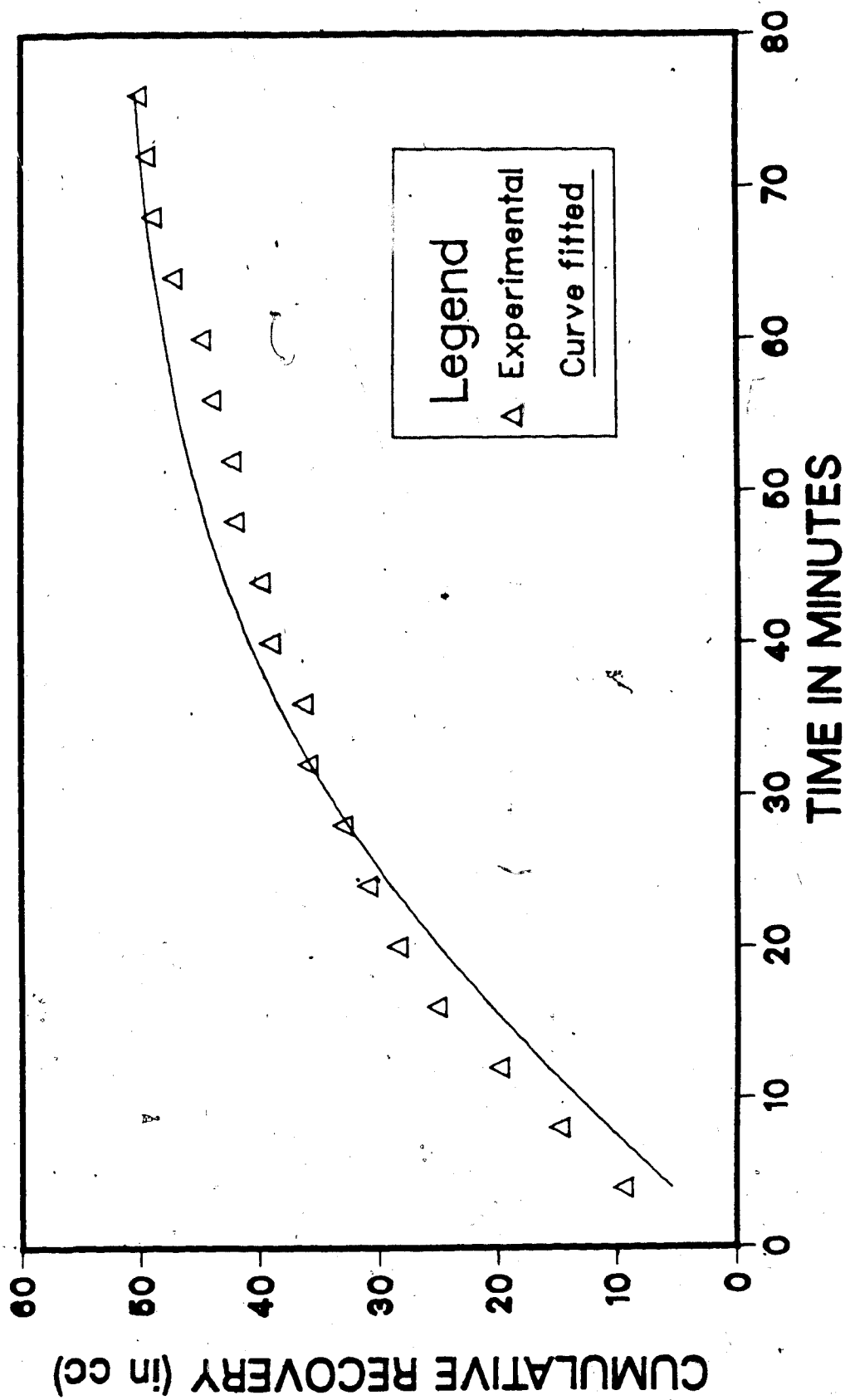


FIG. F-7 CUMULATIVE OIL PRODUCTION CURVE FIT (AT  $\xi = .66$ ) (RUN 9)

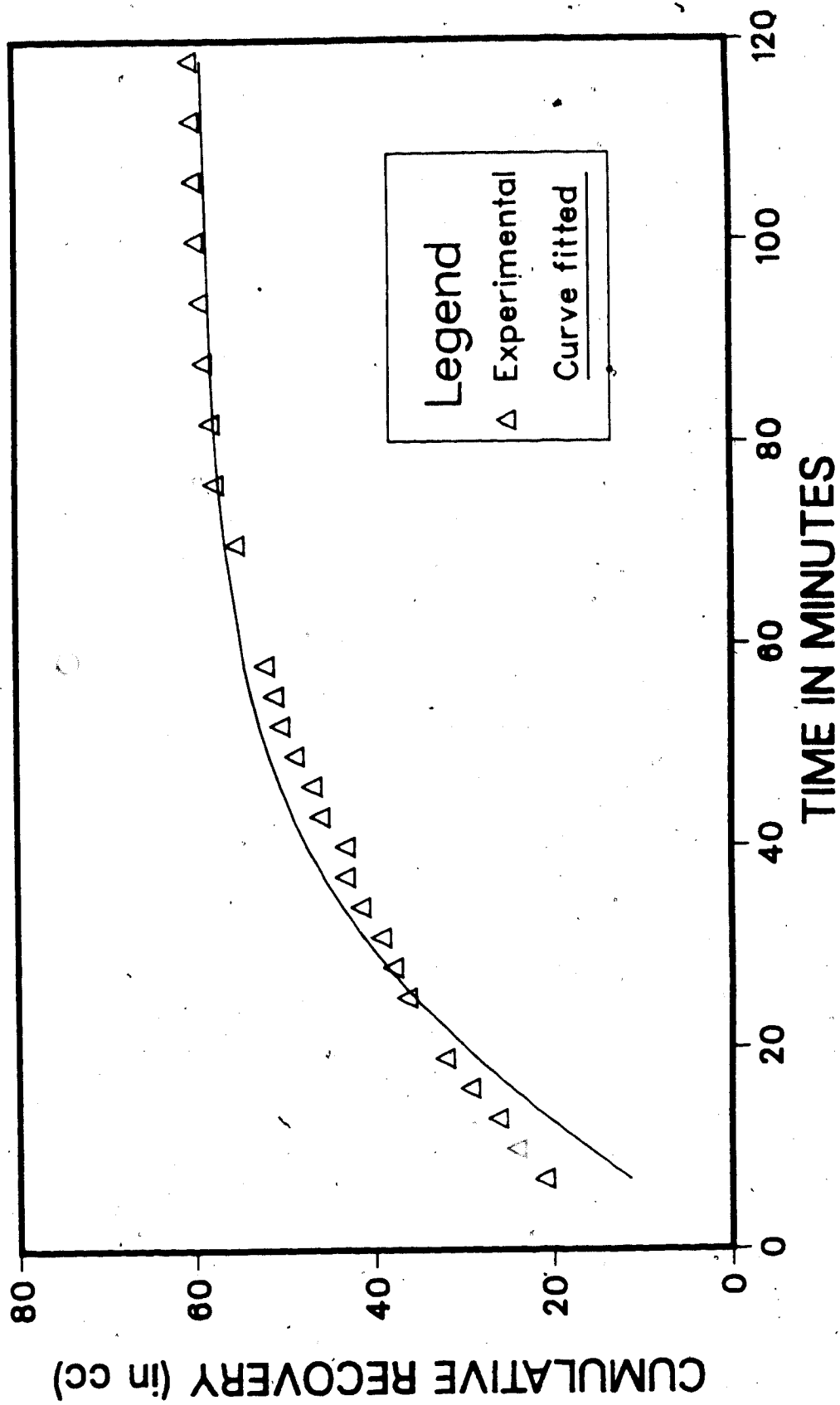


FIG. F-8 CUMULATIVE OIL PRODUCTION CURVE FIT (AT  $\xi = .66$ ) (RUN 10)

15. APPENDIX - G

EXAMPLE OF PRESSURE PROFILE CURVE FIT



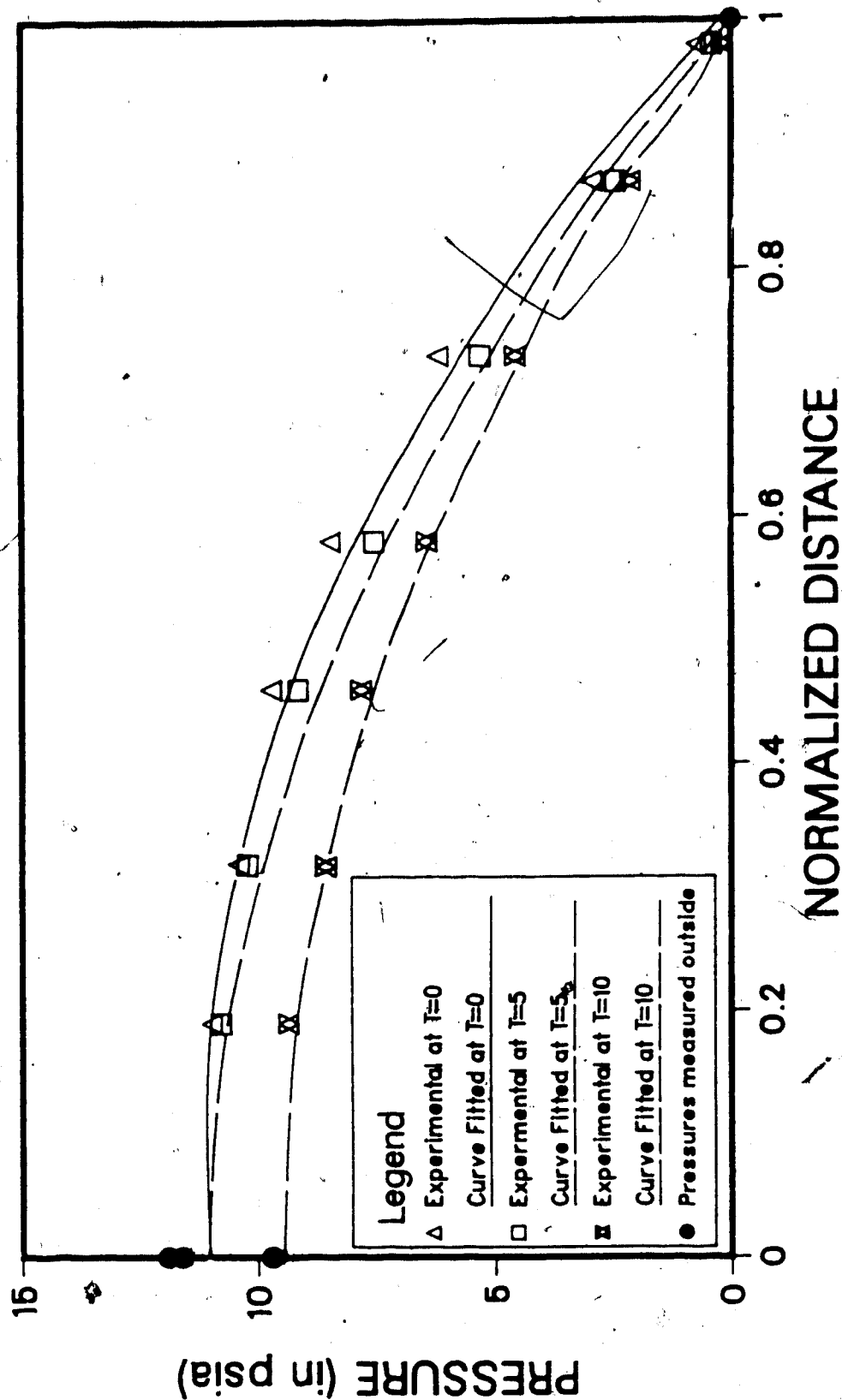


FIG. G-1 EXAMPLE OF PRESSURE PROFILE CURVE-FIT (RUN 5)

16. APPENDIX - H

PARAMETERS OF THE CAPILLARY PRESSURE CURVE FIT

TABLE H-1

## Parameters of the Capillary Pressure Curve Fit

	MCT5+LAGO	DOW-CORNING
$a_c$	0.1085E+01	0.1808E+01
$b_c$	0.6728E+00	-0.4714E-01
$c_c$	0.1212E-04	0.1545E-01
$d_c$	0.9999E+00	0.9256E+00
$e_c$	0.5349E-03	0.9003E-01
$f_c$	0.1000E-02	0.1343E+00

17. APPENDIX - I

COMPUTER PROGRAMS FOR THE SIMPLEX ALGORITHM

# A SIMPLEX METHOD FOR FUNCTION MINIMIZATION

REFERENCE: NELDER, J.A., MEAD, R.  
A SIMPLEX METHOD FOR FUNCTION MINIMIZATION  
COMPUTER JOURNAL, VOL 7  
PP 308, 1965

## VARIABLE DEFINITION:

NAME	DIMENSION	FUNCTION
ALPHA		COEFFICIENT OF REFLECTION
BETA		COEFFICIENT OF CONTRACTION
CENTRO	50	CENTROID COORDINATES
CYCCONT		NO. OF OBJECTIVE EVALUATIONS
CYCLES		MAXIMUM NO. OF CYCCONT ALLOWED
GAMMA		COEFFICIENT OF EXPANSION
GENMAT	51 X 50	MATRIX OF COORDS IN HYPERSPACE
GUESS	50	INITIAL GUESS VECTOR FOR GENMAT
H		ROW POINTER FOR HIGHEST OBJECTIVE
L		ROW POINTER FOR LOWEST OBJECTIVE
N		NUMBER OF ELEMENTS IN A ROW
OBJVAL	51	VECTOR OF OBJECTIVE VALUES
R		WORK VARIABLE
REFLECT	50	VECTOR OF COORDS FOR REFLECTION
S		ROW POINTER FOR SECOND HIGHEST OBJECTIVE
STDERR		STANDARD ERROR OF OBJVAL ABOUT LOWEST
VALUE		STEP SIZES FOR GUESS TO GIVE INITIAL
STEP	50	COUNTER FOR NUMBER OF SIMPLEX SIZE
GENMAT		CONVERGENCE CRITERION FOR STDERR
REDUCTIONS		WORK VARIABLE
STOP		WORK VARIABLE
T1		WORK VECTOR
T2		
TEMP1	50	

```

C      TEMP2      5Q      WORK VECTOR (NOT IN USE WITH THIS LISTING)
C      TEMP3      WORK VARIABLE
C      U          WORK VARIABLE
C      Y          CALCULATED OBJECTIVE VALUE FOR ROW H
C *****
C      USAGE: THE PROGRAM EXPECTS DATA ENTRY TO HAVE THE FOLLOWING
C      STRUCTURE. CARD 1: NUMBER OF SEARCH ELEMENTS. (1<N<52)
C      CARD 2: A VECTOR OF N ELEMENTS (FIRST GUESSES) FROM WHICH
C      THE INITIAL SIMPLEX IS GENERATED. CARD 3: A VECTOR OF N
C      ELEMENTS WHICH REPRESENT THE STEP SIZE FOR PERTURBATION
C      OF THE FIRST GUESSES IN INITIALIZATION OF THE SIMPLEX.
C      NOTE: DATA IS FREE FORMAT AND MUST BE SEPARATED BY A COMMA
C *****
C ***** LOGICAL*1 FREE(1) /'/'/
C      DIMENSION CENTRO(50), GENMAT(51,50), GUESS(50), STEP(50),
C      REFCT(50)
C      DIMENSION OBJVAL(101), TEMP1(101), TEMP2(101)
C      INTEGER CYCLES, H, STEPNO, CYCCNT, S, OUTPUT
C      COMMON GENMAT, OBJVAL, Y, S, L, CYCCNT, N, NPLUS1, OUTPUT, H
C *****
C      VARIABLE INITIALIZATION
C *****
C ***** SET UP STOPPING CRITERION AND CYCLE LIMIT
C      INDEX = 1
C      WRITE (6,10)
C      10 FORMAT (1X, 'ENTER TOLERANCE')
C      READ (5,FREE) STOP
C      WRITE (6,20)
C      20 FORMAT (1X, 'ENTER NO. OF CYCLES')
C      READ (5,FREE) CYCLES
C      OUTPUT = 0
C      SETUP REFLECTION, EXPANSION, AND CONTRACTION COEFFICIENTS
C      ALPHA = 1
C      GAMMA = 2
C      BETA = .5
C      READ IN NUMBER OF ELEMENTS PER SIMPLEX ROW
C      READ (7,FREE) N
C      30 FORMAT (12)

```

```

C READ IN FIRST GUESS VECTOR FOR SIMPLEX GENERATION
  READ (7,FREE) (GUESS(I),I=1,N)
  40 FORMAT (10F5.2)
C READ IN STEP SIZES ASSOCIATED WITH GUESS(I)
  READ (7,FREE) (STEP(I),I=1,N)
C CALCULATE INITIAL SIMPLEX FROM GUESS AND STEP
  50 FORMAT (1X, I2)
  NPLUS1 = N + 1
  DO 90 J = 1, N
    DO 60 I = 1, NPLUS1
      IF (I.EQ. J + 1) GO TO 70
      GENMAT(I,J) = GUESS(J) - ((2/(FLOAT(J) + 1)) * STEP(J))
    CONTINUE
    GENMAT(I,J) = GUESS(J) + ((2/(FLOAT(J) + 1)) * STEP(J)) * FLOAT(J)
  70
    JPLUS2 = J + 2
    DO 80 I = JPLUS2, NPLUS1
      GENMAT(I,J) = GUESS(J)
    CONTINUE
  90 CONTINUE
C SETUP CYCLE COUNTER FOR OBJECTIVE EVALUATIONS
  100 CYCCNT = 0
C SETUP CYCLE COUNTER FOR SIZE REDUCTIONS
  STEPND = 0
C*****
C
C BEGIN SIMPLEX CALCULATIONS
C*****
C EVALUATE OBJECTIVE FOR ALL ROWS IN GENMAT
  110 DO 120 I = 1, NPLUS1
    H = I
    CALL OBJECT(INDEX)
    OBJVAL(I) = Y
  120 CONTINUE
C RANK THE OBJECTIVES ACCORDING TO THEIR MAGNITUDE
  130 CALL RANK
C CALCULATE THE STANDARD ERROR OF THE OBJECTIVE VALUES
    T1 = 0
    T2 = 0
    DO 140 I = 1, NPLUS1
      U = OBJVAL(I) - OBJVAL(L)
      T1 = T1 + U ** 2

```

```

T2 = T2 + U.
140 CONTINUE
  STDERR = SORT((T1 - (T2**2/NPLUS1))/N)
  IF (STDERR .LT. STOP) GO TO 320
  IF (CYCCNT .GT. CYCLES) GO TO 300
C*****
C REFLECTION
C*****
C SAVE ROW CORRESPONDING TO HIGHEST OBJECTIVE VALUE
DO 150 I = 1, N
  TEMP1(I) = GENMAT(H,I)
150 CONTINUE
C CALCULATE THE CENTROID OF THE HYPERPLANE
DO 160 J = 1, N
  CENTRO(J) = 0
  DO 160 I = 1, NPLUS1
    IF (I .EQ. H) GO TO 160
    CENTRO(J) = CENTRO(J) + GENMAT(I,J) / N
  CENTRO(J) = CENTRO(J) + GENMAT(H,J) / N
160 CONTINUE
C CALCULATE REFLECTED VALUE COORDINATES
DO 170 J = 1, N
  REFLCT(J) = (1 + ALPHA) * CENTRO(J) - ALPHA * TEMP1(J)
  GENMAT(H,J) = REFLCT(J)
170 CONTINUE
C CALCULATE OBJECTIVE ASSOC. WITH REFLECTED COORDS.
  CALL OBJECT(INDEX)
  TEMP3 = Y
C REPLACE REFLECTED ROW WITH ORIGINAL H ROW
DO 180 J = 1, N
  GENMAT(H,J) = TEMP1(J)
180 CONTINUE
C COMPARE OBJECTIVE VALUES OF LOWEST ROW AND REFLECTED COORDS.
  IF (TEMP3 .GE. OBJVAL(L)) GO TO 200
C*****
C EXPANSION
C*****
DO 190 J = 1, N
  GENMAT(H,J) = (1 + GAMMA) * REFLCT(J) - GAMMA * CENTRO(J)
190 CONTINUE
C CALCULATE OBJECTIVE ASSOCIATED WITH EXPANSION COORDS.
  CALL OBJECT(INDEX)
C COMPARE OBJECTIVES OF EXPANDED WITH LOWEST ROW
  IF (Y .GT. OBJVAL(L)) GO TO 210
C IF EXPANSION WAS A SUCCESS REPLACE ROW H

```



```

OBJVAL(H) = Y
GO TO 130
C COMPARE OBJECTIVES OF REFLECTED WITH SECOND HIGHEST ROW
200 IF (TEMP3 .GT. OBJVAL(S)) GO TO 230
C IF REFLECTION WAS A SUCCESS REPLACE ROW H
210 OBJVAL(H) = TEMP3
DO 220 J = 1, N
GENMAT(H,J) = REFLCT(J)
220 CONTINUE
GO TO 130
C COMPARE OBJECTIVES OF REFLECTION AND HIGHEST ROW
230 IF (TEMP3 .GT. OBJVAL(H)) GO TO 250
C REPLACE ROW H WITH REFLECTED COORDS.
DO 240 J = 1, N
GENMAT(H,J) = REFLCT(J)
240 CONTINUE
C*****
C***** CONTRACTION *****
C*****
C SAVE ROW H AND CALCULATE CONTRACTION COORDS.
250 DO 260 J = 1, N
TEMP1(J) = GENMAT(H,J)
GENMAT(H,J) = BETA * GENMAT(H,J) + (1 - BETA) * CENTRO(J)
260 CONTINUE
C CALCULATE OBJECTIVE ASSOC. WITH CONTRACTED COORDS.
CALL OBJECT(INDEX)
C COMPARE OBJECTIVES OF CONTRACTED COORDS. AND ROW H
IF (Y .GT. OBJVAL(H)) GO TO 270
C IF CONTRACTION WAS A SUCCESS REPLACE ROW H
OBJVAL(H) = Y
GO TO 130
C*****
C***** STEP CHANGE-----SIZE REDUCTION *****
C*****
C REPLACE CONTRACTED COORDS WITH ORIGINAL ROW H AND REDUCE SIZE
270 DO 280 J = 1, N
GENMAT(H,J) = TEMP1(J)
DO 280 I = 1, NPLUS1
GENMAT(I,J) = (GENMAT(I,J) + GENMAT(L,J)) / 2
280 CONTINUE
C INCREMENT STEP CHANGE COUNTER AND PRINT DATA
STEPNO = STEPNO + 1
290 FORMAT (' STEP CHANGE NUMBER ', I4, ' OCCURRED NEAR CYCLE
1 14)

```





```

SUBROUTINE OBJECT(INDEX)
  LOGICAL*1 FREE(1) /'.*.'/
  DIMENSION GENMAT(51,50), OBJVAL(101)
  INTEGER CYCLES, H, STEPNO, CYCCNT, S, OUTPUT
  COMMON GENMAT, OBJVAL, Y, S, L, CYCCNT, N, NPLUS1, OUTPUT, H
  *****
  C THIS ONE IS FOR CUM OIL PROD. DATA FIT FOR DYNAMIC METHOD
  *****

```

```

C
C CONVENTION: THE SEARCH VARIABLES ARE LOCATED IN ROW
C              H OF THE SIMPLEX MATRIX 'GENMAT'. EG.
C              GENMAT(H,3) WOULD CONTAIN THE VALUE FOR
C              THE THIRD UNKNOWN. YOU MAY REQUIRE TO
C              CONSTRAIN THESE VALUES PRIOR TO YOUR
C              CALCULATIONAL BLOCK (EG. ABSOLUTE VALUES).
C

```

RULES: THE OBJECTIVE FUNCTION VALUE MUST ALWAYS  
BE CALCULATED IN THE VARIABLE 'Y'.

ONCE THE SEARCH IS FINISHED IT WILL OUTPUT  
SOME INFORMATION THEN SET THE 'OUTPUT' FLAG  
TO 1 FROM 0, AND CALL THIS SUBROUTINE WITH  
THE BEST POINT IN THE CURRENT SIMPLEX. THIS  
ALLOWS THE USER TO PROVIDE ADDITIONAL  
PERTINENT OUTPUT.

```

DO NOT REMOVE THE LINE.
  'CYCCNT=CYCCNT+1'
FROM THE SUBPROGRAM AS IT IS USED IN JOB
CONTROL.

```

```

*****
C
C DIMENSION Q(120), QP(120), TIME(120), W(120)
C IF (INDEX.NE. 1) GO TO 40
C WRITE (6,10)
C 10 FORMAT (1X, 'ENTER NO. OF DATA POINTS')
C READ (5, FREE) NDATA
C DO 30 I = 1, NDATA
C 20 READ (1, FREE) TIME(I), Q(I)
C 30 CONTINUE
C 40 CONTINUE
C INDEX = 2
C A = (GENMAT(H,1))

```

```

      B = (GENMAT(H,2))
      Y = O,
      DO 50 II = 1, NDATA
      CC = (TIME(II))
      QP(II) = A * TANH(TIME(II)/B)
      Y = Y + (QP(II) - Q(II)) ** 2
50 CONTINUE
      CYCCNT = CYCCNT + 1
      IF (OUTPUT .EQ. 0) RETURN
      WRITE (6,60) A, B
60 FORMAT ('O', 2(E11.4,1X), 1X, E10.4, 1X, F10.4, /, 4(E10.4,1X))
      WRITE (6,70)
70 FORMAT ('O', 'TIME', 6X, 'OBSERVED', 2X, 'PREDICTED', 1X,
      'RESIDUAL', /, /, 40('-'))
      DO 90 II = 1, NDATA
      PPP = A / B / COSH(TIME(II)/B) ** 2
      RES = (QP(II) - QP(II)) / Q(II) * 100.
      WRITE (6,80) TIME(II), Q(II), QP(II), RES, PPP
80 FORMAT (F6.2, 4X, F6.2, 2X, F6.2, 2X, F6.2, 2X, F7.3)
90 CONTINUE
      RETURN
      END

```

```

SUBROUTINE OBJECT(INDEX)
  LOGICAL*1 FREE(1) /'.'/
  DIMENSION GENMAT(51,50), OBJVAL(101)
  INTEGER CYCLES, H, STEPNO, CYCCNT, S, OUTPUT
  COMMON GENMAT, OBJVAL, Y, S, L, CYCCNT, N, NPLUS1, OUTPUT, H
  *****
  C THIS PROGRAM IS FOR CAPILLARY PRESSURE FIT
  *****

C
C
C CONVENTION: THE SEARCH VARIABLES ARE LOCATED IN ROW
C              H OF THE SIMPLEX MATRIX 'GENMAT'. EG.
C              GENMAT(H,3) WOULD CONTAIN THE VALUE FOR
C              THE THIRD UNKNOWN. YOU MAY REQUIRE TO
C              CONSTRAIN THESE VALUES PRIOR TO YOUR
C              CALCULATIONAL BLOCK (EG. ABSOLUTE VALUES).
C
C
C RULES: THE OBJECTIVE FUNCTION VALUE MUST ALWAYS
C         BE CALCULATED IN THE VARIABLE 'Y'.
C
C
C ONCE THE SEARCH IS FINISHED IT WILL OUTPUT
C SOME INFORMATION THEN SET THE 'OUTPUT' FLAG
C TO 1 FROM 0, AND CALL THIS SUBROUTINE WITH
C THE BEST POINT IN THE CURRENT SIMPLEX. THIS
C ALLOWS THE USER TO PROVIDE ADDITIONAL
C PERTINENT OUTPUT.
C
C
C DO NOT REMOVE THE LINE,
C   'CYCCNT=CYCCNT+1'
C FROM THE SUBPROGRAM AS IT IS USED IN JOB
C CONTROL.
C
C *****
C
C DIMENSION Q(120), QP(120), TIME(120), W(120)
C IF (INDEX.NE. 1) GO TO 40
C WRITE (6,10)
C 10 FORMAT (1X, 'ENTER NO. OF DATA POINTS')
C READ, (5,FREE) NDATA
C DO 30 I = 1, NDATA
C 20 READ (1,FREE) TIME(I), Q(I)
C   TIME(I) = (TIME(I) - 1) / 7
C 30 CONTINUE
C 40 CONTINUE
C INDEX = 2
C A = (GENMAT(H,1))

```

```

IF (GENMAT(H,3) .GE. 1) GENMAT(H,3) = .99
IF (GENMAT(H,4) .GE. 1) GENMAT(H,4) = .99
IF (GENMAT(H,5) .GE. 1) GENMAT(H,5) = .99
IF (GENMAT(H,6) .GE. 1) GENMAT(H,6) = .99
IF (GENMAT(H,3) .LE. 0) GENMAT(H,3) = .001
IF (GENMAT(H,4) .LE. 0) GENMAT(H,4) = .001
IF (GENMAT(H,5) .LE. 0) GENMAT(H,5) = .001
IF (GENMAT(H,6) .LE. 0) GENMAT(H,6) = .001
B = (GENMAT(H,2))
D = (GENMAT(H,4))
C = (GENMAT(H,3))
E = (GENMAT(H,5))
F = (GENMAT(H,6))
Y = 0.
DO 60 II = 1, NDATA
SS = (TIME(II))
FORMAT ('S= ', F10.3)
CA = -A / (1 - D) * (SS - C) ** (1 - D)
CB = -B / (1 - F) * (1 + E - SS) ** (1 - F)
CC = A / (1 - D) * (1 + C) ** (1 - D)
CD = -B / (1 - F) * E ** (1 - F)
QP(II) = CA + CB + CC + CD
Y = Y + (QP(II) - Q(II)) ** 2
60 CONTINUE
CYCCNT = CYCCNT + 1
IF (OUTPUT .EQ. 0) RETURN
WRITE (6,70) A, B, C, D, E, F
70 FORMAT ('O', 2(E11.4,1X), 1X, E10.4, 1X, F10.4, /, 4(E10.4,1X))
WRITE (6,80)
80 FORMAT ('O', 'TIME', 6X, 'OBSERVED', 2X, 'PREDICTED', 1X,
1 'RESIDUAL', /, 40('-'))
AC1 = A * (C**2 - D) - (1 + C)**(2 - D) / (1 - D) / (2 - D)
AC2 = B * ((1 - E)**(2 - F) - E**2 - F) / (1 - F) / (2 - F)
AC3 = A / (1 - D) * (1 + C) ** (1 - D) - B / (1 - F) * E ** (1 -
1F)
AREA = AC1 + AC2 + AC3
WRITE (6,90) AREA, Y
90 FORMAT (1X, 'AREA UNDER THE CURVE= ', E12.6, 2X, 'Y= ', E10.4)
DO 110 II = 1, NDATA
RES = (Q(II) - QP(II)) / Q(II) * 100.
WRITE (6,100) TIME(II), Q(II), QP(II), RES
110 CONTINUE

```

100 FORMAT ( ' ' , F8.4, 4X, F8.4, 2X, F8.4, 2X, F6.2)

110 CONTINUE

RETURN

END



```

SUBROUTINE OBJECT(INDEX)
  LOGICAL*1 FREE(1) /*,
  DIMENSION GENMAT(51,50), OBJVAL(101), QQ(120)
  INTEGER CYCLES, H, STEPNO, CYCNT, S, OUTPUT,
  COMMON GENMAT, OBJVAL, Y, S, L, CYCNT, N, NPLUST, OUTPUT, H
  C *****
  C THIS PROGRAM IS FOR PRESSURE DATA FIT *
  C *****
  C CONVENTION: THE SEARCH VARIABLES ARE LOCATED IN ROW
  C H OF THE SIMPLEX MATRIX 'GENMAT'. EG.
  C GENMAT(H,3) WOULD CONTAIN THE VALUE FOR
  C THE THIRD UNKNOWN. YOU MAY REQUIRE TO
  C CONSTRAIN THESE VALUES PRIOR TO YOUR
  C CALCULATIONAL BLOCK (EG. ABSOLUTE VALUES).
  C
  C RULES: THE OBJECTIVE FUNCTION VALUE MUST ALWAYS
  C BE CALCULATED IN THE VARIABLE 'Y'.
  C
  C ONCE THE SEARCH IS FINISHED IT WILL OUTPUT
  C SOME INFORMATION THEN SET THE 'OUTPUT' FLAG
  C TO 1 FROM 0, AND CALL THIS SUBROUTINE WITH
  C THE BEST POINT IN THE CURRENT SIMPLEX. THIS
  C ALLOWS THE USER TO PROVIDE ADDITIONAL
  C PERTINENT OUTPUT.
  C
  C DO NOT REMOVE THE LINE,
  C 'CYCNT=CYCNT+1',
  C FROM THE SUBPROGRAM AS IT IS USED IN JOB
  C CONTROL.
  C *****
  DIMENSION Q(250), QP(250), TIME(250), W(250)
  IF (INDEX .NE. 1) GO TO 30
  WRITE (6,10)
  10 FORMAT (1X, 'ENTER NO. OF DATA POINTS')
  READ (5,FREE) NDATA
  DO 30 I = 1, NDATA
  20 READ (2,FREE) TIME(I), Q(I)
  30 CONTINUE
  INDEX = 2
  A = (GENMAT(H,1))
  IF (GENMAT(H,3) .LE. - TIME(1)) GENMAT(H,3) = -TIME(1) + .1
  B = (GENMAT(H,2))

```

```

D = (GENMAT(H,4))
C = (GENMAT(H,3))
Y = 0.
DO 40 II = 1, NDATA
  CC = (TIME(II))
  Q2 = A * ALOG(CC + C)
  Q3 = B * (ALOG(CC + C)) ** 2
  Q2 = Q2 + Q3 + D
  QP(II) = EXP(Q2)
  Y = Y + (QP(II) - Q(II)) ** 2
40 CONTINUE
CYCNT = CYCNT + 1
IF (OUTPUT .EQ. 0) RETURN
WRITE (6,50) A, B, C, D, Y
50 FORMAT ('O', 2(E10.4,1X), 1X, E10.4, 1X, F10.4, /, 4(E10.4,1X))
WRITE (6,60)
60 FORMAT ('O', 'TIME', 6X, 'OBSERVED', 2X, 'PREDICTED', 1X,
1 'RESIDUAL', /, 40('-'))
DO 80 II = 1, NDATA
  RES = (Q(II) - QP(II)) / Q(II) * 100.
  WRITE (6,70) TIME(II), Q(II), QP(II), RES
70 FORMAT (' ', F8.4, 4X, F8.4, 2X, F8.4, 2X, F8.4, 2X,
1 F7.3)
80 CONTINUE
RETURN
END

```

```

SUBROUTINE OBJECT(INDEX)
  LOGICAL*1 FREE(1) /* */
  DIMENSION GENMAT(51,50), OBJVAL(101), QO(120)
  INTEGER CYCLES, H, STEPNO, CYCCNT, S, OUTPUT
  COMMON GENMAT, OBJVAL, Y, S, L, CYCCNT, N, NPLUS1, OUTPUT, H

```

```

C*****

```

```

C CONVENTION: THE SEARCH VARIABLES ARE LOCATED IN ROW
C H OF THE SIMPLEX MATRIX 'GENMAT'. EG.
C GENMAT(H,3) WOULD CONTAIN THE VALUE FOR
C THE THIRD UNKNOWN. YOU MAY REQUIRE TO
C CONSTRAIN THESE VALUES PRIOR TO YOUR
C CALCULATIONAL BLOCK (EG. ABSOLUTE VALUES).

```

```

C RULES: THE OBJECTIVE FUNCTION VALUE MUST ALWAYS
C BE CALCULATED IN THE VARIABLE 'Y'

```

```

C ONCE THE SEARCH IS FINISHED IT WILL OUTPUT
C SOME INFORMATION THEN SET THE 'OUTPUT' FLAG
C TO 1 FROM 0, AND CALL THIS SUBROUTINE WITH
C THE BEST POINT IN THE CURRENT SIMPLEX. THIS
C ALLOWS THE USER TO PROVIDE ADDITIONAL
C PERTINENT OUTPUT.

```

```

C DO NOT REMOVE THE LINE,
C 'CYCCNT=CYCCNT+1'

```

```

C FROM THE SUBPROGRAM AS IT IS USED IN JOB
C CONTROL.

```

```

C*****

```

```

C DIMENSION Q(120), QP(120), TIME(120), W(120)
C IF (INDEX.NE. 1) GO TO 30

```

```

C WRITE (6,10)

```

```

C 10 FORMAT (1X, 'ENTER NO. OF DATA POINTS')

```

```

C READ (5, FREE) NDATA

```

```

C DO 20 I = 1, NDATA

```

```

C   READ (1, FREE) TIME(I), Q(I)

```

```

C 20 CONTINUE

```

```

C 30 CONTINUE

```

```

C INDEX = 2

```

```

C A = (GENMAT(H,1))

```

```

C B = (GENMAT(H,2))

```

```

C = (GENMAT(H,3))
D = (GENMAT(H,4))
E = (GENMAT(H,5))
F = (GENMAT(H,6))
Y = 0.
DO 40 II = 1, NDATA
  CC = (TIME(II))
  QP(II) = A - B * CC - C * CC * CC
  Y = Y + (QP(II) - Q(II)) ** 2
40 CONTINUE
CYCUNT = CYCUNT + 1
IF (OUTPUT .EQ. 0) RETURN
WRITE (6,50) A, B, C, Y
  QPIT = B + 2 * C * .45
  QPIT1 = B + 2 * C * .66
WRITE (6,50) QPIT, QPIT1
WRITE (8,50) QPIT, QPIT1
50 FORMAT ('O', 4(E10.4,1X), 1X, E10.4, 1X, F10.4, /, 4(E10.4,1X))
WRITE (6,60)
60 FORMAT ('O', 'TIME', 6X, 'OBSERVED', 2X, 'PREDICTED', 1X,
1  'RESIDUAL', /, 40('-'))
DO 80 II = 1, NDATA
  RES = (Q(II) - QP(II)) / Q(II) * 100.
  WRITE (6,70) TIME(II), Q(II), QP(II), RES
70  FORMAT (' ', F6.2, 4X, F6.2, 2X, F6.2, 2X, F6.2, 2X,
1  F7.3)
80 CONTINUE
RETURN
END

```

```

SUBROUTINE OBJECT(INDEX)
  LOGICAL*1 FREE(1) /*'/'
  DIMENSION GENMAT(51,50), OBJVAL(101)
  INTEGER CYCLES, H, STEPNO, CYCCNT, S, OUTPUT
  COMMON GENMAT, OBJVAL, Y, S, L, CYCCNT, N, NPLUS1, OUTPUT, H
  *****
  C THIS PROGRAM IS FOR CUM OIL PROD. DATA FIT *
  *****

```

```

C CONVENTION: THE SEARCH VARIABLES ARE LOCATED IN ROW
C H OF THE SIMPLEX MATRIX 'GENMAT'. EG.
C GENMAT(H,3) WOULD CONTAIN THE VALUE FOR
C THE THIRD UNKNOWN. YOU MAY REQUIRE TO
C CONSTRAIN THESE VALUES PRIOR TO YOUR
C CALCULATIONAL BLOCK (EG. ABSOLUTE VALUES).

```

```

C RULES: THE OBJECTIVE FUNCTION VALUE MUST ALWAYS
C BE CALCULATED IN THE VARIABLE 'Y'.

```

```

C ONCE THE SEARCH IS FINISHED IT WILL OUTPUT
C SOME INFORMATION THEN SET THE 'OUTPUT' FLAG
C TO 1 FROM 0, AND CALL THIS SUBROUTINE WITH
C THE BEST POINT IN THE CURRENT SIMPLEX. THIS
C ALLOWS THE USER TO PROVIDE ADDITIONAL
C PERTINENT OUTPUT.

```

```

C DO NOT REMOVE THE LINE,
C 'CYCCNT=CYCCNT+1',
C FROM THE SUBPROGRAM AS IT IS USED IN JOB
C CONTROL.

```

```

*****
C DIMENSION Q(120), QP(120), TIME(120), W(120)
C IF (INDEX.NE. 1) GO TO 40
C WRITE (6,10)
C 10 FORMAT (1X, 'ENTER NO. OF DATA POINTS')
C READ (5, FREE) NDATA
C DO 30 I = 1, NDATA
C 20 READ (1, FREE) TIME(I), Q(I)
C 30 CONTINUE
C 40 CONTINUE
C INDEX = 2
C A = (GENMAT(H,1))

```

```

B = (GENMAT(H,2))
IF (GENMAT(H,3) .LE. 0) GENMAT(H,3) = .001
C = (GENMAT(H,3))
IF (GENMAT(H,4) .LE. 0) GENMAT(H,4) = .001
D = GENMAT(H,4)
E = (GENMAT(H,5))
F = (GENMAT(H,6))
G = (GENMAT(H,7))
GG = (GENMAT(H,8))
Y = 0
DO 50 II = 1, NDATA
  CC = (TIME(II))
  QP(II) = A * ALOG(CC + C) + B * (ALOG(CC + D)) ** 2 + E
  Y = Y + (QP(II) - Q(II)) ** 2
50 CONTINUE
CYCCNT = CYCCNT + 1
IF (OUTPUT .EQ. 0) RETURN
WRITE (6,60) A, B, C, D, E, Y
60 FORMAT ('O', 5(E10.4,1X), /, 1X, E10.4, 1X, F10.4, /, 4(E10.4,1X))
WRITE (6,70)
70 FORMAT ('O', 'TIME', 6X, 'OBSERVED', 2X, 'PREDICTED', 1X,
1 'RESIDUAL', /, 40('-'))
DO 90 II = 1, NDATA
  RES = (Q(II) - QP(II)) / Q(II) * 100.
  WRITE (6,80) TIME(II), Q(II), QP(II), RES
80 FORMAT (' ', F6.2, 4X, F6.2, 2X, F6.2, 2X, F6.2)
90 CONTINUE
RETURN
END

```

18. APPENDIX - J

PROGRAMS FOR THE MINICOMPUTER HP-9825

# Monitoring and data storing of the displacement runs

```

0: dim G[500],P[1400],H[500]
1: wrt 723,"00140TB777T"
2: ent "SCAN INTERVAL in min?",r1
3: ent "1st file-1",r11
4: l←W
5: 0←r2
6: red 716,T
7: r2←l←r2
8: if r2>r1;gto "scan"
9: 0←B;l←X
10: for X=1 to 7
11: B←l←B←A
12: dto(2^(A-1))←L;if L>77777;dsp "ERROR";sto
13: for Y=1 to 2
14: fmt 2,c,f4.0,c,z
15: wrt 723.2,"00040TJ",L,"T"
16: wait 500
17: wrt 723,"00240TGT"
18: wrt 723,"GX"
19: red 723,Q;otdQ*.00625←P[X+W-1]
20: next Y
21: next X
22: wrt 701,T,P[W],P[W+1],P[W+2]
23: wrt 701,P[W+3],P[W+4],P[W+5],P[W+6]
24: W←l←W;wait 13000;wait 13000;wait 13000;wait 13000;wait 6000
25: gto 6
26: "scan":
27: wait 600
28: red 716,T;wrt 701,"SCANTIME",T
29: r11←l←r11
30: wrt 723,"0140TBT"
31: 0←J
32: "SCA":
33: J←l←J
34: wrt 723,"00240TIT"
35: red 723,G[J]
36: wrt 723,"00240TIT"
37: red 723,H;otdH←H[J]
38: otdG[J]←G[J];wait 33
39: if J<500;gto "SCA"
40: wrt 723,"00140TB777T"
41: trk 0;rcf r11,G[*]
42: trk 1;rcf r11,H[*]
43: wait 3000;wait 27100
44: gto 5
*5913

```



# Conversion of raw data to microwave output power and storage

```

0: dim G[500],H[500]
1: ent "NO OF FILES",r1
2: ent "first file no.",r2
3: ent "ENTER O INPUT VALUE",r90
4: r2-1→R
5: for Q=1 to r1
6: R+1→R
7: trk 0;ldf R,G[*]
8: rew
9: trk 1;ldf R,H[*]
10: gsb "dec"
11: trk 0;rcf R,G[*];stp
12: next Q
13: "dec":
14: 0→J
15: J+1→J
16: 0→X+Y+Z
17: for I=0 to 11
18: bit(I,G[J])→K
19: if I<=3:I→E;2^E*K+X→X;gto "out"
20: if I<=7:I-4→E;2^E*K+Y→Y;gto "out"
21: I-8→E;2^E*K+Z→Z
22: "out":next I
23: X/100+Y/10+Z→D;fxd 5;fxd 5;(D*10-r90)/1000→G[J]
24: if H[J]=8162;(D*10-r90)/1000→G[J]
25: if H[J]=8164;if D>1;D/10→G[J]
26: if H[J]=8166;D→G[J]
27: if H[J]=8161;(D*10-r90)/1000→G[J]
28: if H[J]=8160;(D-r90)/1000→G[J]
29: if G[J]<0;G[J-1]+G[J]
30: plt J/20,G[J]*5
31: if J<500;nto 15
32: gto 11
*10537

```

# Program for Converting Microwave Response to Saturation Profile

```

0: dim A[500],G[500],B[500],F[500]
1: ent "TRK# FOR READING A0?",r1
2: ent "FILE# FOR READING A0?",r2
3: trk r1
4: ldf r2,A[*]
5: ent "FIL# FOR READING Aw?",r6
6: ent "TRK# FOR READING Aw?",r7
7: trk r7
8: ldf r5,B[*]
9: ent "TRK# FOR READING Sw?",r3
10: for T=1 to 100
11: ent "FILE# FOR READING Sw?",r4
12: ent "Io for Sw data in microwatt?",r5
13: trk r3
14: ldf r4,G[*]
15: for I=1 to 500
16: if G[I]<=0;G[I-1]+G[I]
17: log(G[I]/r5)+3
18: log(B[I]/10)-log(A[I]/10)+r99
19: log(A[I]/10)+A
20: (3-A)/r99+3;S+F[I];if F[I]>1;F[I-1]+F[I]
21: plt I/25,3*10
22: next I
23: stp
24: for F=2 to 333 by 2
25: S+4*F[F]+2*F[F+1]+3
26: next F
27: S+F[1]-F[334]+3;S/3+S;wrt 701,r4,S,F[333]
28: next T
*28120

```

19. APPENDIX - K

PARAMETERS OF THE OIL RECOVERY AND  
PRESSURE CURVE FIT

TABLE K-1  
Parameters of the oil recovery data curve fit  
(For the JBN Method)

Run No.	$a_2$	$b_2$	$c_2$	$d_2$	$e_2$
1.	57.67	-4.083	41.78	56.68	-150.4
2.	68.37	-4.98	26.99	43.13	-163.0
4.	33.2	-2.812	10.72	0.5024	-102.1
5.	20.04	-.6138	3.068	1.475	-37.13
7.	20.17	-.6259	3.188	1.662	-37.53
8.	5.725	10.56	1.944	1.157	-9.041
9.	48.94	-3.332	10.95	0.4936	-117.5
10.	49.69	-3.435	9.555	0.5552	-111.7

TABLE K-2  
Parameters of the  $\Delta P$  data curve fit (for JBN)

Run No.	$a_3$	$b_3$	$c_3$	$d_3$
1.	0.5148	-.1243	2.997	0.9326
2.	0.3548	-.1049	0.9203	1.5484
4.	-1.686	0.1273	17.64	6.0405
5.	2.999	.2479	29.85	9.6875
7.	-3.041	0.2781	19.29	9.2889
8.	-.5847	.00951	6.996	4.1372
9.	-.9269	.04626	6.667	5.0503
10.	-1.466	0.1064	8.428	6.2028

TABLE K-3

Parameters of oil recovery data curve fit  
(For Dynamic Method)

at $\xi=0.66$		at $\xi=0.45$		
Run No.	$a_4$	$b_4$	$a_4$	$b_4$
1.	34.48	50.59		
2.	34.91	40.53		
4.	48.96	26.87		
5.	37.25	23.67	20.80	27.43
7.	53.72	26.34	42.47	29.37
8.	42.67	36.52	42.67	36.52
9.	52.42	38.60	38.65	38.82
10.	58.80	35.8	33.73	54.73